APEX-906

HEAT TRANSFER REACTOR EXPERIMENT NO. 3

Comprehensive Technical Report, General Electric Direct-Air-Cycle Aircraft Nuclear Propulsion Program

By
F. C. Linn

June 15, 1962

Flight Propulsion Laboratory Department
General Electric Company
Cincinnati, Ohio

UNITED STATES ATOMIC ENERGY COMMISSION • DIVISION OF TECHNICAL INFORMATION

Printed in USA. Price $3.00. Available from the Office of Technical Services, Department of Commerce, Washington 25, D. C.

USAEC Division of Technical Information Extension, Oak Ridge, Tennessee

APEX-906
REACTOR TECHNOLOGY

COMPREHENSIVE TECHNICAL REPORT GENERAL ELECTRIC DIRECT-AIR-CYCLE AIRCRAFT NUCLEAR PROPULSION PROGRAM

HEAT TRANSFER REACTOR EXPERIMENT No.3

Author: F. C. LINN
Contributors: F. C. DOMINA, K. F. MERTEN, A. S. HINTZE, R. F. MORAND, J. G. KEPPLER, A. D. SMITH, J. C. McCULLOCH, J. E. Van HOOMISSEN
Editor: D. H. CULVER

June 15,1962

United States Air Force — Contract No. AF 33(600)–38062
United States Atomic Energy Commission — Contract No. AT(11-1)–171

GENERAL ELECTRIC COMPANY
NUCLEAR MATERIALS AND PROPULSION OPERATION
(Formerly Aircraft Nuclear Propulsion Department)
FLIGHT PROPULSION LABORATORY DEPARTMENT
Cincinnati 15, Ohio

ABSTRACT

This is one of twenty-one volumes summarizing the Aircraft Nuclear Propulsion Program of the General Electric Company. This volume describes Heat Transfer Reactor Experiment No. 3 (HTRE No. 3), a solid-moderated nuclear power plant with a horizontal reactor. The objectives and accomplishments of the program are presented in addition to nuclear, thermodynamic, and control system design data. The power plant and components, including the reactor, shield, turbomachinery, controls, and test support equipment are described, and the low-power and operational tests are discussed. Manufacturing techniques, component testing, and materials developments are also presented.

The objective of the HTRE No. 3 program was to provide the technical information needed for the design of a ground test prototype power plant and to test methods of design analysis and performance prediction.

PREFACE

In mid-1951, the General Electric Company, under contract to the United States Atomic Energy Commission and the United States Air Force, undertook the early development of a militarily useful nuclear propulsion system for aircraft of unlimited range. This research and development challenge to meet the stringent requirements of aircraft applications was unique. New reactor and power-plant designs, new materials, and new fabrication and testing techniques were required in fields of technology that were, and still are, advancing very rapidly. The scope of the program encompassed simultaneous advancement in reactor, shield, controls, turbomachinery, remote handling, and related nuclear and high-temperature technologies.

The power-plant design concept selected for development by the General Electric Company was the direct air cycle turbojet. Air is the only working fluid in this type of system. The reactor receives air from the jet engine compressor, heats it directly, and delivers it to the turbine. The high-temperature air then generates the forward thrust as it exhausts through the engine nozzle. The direct air cycle concept was selected on the basis of studies indicating that it would provide a relatively simple, dependable, and serviceable power plant with high-performance potential.

The decision to proceed with the nuclear-powered-flight program was based on the 1951 recommendations of the NEPA (Nuclear Energy for the Propulsion of Aircraft) project. Conducted by the Fairchild Engine and Airplane Corporation under contract to the USAF, the five-year NEPA project was a study and research effort culminating in the proposal for active development of nuclear propulsion for manned aircraft.

In the ensuing ten years, General Electric's Aircraft Nuclear Propulsion Department carried on the direct air cycle development until notification by the USAF and USAEC, early in 1961, of the cancellation of the national ANP program. The principal results of the ten-year effort are described in this and other volumes listed inside the front cover of the Comprehensive Technical Report of the General Electric Direct Air Cycle Aircraft Nuclear Propulsion Program.

Although the GE-ANPD effort was devoted primarily to achieving nuclear aircraft power-plant objectives (described mainly in APEX-902 through APEX-909), substantial contributions were made to all aspects of gas-cooled reactor technology and other promising nuclear propulsion systems (described mainly in APEX-910 through APEX-921). The Program Summary (APEX-901) presents a detailed description of the historical, programmatic, and technical background of the ten years covered by the program. A graphic summary of these events is shown on the next page.

Each portion of the Comprehensive Report, through extensive annotation and referencing of a large body of technical information, now makes accessible significant technical data, analyses, and descriptions generated by GE-ANPD. The references are grouped by subject and the complete reference list is contained in the Program Summary, APEX-901. This listing should facilitate rapid access by a researcher to specific interest areas or

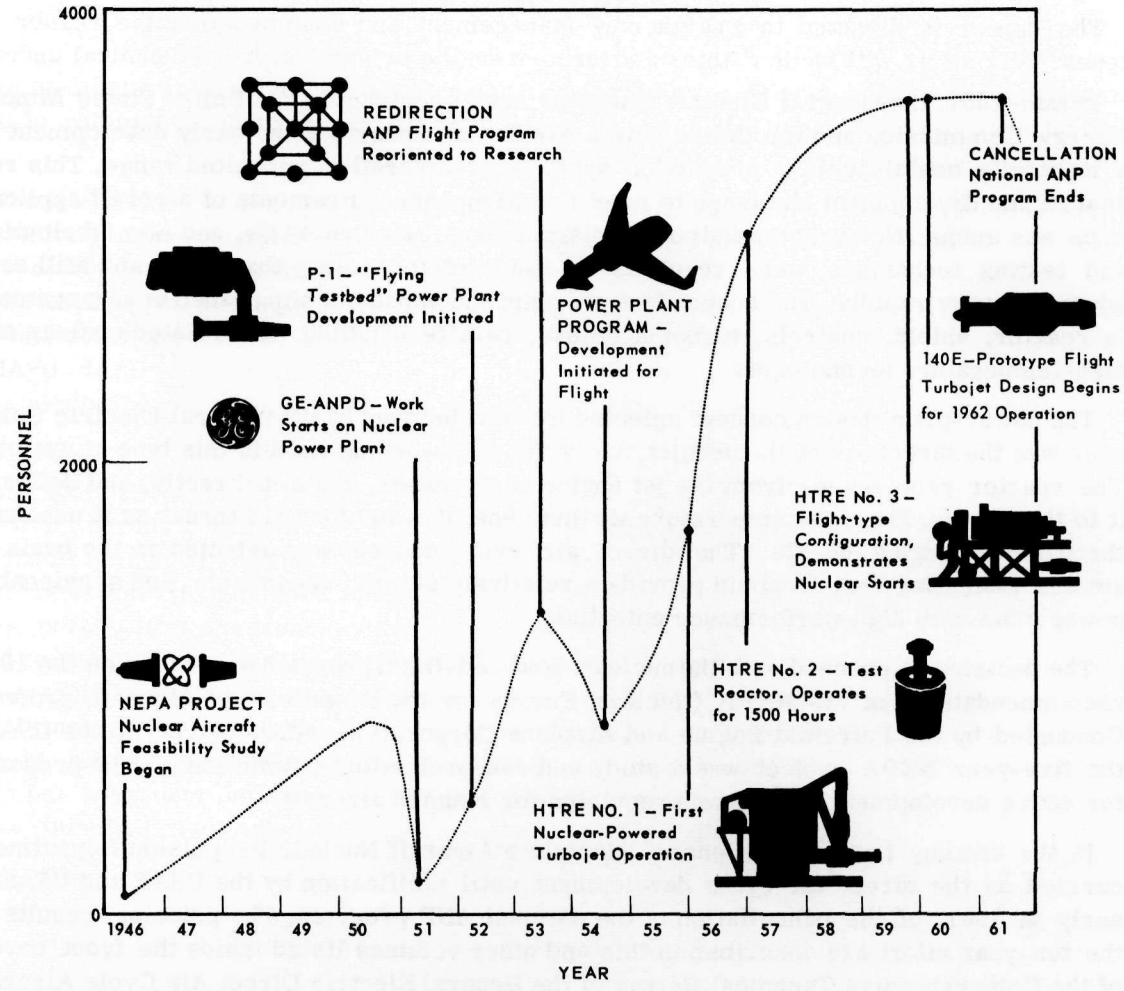

Summary of events – General Electric Aircraft Nuclear Propulsion Program*

*Detailed history and chronology is provided in Program Summary, APEX-901. Chronology information extracted from: Aircraft Nuclear Propulsion Program hearing before the Subcommittee on Research and Development of the Joint Committee on Atomic Energy, 86th Congress of The United States, First Session, July 23, 1959, United States Government Printing Office, Washington 1959.

sources of data. Each portion of the Comprehensive Report discusses an aspect of the Program not covered in other portions. Therefore, details of power plants can be found in the power-plant volumes and details of the technologies used in the power plants can be found in the other volumes. The referenced documents and reports, as well as other GE-ANPD technical information not covered by the Comprehensive Report, are available through the United States Atomic Energy Commission, Division of Technical Information Extension, Oak Ridge, Tennessee.

The Report is directed to Engineering Management and assumes that the reader is generally familiar with basic reactor and turbojet engine principles; has a technical understanding of the related disciplines and technologies necessary for their development and design; and, particularly in APEX-910 through APEX-921, has an understanding of the related computer and computative techniques.

The achievements of General Electric's Aircraft Nuclear Propulsion Program were the result of the efforts of many officers, managers, scientists, technicians, and administrative personnel in both government and industry. Most of them must remain anonymous, but particular mention should be made of Generals Donald J. Keirn and Irving L. Branch of the Joint USAF-USAEC Aircraft Nuclear Propulsion Office (ANPO) and their staffs; Messrs. Edmund M. Velten, Harry H. Gorman, and John L. Wilson of the USAF-USAEC Operations Office and their staffs; and Messrs. D. Roy Shoults, Samuel J. Levine, and David F. Shaw, GE-ANPD Managers and their staffs.

This Comprehensive Technical Report represents the efforts of the USAEC, USAF, and GE-ANPD managers, writers, authors, reviewers, and editors working within the Nuclear Materials and Propulsion Operation (formerly the Aircraft Nuclear Propulsion Department). The local representatives of the AEC-USAF team, the Lockland Aircraft Reactors Operations Office (LAROO), gave valuable guidance during manuscript preparation, and special appreciation is accorded J. L. Wilson, Manager, LAROO, and members of his staff. In addition to the authors listed in each volume, some of those in the General Electric Company who made significant contributions were: W. H. Long, Manager, Nuclear Materials and Propulsion Operation; V. P. Calkins, E. B. Delson, J. P. Kearns, M. C. Leverett, L. Lomen, H. F. Matthiesen, J. D. Selby, and G. Thornton, managers and reviewers; and C. L. Chase, D. W. Patrick, and J. W. Stephenson and their editorial, art, and production staffs. Their time and energy are gratefully acknowledged.

THE EDITORIAL BOARD:

Paul E. Lowe
Arnold J. Rothstein
James I. Trussell

November 8, 1961

CONTENTS

	Page
1. Introduction and Summary	15
1. 1 Introduction	15
1. 2 Summary	16
2. HTRE No. 3 Power Plant Program	21
2. 1 Program Objectives	21
2. 2 Program Accomplishments	21
2. 3 Description of Equipment	22
2. 3. 1 Over-All Power Plant	22
2. 3. 2 Reactor	22
2. 3. 3 Shield	22
2. 3. 4 Airflow Pattern	22
2. 3. 5 Engine Control	22
2. 3. 6 Reactor Control	27
2. 3. 7 Turbomachinery	28
2. 4 Specifications and Design Data	28
2. 4. 1 Physical Characteristics	29
2. 4. 2 Aerothermal Characteristics	31
2. 4. 3 Nuclear Characteristics	31
2. 5 Assembly of HTRE No. 3 at ITS	32
2. 6 References	37
3. HTRE No. 3 Tests	39
3. 1 Summary	39
3. 1. 1 First Low Power Test (LPT 2)	39
3. 1. 2 Initial Power Test (IET No. 13)	39
3. 1. 3 Second Low Power Test (LPT 2-2)	40
3. 1. 4 Phase I Testing (IET No. 16)	40
3. 1. 5 Endurance Run (IET No. 18)	40
3. 1. 6 Full Nuclear Start and Elevated Performance Demonstration (IET No. 25)	41
3. 1. 7 Summary of HTRE No. 3 Performance	42
3. 2 Reactor Performance	42
3. 2. 1 Low Power Tests	42
3. 2. 2 Power Tests	47
3. 3 Shield Performance	58
3. 3. 1 Shield Heating Rates	58
3. 3. 2 Radiation Levels Outside the Shield	58
3. 4 Nuclear Starts	58
3. 5 References	64
4. Reactor	65
4. 1 Objectives and Requirements	65

Page

4.2 Reactor Design 66
4.2.1 Over-All Core 66
4.2.2 Fuel Cartridges 68
4.2.3 Moderator 84
4.2.4 Reflector 88
4.2.5 Control Rods 88
4.2.6 Tube Sheets 90
4.2.7 Critical Experiments 96
4.2.8 Supporting Analytic Program 96
4.3 References 97
5. Shield 99
5.1 Objectives and Requirements 99
5.1.1 Primary Shield 101
5.1.2 Auxiliary Shield 102
5.1.3 Combustor Shield 102
5.1.4 Scroll, Elbow, and Transition Ducting 102
5.1.5 Stress Criteria and Loads 102
5.2 Design Description 103
5.2.1 Mechanical Design 103
5.2.2 Aerothermal Design 118
5.2.3 Nuclear 126
5.2.4 Stress and Weight 138
5.3 Manufacture and Assembly 138
5.4 Component Testing 142
5.4.1 Mechanical Testing 142
5.4.2 Nuclear Testing 148
5.4.3 Aerothermal Testing 148
5.5 Operations 156
5.5.1 Mechanical (Insulation) 156
5.5.2 Nuclear 156
5.5.3 Aerothermal 156
5.6 References 166
6. Turbomachinery 169
6.1 General Description 169
6.1.1 Design 169
6.1.2 Design Requirements 170
6.2 Components 170
6.2.1 Inlet Section 170
6.2.2 Gearbox 170
6.2.3 Compressor 170
6.2.4 Midframe and Aftframe 171
6.2.5 Compressor and Turbine Scrolls 171
6.2.6 Turbine 172
6.2.7 Exhaust Nozzle 172
6.2.8 Auxiliary Flow Systems 172
6.2.9 Combustor 172
6.3 Engine Controls and Instrumentation 172
6.3.1 Engine Control System Philosophy 172
6.3.2 Control System Design and Mechanization 174
6.3.3 Engine Operating Instrumentation 174

Page

6. 3. 4 Accessory Components 174
6. 3. 5 Data-Instrumentation 176
6. 3. 6 Parameter Tabulation 176
6. 4 References 177
7. Controls 179
7. 1 System Requirements 179
7. 2 Control Description and Operation 180
7. 2. 1 Source Range Control 181
7. 2. 2 Shim Control System 181
7. 2. 3 Intermediate Range 181
7. 2. 4 Power Range 182
7. 2. 5 Flux Monitoring Channel 182
7. 2. 6 Temperature Control Loop 183
7. 2. 7 Safety Features 186
7. 2. 8 Nuclear Sensor System 188
7. 3 Components and Materials 190
7. 4 Component Testing 190
7. 5 Operations 190
7. 6 References 195
8. Test Assemblies and Reactor Accessories 197
8. 1 Dolly Assembly 197
8. 2 Reactor Accessories 197
8. 2. 1 External Ducting 197
8. 2. 2 Duct Valves and Actuators 198
8. 2. 3 Service-Air System 199
8. 2. 4 Primary Shield Liquid System 199
8. 2. 5 Shield Augmentation System 200
8. 3 References 201
9. Remote Handling Equipment 203
9. 1 Objectives and Requirements 203
9. 2 References 204
10. Hazards 205
10. 1 References 206

FIGURES

		Page
1.1	- HTRE No. 3 test assembly	16
2.1	- HTRE No. 3 key components	23
2.2	- HTRE No. 3 test assembly	24
2.3	- HTRE No. 3 reactor shield assembly (artist's concept)	25
2.4	- HTRE No. 3 reactor shield assembly (side and section views)	26
2.5	- D102A airflow cycle	27
2.6	- HTRE No. 3 dolly	32
2.7	- HTRE No. 3 dolly during superstructure assembly	33
2.8	- X39-5 engine ready for assembly onto HTRE No. 3 dolly	34
2.9	- Master jig containing core and front shield plug	35
2.10	- Core removal fixture on top of erection stand	36
3.1	- Comparison of gross radial power distributions from preliminary and final power maps (LPT 2)	44
3.2	- Comparison of gross radial power distributions for hot and cold power maps	45
3.3	- Comparison of circumferential power distribution with two different poison liner configurations (Cell 241, Cylinder 4)	45
3.4	- Core radial temperatures	49
3.5	- Core longitudinal temperatures	50
3.6	- Circumferential temperatures and power	50
3.7	- Individual fuel element radial temperatures	51
3.8	- Rear tube sheet temperatures	52
3.9	- Core temperatures during endurance and elevated-performance runs	53
3.10	- Power to air and weight flow for endurance and elevated-performance runs	54
3.11	- Afterheat temperature rise	55
3.12	- Shutdown power decay	56
3.13	- Location of shield-heating-rate sensors	59
3.14	- Gamma-ray dose rate in the vertical midplane at a 10-foot radius about the center of the active core	60
3.15	- Fast neutron flux in vertical midplane at a 10-foot radius about the center of the active core	61
3.16	- Transient parameters recorded during the first all-nuclear start	62
3.17	- Predicted and measured data of the first all-nuclear start	63
4.1	- HTRE No. 3 core assembly	67
4.2	- HTRE No. 3 fuel-moderator cell assembly	69
4.3	- HTRE No. 3 moderator assembly	70
4.4	- Insulation liner assembly	71
4.5	- Side view of fuel cartridge assembly	72

Page

4.6 - Longitudinal cross section and loading diagrams of fuel stage used in HTRE No. 3 fuel cartridges 76
4.7 - Design evaluation in fuel element design process 78
4.8 - XR-13 fuel element 79
4.9 - XR-26 fuel element 80
4.10 - Fuel element for core regions A and B 81
4.11 - HTRE No. 3 fuel cell components 82
4.12 - Distribution of control rods, fuel elements, and N_H regions 83
4.13 - First three steps in moderator assembly procedure 85
4.14 - Final three steps in moderator assembly procedure 86
4.15 - Typical moderator blocks 89
4.16 - Typical HTRE No. 3 moderator assembly 90
4.17 - Front tube sheet detail 91
4.18 - Maximum ligament stresses in the front tube sheet 94
4.19 - Maximum ligament stresses in the rear tube sheet 95

5.1 - HTRE No. 3 airflow stations 100
5.2 - External auxiliary shield 104
5.3 - Combustor shield 105
5.4 - General arrangement of the primary and auxiliary shields 106
5.5 - Side view of front shield plug assembly 107
5.6 - Control rod passing through front shield plug and core 108
5.7 - Tandem pneumatic cylinder 109
5.8 - Rear shield plug assembly 110
5.9 - The forward annulus 111
5.10 - The island plug 112
5.11 - Thermal barrier 113
5.12 - Thermal barrier fastening device 113
5.13 - Primary shield assembly 114
5.14 - Inner pressure vessel 115
5.15 - Upper half of auxiliary shield after installation of boral sheets on outside surface 116
5.16 - Combustor shield less sliding doors 117
5.17 - Scroll, elbows, and transition ducts 118
5.18 - Scroll 119
5.19 - Elbow 120
5.20 - Mockup of HTRE No. 3 assembly showing external auxiliary shield raised and primary shield cut away 121
5.21 - Primary shield structural temperatures based on X211 engine operation .. 122
5.22 - Temperature profile in front shield plug, point A 122
5.23 - Temperature profile in front shield plug, point B 123
5.24 - Temperature profile in front shield plug, point C 123
5.25 - Temperature profile of side shield considering no contact resistance 124
5.26 - Temperature profile of side shield considering a 20-mil air gap on one side 124
5.27 - Temperature profile of pressure shell midplane 125
5.28 - Temperature distribution in region of point D 126
5.29 - Temperature distribution in region of point E 127
5.30 - Calculated HTRE No. 3 gamma-ray dose rate during operation 128
5.31 - Calculated HTRE No. 3 fast neutron dose rate during operation 129
5.32 - Calculated HTRE No. 3 gamma-ray dose rate 18 hours following shutdown after 100 continuous hours of operation 130

Page

5.33 - Calculated heating rates in the longitudinal traverse of the HTRE No. 3 front shield plug 131
5.34 - Calculated radial distribution of the total heating rate in the front shield plug of HTRE No. 3 134
5.35 - Calculated heating rates in the radial traverse of the HTRE No. 3 primary shield 135
5.36 - Calculated longitudinal distribution of the heating rate in the primary shield of HTRE No. 3 for the three lead slabs 138
5.37 - Insulated rear shield plug 140
5.38 - Insulated rear shield plug island 141
5.39 - Rear shield plug annulus 142
5.40 - Rear shield plug assembly 143
5.41 - Portion of the test tank for proof-testing the insulation of the HTRE No. 3 rear shield 144
5.42 - Insulated rear shield test tank in the test rig 145
5.43 - Insulation test tank during a proof test 146
5.44 - Insulation pads after proof testing 147
5.45 - 1/4-scale scroll-shield-tube bundle mockup for aerodynamic testing 150
5.46 - Alternative configuration of various front and rear header plugs in 1/4-scale aerodynamic test mockup 151
5.47 - Front view of the HTRE No. 3 inlet scroll 152
5.48 - Configuration of several front shield plugs tested for the HTRE No. 3 153
5.49 - Reactor simulator showing the tube bundle 154
5.50 - Rear plug No. 4 155
5.51 - Weight flow distribution radially in core for various front plug configurations 157
5.52 - Weight flow distribution radially in core for various rear plug configurations 158
5.53 - Front end of insulated HTRE No. 3 rear plug after operation 159
5.54 - Aft end of HTRE No. 3 rear plug seen through the combustor 160
5.55 - Comparison of calculated and measured thermal neutron flux distribution in HTRE No. 3 sensor well plug 161
5.56 - Comparison of calculated and measured fast neutron flux distribution in HTRE No. 3 sensor well plug (neutron energy > 2.9 Mev) 161
5.57 - Comparison of calculated and measured fast neutron flux in the vertical longitudinal midplane of the HTRE No. 3 at a radius of 10 feet from the center of the core (neutron energy > 2.9 Mev) 162
5.58 - Comparison of calculated and measured gamma-ray dose rate in the vertical longitudinal midplane of the HTRE No. 3 at a radius of 10 feet from the center of the core 163
5.59 - HTRE No. 3 core discharge air temperature, surge tank level, and rear shield temperature as a function of time during Run No. 13 164

6.1 - X39-5 engine 169
6.2 - Configuration of HTRE No. 3 engine scrolls 171
6.3 - HTRE No. 3 combustor 173

7.1 - Source range control 181
7.2 - Intermediate range control 182
7.3 - Power range control 183
7.4 - Temperature loop 184
7.5 - Measured open loop frequency response of the temperature loop 184

Page

7.6 - Measured closed loop attenuation response of the temperature loop 185
7.7 - Temperature loop transient response to demand (50° step input) 185
7.8 - Safety system 186
7.9 - Response characteristics of the basic interlock and manual override actions 188
7.10 - Rate of power decrease during a manual scram safety action 188
7.11 - Safety-system monitoring of a demand power rise in the event of a period violation 189
7.12 - Sequence of events in a scram action 189
7.13 - Fission chamber 191
7.14 - Compensated ionization chamber 192
7.15 - Uncompensated ionization chamber 193

8.1 - Louvered weather protection for HTRE No. 3 test assembly 198

TABLES

Page

1.1 - Predicted and Measured HTRE No. 3 Performance 18

3.1 - HTRE No. 3 Performance Data 42
3.2 - Low-Power Test Excess Reactivity 43
3.3 - Control System Reactivity Values 43
3.4 - Rod Worth Comparison 44
3.5 - Core Power Comparison Data 46
3.6 - Final Core Power Profiles (LPT 2-2) 46
3.7 - Symmetry Study of Final Configuration (LPT 2-2) 48
3.8 - Clean Excess Reactivity Values During IET No. 18 56
3.9 - Total Poison in HTRE No. 3 Reactor After 65 Hours of Continuous Operation 57
3.10 - Shield Heat Generation Rates in IET No. 16 and IET No. 18 60

4.1 - HTRE No. 3 Performance with X211 and X39 Engines 65
4.2 - HTRE No. 3 Reactor Dimensions and Characteristics 73
4.3 - Data on Hydrogen Content and Bonding of HTRE No. 3 Moderator Sections Selected for Testing in HTRE No. 2, Insert 1B 87

6.1 - Characteristics of the Overspeed Governor 174
6.2 - Engine Operating Instrumentation 175
6.3 - Engine Test Instrumentation 176

7.1 - Control System Parameters 179
7.2 - HTRE No. 3 Safety Parameters 187

1. INTRODUCTION AND SUMMARY

1.1 INTRODUCTION

Heat Transfer Reactor Experiment No. 3 (HTRE No. 3) was the third nuclear power plant developed by the Aircraft Nuclear Propulsion Department of the General Electric Company (GE-ANPD). The primary purpose of the HTRE series was to confirm the methods of design analysis and performance prediction, developed by GE-ANPD, to be used in the design of high-performance nuclear power plants capable of meeting the levels of performance established by the Department of Defense.

The HTRE reactors were of two distinct but related types. The first two, HTRE No. 1 and HTRE No. 2, used water as the moderator, had vertical cores, and powered a single turbojet or were cooled by one or two turbojet engines operating wholly or partially on chemical power. HTRE No. 2 is virtually identical to HTRE No. 1 except for a longitudinal void provided in the center of the core. HTRE No. 2 was designed to serve as a facility in which tests of advanced fuel elements could be carried out under conditions of irradiation, temperature, and airflow approximating those to be encountered in a flight reactor.

The design of HTRE No. 3 (shown in Figure 1. 1) differs from the first two power plants in three basic ways: (1) it has a solid moderator, (2) the reactor is horizontal, and (3) a single reactor supplies the heat for two turbojet engines operating simultaneously. Using lightweight hydrided zirconium as a moderator instead of water in the HTRE No. 3 eliminated the necessity for circulating and removing heat from the moderator water, reducing weight and complexity, increasing the power-to-weight ratio, and freeing the power plant from the cooling ram-air temperature limitation. HTRE No. 3 was intended to provide the technical information needed for the design of a ground test prototype power plant (designated the XMA-1A and discussed in APEX-907, "XMA-1 Nuclear Turbojet," of this Report), and also to evaluate and confirm methods of design analysis and performance prediction. The objectives of the operating tests of the power plant were to achieve maximum exit-air temperatures for a given maximum fuel element temperature (because it is the maximum fuel element temperature that limits the power that can be extracted from the reactor), and, concurrently, to hold the pressure drop through the reactor to the level required by the characteristics of the compressor and turbine.

The dimensions of the core and its structural characteristics as well as the design temperatures were those of a power plant capable of providing useful flight propulsion. The power generated by HTRE No. 3 ranged up to about 35 megawatts. As a flight reactor would be required to produce many times this level, HTRE No. 3 was designed to generate such power levels when provided with suitable turbojet engines. In the HTRE No. 3 tests, the power levels were so chosen that the fuel element temperatures, the key parameter, would be characteristic of flight service.

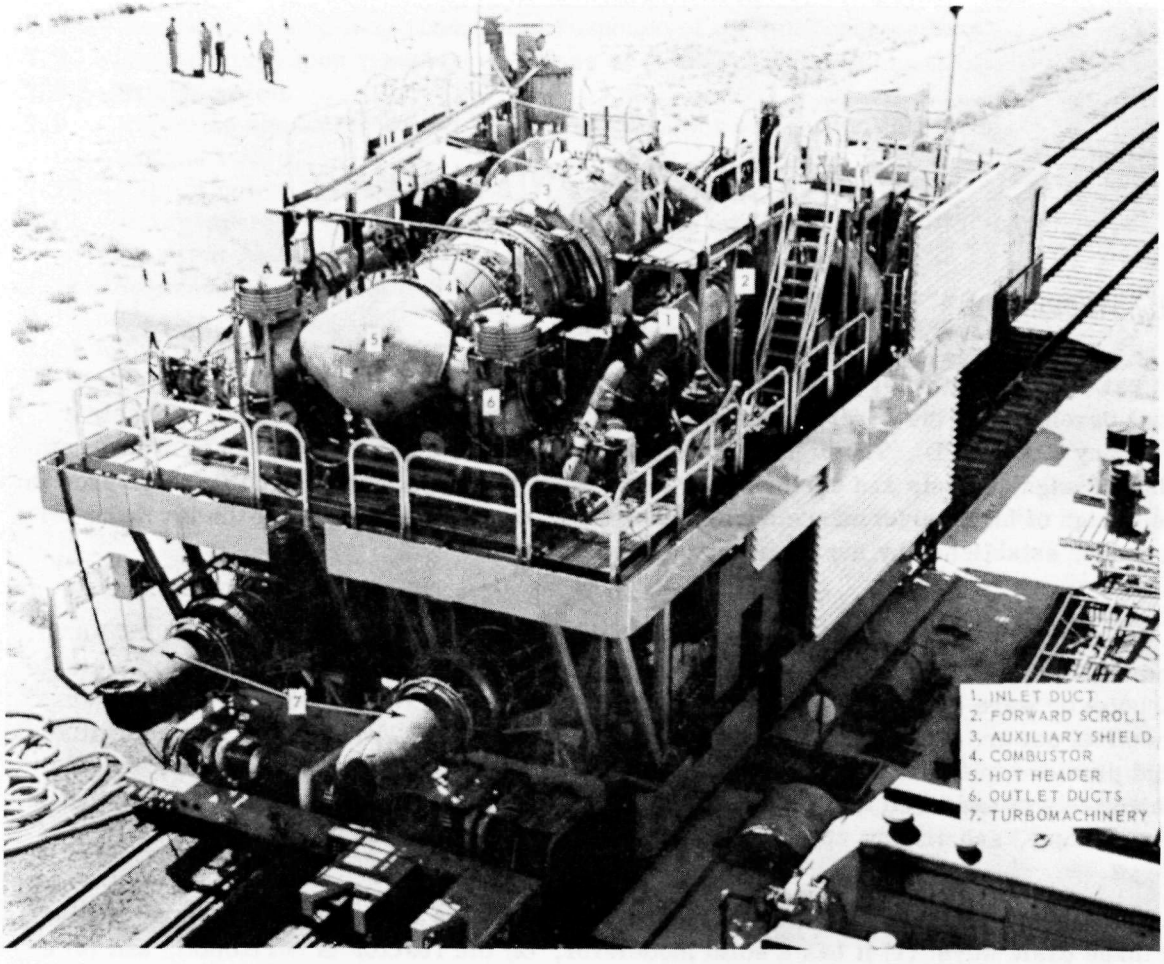

Fig. 1.1 – HTRE No. 3 test assembly (Neg. U-2700-11)

For purposes of convenience, the HTRE No. 3 shield mechanically resembles the shield that was planned for a prototype flight power plant but was water-cooled. HTRE No. 3 also differs in other respects from the final power plant; e.g., some features of the control system would not have been flight-worthy. Although such deviations from a flight design could have become significant if not eventually corrected, they did not interfere with the primary objective of confirming the methods of design analysis and performance prediction. Other work showed that the shield, controls, etc., were also in a satisfactory state of development. Even though the HTRE No. 3 did not incorporate all the design refinements that are now known to be practical, it is probably the most sophisticated gas cooled reactor that has been built to date.

1.2 SUMMARY

The active core of HTRE No. 3 is 30 inches long and 51 inches in diameter. It is made up of 150 cells which are surrounded by a 3-inch beryllium reflector. Each cell consists of a fuel cartridge inside a hydrided zirconium moderator. The fuel cartridges consist of 19 stages, each of which is made up of 12 concentric metallic rings. These fuel elements operated satisfactorily at temperatures up to 1900°F for over 100 hours and up to 2050°F for more than 25 hours.

In cross section, the moderator tubes are hexagonal on the outside and circular on the inside. Gross radial power flattening is achieved by varying the hydrogen content of the moderator radially outward from the center of the core. The moderator demonstrated an operating temperature capability of up to 1300°F for 100 hours without experiencing excessive oxidation or hydrogen loss.

The beryllium reflector consists of hexagonal blocks provided with longitudinal cooling holes. Insulation separating it from the active core held the operating temperature of the reflector to a maximum of 1200°F.

The lead and water shielding is cooled by circulating the water between the lead slabs and rejecting the heat to a water-to-water heat exchanger on the dolly. All other components of the reactor are cooled by the primary air from the turbojet compressor.

The reactor, front and rear shield plugs, and the radial shield are supported by the Inconel X pressure vessel.

Control of the reactor is achieved by control rods located at the interstices of the moderator tubes; there are 30 shim rods, 3 dynamic rods for power changes, and 15 safety rods which are normally withdrawn except for shutdown. The control rods are made up of short segments of clad europium oxide held together by straps. This articulated design permits the necessary deflection as the rod traverses its guide tube. These rods operated satisfactorily at temperatures up to 1600°F. With a rate of travel of 5 feet per second and a stroke of 20 inches, the rods were subjected to 34,000 cycles under varying conditions without failure or malfunction.

Achieving the objectives of the HTRE No. 3 series of tests required that the highest possible exit air temperature be maintained without exceeding the allowable fuel element temperatures. Thus, careful design in many areas was necessary to eliminate the causes of hot spots wherever possible.

1. The inlet plenum chamber was carefully shaped to provide a uniform distribution of airflow over the face of the core (actual measurements showed that the least well-cooled channel received only 2 percent less air than the average channel).
2. The hydrogen content of the hydrided zirconium moderator was increased radially outward from the center of the core to flatten the power distribution across the reactor.
3. Within individual fuel elements, power flattening was achieved by varying the loading of UO_2 in the concentric rings; the outermost rings were loaded least heavily.
4. The number of concentric rings per fuel element stage was increased toward the outlet end of the reactor. This created a greater heat transfer area to compensate for the smaller differential between fuel element surface temperature and the cooling air temperature in that area of the core. It also had the desirable effect of minimizing the pressure drop through the reactor.
5. The moderator was extended 5 inches forward of the upstream face of the fuel elements to shift the longitudinal power peak in the direction of the inlet end. This further diminished the difference between local air temperature and allowable fuel temperature.
6. Measured circumferential power scalloping around the individual fuel elements was trimmed by using thin shims of boron-steel along each streak of high power.
7. Allowance was made for the effects of control rod insertion depth, burnup, fission product poisoning, thermal expansion of fuel elements causing reduced area for cooling air, deviations in flow passages resulting from unavoidable manufacturing inaccuracies, possible variations in the fuel content of the fuel rings, radiation of heat from fuel ring to fuel ring, turbulence caused by airflow over structural hardware, etc.

8. Extensive calculations were performed in an effort to solve the difficult problem of the rate of heat generation in the reactor components other than the core; e.g., moderator, control rods, control rod guide tubes, reflector, structure, etc. This proved to be very difficult. Non-fueled components, for example, can acquire or generate heat by at least five different mechanisms, each of which had to be evaluated.

Table 1.1 presents a comparison of the predicted and the measured performance of the HTRE No. 3 power plant. In general, excellent agreement was obtained, demonstrating the reliability of the methods of analysis and performance prediction developed during the ANP program. Of particular interest was the differential between maximum fuel temperature and average exit-air temperature. In HTRE No. 3 this difference was 465°F (1900° minus 1435°); in HTRE No. 1 the difference was 515°F. The difference is indicative of the refinement of the design of HTRE No. 3 over HTRE No. 1. It was estimated that the temperature differential in HTRE No. 3 could have been reduced to 400°F by incorporating further improvements. Turbine inlet temperatures of 1500° to 1650°F could probably be achieved for times of 1000 hours or more by reactors of this type, based on information acquired during the HTRE No. 3 tests.

TABLE 1.1

PREDICTED AND MEASURED HTRE NO. 3 PERFORMANCE

	Predicted	Measured
Maximum fuel temperature, °F	1880	1900
Maximum moderator temperature, °F	1175	1120
Maximum reflector temperature, °F	1100	1030
Maximum fuel air discharge temperature, °F	1640	1640
Average fuel air discharge temperature, °F	1430	1435
Average moderator air discharge temperature, °F	968	880
Average reflector air discharge temperature, °F	955	940
Average control rod discharge temperature, °F	805	480
Reactor pressure drop, psi	6.05	6.2
Pressure drop, compressor to turbine, psi	10.8	9.3

The development and operation of the HTRE No. 3 power plant represented several significant technological advances in the national Aircraft Nuclear Propulsion Program.

1. The reactor core was moderated with hydrided zirconium whereas previous GE-ANPD power plants had been water-moderated. The hydriding of the solid material to improve the moderating capability was also a major achievement.
2. Starting the HTRE No. 3 turbojet engines on nuclear heat only represented the first known demonstration of the feasibility of all-nuclear starts.
3. HTRE No. 3 was the first power plant whose core and primary shield were designed for the stresses of flight airflow, pressure, temperature, and G loadings.
4. The primary shield was the first to be built to withstand the radiation levels expected in flight.
5. The flight-type control system was the first to operate in the horizontal position.

The measured performance of HTRE No. 3 was found to be essentially as predicted, thus confirming the nuclear and aerothermodynamic calculations. The ability to control the power distribution to a fine degree was proved. HTRE No. 3 operation led to improve-

ments and modifications in the control system that were subsequently developed and tested. HTRE No. 3 demonstrated that a reactor of this type, with a peak-to-average power ratio of less than 1.10, is entirely feasible and practicable. In addition, by demonstrating that airflow perturbations can be held to an insignificant amount, HTRE No. 3 also proved that near-maximum power can be produced within the temperature limitations of the materials.

The data obtained on the heating rates of moderator, shield, control rods, and structural components reduced the tolerance, and the resulting degradation of performance, that was previously necessary because of the uncertainties concerning these values. The automatic flux and temperature controls were shown to be quite adequate for any transients that could be expected in a system of this type. The ability to handle the assembly remotely was demonstrated in several assembly and disassembly operations. Much fabrication experience was gained in the manufacture of lightweight structures of Inconel X and 17-7PH stainless steel, metallic fuel elements, hydrided zirconium moderator, control rod poison sections, etc. Operation was demonstrated from startup to full power with nuclear heat only, thus showing that auxiliary heat is not required in any portion of the operating range.

The examination of HTRE No. 3 at the conclusion of power tests revealed no deterioration that would have prevented continued operation for an even longer additional period of time.

2. HTRE NO. 3 POWER PLANT PROGRAM

2.1 PROGRAM OBJECTIVES

The general goals set for Heat Transfer Reactor Experiment No. 3 were the design, development, manufacture, and test of a nuclear reactor with components that could be used on the XMA-1 power plant or the establishment of fundamentals applicable to the XMA-1. The reactor size, shape, neutron spectrum, control system, and structure were thus to be similar to those anticipated for the XMA-1 system.

The structural portion of the core, the reflector, the inlet plenum chamber, the shields (front, rear and primary or side shield), and the flow passages through them were designed for operation with two X211 turbojet engines. Since the air supply for HTRE No. 3 was from two X39-5 engines (modified J47's) and since HTRE No. 3 was operated with this air supply, the reactor was designed to meet the conditions imposed upon it by the X39 engines.

2.2 PROGRAM ACCOMPLISHMENTS

Many engineering advances constituting "firsts" with respect to the Aircraft Nuclear Propulsion Program were realized in the manufacture and operation of HTRE No. 3. Listed below are some of these accomplishments.

1. The reactor core was moderated with hydrided zirconium. Previous cores had been water-moderated. (The hydriding of the solid material to provide a better moderating capability was in itself a noteworthy achievement.)
2. The turbojet engines used in the tests were started for the first time on nuclear heat only. In previous HTRE tests, the engines had been started on heat from chemical combustors.
3. The core and primary shield were designed to withstand the stresses of flight airflow, pressure, temperature, and G loadings.
4. The primary shield was designed to withstand the radiation levels expected in flight.
5. Since the reactor was operated in the horizontal attitude, the control system was the first version of a flight-type system in which the control rods operated horizontally.

Some of the work, although not unique with this power plant, was large enough in scope or difficult enough to accomplish to merit mention. Preoperation component testing was performed on the forward and rear shields and control equipment. Experience was gained from designing and building the lightweight, complex structure from Inconel X and 17-7 PH stainless steel. Reactivity temperature coefficient and aftercooling characteristics were determined. Nuclear and aerothermodynamic performance calculations, including determination of perturbations and interactions, were confirmed. Also significant were the improved techniques and equipment for remote handling of the power-plant components during assembly and disassembly.

2.3 DESCRIPTION OF EQUIPMENT

2.3.1 OVER-ALL POWER PLANT

The HTRE No. 3 (D102A) power plant consists of a reactor, side shield, front and rear shields, external auxiliary shielding, engine-reactor ducting, a single chemical combustor with surrounding auxiliary shield, accessories, controls, and two X39-5 turbojet engines. The key components of the power plant are shown, without structure and associated equipment, in Figure 2.1.

Figure 2.2 shows the fully assembled power plant. The power plant is mounted on a dolly so that is can be serviced with the facilities in the shop area at the Idaho Test Station and then moved out to the Initial Engine Test facility, about a mile away, for testing.

2.3.2 REACTOR

The reactor core has a nominal diameter of 51 inches, an active core length of 30.7 inches, and an over-all length of 43.5 inches. The core is composed of a hexagonal array of 151 moderator cells surrounded by a beryllium reflector approximately 3 inches thick. Each cell consists of a moderator of hydrided zirconium (a hexagonal bar 4 inches across flats with a 3-inch-diameter hole through its center), metallic fuel elements of 80Ni - 20Cr and uranium oxide, an insulation liner, and a structural tube.

A fuel element consists of 19 stages, each 1.5 inches in length. These stages are composed of 12 concentric rings. The fuel inventory consists of fully enriched uranium in the form of the oxide with an equivalent total U^{235} investment of 390 pounds. A total of 1478 pounds of 80Ni - 20Cr is used. The uranium oxide is embedded in the 80Ni - 20Cr matrix and is clad with 80Ni - 20Cr. The core components are air cooled by proper division of the primary airflow.

A cutaway view of the reactor-shield assembly is shown in Figure 2.3.

2.3.3 SHIELD

The water, lead, steel, and boral shielding was designed for a 1000-hour life at 175-megawatt reactor operation. The primary shield, approximately 20 inches thick, was designed to simulate a flight-type shield structure and to attenuate the radiation expected during flight. In the external auxiliary shield, the radiation levels are expected to fall within the limits of 10^4 rep per hour for fast neutrons and 10^5 roentgens per hour for operating gammas. The complete reactor-shield assembly showing both shields is illustrated in Figure 2.4.

2.3.4 AIRFLOW PATTERN

As shown in Figure 2.5, air enters the compressor of the turbojet engine and passes through the cold ducting to the forward transition scroll, where it is distributed radially around the front shield plug and into the core through the front tube sheet. Three percent of this air cools the beryllium reflector and the control rods; the other 97 percent passes through the active core. The air is heated to approximately 1300°F and exhausted into a plenum, from which it passes through the combustor, aft header, and turbines. The air is exhausted to the atmosphere via an exhaust-handling system. When the power plant is operating on chemical fuel, the compressor air passes through the cold reactor. Single-engine operation can be obtained by closing the compressor and turbine shutoff valves in the external ducting of the inactive engine.

2.3.5 ENGINE CONTROL

Each engine is independently and automatically controlled during either chemical or nuclear operation by automatic speed control systems. The turbine inlet temperature (T_4) of

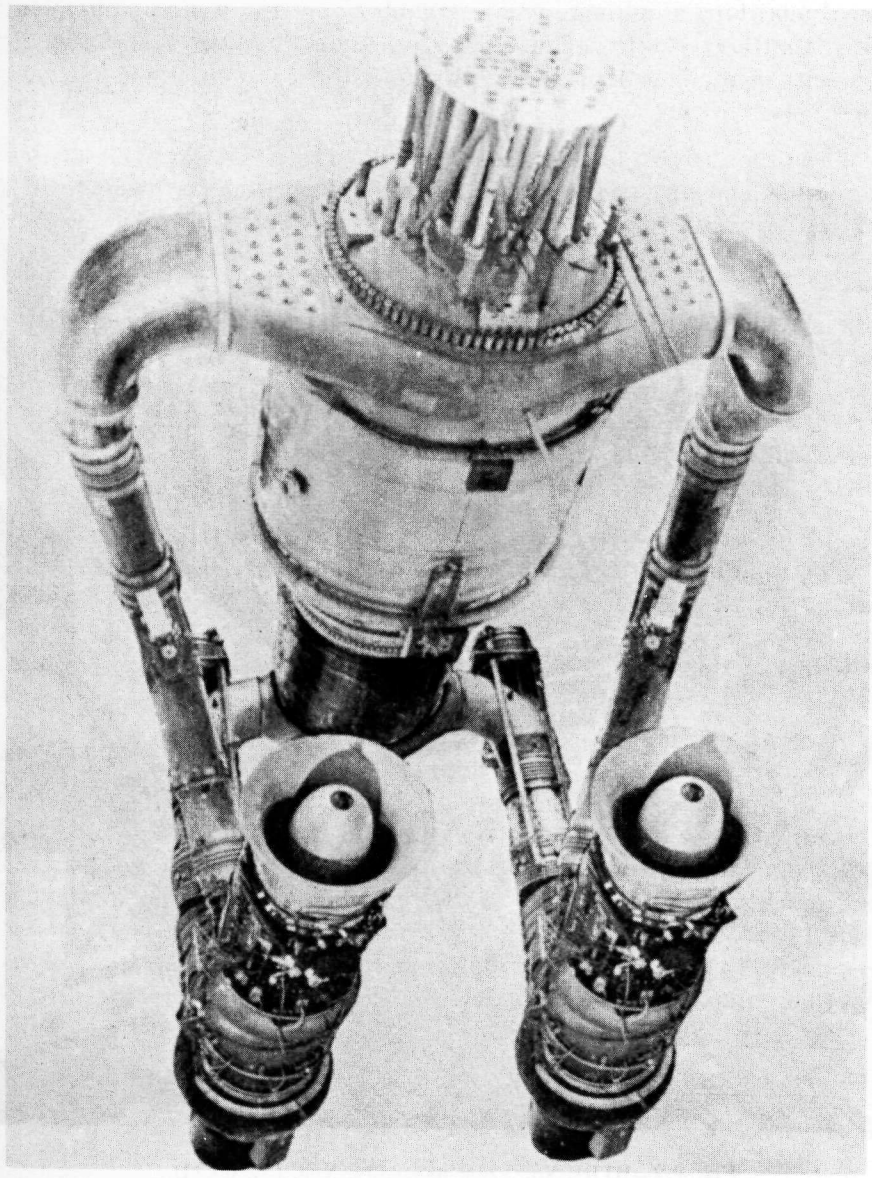

Fig. 2.1 – HTRE No. 3 key components (ANP Chart 95)

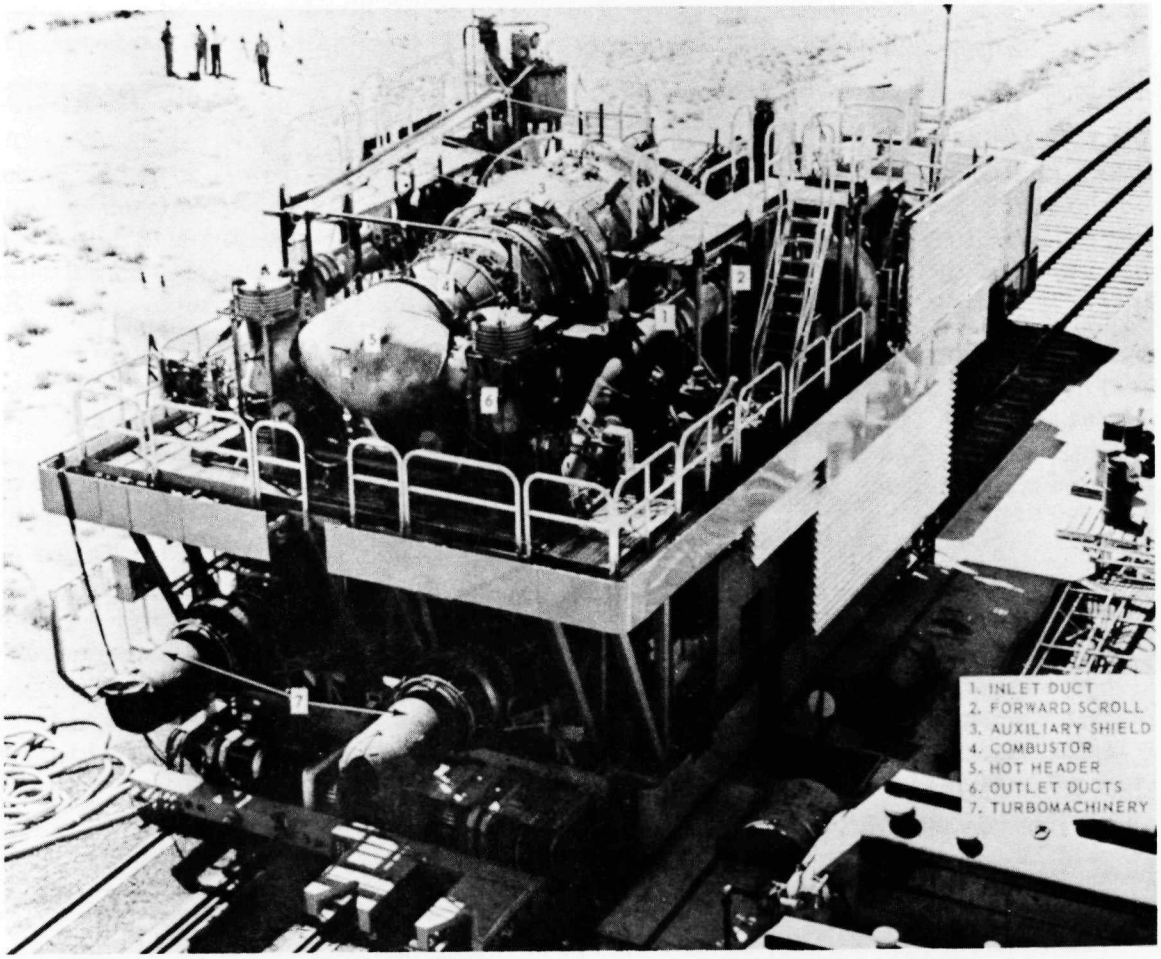

Fig. 2.2 – HTRE No. 3 test assembly (Neg. U-2700-11)

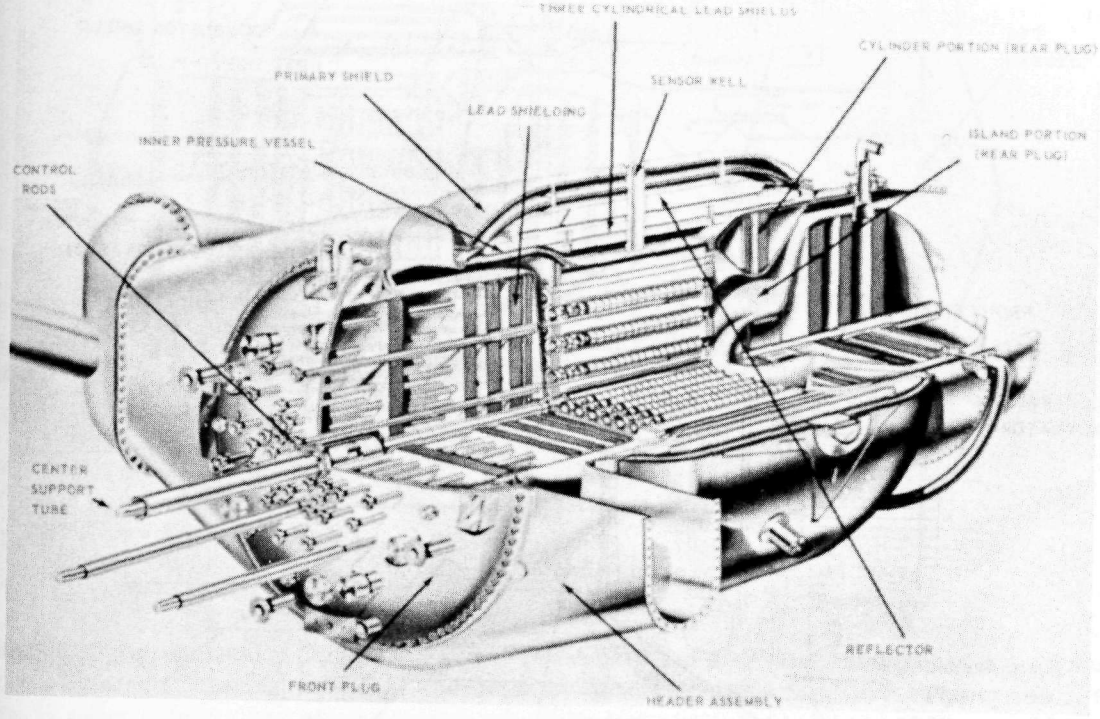

Fig. 2.3 – HTRE No. 3 reactor shield assembly (artist's concept)

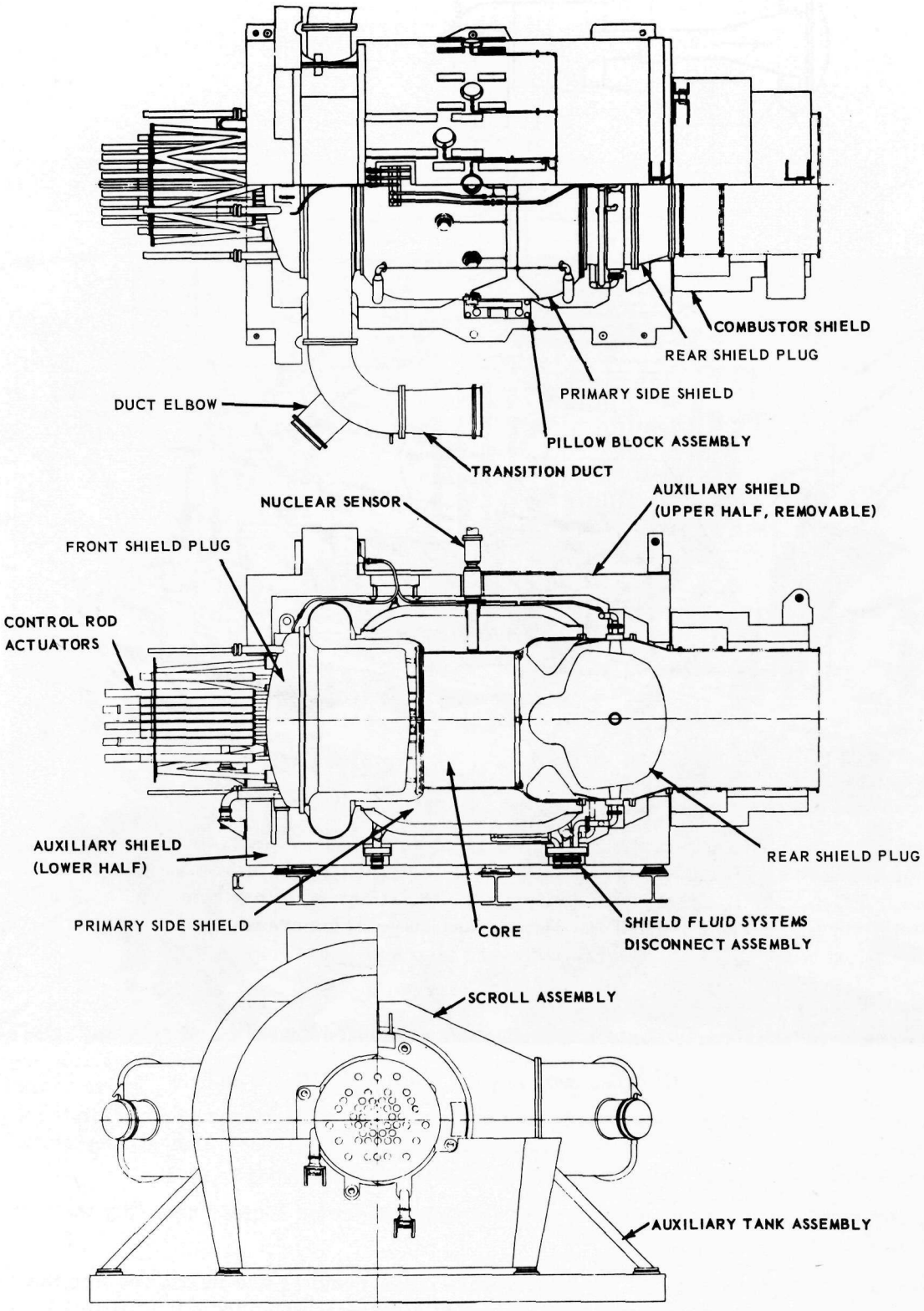

Fig. 2.4 – HTRE No. 3 reactor shield assembly (side and section views)

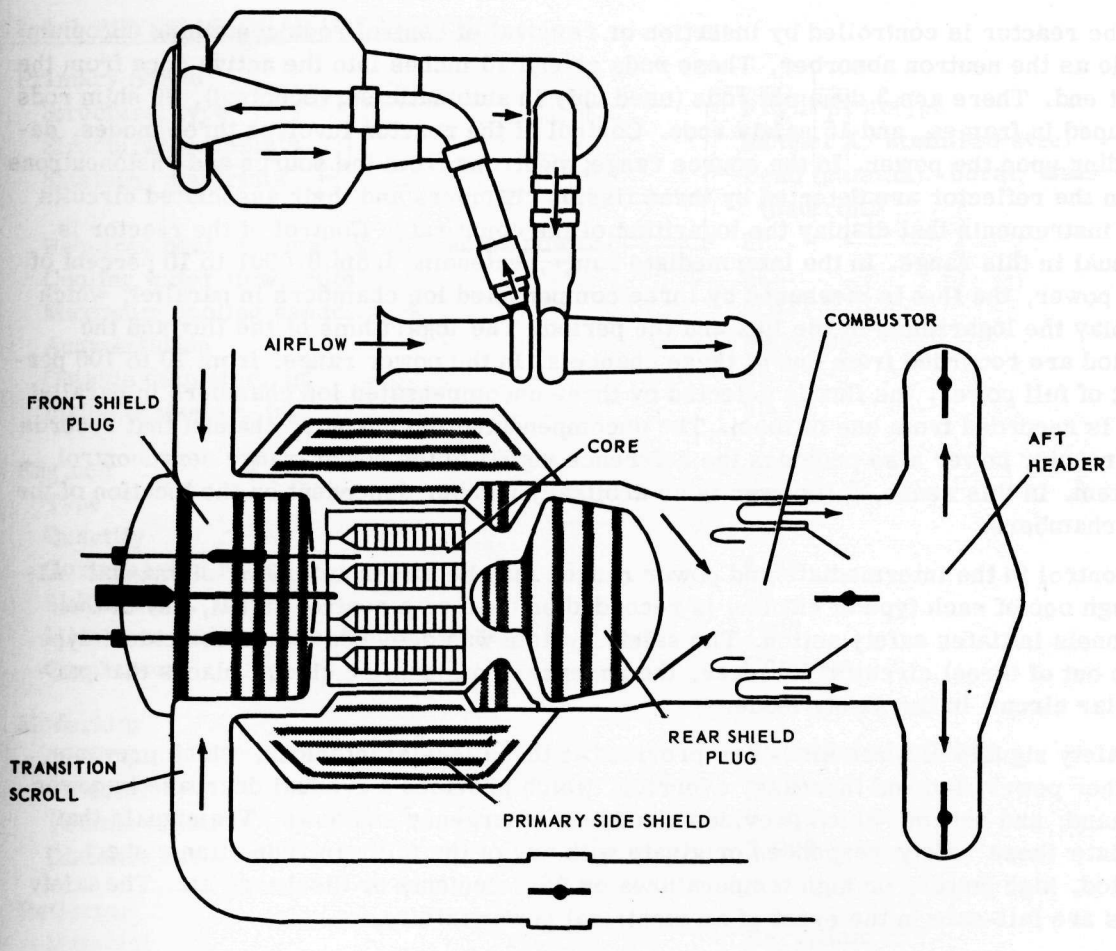

Fig. 2.5 – D102A airflow cycle

the engine is automatically controlled at any point between 800° and 1600°F, with an accuracy of ±1 percent, during chemical operation by controlling the fuel flow. The speed of the engine is independently and automatically controlled at any point between 5500 and 7950 rpm, with an accuracy of ±0.5 percent, by the opening and closing of the nozzle. Manual methods of controlling the fuel flow and nozzle area are also provided.

2.3.6 REACTOR CONTROL

The power plant is started on chemical fuel with compressor air passing through the cold reactor. Then, with the engine speed and turbine inlet temperature controls set at a predetermined level, the reactor is started and its power increased. When T_4 starts to increase because of the addition of nuclear heat, the chemical fuel valve closes to maintain the T_4 at the predetermined level. As reactor power increases, the fuel valve closes completely. Engine speed is held approximately constant throughout the transfer cycle.

During HTRE No. 3 tests, starting of the turbojet engine on nuclear heat only was demonstrated.

Reactor fuel element and exit air temperature measurements are integrated into the overall control. The flux system automatically controls reactor power from 0.0001 to 100 percent of full power, with the range from 10 to 100 percent of full power controlled within an accuracy of ±1 percent of full power. The temperature system automatically controls T_4 from 1000° to 1600°F ±10°.

The reactor is controlled by insertion or removal of control rods containing europium oxide as the neutron absorber. These rods extend 20 inches into the active core from the inlet end. There are 3 dynamic rods (used only in automatic servocontrol), 30 shim rods grouped in frames, and 15 safety rods. Control of the reactor involves three modes, depending upon the power. In the source range, neutrons from the source and photoneutrons from the reflector are detected by three fission chambers and their associated circuits and instruments that display the logarithm of the count rate. Control of the reactor is manual in this range. In the intermediate range, extending from 0.0001 to 10 percent of full power, the flux is measured by three compensated ion chambers in parallel, which display the logarithms of the flux and the period. The logarithms of the flux and the period are recorded from one of these channels. In the power range, from 10 to 100 percent of full power, the flux is detected by three uncompensated ion chambers in parallel and is recorded from one of them. The uncompensated ion chamber channel that records the reactor power also provides the reference signal to the power-range servocontrol system. In this sense, full power is an arbitrary number dependent on the location of the ion chambers.

Control in the intermediate and power ranges may be either automatic or manual. Although one of each type of channel is recorded or used as a control signal, any of the channels initiates safety action. The safety system was designed to use coincident-type (two out of three) circuits; however, the absence of a signal or circuit places that particular circuit in the safety mode.

Safety signals of three kinds are provided at three levels: interlock, which prevents further power-demand increase; override, which provides a gradual decrease in power demand; and scram, which provides a sudden, emergency shutdown. The signals that initiate these safety responses originate with any of the following conditions: short period, high power, or high temperatures on fuel elements or discharge air. The safety rods are fail-safe in the event of an electrical power failure.

A scram action is entirely independent of the control system. Scram normally is initiated only after the lesser safety actions - interlock, which prevents shim rods from withdrawing, and override, which reduces power demand - have failed to correct a safety violation. A scram signal releases the latching current of all safety rods, which are spring-loaded, and allows them to drive in. To insure shutdown at a maximum rate, a followup action fully inserts the dynamic rods and drives all shim rods in at their maximum speed.

2.3.7 TURBOMACHINERY

The turbomachinery in HTRE No. 3 consists of two X39-5 engines (modified General Electric J47 engines). The combustion section of the engine was removed and replaced by a compressor discharge scroll, an external chemical combustion chamber, and ducting to the turbine inlet annulus. Component arrangement and the airflow pattern are shown in Figure 2.5.

The reduction of compressor airflow to match the new requirements for the turbine, and the installation of a new engine-control system, were other major changes.

2.4 SPECIFICATIONS AND DESIGN DATA

The following is a list of general physical, aerothermal, and nuclear characteristics of HTRE No. 3 with the X39-5 engines. Data are based on Idaho Standard Day operating conditions.

2.4.1 PHYSICAL CHARACTERISTICS

Primary Shield	
Structural type	Flight prototype
Structural materials	Inconel X, stainless steel
Shielding materials	Lead (gamma), boral, water (neutron)
Required heat removal, % of reactor power	2†
Cooling water flow, gpm	612
Maximum cooling capacity, %	2.5‡
Augmentation	Mercury
Outside diameter, in.	97.5
Inside diameter, in.	58.0
Engines	
Type	X39-5
Quantity	2
Compression ratio	4.95
SLS airflow, lb/sec	75
Maximum turbine inlet temperature, ^{o}F	1600
Combustor	Common
Moderator	
Material	Hydrided zirconium
Cladding	None
Volume fraction	0.358
Distance across flats, in.	3.923
Reflector	
Material	Beryllium
Outside diameter, in.	57.0
Configuration	Hexagonal shapes
Cooling configuration	7 holes per segment
Fuel Elements	
Material (structural)	80Ni - 20Cr
Number of identical stages per cartridge	19
Control Rods	
Material (poison)	Europium oxide
Density, g/cm^3	3.0
Type and quantity - dynamic	3
- shim	30
- safety	15
Core, General	
Structural material	Inconel X
Over-all length, in.	43.5
Active length, in.	30.7
Over-all diameter, in.	57.0
Nominal diameter, in.	51.0

†Found to be 4 percent during IET tests.
‡Figure is for X211 operation at sea-level-static conditions.

As-Built Component Weights, lb

	Dry	Water Added	Mercury Added
Dolly	87,000	*	*
Superstructure	35,300	*	*
Auxiliary shield	85,100	103,800	*
Primary side shield	51,000	54,200	106,900
Front shield plug	20,600	26,000	*
Rear shield plug	20,000	22,000	*
Reactor	14,600	*	*
Scroll assembly (20-in. ducts)	6,600	*	*
Chemical fuel combustor	1,700	*	*
Shield for combustor	21,100	22,000	*
Cold ducting assembly (engines)	5,800	*	*
Hot header and duct assembly	8,000	*	*
X39-5 engines (2)	10,600	*	*
Shield liquid system	13,400	17,400	19,500
Shield liquid vent system	500	*	*
Aftercooling system	25,900	*	*
Fuel system	400	*	*
Lubrication system	600	*	*
Fire-extinguisher system	800	*	*
Electrical system (including trays, panels, boxes, and instrumentation)	12,000	*	*
Actuators, powerpack, and control rods	3,500	*	*
Service air systems	500	*	*
Walkways installation	21,600	*	*
External structures assembly	5,000	*	*
Total Weight	451,600	485,800	539,600

*Weight not affected by augmentation.

Requirements for Mechanical Design of Components

The inlet scroll, front shield plug, primary shield, structural part of the core, reflector, and rear shield plug were designed to meet the following operating conditions with two X211 engines:

Flow, lb/sec	850
Inlet pressure, psia	175
Inlet temperature, °F	700
Pressure drop across core, psi	35
Discharge pressure, psia	140
Discharge temperature, °F	1600
Structural metal operating temperature, °F	1000
Air-passage hydrostatic-test pressure, psig	225
Reactor power, mw	175

The fuel elements, moderator, combustor, header, piping, and engine were designed to meet the following operating conditions with two X39 engines:

Total flow, lb/sec	150
Pressure, psia	75

Compressor discharge temperature, °F	450
Turbine inlet temperature, °F	1600
Structural metal operating temperature, °F	1000
Reactor power, mw	35

2.4.2 AEROTHERMAL CHARACTERISTICS*

Power, mw	32.3
Compressor airflow (2 engines), lb/sec	126.0
Compressor discharge pressure, psia	53.5
Compressor discharge temperature, °F	385
Core inlet pressure, psia	50.3
Pressure ratio across core	0.91
Pressure ratio, turbine to compressor	0.79
Reactor airflow, lb/sec	122.3
Fuel cartridge airflow, lb/sec	102.8
Moderator airflow, lb/sec	17.4
Reflector airflow, lb/sec	1.2
Control rod airflow, lb/sec	0.9
Core discharge air temperature, °F	1330
Fuel cartridge discharge air temperature, °F	1425
Moderator discharge air temperature, °F	925
Reflector discharge air temperature, °F	850
Control rod discharge air temperature, °F	810
Reactor discharge pressure, psia	46.0
Turbine inlet pressure, psia	42.2
Turbine inlet temperature, °F	1310
Fuel-element maximum design temperature, °F	1850 ± 100
Maximum design dynamic head within fuel element, psi	6.0
Maximum operating dynamic head within fuel element, psi	0.8
Moderator maximum operating temperature, °F	1200
Control rod maximum temperature, °F	1650

2.4.3 NUCLEAR CHARACTERISTICS

Expected final cold, clean excess reactivity, % Δk/k	+2.7 ± 1.0
Expected maximum effect of temperature increase from 68° to 1000°F, % Δk/k	1.0
Worth of control rods, shadowed, % Δk/k	
30 shim rods	4.44 ± 0.40
3 dynamic rods	0.43 ± 0.05
15 safety rods	1.99 ± 0.20
Xenon equilibrium expected at 35 mw, % Δk/k	1.33
Power distribution	
Heat generated in core to air, %	98.0
Heat generated in shield to water, %	2.0†

Detailed specifications appear in references 1, 2, and 3.

*In X39-5 engines only at sea-level-static conditions.
†Actual 4 percent.

2.5 ASSEMBLY OF HTRE NO. 3 AT ITS

The dolly bed, Figure 2. 6, consists of a durable platform mounted on four railroad tracks. The superstructure with a few components assembled is shown in Figure 2. 7. Components were assembled onto the dolly as shown in Figure 2. 1. Figure 2. 8 shows the final assembly of the X39-5 engine ready for assembly onto the dolly.

Most of the assembly and repair work was to have been done manually at ITS. The core assembly, the front shield plug, and the pressure shell of the primary shield were maintained remotely because of radiation. The front shield plug, core, front scroll, and pressure shell were manufactured to match a master jig. If a new component should be required in the future, it can be manufactured to the jig and remotely assembled to the used parts. The master jig was used to check the component parts at ITS. Figure 2. 9 shows the front shield plug and core assembled in the male portion of the master jig.

Jigs and fixtures are provided for remote assembly and disassembly of components that become radioactive. Figure 2. 10 shows the primary shield in the erection stand and the core and front shield plug in the core removal fixture. The final assembly of these components was performed with remote handling equipment.

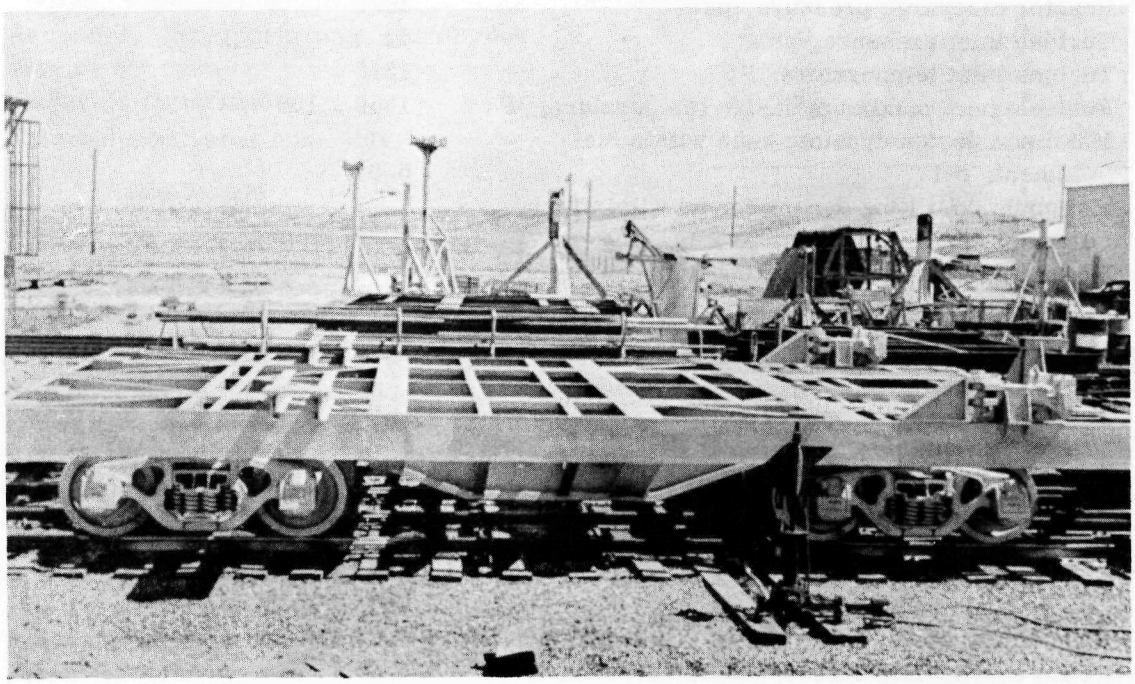

Fig. 2.6 – HTRE No. 3 dolly (U1278-2)

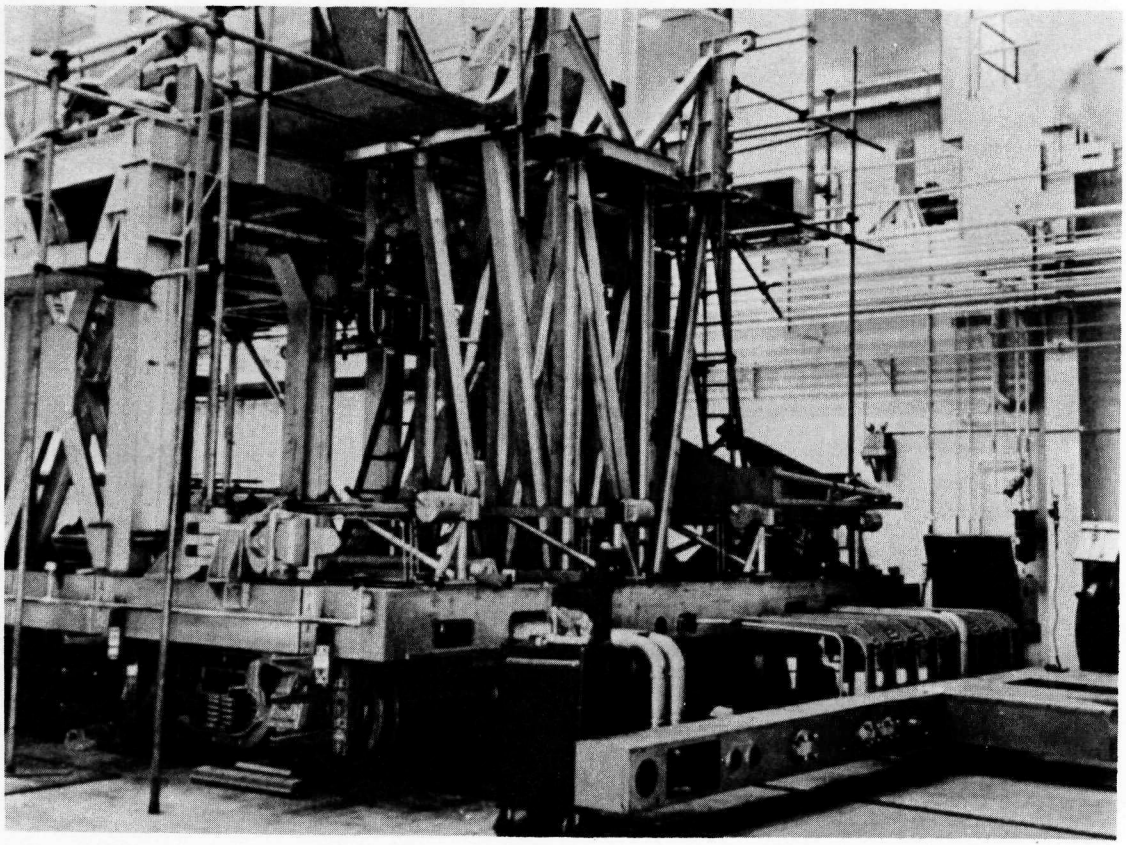

Fig. 2.7 – HTRE No. 3 dolly during superstructure assembly (C13560)

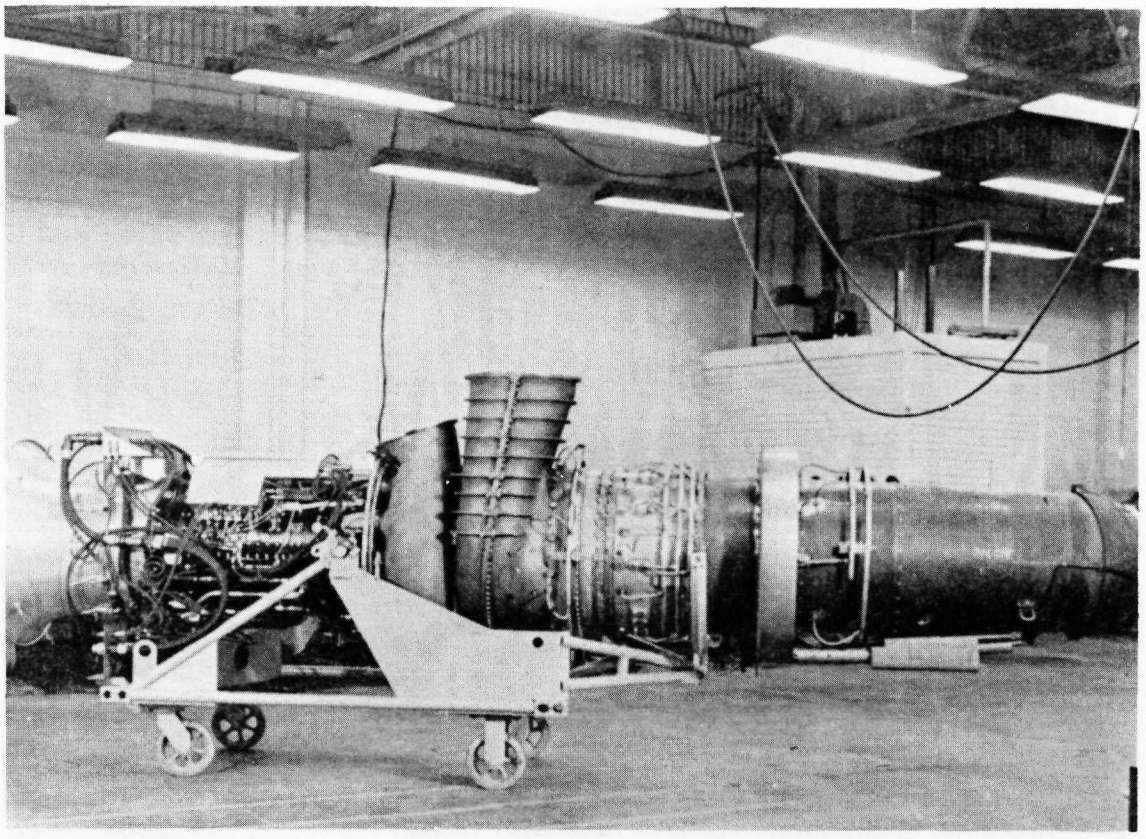

Fig. 2.8 – X39-5 engine ready for assembly onto HTRE No. 3 dolly (U35156C)

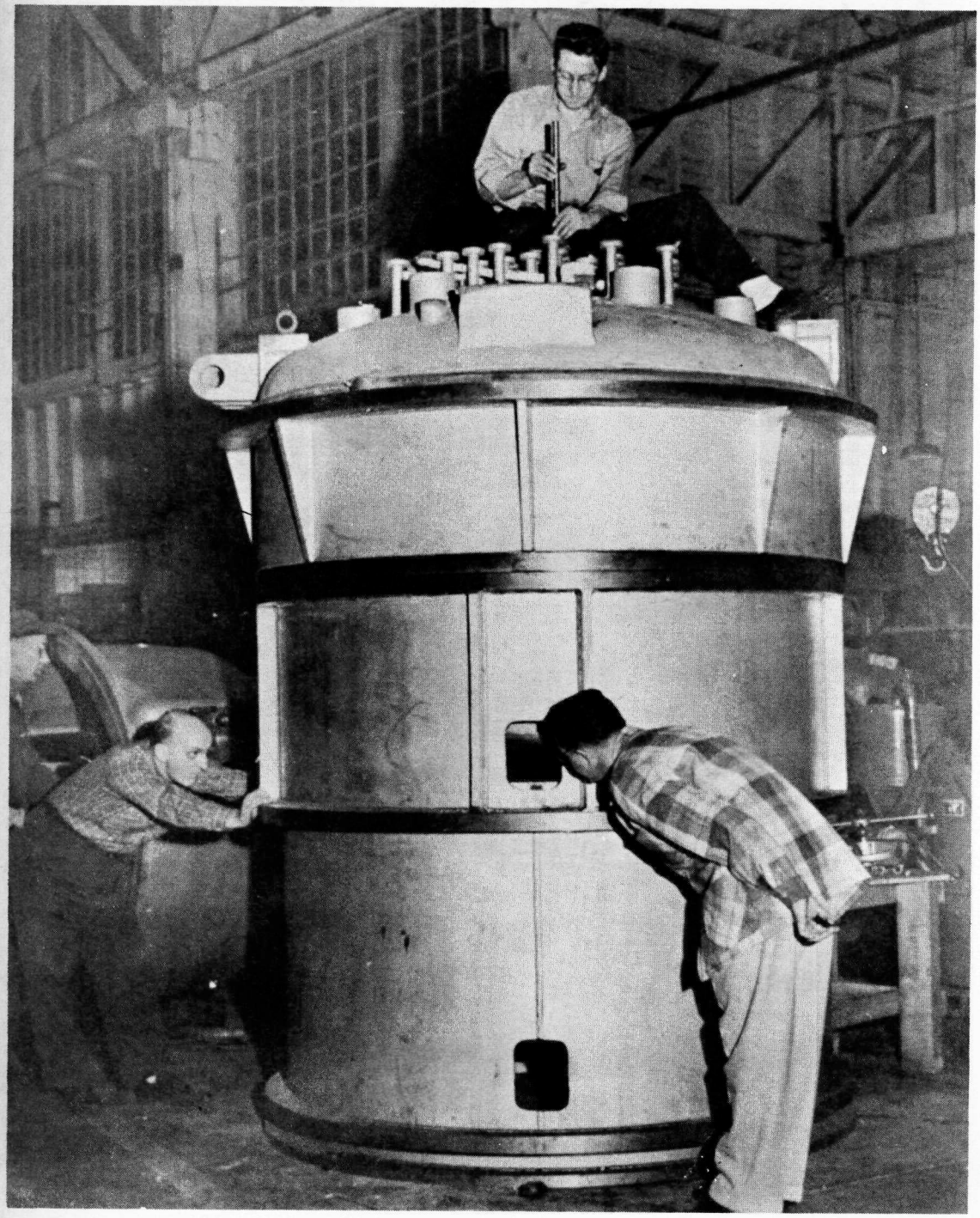

Fig. 2.9 – Master jig containing core and front shield plug (783-1)

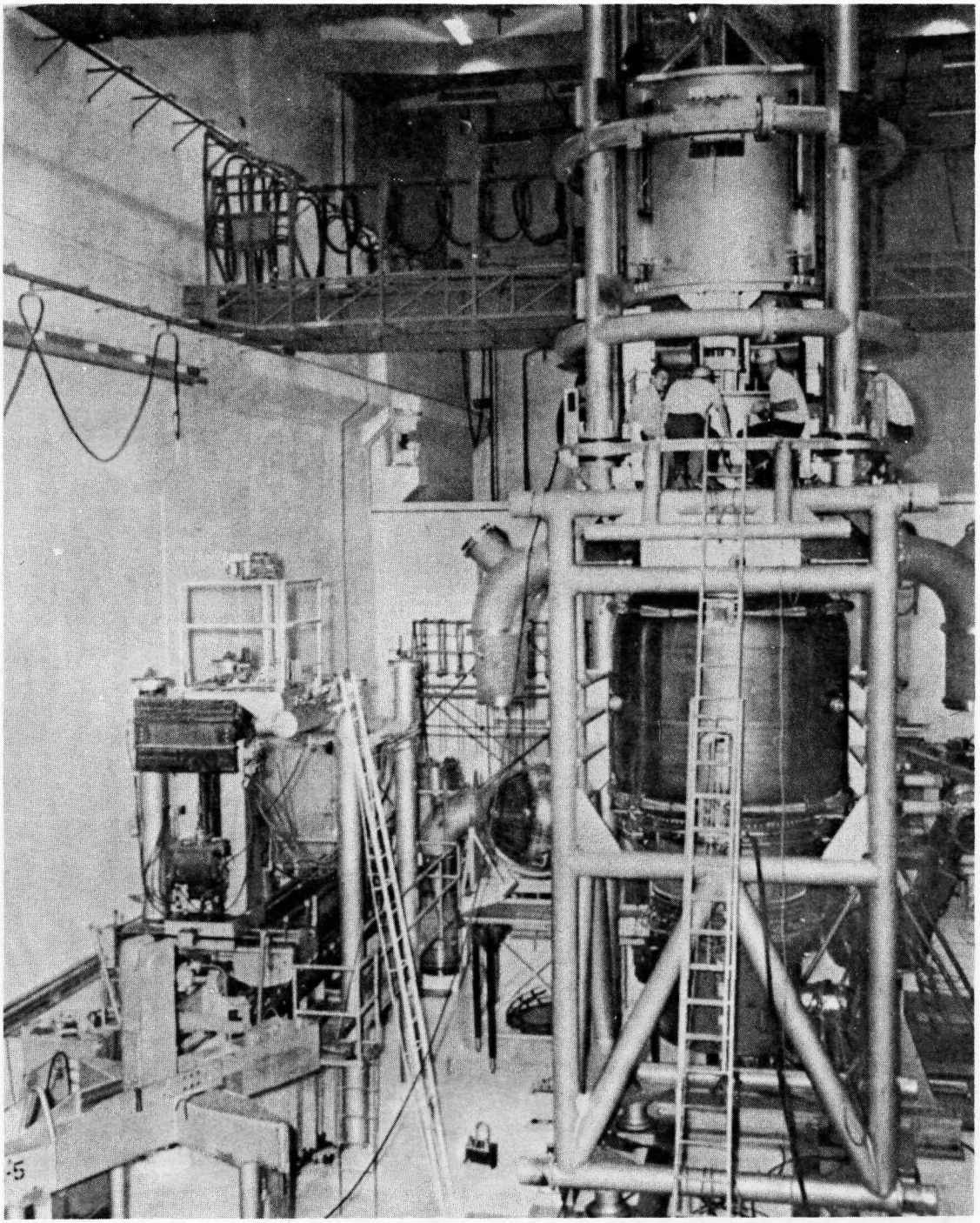

Fig. 2.10 – Core removal fixture on top of erection stand (C-14022)

2.6 REFERENCES

1. Schoenberger, T. W., "102 Project Data Book - 6th Issue," GE-ANPD, DC 58-2-118, February 14, 1958.
2. Schoenberger, T. W., "102 Project Data Book - 7th Issue," GE-ANPD, DC 58-10-159, October 22, 1958.
3. Schoenberger, T. W., "102 Project Data Book - 8th Issue," GE-ANPD, DC 59-8-22, July 29, 1959.

3. HTRE NO. 3 TESTS

Testing of the D102A reactor for the HTRE No. 3 power plant started in April 1958 and was completed on December 19, 1960. Essentially all test objectives were met. Approximately 126 hours of operation under "on-test" conditions were accumulated, 65 of which were continuous. In addition to the first known demonstration of a full-nuclear start of a nuclear powered turbojet, the HTRE No. 3 power plant was also the first successful operation of two turbojet engines from a single nuclear heat source. The reactor was found to be in excellent condition at the conclusion of all tests. Presumably, many additional hours of operation at full power could have been achieved.

3.1 SUMMARY

3.1.1 FIRST LOW POWER TEST (LPT 2)

The initial low-power testing of the D102A reactor was conducted at the Low Power Test (LPT) Facility during the months of April, May, and June 1958. These tests were conducted to confirm design parameters and to provide basic nuclear data on the as-built system prior to high-temperature operation at the Initial Engine Test Facility (IET). The first series of tests included initial loading, reactivity measurements, power mapping, power profile alterations, and elevated-temperature power mapping. Essentially all test objectives were attained and the reactor was found to conform with the design parameters within the specified tolerances. The reactor poison configuration was altered four times during this series to achieve a radial power profile calculated to be flat within ±7 percent across the core. The maximum fuel plate local-to-average core power scallop was 1.14.

3.1.2 INITIAL POWER TEST (IET No. 13)

On September 8, 1958, the HTRE No. 3 was moved to the IET and preparations were started for Phase 1 testing. Since this test series was to provide a shakedown of the power plant, the first operations were a series of tests of the service air system to insure that it would supply adequate cooling to various components on the engines and dolly during reactor operation. Next, the increase in reactivity resulting from draining the front, side, and rear shield compartments was determined. The increase was found to be 3 percent $\Delta k/k$. The worth of shim rod 243 was measured as 0.156 percent $\Delta k/k$ as compared to 0.161 percent $\Delta k/k$ at LPT. The excess reactivity was determined to be 1.88 percent $\Delta k/k$ with the shield full of water.

Reactor power was determined by exposing foils attached to dummy control rods placed in the active core. Foil count rate was corrected to saturated activity and then compared to the LPT dummy rod foil activity for which the core power had been determined by a detailed flux map. A correlation was also obtained in order to calibrate the nuclear instruments.

The moderator and control rod heating rates were measured with Bragg-Gray ion chambers. The maximum heating rate measured was 0.0755 watts/g-mw.

Rather extensive gamma ray measurements were made external to the shield by suspending pocket dosimeters and film packs from the test cell ceiling. This system of measurement worked fairly well and showed a reproducibility within a range of 20 to 30 percent.

3.1.2.1 IET No. 13 Excursion

On November 18, 1958, a power excursion occurred,[1*] the result of the dynamic and shim rods being withdrawn by the control system under the influence of an erroneous reactor power indication. The false power indication was due to a high-series-resistance noise filter in the output of each ion chamber power supply. Another contributing factor was an improper voltage setting for these power supplies. The mechanism of reactor shutdown was partially self-initiated. It appears that a scram due to fuel element temperature indication (or due to melting of the thermocouple lead wires) and a reactivity loss of about 2 percent caused by melting and collapse of fuel rings occurred within a very short time interval and that both contributed to reactor shutdown. Following this excursion, the power plant was returned to the Hot Shop for inspection and replacement of the fuel elements.

It is significant to note that in the event of a complete failure of the safety systems, the reactor would probably have shut itself down due to the local redistribution of the fuel prior to any major damage to the reactor components other than the fuel elements.

3.1.3 SECOND LOW POWER TEST (LPT 2-2)

On June 4, 1959, the rebuilt core, designated the D102A2(A), was returned to the Low Power Test Facility. Further tests were undertaken for purposes of comparison with the original D102A core, further evaluation of system parameters, and additional refinements to the power profile. This series was completed in one month and included initial loading, reactivity measurements, power mapping, and additional power profile alterations. The rebuilt core was found to duplicate the original core within all the specified tolerances. One additional alteration in the poison configuration was performed to further improve the power profile.

3.1.4 PHASE I TESTING (IET No. 16)

The power plant was delivered to the IET on July 28, 1959, to begin final checkout prior to testing. Criticality was achieved on September 8, 1959. Testing then continued until the test program was completed on October 9, 1959.

Rod worth, excess reactivity, reactor power, and moderator and control rod heating rates were determined. The results of these measurements compare closely with those obtained during IET No. 13. The reactor was brought to a power of 10 megawatts in the normal stepwise fashion for a new or modified reactor at IET. A complete data scan was taken at each step. Power was limited to 10 megawatts at this stage pending alterations to the effluent monitoring system.

After the completion of the power tests, the power plant was returned to the Hot Shop. Analysis of the data obtained during the power steps verified that the performance of the reactor and its controls met or exceeded the expected performance. Inspection of the power plant revealed no defects of any consequence. Some heat damage to the insulation was discovered in the aft header and the ducting downstream of the reactor.

3.1.5 ENDURANCE RUN (IET No. 18)

The HTRE No. 3 dolly was transported to the IET on December 14, 1959, for endurance testing. First engine operations were accomplished on December 22, 1959; the reactor was made critical on December 23, 1959. After successful completion of all test requirements, the test dolly was returned to the Hot Shop on February 8, 1960. During

*Superscripts refer to the reference lists that appear at the end of each section.

the test period, the reactor was operated for 166.5 hours at more than 1 percent of design power. One run of 126 hours at full power was operated almost continuously.

As customary, one of the first operations conducted on the power plant was a check of the chemical engine performance to establish temperature, pressure, and flow rates over the range of engine speed and nozzle position. The reactor was then brought to full nuclear power in steps: 13.0, 16.2, 20.2, 24.0, 31.3, and 31.8 megawatts. A data scan was taken at each power step and, at the 13.0-, 16.2-, and 20.2-megawatt steps, engine speed runs were also made to determine the part-chemical, part-nuclear characteristics of the power plant prior to transfer to full nuclear power. Subsequently, six transfers to full nuclear power were made.

Because this was the first time that two turbojet engines had been run from a single nuclear power source, system variables were examined over a range of engine speeds and reactor powers, including the lowest possible engine speed to examine some of the system characteristics associated with a full nuclear start.

Other tests conducted during IET No. 18 were afterheat evaluation, auxiliary blower starting characteristics, reactivity measurement, nuclear versus thermodynamic power calibration, fast neutron mapping, and effluent radiation monitoring.

The most significant accomplishment of this test series was the accumulation of 126.1 hours of operation at "on test" conditions, defined as a mixed core exit air temperature of $1330^{\circ} \pm 20^{\circ}$F. The total endurance hours were accrued in units of 1.4, 29.0, 5.5, 25.4, and 64.9 hours of continuous operation. The reactor performance exceeded expectations during the endurance runs. Some difficulties were experienced such as boiling in the rear shield plug and failure of some of the insulation in the aft header.

During all of IET No. 18, thermocouples on fuel elements 340 and 460 recorded relatively high temperatures of 1880°F and 1915°F, respectively. These fuel elements were removed from the core after the power plant had been returned to the Hot Shop. Visual inspection revealed that the fuel elements were in excellent condition. Detailed radiochemical analysis verified that power generation was within the predicted range.

3.1.6 FULL NUCLEAR START AND ELEVATED PERFORMANCE DEMONSTRATION (IET No. 25)

The purposes of test series IET No. 25 were to demonstrate the capabilities of the fuel elements above design temperatures and to confirm that the power plant could achieve a full nuclear start as predicted. The reactor went critical on November 14, 1960, and the test program was completed on December 19, 1960.

The first test conducted, an increasing power test, compared system parameters with those obtained on previous tests. After a series of runs to obtain steady-state performance maps of reactor and engine parameters, a full nuclear start was made on December 12, 1960. Subsequently, two more nuclear starts were made. The reactor control system, together with a proficient operator, was able to compensate for the transients involved in the nuclear start. The procedure for the start, which was established with the aid of an analog computer, worked very well, and the system behavior closely duplicated that anticipated by the analog studies.

Following the second nuclear start, the reactor was maintained at a power of approximately 29 megawatts for one hour and then was manually scrammed. One aftercooling blower supplied a flow of 8.6 pounds of cooling air per second to the reactor after scram. Transient recordings were made of selected system parameters. All temperatures started to decline after the scram and, in all cases, the trend established during the first 10 minutes following the scram was maintained for the remainder of the recording period of one hour.

A total of 20.3 hours of elevated performance was accumulated at the conclusion of the full nuclear starts. Elevated performance was defined as full nuclear operation with a peak fuel element temperature of 2030°F ± 20°F. All reactor variables remained quite stable during this run and the reactor operation was completely normal. At the termination of this operation, the instrumentation indicated that the reactor was fully capable of continued operation.

Additional low airflow tests were run during this test series to supplement the low-flow data taken in previous tests.

3.1.7 SUMMARY OF HTRE NO. 3 PERFORMANCE

Table 3.1 presents a summary of performance data accumulated during the HTRE No. 3 tests. When the fuel was unloaded in May 1961, HTRE No. 3 was found to be in excellent condition.

TABLE 3.1

HTRE NO. 3 PERFORMANCE DATA

	Endurance Run		Elevated Performance
Reactor power to air, mw	32.4		34.2
Reactor airflow, lb/sec	123		125.6
Mixed core discharge air temperature, °F	1330		1370
Compressor discharge temperature, °F	385		376
Compressor discharge pressure, psia	53.5		
	Predicted	Measured	Measured
Maximum temperature, °F			
Fuel element	1880	1900	1986 2050 (extrapolated)
Moderator	1175	1120	1160
Reflector	1100	1030	1010[a]
Discharge air from fuel	1640	1640	1720
Average temperature, °F			
Discharge air from moderator	968	880	900[a]
Discharge air from reflector	955	940	845[a]
Discharge air from control rods	805	480	485[a]

[a]Thermal equilibrium not reached.

3.2 REACTOR PERFORMANCE

3.2.1 LOW POWER TESTS

A summary of the results of the two low-power tests are presented together for comparative purposes. Complete information concerning these tests is contained in the final data reports.[2, 3, 4]

3.2.1.1 Test Equipment

To conduct the low power testing, the D102 core was placed in a horizontal stainless steel tank that closely duplicated the dimensions and nuclear properties of the prototype pressure vessel. An electric heater and blower were connected to the test tank so that high-temperature (1000°F) air could be blown through the core to perform the elevated-temperature portions of the experiment. The prototype front shield plug was used as were the prototype actuators. In the first series of tests (LPT 2) the rear shield plug was not duplicated, but a rear shield plug mockup was used in the second series (LPT 2-2).

3.2.1.2 Summary of Results

Initial Loading, Excess Reactivity, and Control System Worths - Core loading was accomplished using standard inverse multiplication procedures. During LPT 2, the reactor achieved criticality when 136 of the 150 elements were loaded, while for LPT 2-2, criticality was achieved with 146 elements. The difference may be attributed to the increased poison inventory in the second configuration. Excess reactivity values are summarized in Table 3.2. Note the close comparison between the excess reactivity values of the original core and the rebuilt core of the same configuration (1.37% Δk/k versus 1.33% Δk/k).

Control system reactivity values are tabulated in Table 3.3.

TABLE 3.2

LOW-POWER TEST EXCESS REACTIVITY

Configuration	Excess Reactivity,[a] % Δk/k
LPT 2 configuration with 13 poison liners	3.19
LPT 2 configuration with 84 poison liners	1.37
LPT 2-2 configuration with 13 poison liners	1.33
LPT 2-2 configuration with 78 poison liners (rear shield plug mockup in place)	1.88

[a]At 70°F.

TABLE 3.3

CONTROL SYSTEM REACTIVITY VALUES

	LPT 2 Rod Worth,[a] % Δk/k	LPT 2-2 Rod Worth,[b] % Δk/k
Shim	5.35	5.14
Dynamic	0.42	0.45
Safety	1.85	1.90
Total	7.62	7.48

[a]Temperature coefficient of reactivity = + (0.7 ± 0.3) x 10^{-3}% Δk/k/°F.
[b]Plug worth = + 0.57% Δk/k.

To compare the two cores, six typical rods were calibrated with the cores in the same configuration (no rear shield plug, 84 poison liners). The results are tabulated in Table 3.4. The relative effectiveness curves for the rods of both cores were found to be essentially identical; however, addition of the rear shield plug mockup in LPT 2-2 altered the shape of the curve so that the relative worth was decreased towards the withdrawn position.

Power Mapping and Power Profile Alteration - Power mapping was performed using catcher-foil techniques and mockup cartridges during cold mapping, and stainless-clad uranium-filled tapes for the elevated-temperature mapping. During LPT 2, power mapping was performed to locate and correct for unwanted power peaks in both the gross and fine distribution. Of primary concern was the establishment of a flat radial power

TABLE 3.4

ROD WORTH COMPARISON

Rod No.	Rod Worths, % Δk/k LPT 2	LPT 2-2
110	0.185	0.189
610	0.185	0.189
621	0.174	0.185
620	0.170	0.180
521	0.175	0.183
631	0.167	0.171

distribution with a minimum of power scalloping around individual elements. During the second series of tests, LPT 2-2, power mapping was performed to compare cores and to further reduce power peaks. Alterations to the power profile and reduction of scalloping was accomplished by selectively poisoning portions of the core by the use of poison liners. For the purposes of the low-power test, the poison liners consisted of stainless steel tubes that were fitted over the fuel elements. Boron steel strips of varying thickness, width, and angular orientation were spot-welded to the outer surface of these tubes to achieve the particular poison arrangement. During these tests no alterations to the longitudinal power profile were performed.

The extent to which the radial profile of the core was improved by four basic poison liner changes during the initial test, LPT 2, is illustrated in Figure 3.1. Figure 3.2 illustrates the radial power profile obtained using uranium-filled tapes at 700°F.

Figure 3.3 illustrates the manner in which local circumferential power peaks were reduced by alteration or addition of poison.

Table 3.5 tabulates and compares local-to-average power ratios for the original and rebuilt cores. Also shown in this table are normalized cell powers for both tests. Again, good correlation between the original and the rebuilt core is evident.

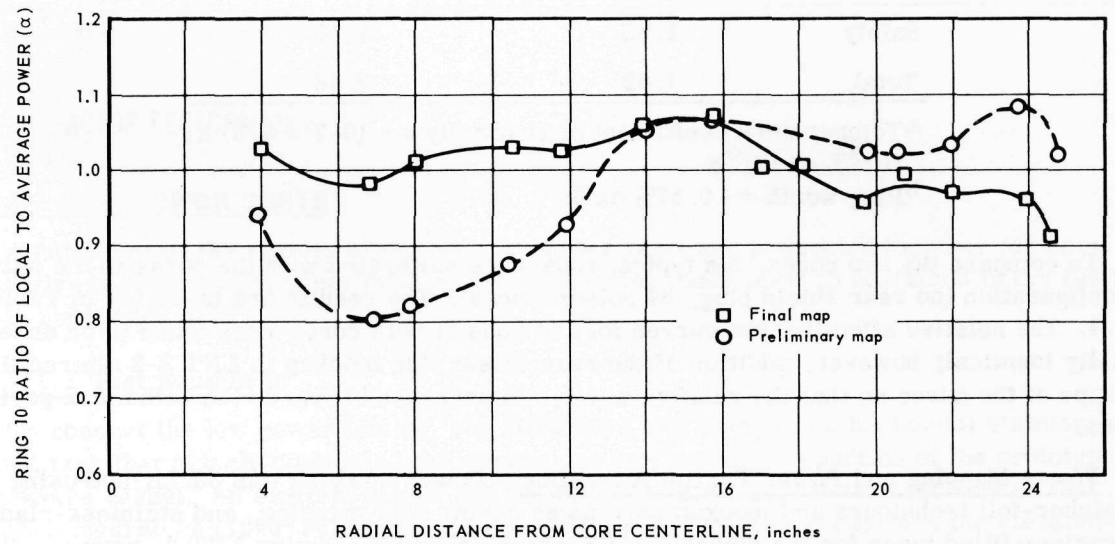

Fig. 3.1 – Comparison of gross radial power distributions from preliminary and final power maps (LPT 2)

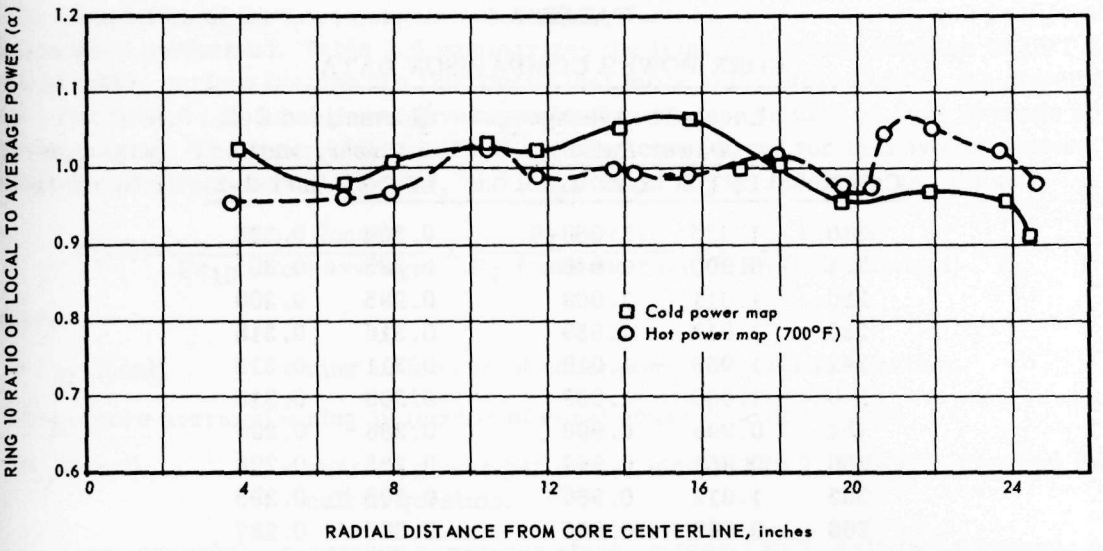

Fig. 3.2 – Comparison of gross radial power distributions for hot and cold power maps

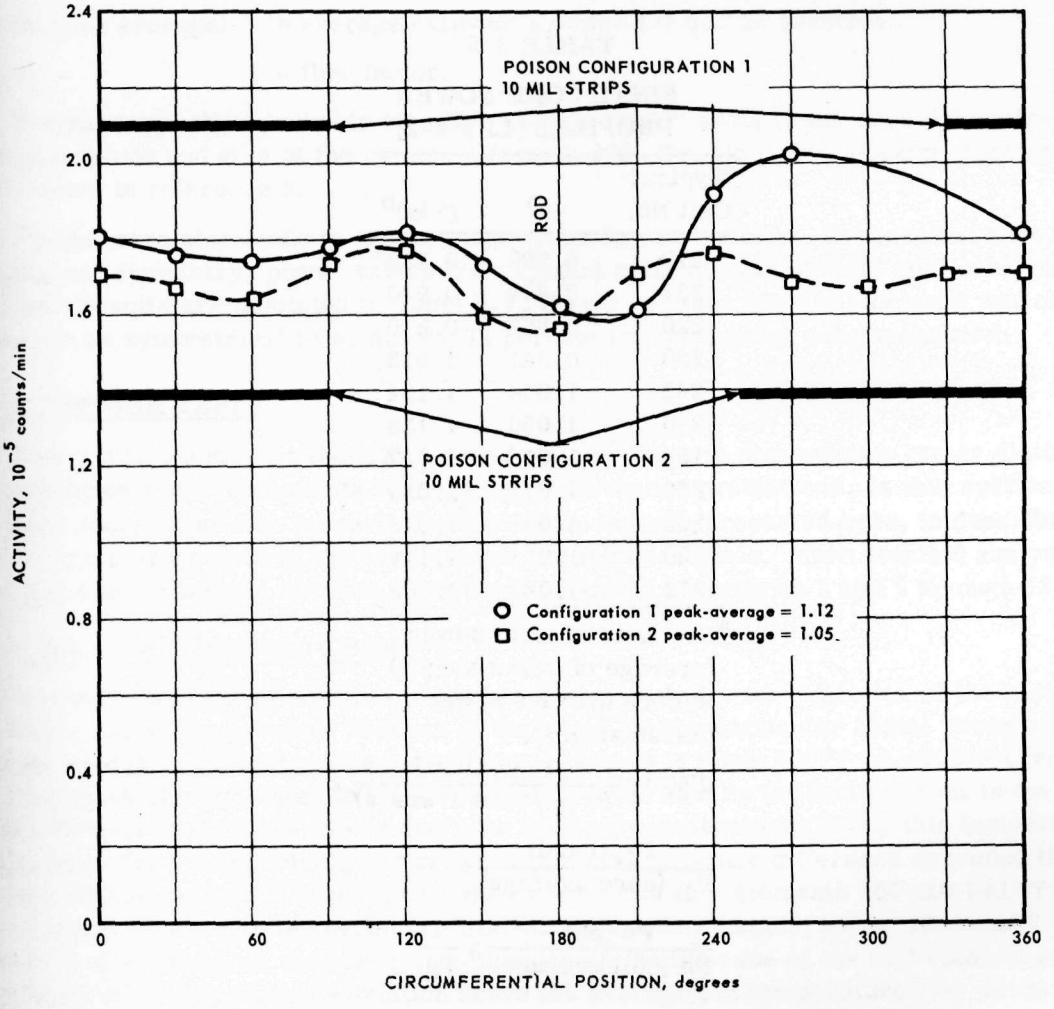

Fig. 3.3 – Comparison of circumferential power distribution with two different poison liner configurations (Cell 241, Cylinder 4)

TABLE 3.5

CORE POWER COMPARISON DATA

Cell No.	Local-To-Average Power Ratio		Normalized Cell Power, watt	
	LPT 2	LPT 2-2	LPT 2	LPT 2-2
210	1.035	1.068	0.304	0.326
221	0.900	1.040	0.285	0.305
220	1.011	1.009	0.285	0.300
230	1.019	1.039	0.316	0.318
242	1.036	1.018	0.311	0.315
240	1.060	1.059	0.309	0.316
154	0.998	0.998	0.286	0.296
250	0.951	0.967	0.285	0.298
262	1.012	0.966	0.205	0.295
260	0.992	0.956	0.295	0.287
272	0.906	0.883	0.265	0.266

TABLE 3.6

FINAL CORE POWER PROFILES (LPT 2-2)

Typical Cell No.	α[a]	$\Gamma(4a)$[b]
210	0.909	0.988
221	0.874	0.940
220	0.865	0.870
230	0.941	1.013
242	1.054	1.134
240	1.050	1.138
154	1.018	1.057
250	1.011	1.024
262	1.028	1.048
260	1.071	1.114
272	1.041	1.006

[a] α = ratio of local power (average of seven stages) to core average power (seven stages).

[b] $$\Gamma 4(a) = \frac{Pr_{10}\ (\text{local})}{Pr_{10}\ (\text{core average})} \times \frac{P_L\ (\text{local})}{P_L\ (\text{core average})} \times \frac{Pn\ (pk)}{Pn\ (\text{cell average})} \times \frac{1}{F_k}$$

On completion of the core comparison studies, further power mapping and profile alterations were performed. Table 3.6 summarizes the final core power profiles in LPT 2-2. In this table, various factors are introduced that more completely identify the power profile. The first, α, is local power (average of seven stages) divided by core average power (seven stages). The second factor, $\Gamma(4a)$ includes corrections for relative cell power, relative cell circumferential power, and longitudinal power and flow, as follows:

$$\Gamma(4a) = \frac{Pr_{10}\ (\text{local})}{Pr_{10}\ (\text{core average})} \times \frac{P_L\ (\text{local})}{P_L\ (\text{core average})} \times \frac{Pn\ (\text{pk})}{Pn\ (\text{cell average})} - \times \frac{1}{F_k}$$

where:

Pr_{10} (local) = ring 10 (center of core) power for cell in question.

Pr_{10} (core average) = ring 10 (center of core) power (core average).

P_L (local) = average power per stage, stages 1 to 7, cylinder 4 (outer) for cell in question.

P_L (core average) = average power per stage, stages 1 to 7, cylinder 4 (outer), entire core.

Pn (pk) = cylinder 4 peak circumferential power for cell in question.

Pn (cell average) = average cylinder 4 power for cell in question.

F_k = flow factor.

The values of $\Gamma(4a)$ serve to identify "hot" or "cold" spots in the core determined by the magnitude and sign of the variation from 1.000. Details of the mockup cartridge are presented in reference 3.

Studies were also made to examine the symmetry of the core. Because the core has hexagonal symmetry, power values from typical cells in symmetrical sections were compared. Results are tabulated in Table 3.7. Based on these results, the core was calculated to be symmetrical to within ±1.74 percent for the typical cells measured.

3.2.2 POWER TESTS

The primary goals for the HTRE No. 3 reactor were to demonstrate power-flattening capabilities and to obtain data for making performance predictions. In this section of the report some of the data taken during the power tests is presented here, to describe, in general, the performance of the core against the intended goals. More detailed analyses will be found in subsequent sections of this report and in references 1 and 5 through 13.

3.2.2.1 Core Temperature Profiles

The core radial temperatures plotted in Figure 3.4 give an indication of the over-all relative radial temperature flatness of the core. On the particular radial shown, the maximum spread in the fuel element plate temperatures is about 120°F or ±3.5 percent. A figure more closely linked to the actual power generated by the fuel element is the difference between plate temperature and core inlet air temperature. Using this temperature difference for a comparison, the greatest plate temperature difference exceeded the average difference by 5.2 percent with the exception of fuel elements 460 and 340. For these two fuel elements this temperature difference exceeded the average by 12.2 and 9.8 percent, respectively, on the lower side of stage 15. In the case of the fuel element exit air, the maximum temperature deviation above the average air temperature rise across the core was 10 percent except for fuel elements 340 and 460, which deviated 14 and 11.3 percent, respectively.

TABLE 3.7

SYMMETRY STUDY OF FINAL CONFIGURATION
(LPT 2-2)

Cell No.	Deviation From Average Power, %	RMS Deviation From Average For Typical Cells, %
210	-1.15	±0.80
410	+1.15	
141	+0.42	±0.39
541	-0.42	
140	-0.77	±0.88
240	-0.96	
340	-0.48	
440	+1.74	
540	+0.48	
640	-0.29	
142	+0.38	±0.80
342	-1.33	
542	+1.04	
242	+0.38	±1.06
442	-1.63	
642	+1.24	
160	+0.57	±0.96
260	-1.04	
360	+0.85	
460	+0.38	
560	-1.70	
660	-0.94	

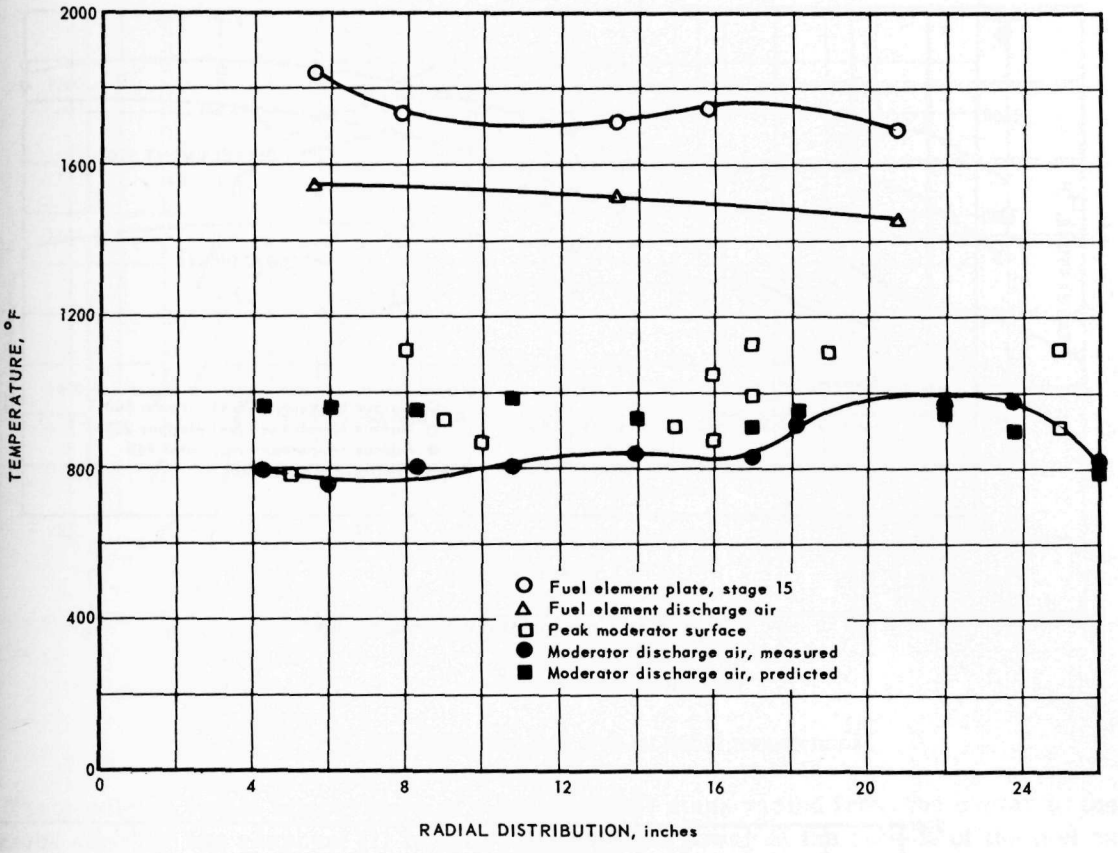

Fig. 3.4 – Core radial temperatures

Fuel cartridge longitudinal temperature measurements compared with predictions are shown in Figure 3.5; actual temperatures were higher than predicted in the rear half of the cartridges and lower in the front half. This indicated that the cartridge power is distributed more to the rear than predicted. Power measurements of fuel element punchings confirmed this. The slight error in this prediction was probably due to an insufficient rear shield plug mockup in the original low-power mapping.

Fuel element circumferential temperatures and power generation ratios are shown in Figure 3.6. All data are for stage 15, ring 11. The temperatures shown are for fuel element 140; for the curve shown, the maximum deviation of the measured fuel element temperature from the average temperature of stage 15, ring 11 is 1.4 percent as compared to 11 percent for all of the temperatures of stage 15, ring 11 (of fuel element 460).

The measured individual fuel element radial temperature distributions shown in Figure 3.7 agree quite well with the predictions. This confirms the individual fuel element radial power distributions used in the predictions and also confirms the power mapping performed during LPT 2-2. The main difference between measurements and predictions seems to be in predicting the fuel element temperatures of rings 11 and 12, as evidenced by the data shown for fuel element 465. The ring temperatures were predicted to decrease from ring 10 to ring 12. Generally this was true, as the average surface temperatures for stage 15, rings 10, 11, and 12 were 1762°, 1726°, and 1698°F, respectively. There were these exceptions to the rule, however, where the temperature of ring 12 was higher than the temperature of ring 10.

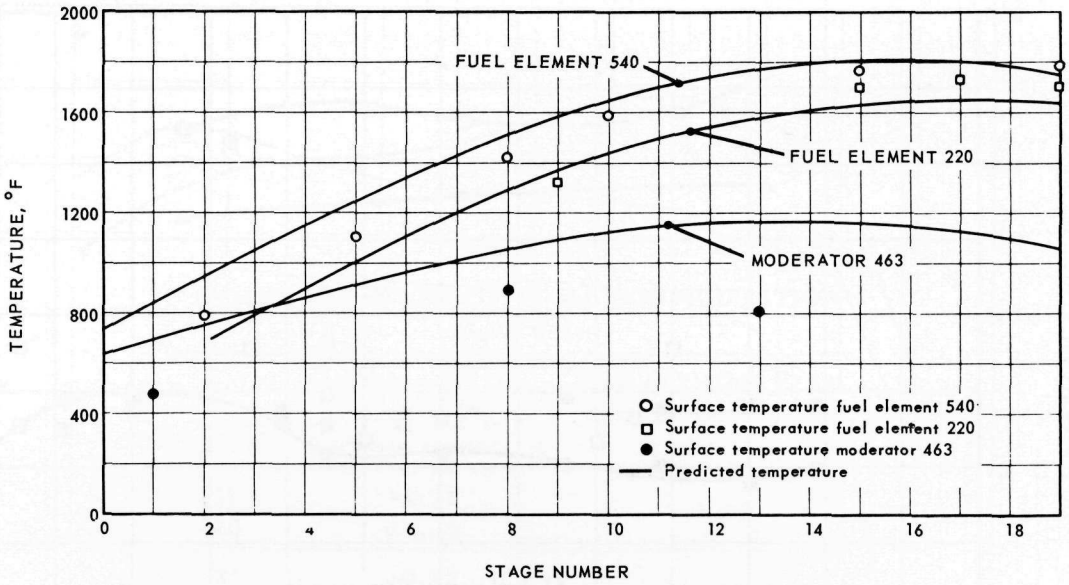

Fig. 3.5 – Core longitudinal temperatures

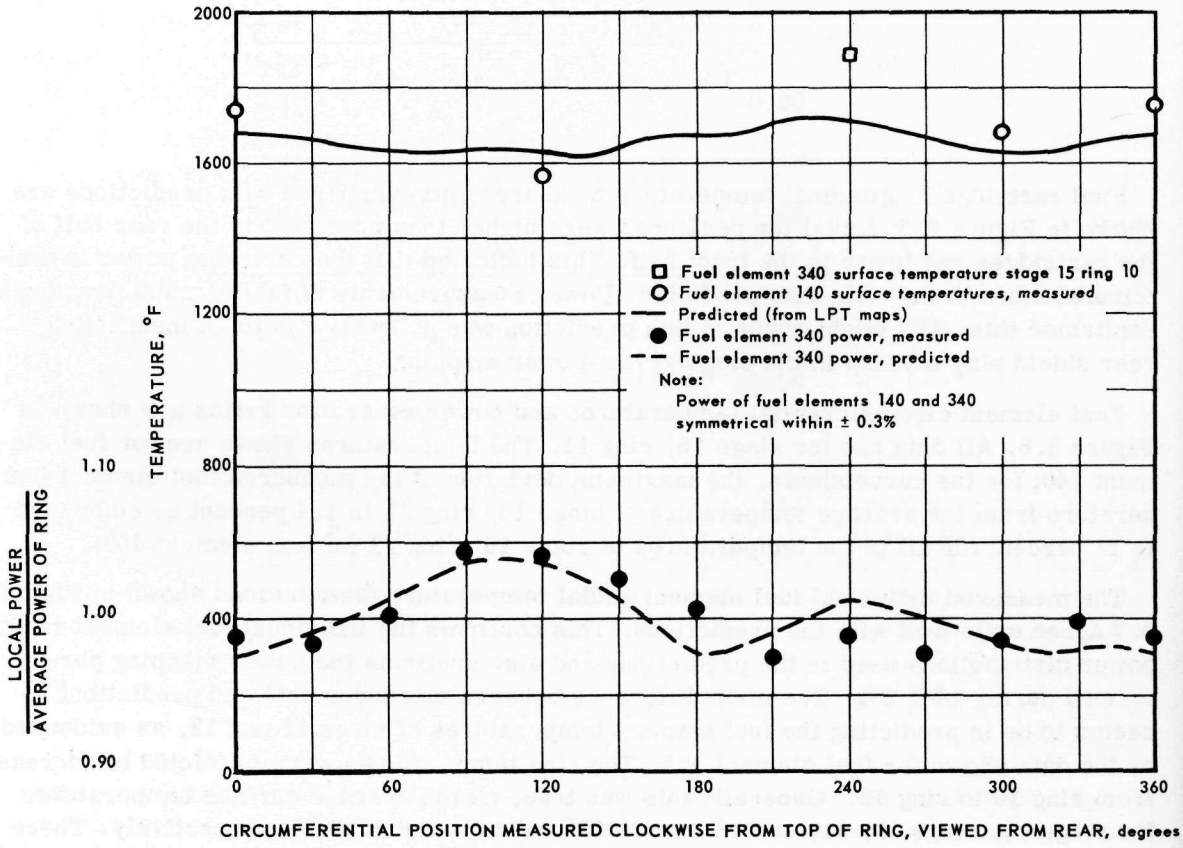

Fig. 3.6 – Circumferential temperatures and power

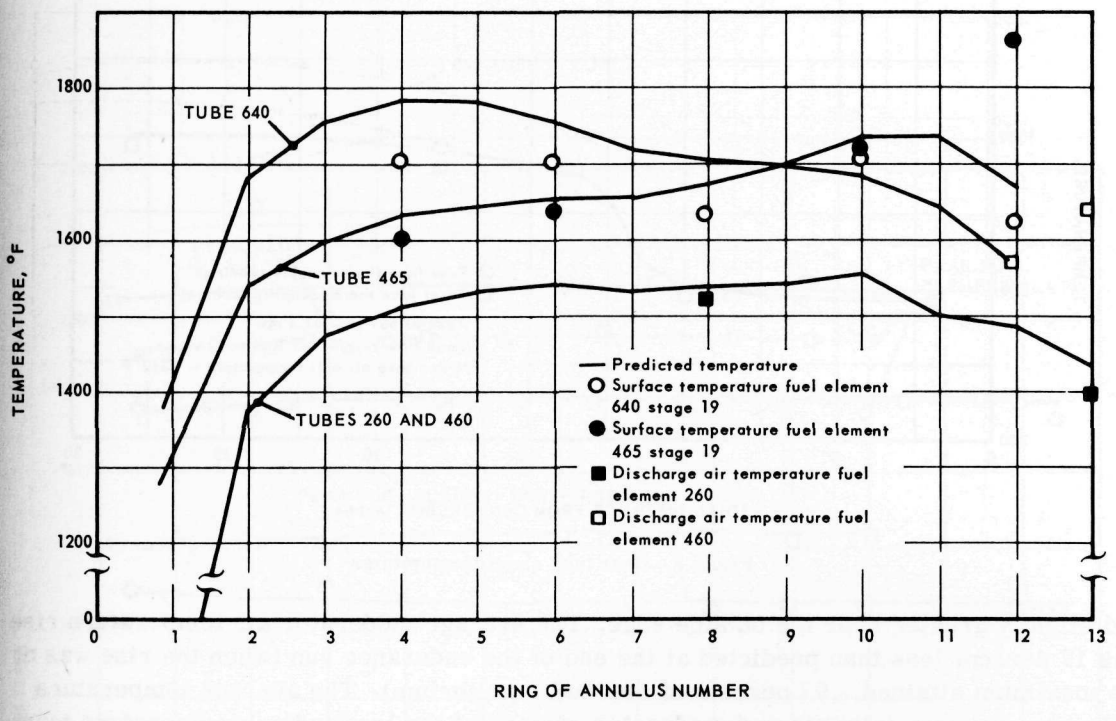

Fig. 3.7 – Individual fuel element radial temperatures

The predicted radial temperature of a fuel element stage varied from the center to the outside edge for two reasons: (1) intentionally reduced power at the outside of the fuel cartridge because of space variations between the cartridge and the insulation liner, and (2) lower-than-average power in the center of the cartridge because of manufacturing limitations at that time.

At the end of the 125 hours of endurance testing, fuel elements 340 and 460 were removed from the reactor for inspection and for determination of the relative power flatness of the stages. To make this determination, punchings taken from the fuel rings were gamma-scanned to determine their gamma decay power. Since the decay power is proportional to the generated power, accurate ratios of local power to the ring average power could be worked out. A curve of this ratio for fuel element 340 is shown in Figure 3.5. The predicted ratio agrees quite well with the measured; the maximum spread is less than 5 percent. The agreement between predicted and measured power ratios is equally good for fuel element 460.

In summary, the peak temperature rise (with only one exception) varied from the average by no more than ±8 percent in the maximum power area of the fuel element, i.e., the area between the inner and outer low-power sections. Although fuel elements 340 and 460 indicated the highest temperatures, visual inspection at the end of the endurance run showed no heat damage.

The variation of rear tube sheet temperatures with distance from the reactor centerline are shown in Figure 3.8. The step in the curve at about the 10-inch line did not seem to present a problem from the standpoint of thermal stress.

Variation of moderator discharge air temperature and moderator slab maximum temperatures with radial distance from the reactor centerline are also shown in Figure 3.4. The predictions shown are for the final orificing of the individual moderator slabs. The moderator air temperature rise was smaller than predicted near the center of the core

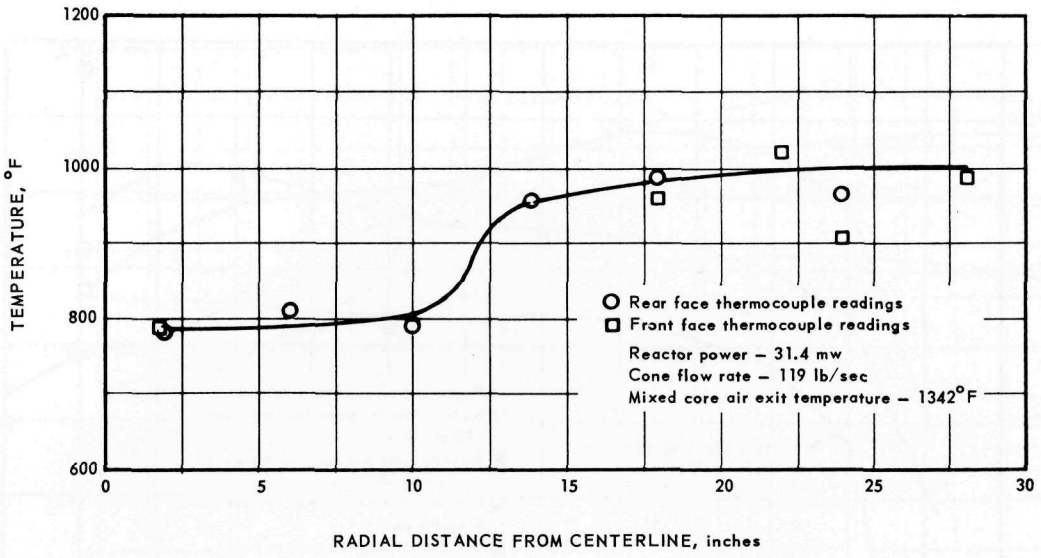

Fig. 3.8 – Rear tube sheet temperatures

and slightly greater near the outside edge. The average moderator air temperature rise was 12 percent less than predicted at the end of the endurance run (when the rise was at the maximum attained - 97 percent of thermal equilibrium). The average temperature difference between inlet air and moderator surface at the longitudinal temperature maximum was 27 percent less than predicted, or 24 percent if thermal equilibrium had been reached. This conservative deviation between the measured and calculated values is probably due to a greater-than-predicted convective heat transfer coefficient, a greater-than-calculated effective conduction between fuel and moderator support tube, and cooling airflow along unexpected paths. None of these explanations are sufficient in themselves, but collectively they could easily cause the observed deviations.

3.2.2.2 Core Parameter Variations During Endurance Testing

The fuel element and moderator temperature variations with operating time are shown in Figure 3.9. The peak fuel element plate and exit air temperatures remained fairly constant with time for the duration of both the endurance and the elevated-performance run. The moderator temperatures show a step decline and slow buildup each time the power plant was shut down and then brought back to power; this is due to the time required for the moderator to reach thermal equilibrium.

The core mixed-air temperatures are also shown in Figure 3.9. Again, the exit temperature was fairly stable and constant during both the endurance and the elevated-performance runs.

The weight flow and power-to-air curves for both the endurance and elevated-performance runs are shown in Figure 3.10. These curves show more changes than the other endurance curves because the weight flow and power to air had to be adjusted in order to hold constant the desired test parameters - core mixed-exit-air temperature and engine speed for the endurance run, and hottest extrapolated fuel element plate temperature and engine speed for the elevated-performance run.

Actually, detailed analyses showed some shifting of the relative power generation of the fuel elements during testing. This was expected because of the following effects:

1. A gross power shift from outer cells to inner cells as excess reactivity was used and control rods were withdrawn, occurring gradually during the test as a function of megawatt-hours.

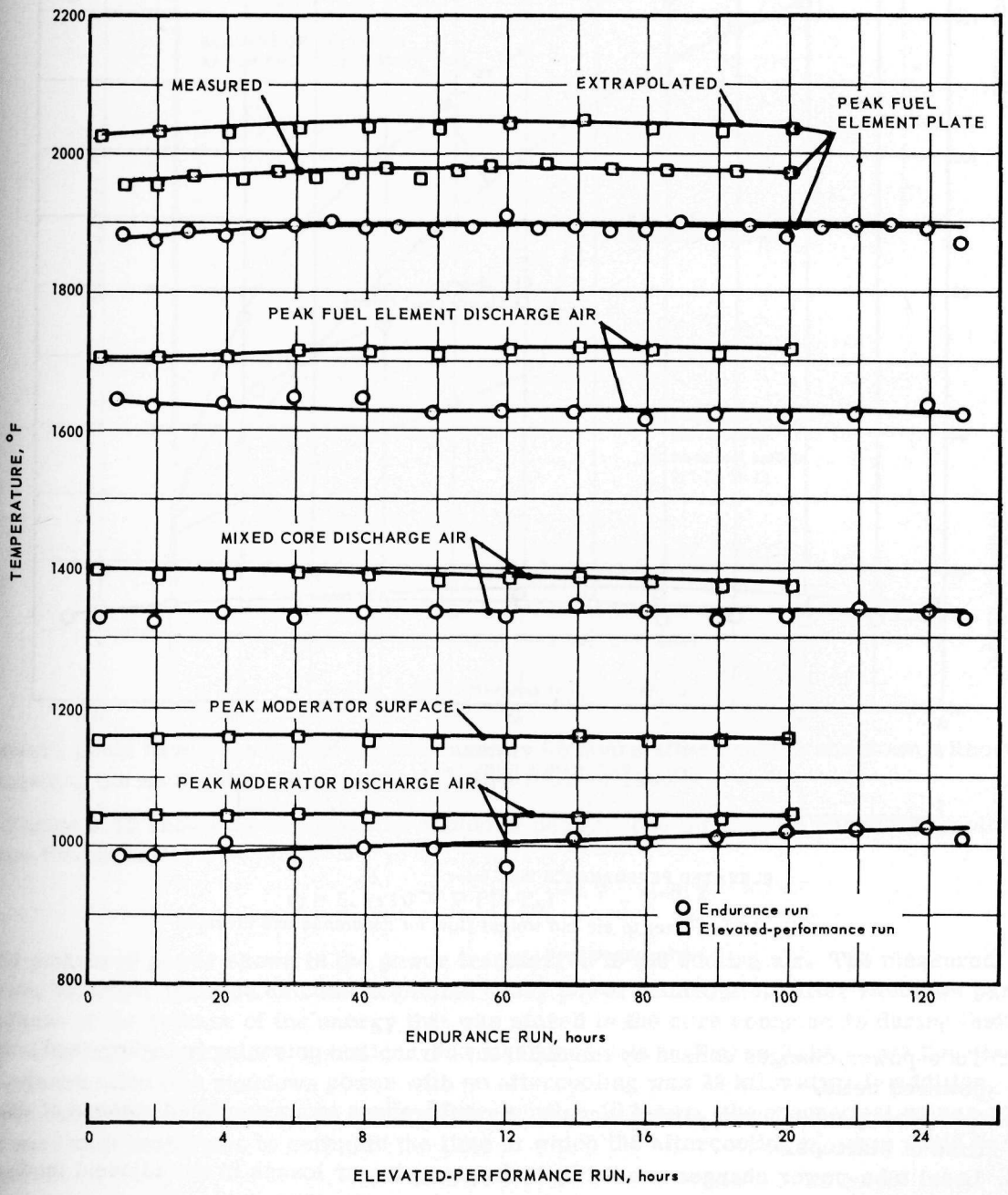

Fig. 3.9 – Core temperatures during endurance and elevated-performance runs

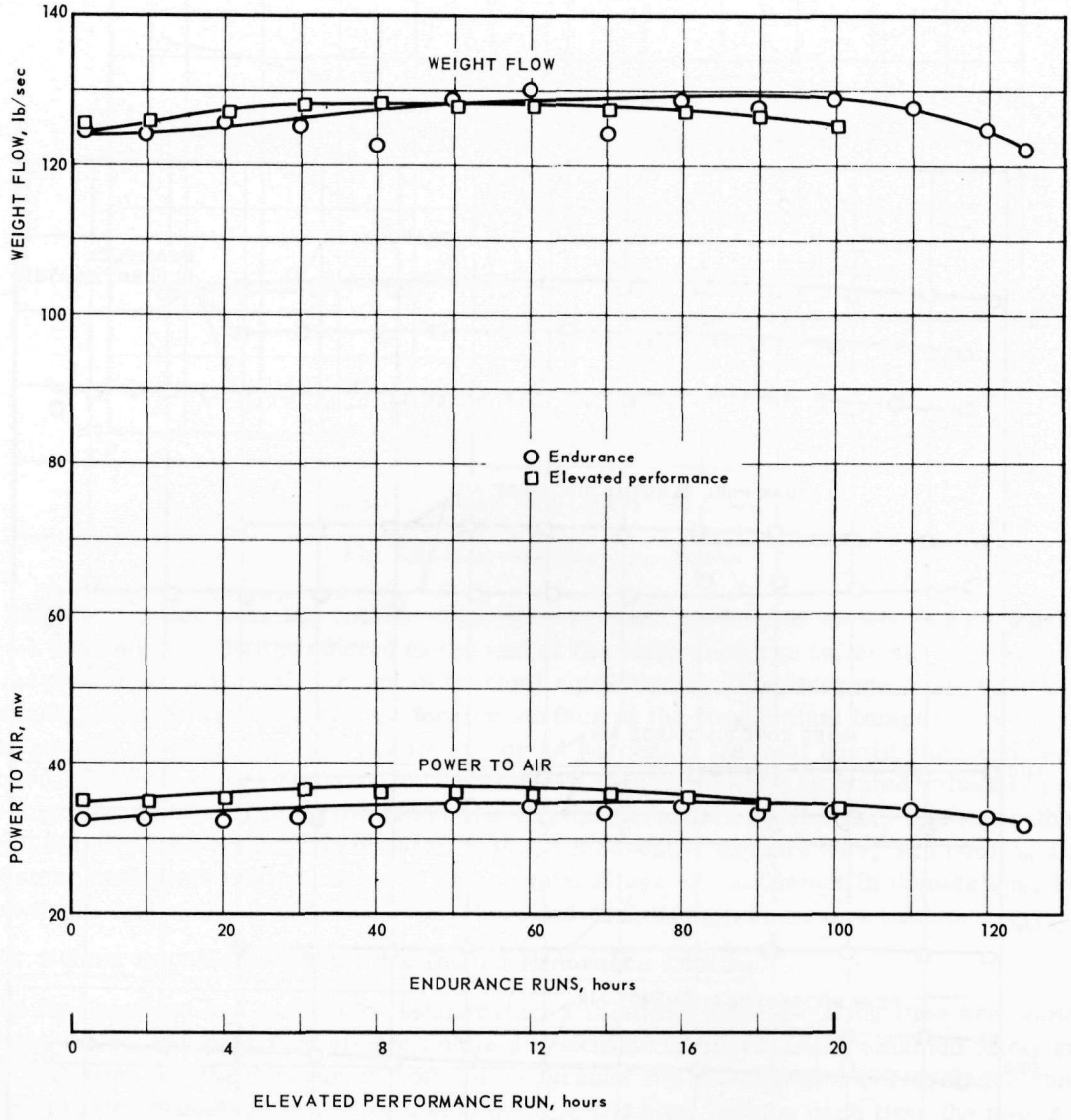

Fig. 3.10--Power to air and weight flow for endurance and elevated-performance runs

2. Tube-power changes caused by the different burnup and poisoning in higher- and lower-powered cells.
3. Temporary tube-power changes caused by differences in accumulated poisons at the time of startups.
4. Local tube-power changes caused by hydrogen gains or losses in the adjacent moderator.

3.2.2.3 Afterheat Evaluation

The core component heating rates caused by afterheat were measured after most of the power runs. These measurements were made by turning off the aftercooling blowers at specific times following a power run and then observing the temperature rise of reactor components as indicated by the thermocouples. Some of the measurements made after the endurance run of 65 hours are presented in Figure 3.11. Apparently the aftercooling

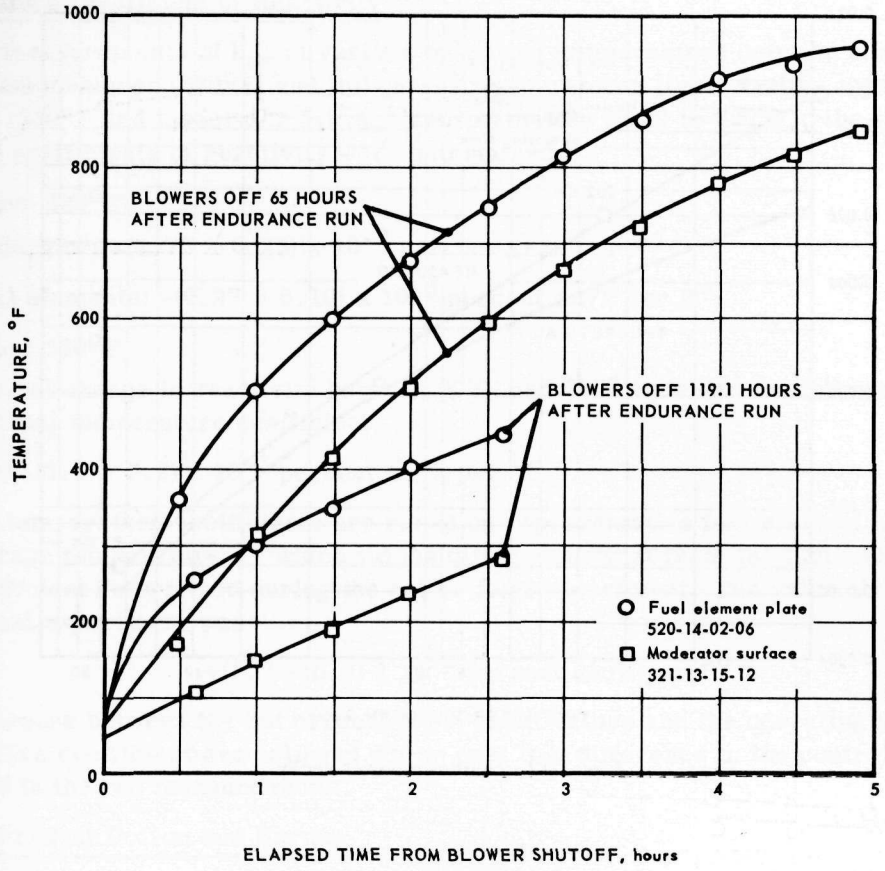

Fig. 3.11 – Afterheat temperature rise

blowers could have been turned off permanently 65 hours after reactor shutdown without exceeding the moderator surface-temperature limit of 1200°F.

Figure 3.12 shows the decay of the shutdown power. The theoretical curve was plotted from the equation*

$$Q = 5.9 \times 10^{-3} P \left(T-T_0\right)^{-0.2} - T^{-0.2}$$

The measured power shown is the power transferred to the cooling air. The measured power is larger than the calculated gamma decay power immediately after shutdown partly because of the release of the energy that was stored in the core components during their previous high-temperature operation. The measured data in Figure 3.12 shows that the maximum allowable shutdown power with no aftercooling was 22 kilowatts. In addition, since the theoretical curve was fairly accurate after 10 hours, the theoretical values could be used with confidence to estimate the time at which the aftercooling blowers could be shut off.

3.2.2.4 Reactivity Measurements

Clean k Excess Reactivity at Various Reactor Conditions

Measurements of k_{ex} were made during power operation by using a representative isothermal rod shape curve for a banked rod configuration and the value of the worth of the bank of rods at ambient temperature.[14] The worth of the control rods at ambient temper-

*Samuel Glasstone, "Principles of Nuclear Reactor Engineering," D. Van Nostrand Co., Princeton, New Jersey.

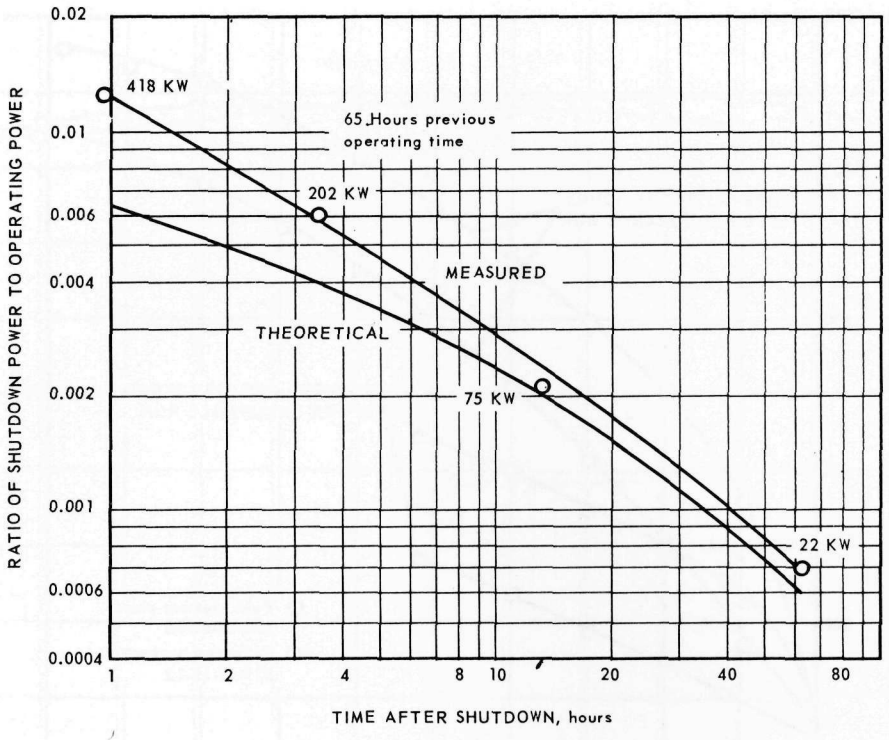

Fig. 3.12 – Shutdown power decay

ature was used in the absence of any conclusive experimental evidence of the effect of temperature on control rod worth in the HTRE No. 3. Hot critical experiments have indicated, however, that temperature increases up to 1000°F increase the rod worth as much as 25 percent in the case of control rod materials used in the HTRE No. 3. Evidence indicated that the temperature effect on rod worth is primarily a function of moderator temperature rather than fuel element temperature.

Table 3.8 presents the basic clean k_{ex} values under various operating conditions, as determined during IET No. 18. The uncertainty in the measurements averages ±0.02 percent Δk.

TABLE 3.8

CLEAN EXCESS REACTIVITY VALUES DURING IET NO. 18

		Excess Reactivity, % Δk
Ambient temperature - water shield coolant		1.82
Compressor discharge (320°F) - water		2.08
	- ethylene glycol	2.13
On test at 33.5 mw	- water	2.57
	- ethylene glycol	2.63

Temperature Coefficient of Reactivity

From measurements of k_{ex} at various operating temperatures between compressor discharge temperatures (320°F) and full-power temperatures (fuel average approximately equal to 1330°F and moderator average approximately equal to 750°F), the following temperature coefficients of reactivity were determined.

1. Above 320°F

   Moderator: $+(1.75 \pm 0.25) \times 10^{-3}$ percent $\Delta k/k$ per F^{o}

   Fuel elements: $-(0.27 \pm 0.10) \times 10^{-3}$ percent $\Delta k/k$ per F^{o}

2. Below 320°F

   The net change in reactivity between 60°F and 320°F yielded the following net isothermal temperature coefficient:

   Net: $+(1.1 \pm 0.2) \times 10^{-3}$ percent $\Delta k/k$ per F^{o}

These temperature coefficients are based on representative fuel element and moderator "average temperatures," which values differ somewhat from the isothermal temperature coefficient determined during the hot critical experiment. The value obtained during the critical experiment was

$$+(0.7 \pm 0.3) \times 10^{-3} \text{ percent } \Delta k/k \text{ per } F^{o}$$

The difference between the hot critical experiment values and the operating values of the temperature coefficient are believed due in part to a difference in the control rod pattern employed in the two measurements.

Fission Product Poison and Burnup

Following the last period of continuous operation for 65 hours at nominally 33 megawatts, the values of total poison (measured) and individual contributions to the poison (calculated) shown in Table 3.9 were determined by fitting k_{ex} measurements to the xenon program throughout the test period. From the fitting of the k_{ex} measurements to a one-group xenon, samarium, burnup program, a set of parameters was obtained that gave quite good agreement throughout the two weeks of operation during which the 126 hours at full power were accumulated.[7,15]

TABLE 3.9

TOTAL POISON IN HTRE NO. 3 REACTOR AFTER 65 HOURS OF CONTINUOUS OPERATION

	Total Poison, % Δk
Xenon (equilibrium)	1.32
Samarium	0.08
Burnup and long-lived fission products	0.05
Total poison	1.45

The maximum value of samarium poison obtained from this program, i.e., after complete decay of its precursor, was 0.10 percent Δk. The parameter adopted for burnup and long-lived fission product accumulation was

$$0.9 \times 10^{-5} \text{ percent } \Delta k/\text{mw-hr}$$

of which 42 percent is attributed to the burnup of fuel. Of the above value, 58 percent rep-

resents an approximation of the accumulation of long-lived fission products for fractional fuel burnup of less than 10 percent. As higher fuel burnup is achieved, the accumulation rate of the long-lived fission products should lessen appreciably.

3.3 SHIELD PERFORMANCE

3.3.1 SHIELD HEATING RATES

During the phase I (IET No. 16) and the phase II (IET No. 18) testing, shield heat generation rates were measured by means of calorimeter-type sensors placed in various locations in the side shield and the front and rear shield plugs. Sensor locations and designations are shown in Figure 3.13. Table 3.10 summarizes the measured and predicted heating rates for the two-test series.

3.3.2 RADIATION LEVELS OUTSIDE THE SHIELD

The gamma-ray dose rates outside the shield, shown in Figure 3.14, were measured with pocket dosimeters suspended from the IET building in the vertical midplane of the reactor shield assembly. The predicted dose rates are within a factor of 3 of the measured dose rates from 55 to 150 degrees, at a distance of 10 feet from the center of the active core. The effect of the front duct apparently was underestimated.

The fast neutron flux levels outside the shield are presented in Figure 3.15; the calculated values agree very well with the measured values.

3.4 NUCLEAR STARTS

Another significant accomplishment achieved during the HTRE No. 3 program was the first known start of a turbojet engine with a standard starter on nuclear power only. Since the all-nuclear start presented some unique problems in the analysis of the dynamic properties and control of the reactor, it is briefly summarized here. More complete details are contained in references 8 and 16.

An analog study showed that the engine-reactor combination was unstable over part of the possible range of engine speeds. This is because there is a dip in the relationship of turbine inlet temperature to engine speed in a turbojet engine operating with a fixed nozzle area. In other words, the engine is capable of operating at two different engine speeds for a single turbine inlet temperature. The weight of air flowing through the engine is different at the two speeds, however. The HTRE No. 3 engine-reactor combination was inherently unstable in the area below this reversal in the turbine inlet temperature curve because of the thermal lag of the reactor. Nevertheless, the analog study indicated that a successful nuclear start could be made, and the decision was made to attempt it.

To traverse the area of instability, the operator was required to maintain control between close limits of engine speed and fuel element plate temperature. During one phase of the nuclear start, it was necessary to adjust reactor power in direct opposition to the oscillations in engine speed. In spite of the relative delicacy of the operation, three successful nuclear starts were achieved, adequately demonstrating the feasibility of this type of operation as a routine method for starting a reactor-turbojet system.

Transient temperature, power, and engine data which were recorded continuously from 3400 rpm to the final steady-state condition are shown in Figure 3.16. These curves show that the measured power to air peaked at 28.5 megawatts during the period in which the generated power was held constant at about 18.9 megawatts. This was due to the release

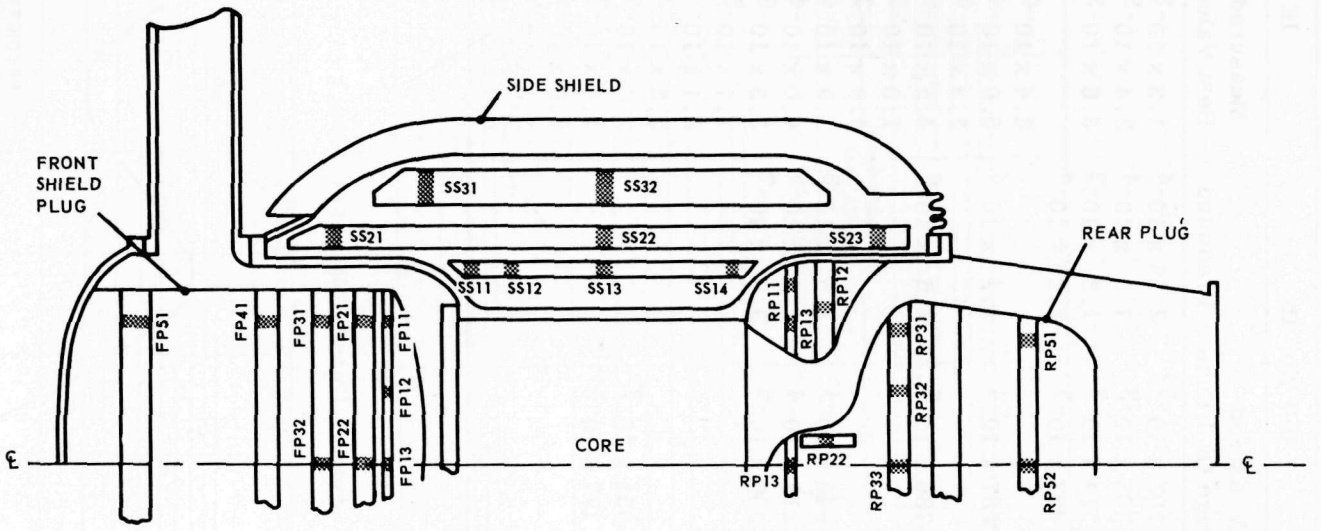

Fig. 3.13 – Location of shield-heating-rate sensors

TABLE 3.10

SHIELD HEA . GENERATION RATES IN IET NO. 16 AND IET NO. 18

	Shield Heat Generation Rates, w/g-mw			
	IET No. 16		IET No. 18	
Sensor	M asured Average Of 3 Runs	Predicted	Measured Best Value	Calculated
SS1-1	1.302×10^{-3}	2.26×10^{-4}	1.3×10^{-3}	
SS1-2	2.705×10^{-3}	7.8×10^{-4}	2.4×10^{-3}	
SS1-3	4.714×10^{-3}	1.5×10^{-3}	3.6×10^{-3}	
SS1-4	2.692×10^{-3}	2.26×10^{-4}		
SS2-1			3.4×10^{-4}	
SS2-2	2.267×10^{-4}	1.1×10^{-4}	6.0×10^{-4}	
SS3-1			3.3×10^{-6}	
SS3-2	3.736×10^{-6}	1.6×10^{-6}	4.5×10^{-6}	
FP1-2			1.0×10^{-3}	0.795×10^{-3}
FP1-3			1.9×10^{-3}	0.870×10^{-3}
FP2-1	0.946×10^{-4}	7.5×10^{-6}	1.9×10^{-4}	1.14×10^{-4}
FP2-2	3.219×10^{-4}	1.5×10^{-5}	4.0×10^{-4}	1.72×10^{-4}
FP3-2	4.306×10^{-6}	3.0×10^{-7}	3.3×10^{-6}	2.44×10^{-5}
FP4-1			1.7×10^{-5}	1.84×10^{-5}
FP5-1			8.1×10^{-7}	
RP1-1			2.2×10^{-3}	
RP1-2	4.951×10^{-3}		3.1×10^{-3}	
RP1-3	2.177×10^{-3}		1.6×10^{-3}	
RP3-1			6.9×10^{-4}	
RP5-1			5.0×10^{-5}	
RP5-2			1.7×10^{-5}	

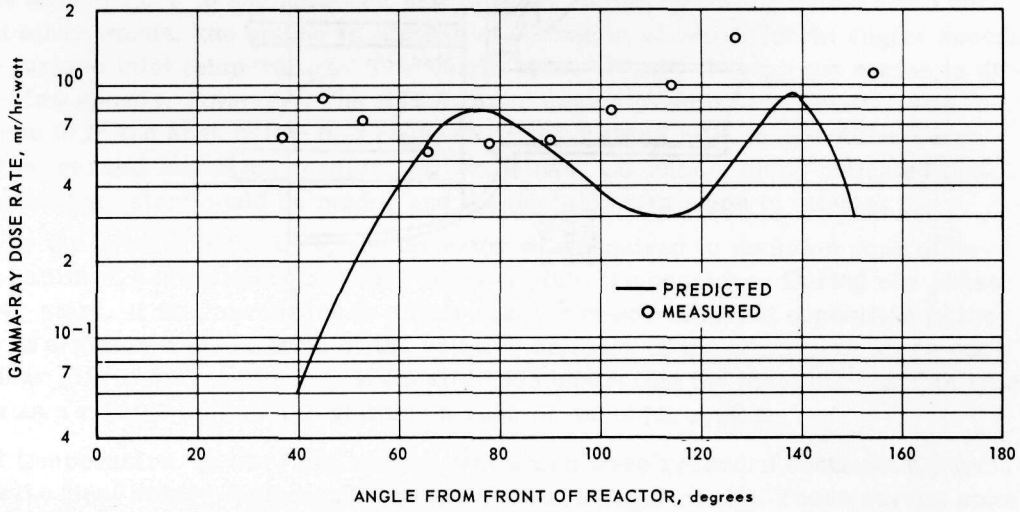

Fig. 3.14 – Gamma-ray dose rate in the vertical midplane at a 10-foot radius about the center of the active core

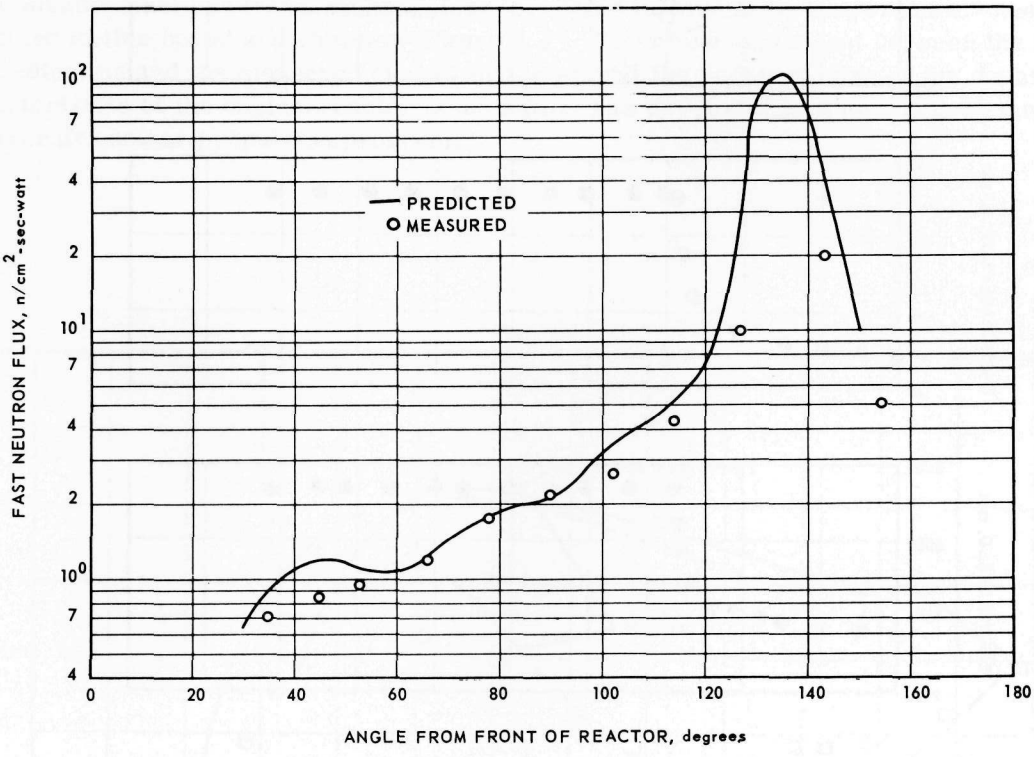

Fig. 3.15 – Fast neutron flux in vertical midplane at a 10-foot radius about the center of the active core

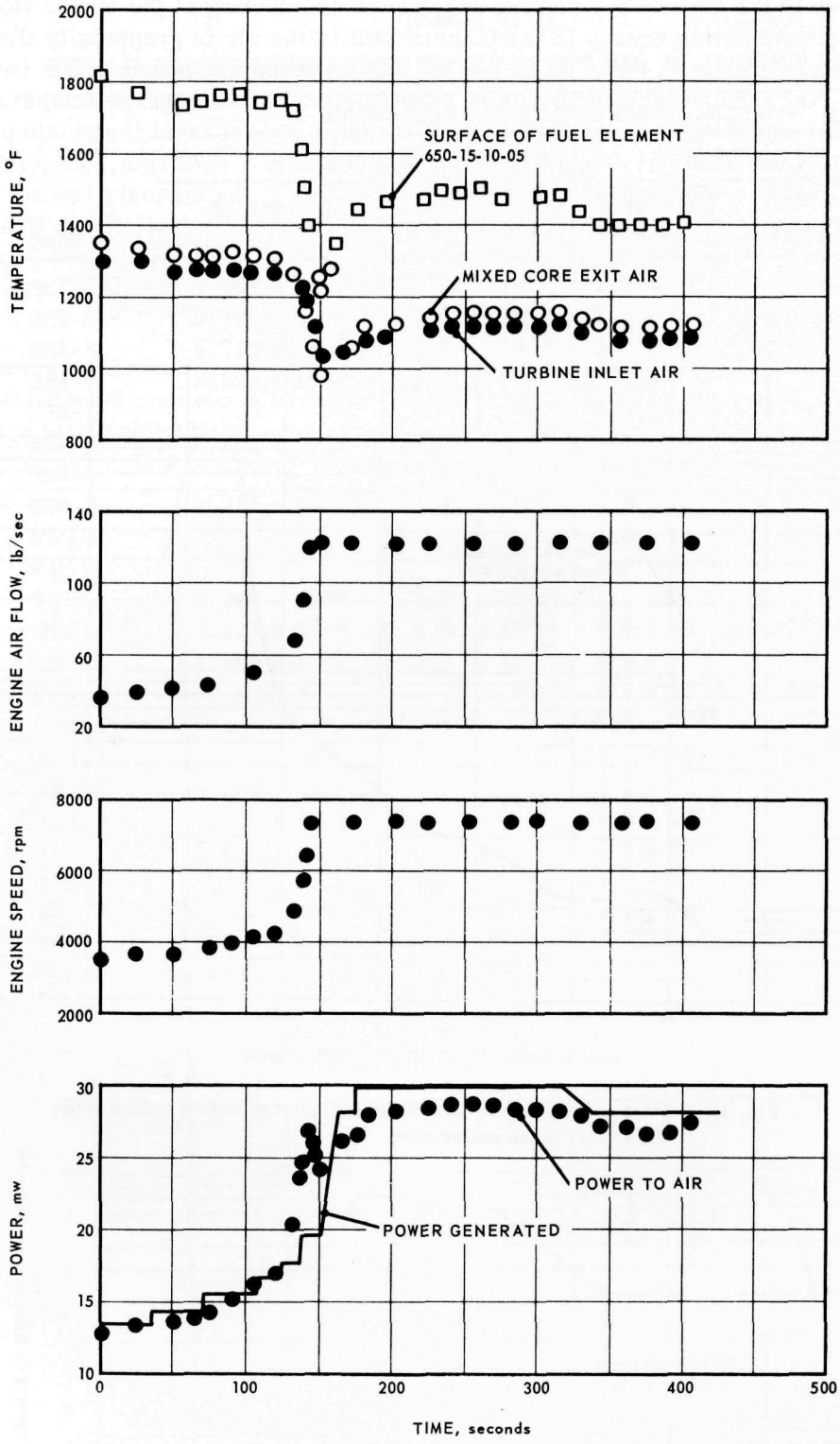

Fig. 3.16 – Transient parameters recorded during the first all-nuclear start

of stored energy in the core; i.e., cooling of the core and ducting at the higher flow conditions. The release of this energy in the form of heat to the air is graphically illustrated by the temperature traces on these plots. As the engine speed and power to air increased to a maximum, the turbine inlet temperature exceeded the core discharge temperature for several seconds, indicating a large, momentary transfer of heat from the shield plug and ducting to the turbine inlet air. When the engine speed reached 7070 rpm, the jet nozzle on the control engine closed to hold this speed. At this point, the measured power to air decreased sharply as the turbine inlet air temperature continued to fall off. A final reactor power step of 8.5 megawatts was taken at a rate of about 36 megawatts per minute within ten seconds of attaining 7070 rpm. The core discharge air temperature reflected this power burst a few seconds later.

The steady-state and transient curves of corrected turbine inlet temperature versus corrected engine speed are shown in Figure 3.17. The close agreement between the analog predictions and the measured curves indicates that the understanding of the dynamic characteristics of the engine-reactor combination was developed to a high degree during the aircraft nuclear propulsion program.

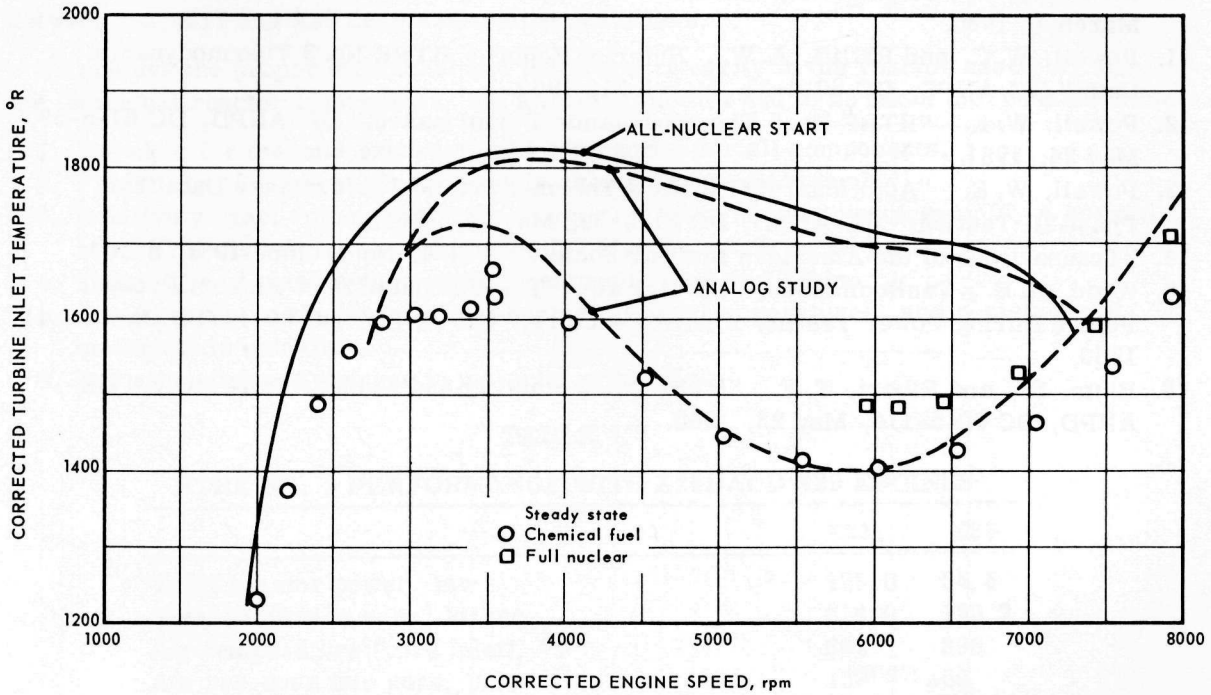

Fig. 3.17 – Predicted and measured data of the first all-nuclear start

3.5 REFERENCES

1. "Summary Report of HTRE No. 3 Nuclear Excursion," GE-ANPD, APEX-509, August 1959.
2. Feinauer, E., Highberg, J. W., Luke, C. W., Masson, L. S., and Tuck, G., "Summary Report for Testing of the D102A Reactor Assembly During LPT 2," GE-ANPD, DC 58-9-705, August 29, 1958.
3. Skow, K. J., Hendricks, T. J., and Kunze, J. F., "Preliminary Data Report, LPT 2-2, D102A2(A)," GE-ANPD, XDCL 59-7-716, July 20, 1959.
4. Becar, M. J., "Final Data Report, LPT 2-2, D102A2(A)," GE-ANPD, DC 61-2-725, February 17, 1961.
5. Devens, F. G., "D102A Power Plant Testing IET #13," GE-ANPD, DC 59-4-710, April 3, 1959.
6. Showalter, D. E., "Preliminary Data Report - IET 16 - D102A2(A)," GE-ANPD, XDCL 59-11-715, October 28, 1959.
7. Cannon, C. B., "Preliminary Data Report - IET 18 - D102A," GE-ANPD, DC 60-6-735, June 17, 1960.
8. Cannon, C. B., "Preliminary Data Report - IET 25 - D102A2 Power Plant," GE-ANPD, DC 61-2-724, February 10, 1961.
9. Miller, C. L., and Nassano, R. N., et al., "Interim Report on HTRE No. 3 (D102A2) Operations," GE-ANPD, DC 60-1-50, January 7, 1960.
10. Blumberg, B., "HTRE No. 3 Performance Demonstration," GE-ANPD, DC 60-3-53, March 3, 1960.
11. Powell, W. C, and Ratliff, A. W., "Interim Report - HTRE No. 3 Thermodynamic Data," GE-ANPD, DC 60-4-22, March 31, 1960.
12. Powell, W. E., "HTRE No. 3 Thermodynamic Performance," GE-ANPD, DC 61-5-59, May 24, 1961.
13. Powell, W. E., "Additional HTRE No. 3 Thermodynamic Performance Data from Phase III Testing," GE-ANPD, DC 61-5-59, May 24, 1961.
14. "Transactions of the American Nuclear Society," Vol. 4, No. 1, June 1961, p. 106.
15. Wood, R. E., VanHoomissen, J. E., et al., "The Computation of Fission Product Poison During Power Testing of ANP Reactors," GE-ANPD, DC 60-1-714, January 14, 1960.
16. Blum, S., and Elbert, T. F., "HTRE No. 3 Stability and Nuclear Start Study," GE-ANPD, DC 60-5-114, May 23, 1960.

4. REACTOR

4.1 OBJECTIVES AND REQUIREMENTS

The objectives of the HTRE No. 3 reactor program were to design, build, and test an air-cooled, solid-moderator reactor assembly. The assembly was limited to a diameter of 57 inches and a length of 43 inches; these dimensions include the side reflector and support structures.

Original specifications required a reactor system that could operate either with X39 engines at 32.3 megawatts and an airflow of 122 pounds per second or with X211 engines at 175 megawatts with 850 pounds of air per second. The reactor support structure and the fuel elements were designed to accommodate the aerothermodynamic loads encountered under the X211 conditions. The reactor was actually built, however, to operate only under the X39 conditions. Table 4.1 presents typical performance data that show the differences between the X211 and X39 design operating conditions.

To achieve the proper structural and functional integrity in the reactor assembly and the individual reactor components, the following factors had to be taken into consideration:

1. Freedom for thermal expansion and contraction for all components.
2. Flexibility of components for remote assembly and disassembly.
3. Relatively exact volume fractions to accommodate nuclear requirements. A normal statistical distribution was assumed for size variation on all parts.
4. Feasibility of manufacture within reasonable time and costs.
5. Compatibility of the materials in contact at high temperatures, and resistance of materials to oxidation.
6. Radiation-induced changes in material properties.

TABLE 4.1

HTRE NO. 3 PERFORMANCE WITH X211 AND X39 ENGINES[a]

	X211	X39
Total reactor power, mw	128.0	35.5
Total airflow to core, lb/sec	624.0	122.2
Air temperature (core inlet), °F	662	396
Air pressure into core, psia	159	56
Air temperature (core outlet), °F	1390	1438
Air temperature from fuel elements, °F	1500	1590
Core outlet pressure, psia	123	49
Pressure drop across the core, psi	36	7
Maximum average fuel element temperature, °F	1770	1770
Maximum fuel element temperature, °F	1950	1950

[a]These statistics are preliminary and are not in agreement with the final data given later in the report.

7. Freedom of parts to bend under load without damaging adjacent parts.
8. Relative position of component at full loads and maximum temperatures compared to their as-built positions.
9. Closely controlled cooling passages.

Limited precedence existed for establishing the preliminary requirements for physical characteristics such as reactor size, volume fractions, and fuel-loading manufacturing tolerances. The size limitations placed on the reactor at the beginning of design were held throughout the work because any changes would have caused changes in other subassemblies, such as shielding and ducting.

The concentric-ring fuel elements consisted of the same material used previously in HTRE No. 1 and HTRE No. 2, but in HTRE No. 3 the dynamic loads were higher by a factor of about 6. This more difficult dynamic loading condition was further intensified by an increased surface-to-volume ratio of the fuel elements and by a temperature increase of about 100°F.

Maintenance requirements also presented difficult design problems. The capability to completely disassemble the power plant and install most of the structure and all of the active core components was a requirement. Remotely operated fasteners and release mechanisms were required for each component.

Very little was known of the behavior of the hydrided zirconium moderator or the cladding requirements for hydrogen retention. Inconel X was chosen early in the program to meet the structural requirements at the temperatures expected; but only small quantities of sheet and strip had been produced previously, and knowledge of welding, machining, and forming of this material was limited.

An early hope of the designers was to operate the two X39 engines on full nuclear power and to accomplish a full-nuclear start.

Although the HTRE No. 3 reactor was a prototype flight model, it did not have all possible refinements. The program was intended to solve many of the problems in design, fabrication, and operation of a flight system; raise the general knowledge; and clear the way for a flight-system effort.

4.2 REACTOR DESIGN

4.2.1 OVER-ALL CORE

The core of HTRE No. 3 is air-cooled, has a hydrided zirconium moderator, and contains 80Ni - 20Cr fuel elements. The hydrogen concentration (N_H = number of hydrogen atoms per cubic centimeter) in the moderator is varied radially for radial power flattening, and two types of fuel cartridges are used to improve the fine power characteristics of the elements. Cross-sectional views of the core are shown in Figure 4.1.

The active core contains 150 fueled cells, each of which includes a moderator section and a fuel cartridge. A typical cell installation is shown in Figure 4.2.

The moderator cells are hexagonal bars of hydrided zirconium 3.923 inches across flats with a 3.090-inch bore, as shown in Figure 4.3. A 310 stainless steel support tube, 0.020 inch thick, inside the bars provides a cylindrical cell for the insulation liner and fuel cartridge. The support tube is attached to the ball joint and remote disconnect at the entrance end and to a tail section that extends into the rear tube sheet. The insulation liner, a cylindrical tube 3.00 inches in outside diameter, is inserted into the moderator cell to separate it from the fuel cartridge and to form a cooling annulus around the outside fuel

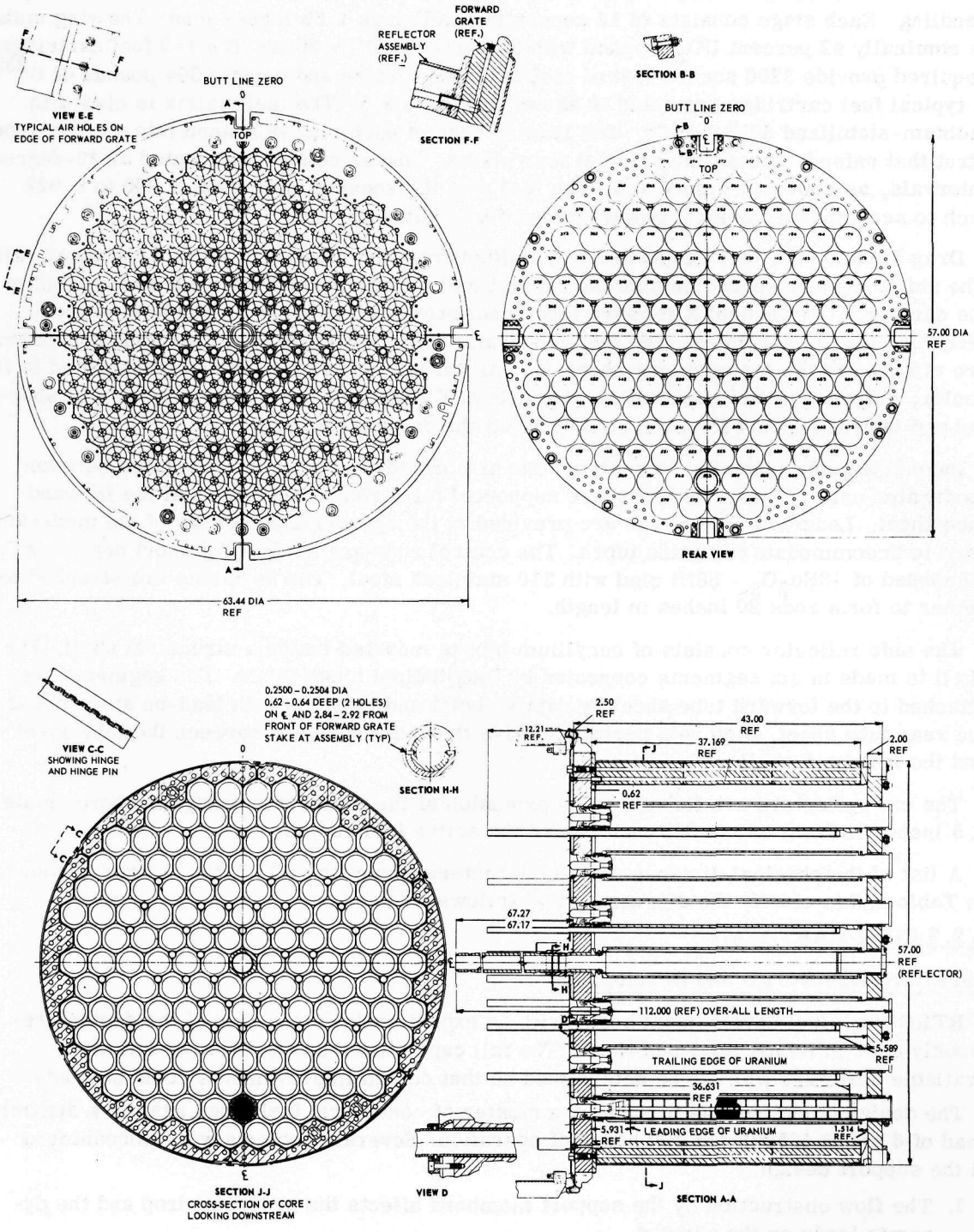

Fig. 4.1 – HTRE No. 3 core assembly (Dwg. 7018R51)

ring. A resilient seal ring at the forward end forms a seal with the moderator support tube. The insulation liner is shown in Figure 4.4.

Each fuel cartridge is made up of 19 fuel stages, a nose section, and a tail assembly for handling. Each stage consists of 12 concentric fuel rings 1.55 inches long. The ring matrix is nominally 42 percent UO_2 blended with 58 percent 80Ni - 20Cr. The 150 fuel cartridges required provide 3200 square feet of heat transfer surface and contain 394 pounds of U^{235} A typical fuel cartridge assembly is shown in Figure 4.5. The fuel matrix is clad with niobium-stabilized 80Ni - 20Cr. The leading edge of each ring is brazed into a comb-type strut that extends across the stage at four places. Spacer combs are located at 22-degree intervals, as shown in Figure 4.5. The fuel ring thicknesses vary from 0.020 to 0.027 inch to accomodate the local power-generation requirements.

Drag loads on the fuel stages are transmitted from the comb struts to four support rails. The rails, equally spaced outside the largest fuel ring, transmit the loads to the front of the cartridge. An Inconel X forward tube sheet provides the basic longitudinal support structure for the assembly. The fuel-moderator cells and longitudinal structural members are attached to the forward tube sheet, and all thrust and drag loads are transmitted to the cooler, entrance end of the reactor. An Inconel X rear tube sheet provides for cell spacing and lateral support for each component at the downstream end.

Inconel X guide tubes for 48 control rods are provided at alternate positions between moderator cells. The guide tubes are supported for fore and aft motion at the forward tube sheet. Longitudinal grooves are provided at the appropriate corners of the moderator bars to accommodate the guide tubes. The control rods are made up of short segments composed of $42Eu_2O_3$ - 58Ni clad with 310 stainless steel. The segments are strapped together to form rods 20 inches in length.

The side reflector consists of beryllium blocks mounted inside a structural shell. The shell is made in six segments connected by longitudinal hinge joints. The segments are attached to the forward tube sheet by captive bolts and by studs with lead-on stop nuts at the rear tube sheet. Stop nuts permit relative thermal expansion between the tube sheet and the reflector shell.

The end reflectors are formed by an extension of the moderator hexagons approximately 4.5 inches in front of and 0.5 inch behind the active fuel region.

A list of the physical dimensions and characteristics of the HTRE No. 3 core is shown in Table 4.2 to clarify the discussion that follows.

4.2.2 FUEL CARTRIDGES

Fuel Cartridge Design and Development

HTRE No. 3 fuel development began with an experimental evaluation of the design previously used in HTRE No. 1 and No. 2. The full capabilities and methods of failure of available hardware were to be determined so that design improvements could be made.

The design objective was to support a cluster of concentric fuel rings against a dynamic head of 6 psi at 1850°F for 100 hours of operation. Several problems were encountered in the support design:

1. The flow obstruction by the support members affects the pressure drop and the dynamic loads on the support.
2. The addition of neutron-absorbing metals in the active core increases the fuel requirements.
3. In a reactor for aircraft applications, the problem of weight is significant.
4. Increased depth of the struts presented a greater restriction for relative thermal expansion between the rings and the unfueled combs.

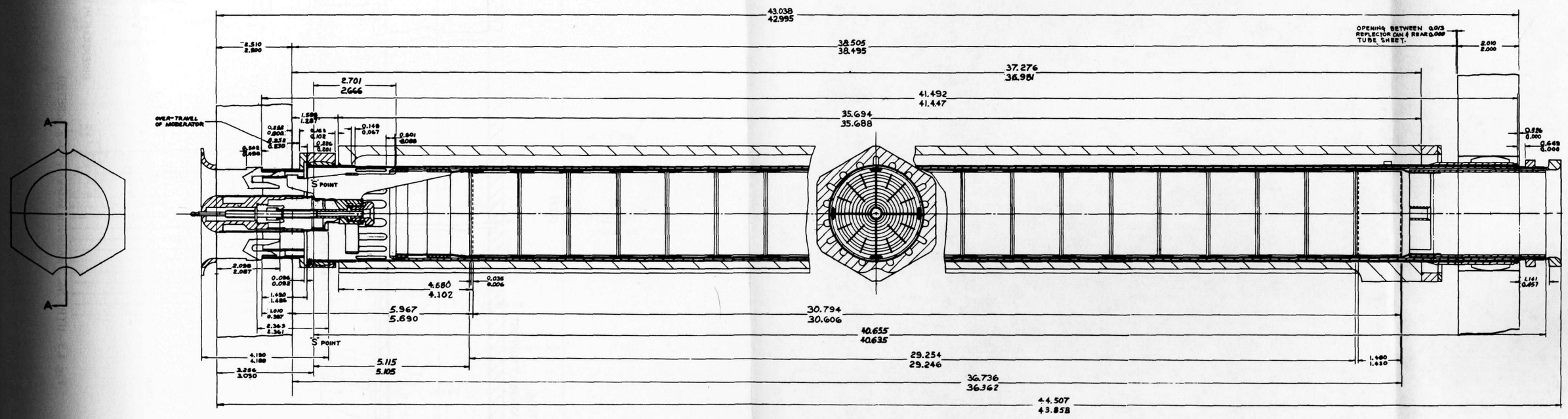

SECTION A-A

Fig. 4.2—HTRE No. 3 fuel-moderator cell assembly (Dwg. 7016R71)

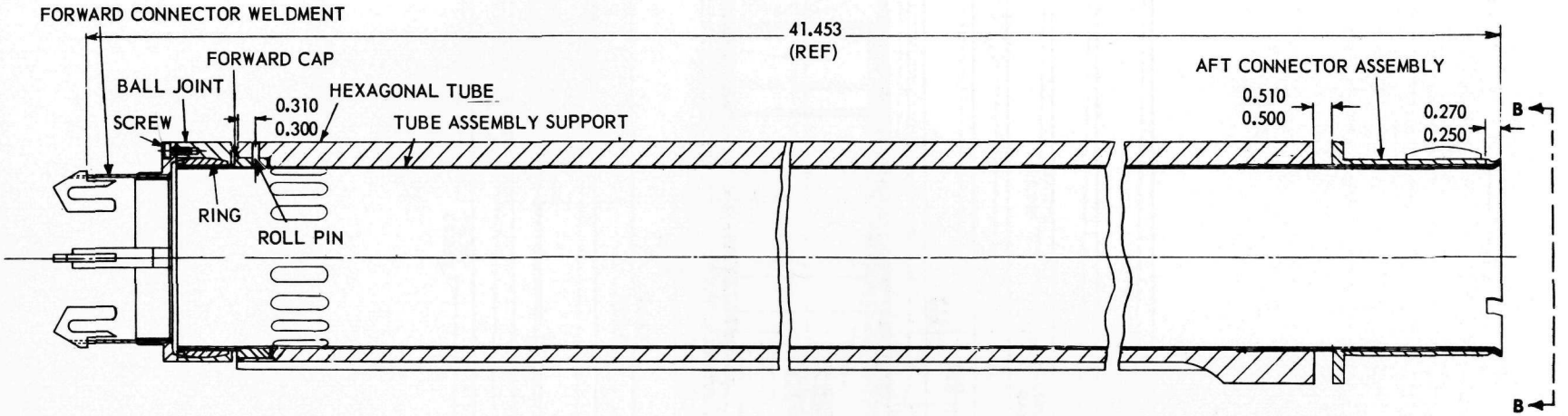

SECTION A-A

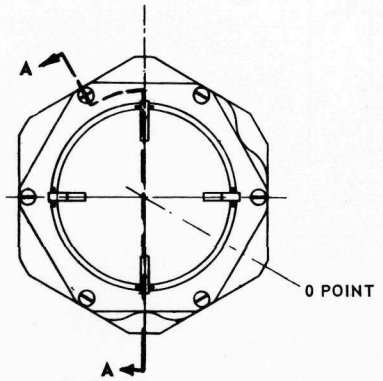

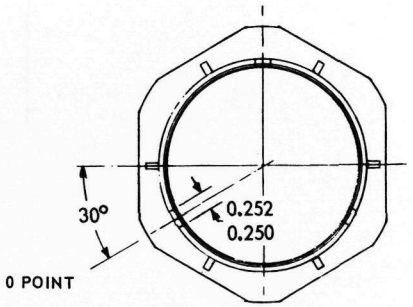

VIEW B-B

DIMENSIONS IN INCHES

Fig. 4.3 – HTRE No. 3 moderator assembly (Dwg. 628E720)

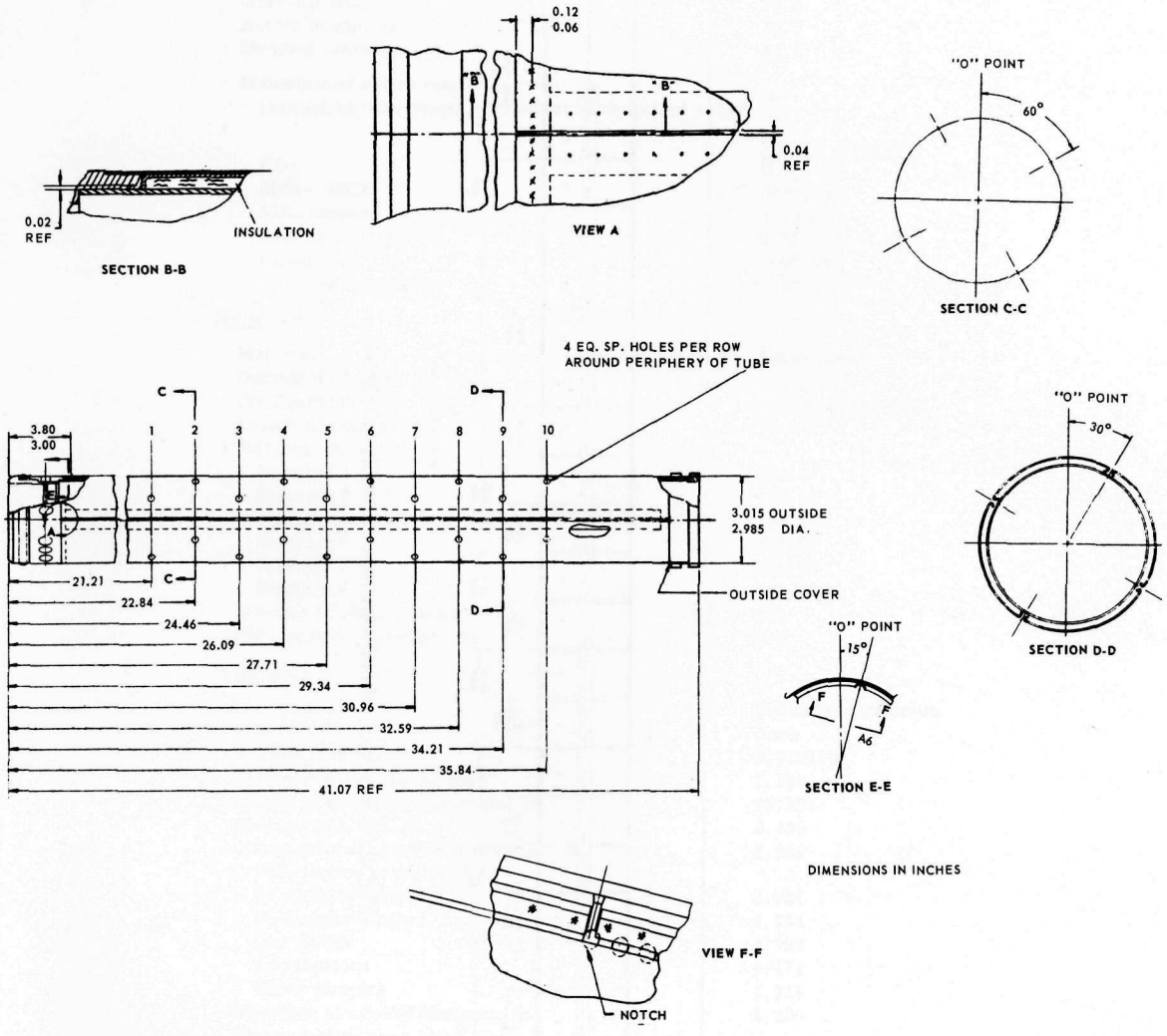

Fig. 4.4 – Insulation liner assembly (665D129)

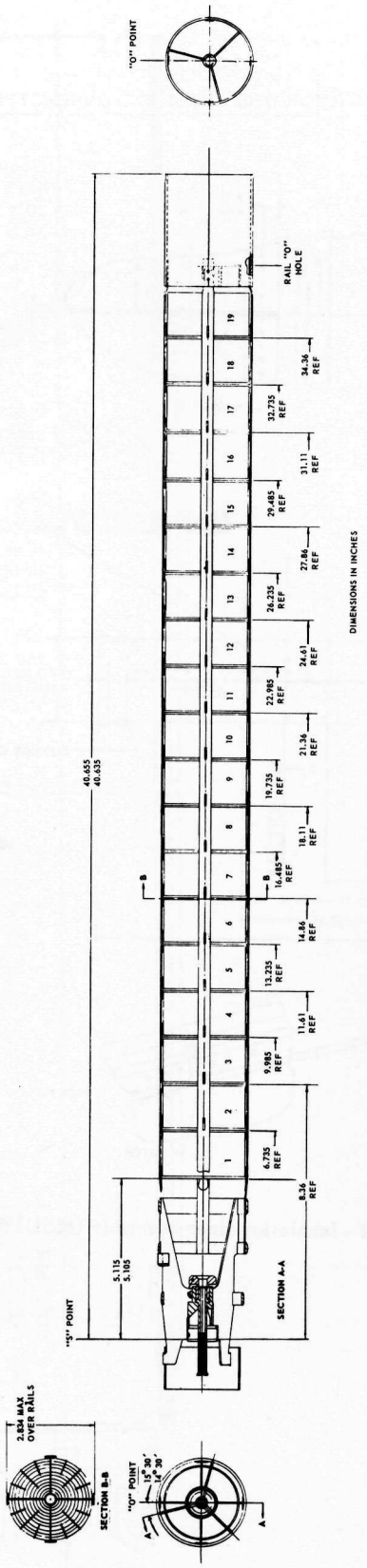

Fig. 4.5 – Side view of fuel cartridge assembly (7018R94)

TABLE 4.2

HTRE NO. 3 REACTOR DIMENSIONS AND CHARACTERISTICS

Core - General		
Structural material		Inconel X
Over-all length, in.		43.5
Active length, in.		30.7
Nominal diameter, in.		51.0
Materials of active core (excluding tube sheets, reflector, and control rods)		
		Volume Fraction
UO_2		0.019568
80Ni - 20Cr		0.078086
310 stainless steel		0.032463
Hydrided zirconium		0.348170
Inconel X		0.001940
Void and insulation		0.519770
Reflector		
Material		Beryllium
Outside diameter, in.		57.0
Configuration		Hexagonal prisms
Length of each block, in.		12.123
Weights, lb.		
Segment 1		150.56
Segment 2		150.56
Segment 3		147.68
Segment 4		150.56
Segment 5		150.56
Segment 6		148.90
Number of cooling holes		211
Cooling hole diameter, in.		0.5
Moderator		
Material		Hydrided zirconium
Clad		None
Volume fraction		0.348170
Distance across flats, in.		3.923
Length of hydrided zirconium, in.		35.332
Element spacing, in.		0.030
Diameter of forward-end hexagon, in.		3.089
Cross-section area, in. ^{2}		
No dimples (outer)		5.031
No dimples (inner)		4.943
One dimple		4.707
Two dimples		4.471
Three dimples		4.234
Diameter of aft-end hexagon, in.		3.100
Cross-section area, in. ^{2}		
No dimples (outer)		4.995
No dimples (inner)		4.912
One dimple		4.675
Two dimples		4.437
Three dimples		4.199
	Depth, in.	Width, in.
Cooling slots, cells X10-X65		
Corner slots	0.320	0.147 ± 0.005
Middle slots	0.215	0.194 ± 0.005
Cooling slots, cells X72-X75		
Corner slots	0.320	0.161 ± 0.005
Middle slots	0.229	0.207 ± 0.005
Insulation-liner - fuel-annulus hydraulic diameter, in.		0.18

TABLE 4.2 (cont'd.)

HTRE NO. 3 REACTOR DIMENSIONS AND CHARACTERISTICS

Moderator (cont'd.)

Cells	N_H	Quantity
X10, 121, 321, 521, X32, X31, X30	2.90	27
221, 421, 621, X20, 143, 343, 543, 242, 442, 642, 141, 341, 541, X40	3.00	24
243, 443, 643, 142, 342, 542, 241, 441, 641	3.10	9
X5X	3.25	30
X6X	3.45	36
X72, X73, X74, X75	3.95	24
700	0	1

Moderator Support Tube	
Material	310 stainless steel
Thickness, in.	0.025
Outer diameter, in.	3.080
Moderator Insulation Liner	
Material	310 stainless steel
Thickness, in.	0.020
Outer diameter, in.	2.890
Insulation	Refrasil
Insulation container	310 stainless steel
Thickness, in.	0.002

Fuel Elements

Material	80Ni - 20Cr	
Number of identical stages per cartridge	19	
Distance from leading edge of stage 1 to leading edge of stage 19, in.	29.250 ± 0.020	
Nominal spacing between successive stages, in.	0.134	
Number of rings per stage	12	
Ring-spacing tolerance, in.		
Outside of rings 1, 2, 3, 4	± 0.004	
All others	± 0.005	
Active cartridge length, in.	30.741	
Meat width of rings, in.	1.450 ± 0.030	
Dead-edge width, in.	0.0205 ± 0.0145	
Over-all width of rings, in.	1.491 ± 0.059	
Ring thickness tolerance, in.		
Maximum per ring	± 0.001	
Weighted average	± 0.005	
Cut length tolerance, in.	± 0.015	
Cladding thickness, in.	0.004 ± 0.0006	
Linear density tolerance, %	± 3.5	
Area density tolerance (reference), %	± 6.0	
Weight percentage uranium in UO_2, %	81.6 ± 0.7	
Weight percentage U^{235} in uranium (enrichment), %	93.2 ± 0.5	

	Type A[a]	Type B[a]
Total UO_2 weight per stage, lb	0.1697 ± 0.005	0.1700 ± 0.005
Total UO_2 weight per cartridge, lb	3.224 ± 0.060	3.230 ± 0.060
Total weight of assembled cartridge, lb	13.114 ± 0.430	13.057 ± 0.430
Uranium-235 weight per core, lb	394 ± 6	
Inside diameter (cold) of insulation liner, in.		2.853
Center-to-center distance of cells, in.		3.953
Fuel and air frontal area, $in.^2$		963
Heat transfer area, ft^2		3200
Moderator cooling air frontal area, $in.^2$		87

	Nominal 80Ni - 20Cr Weight Per Stage, g	
	Type A	Type B
Cladding plus dead edge	97.5	95.8
Inner structure (combs, spacers, etc)	21.7	21.7
Rails	8.8	8.8
Wire seals	2.1	2.2
80Ni - 20Cr weight in core, lb	1478	

[a]Fuel elements for regions A and B are shown in Figure 4.10.

TABLE 4.2 (cont' d.)

HTRE NO. 3 REACTOR DIMENSIONS AND CHARACTERISTICS

Control Rod Guide Tubes	
Material	Inconel X
Number	48
Inner diameter, in.	0.841
Wall thickness, in.	0.060
Control Rods	
Poison material	Europium oxide
Density, g/cm^3	3.0
Clad	310 stainless steel
Clad thickness, in.	0.040
Diameter of rod, in.	0.700
Active length, in.	20
Type and quantity	
Dynamic	3
Shim	30
Safety	15
Location	
Center	23
Outer	25

The general configuration of an individual fuel stage is shown in Figure 4.6 together with the loading diagrams. Because of the complexity of the ring-type fuel element, the following simplifying assumptions were necessary to facilitate the stress analysis of the support members.

1. The main cross combs act as independent beams, simply supported at the rails. This assumption is thought to be slightly conservative since the conclusion assumed is that the support rails provide no supporting moment.
2. The bending restraint of the fuel rings on the combs is neglected.
3. The air velocity profile across the face of the element is essentially flat, and the drag on each ring is proportional to the surface area. With this assumption, the load on the beam is approximately linear with radial position.

To provide a passage for the cartridge release rod within the smallest fuel ring, the comb struts are brazed into an unfueled reinforcing ring at midspan. The reinforcing ring must be sufficiently strong to bridge the gap in the combs and provide a continuous beam across the complete stage.

The combs are slotted at each fuel ring intersection and brazed onto the fuel rings.

The fuel rings are a sandwich-type construction with a cermet core clad on each surface with 0.004 inch of 80Ni - 20Cr stabilized with 1 percent niobium. The core is a pressed and sintered matrix of uranium oxide and 80Ni - 20Cr powder. The leading and trailing edge of the rings are sealed with about 0.020 inch of stabilized 80Ni - 20Cr.

Since the downstream edge of the support comb is not continuous it is assumed to be in tension. This situation requires that the fuel rings form part of the support beams and creates a condition in which the bond between the fuel ring cladding and matrix is in tension.

Based on the design assumptions, a dynamic head of 6 psi, and a temperature of 1900°F, the analysis indicated a minimum margin of safety of -0.1. This is for the shear stress in the comb at the comb-rail junction.

$$\text{Margin of safety} = \left(\frac{\text{calculated stress} \times 1.5}{0.5 \times \text{100-hr stress rupture}} - 1 \right)$$

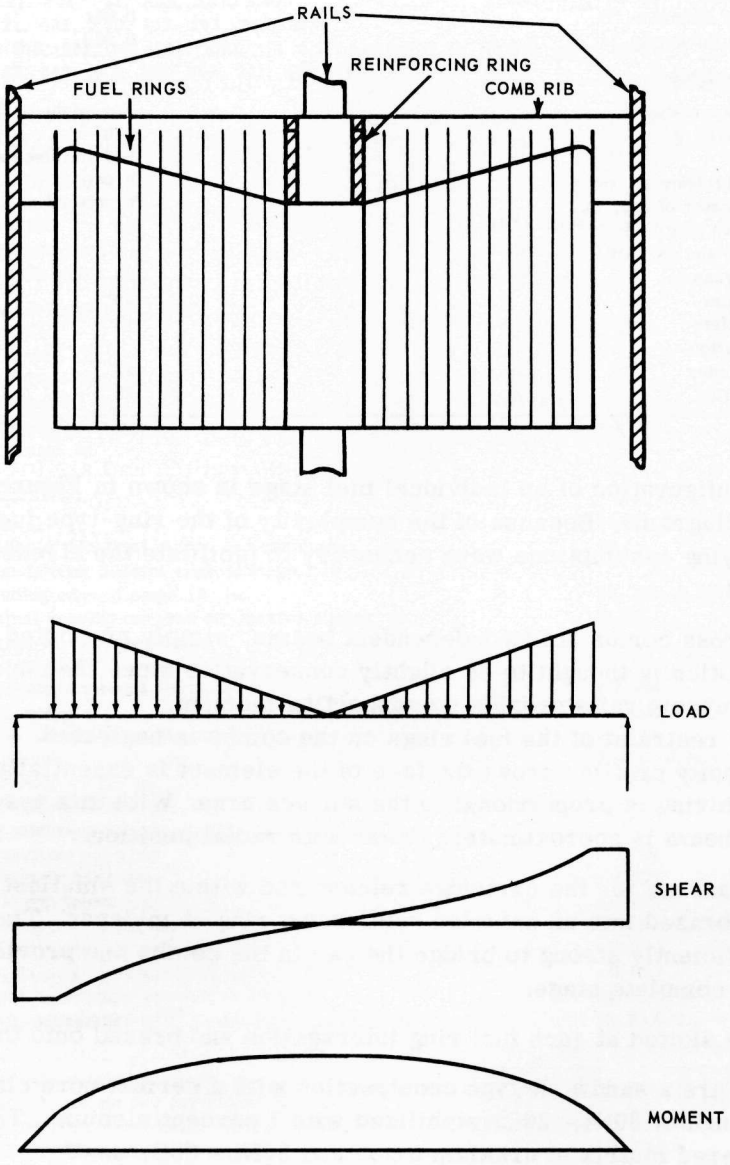

Fig. 4.6 – Longitudinal cross section and loading diagrams of fuel stage used in HTRE No. 3 fuel cartridges

In actual reactor operation, the unfueled comb would operate at a lower temperature than the fueled ring and, conversely, the comb would act as a cooling fin to create local temperature depressions in the rings.

Minor deflections in the support beams would result in misalignment of the fuel rings and introduce aerodynamic forces in a lateral direction on the fuel rings that could create conditions for catastrophic failure.

Laboratory tests on fuel stages were performed by flowing hot combustion gases through the assembly at the desired dynamic head. These tests did not introduce thermal stresses in the fuel stage assembly during steady-state operation, and the support combs and the fuel rings operated at the same temperature. The series of tests for a particular design required a proof test in the combustion gas burner rig before operation in the MTR or ETR testing facilities. The laboratory isothermal test specimens were identical to the in-pile test specimens except that depleted fuel was used in the laboratory sample. This series of tests presented the designer with the problem of designing for both the isothermal situation that introduced a temperature penalty on the structure and the in-pile test condition that introduced internal heating and thermal stresses in the material.

The in-pile test specimens required special design considerations because of nuclear heating. Special fuel concentrations compatible with the test reactor power and local flux levels were required to obtain the desired element temperature and airflow rate. Even with the best effort the in-pile tests do not present operating situations identical to those found in the reactor for which the fuel is designed. Temperature variations from fuel ring to fuel ring and temperature scallops in individual rings cannot be precisely duplicated.

The series of fuel element designs considered in arriving at a final configuration are shown in Figure 4.7. XR-13 and -14 are almost identical to the fuel stages used in HTRE No. 1. Extreme permanent deflection occurred in both samples early in the test with a dynamic head of 6 psi at 1850°F.

In the early test specimens downstream spacers were used in an attempt to prevent distortion of the rings at the trailing edge. The spacers did not prevent ring distortion, and observations after test indicated that the spacers may have caused distortion. In most cases ring distortion could be related to permanent bending of the support struts at the leading edge of the fuel stage.

The design approach of eliminating the extraneous obstructions in the flow channels and concentrating on a design for minimum deflection of the ring package proved successful. The comb ribs were shaped to accommodate the local bending moment, as shown in the XR-25 design in Figure 4.7. To further reduce the pressure drop and the resulting loads on the struts, the leading edges of the fuel and combs were rounded off and the trailing edges left square.

To point out the gains made in streamlining and strengthening the fuel ring package, elements XR-13 and XR-26 are shown in detail in Figures 4.8 and 4.9. The final-design fuel stages for the A and B regions of the core are shown in Figure 4.10.

The 90-degree fuel ring span between the major support combs is supported at three places to prevent local buckling of the fuel stage. Support of the rings at 45-degree intervals proved to be inadequate. Ring stability is a function of ring thickness and diameter, and the intermediate ring supports do not span across the stage but are limited to the larger rings. The smaller rings are stable with support points every 90 degrees. As the fuel rings become larger, they more nearly approach a flat plate configuration, and more frequent supports are required.

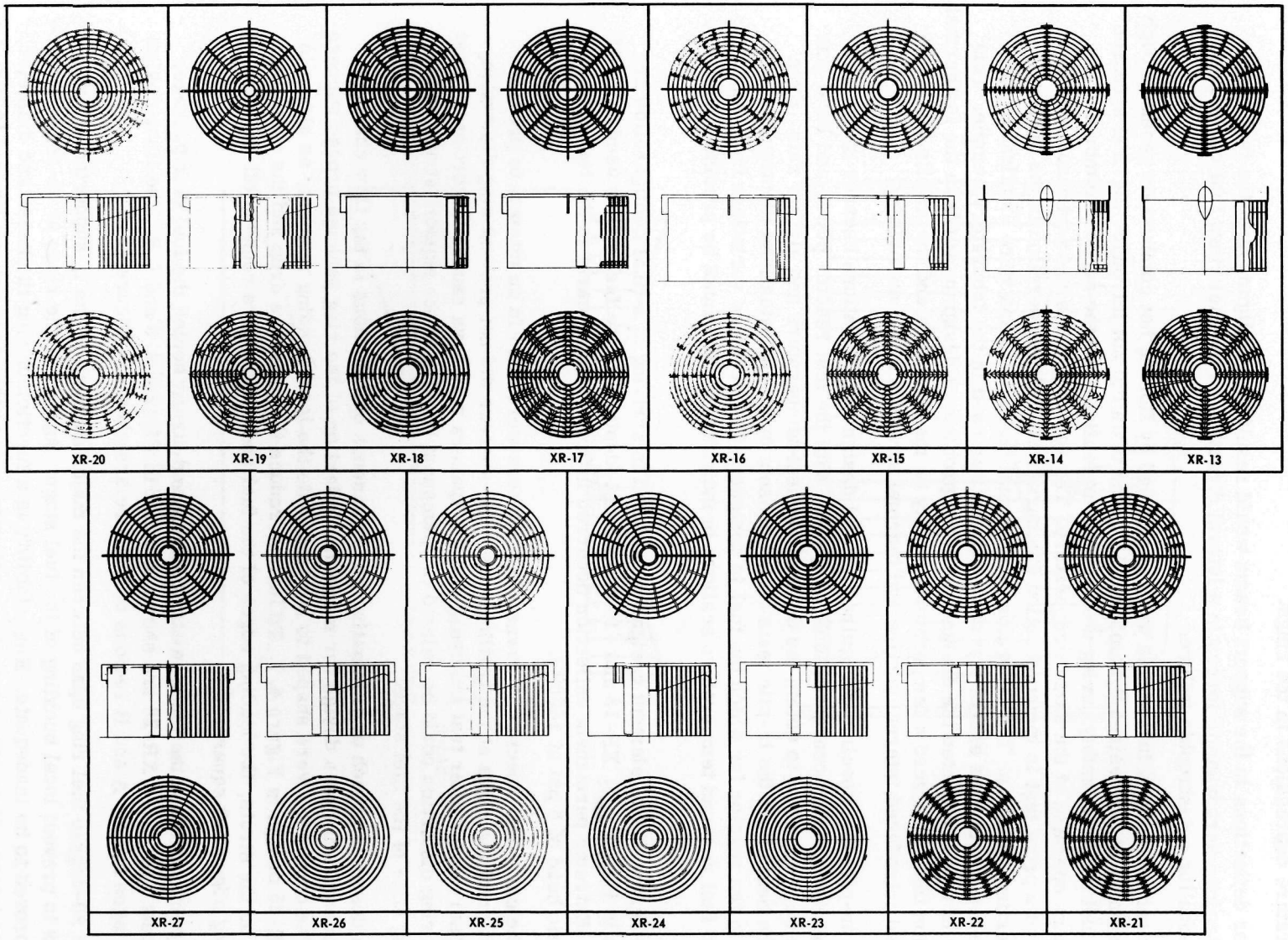

Fig. 4.7 – Design evaluation in fuel element design process

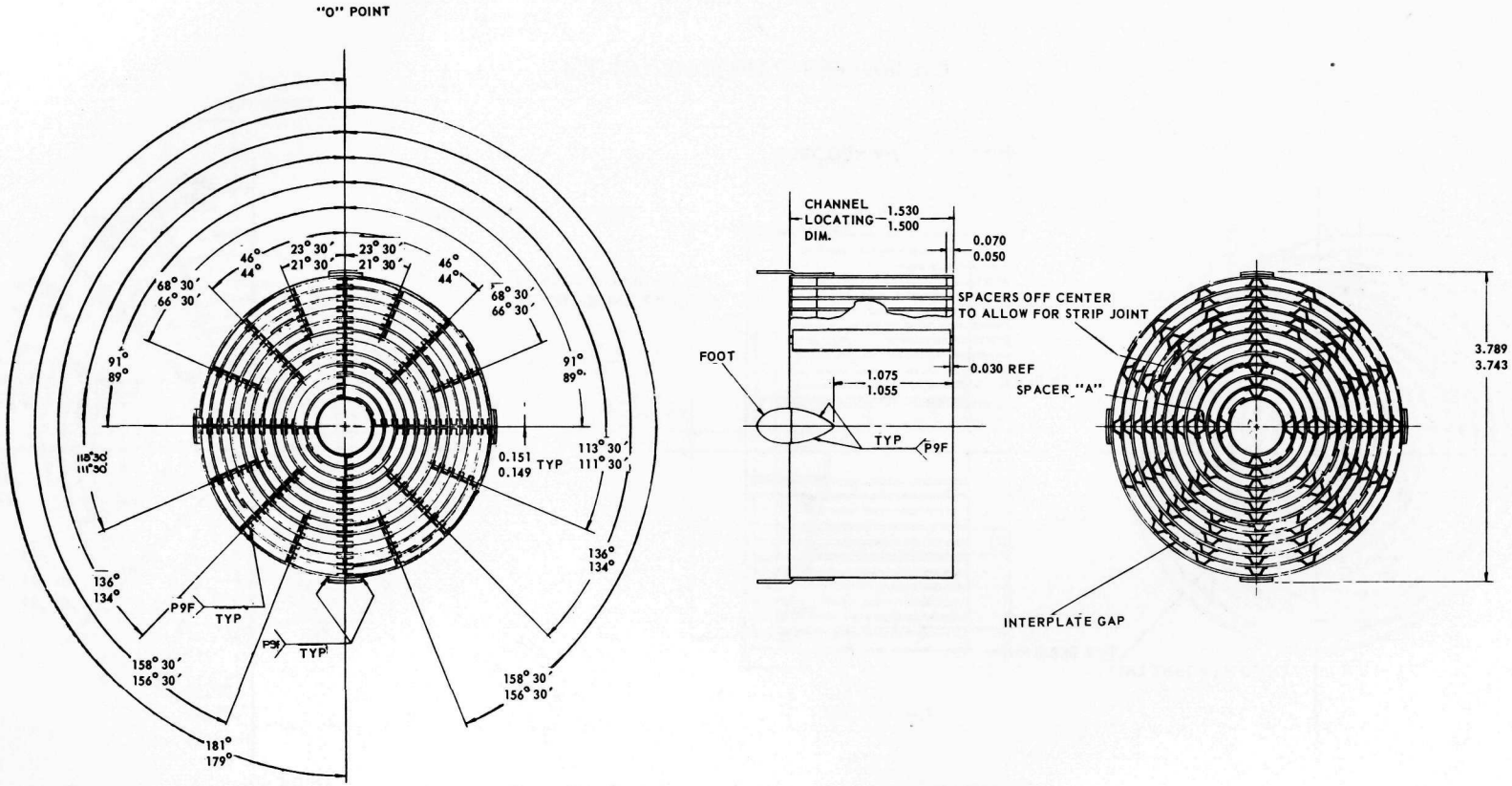

Fig. 4.8 – XR-13 fuel element (294D529)

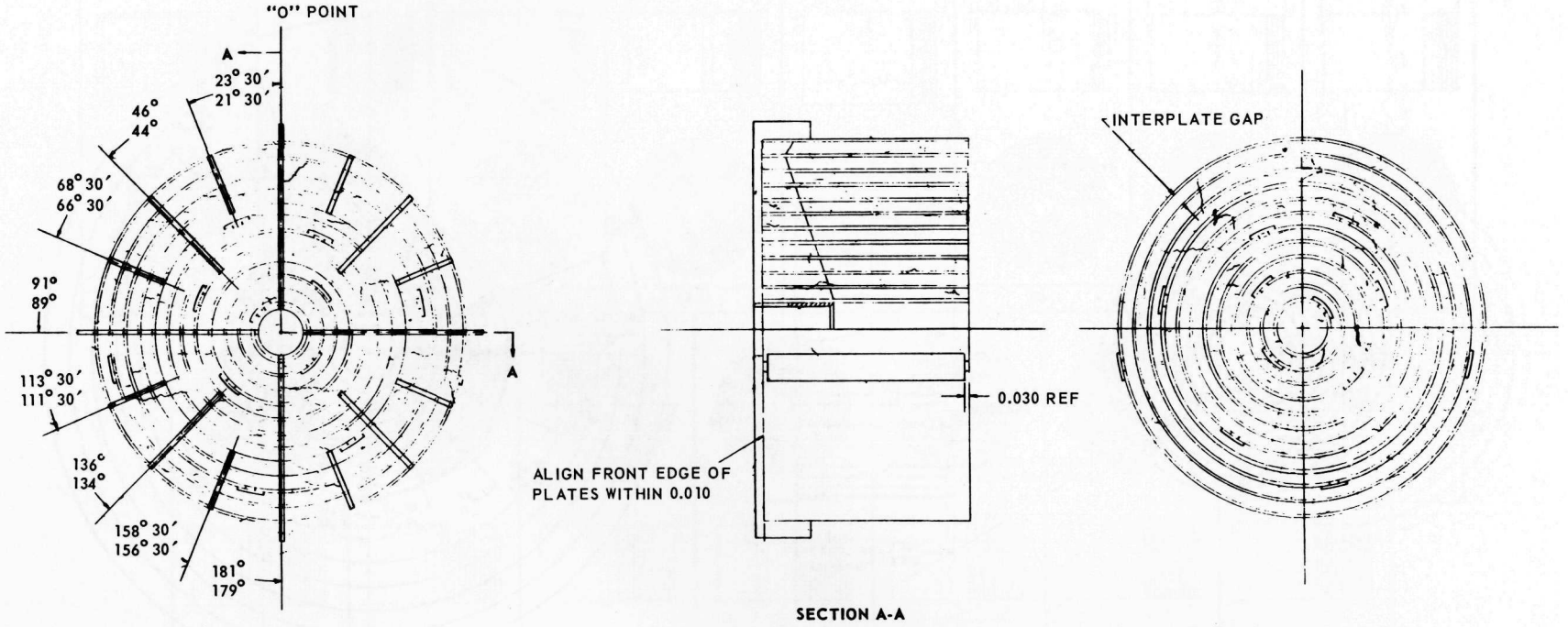

Fig. 4.9 – XR-26 fuel element (568D345)

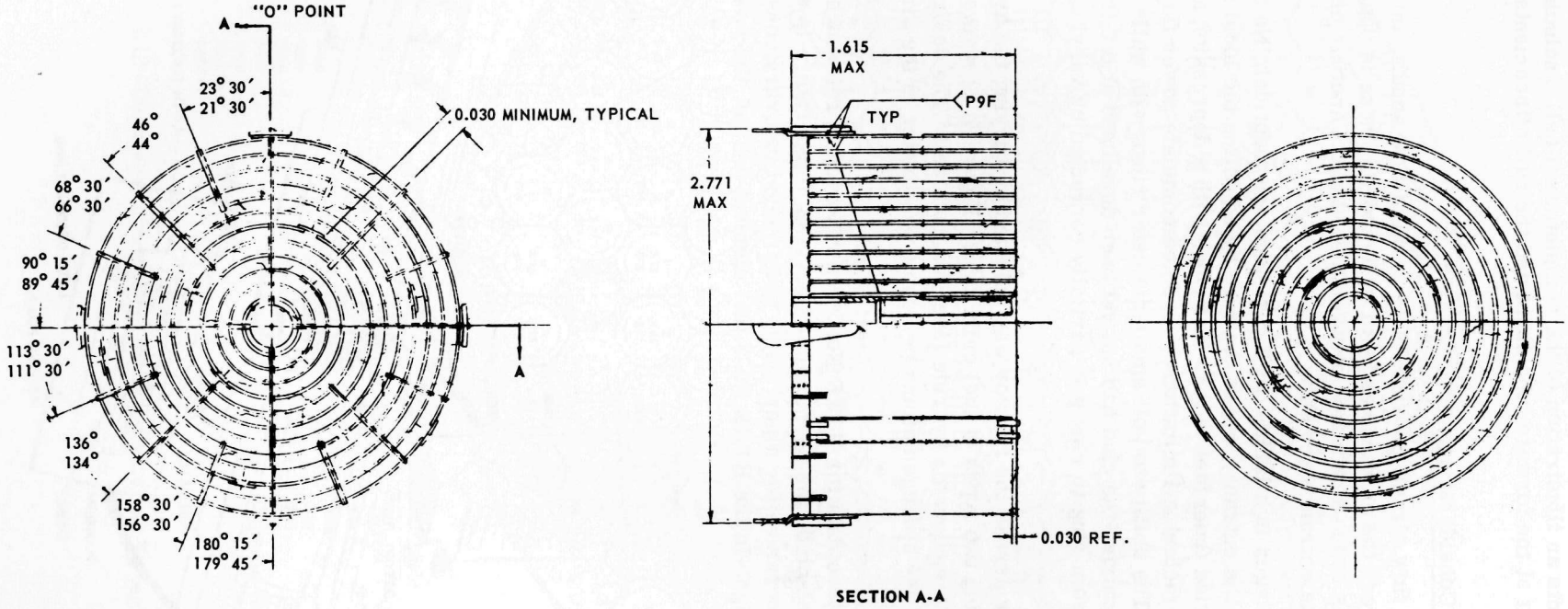

Fig. 4.10 – Fuel element for core regions A and B (295D535)

Figure 4. 11 presents an illustration of the complete fuel cell, including the cartridge fastener arrangement at the forward tube sheet and the rail attachments along the cartridge.

Aerothermodynamic Considerations

The fuel cartridge flow circuit consists of 12 parallel flow annuli, interrupted at each of the 18 stages between the entrance and exit of the core. There is opportunity for cross flow between channels at the separation between fuel stages. Another problem is that of pressure losses at the entrance and exit.

All of the 19 fuel stages in a HTRE No. 3 cartridge are identical. No attempt was made to increase power at the entrance end of the core by adjusting the local fuel loading. The power generation varied from fuel ring to fuel ring, with a depression at the smallest ring. Fuel ring manufacturing limitations prevented complete power flattening by varying fuel ring thickness. The ability to roll small-diameter rings with walls more than 0. 027 inch thick without rupturing the clad had not yet been developed at the time. The fine radial temperature from ring to ring was partially corrected by varying the cooling channels.

Gross radial power across the reactor was adjusted by varying the hydride level of the moderator and by using two types of fuel cartridges. Figure 4. 12 shows the type of fuel cartridge used and the moderator hydride level for each cell. The designation N_H in the figure is in units of 10^{22} hydrogen atoms per cubic centimeter in the zirconium moderator.

The basic temperature data for HTRE No. 3 are reported in references 1, 2, and 3. Once a material is selected, the permissible operating temperature is essentially fixed, but the required temperature for a particular power level can vary considerably and is dependent on the design. In the HTRE No. 3 fuel element design, the power output can be

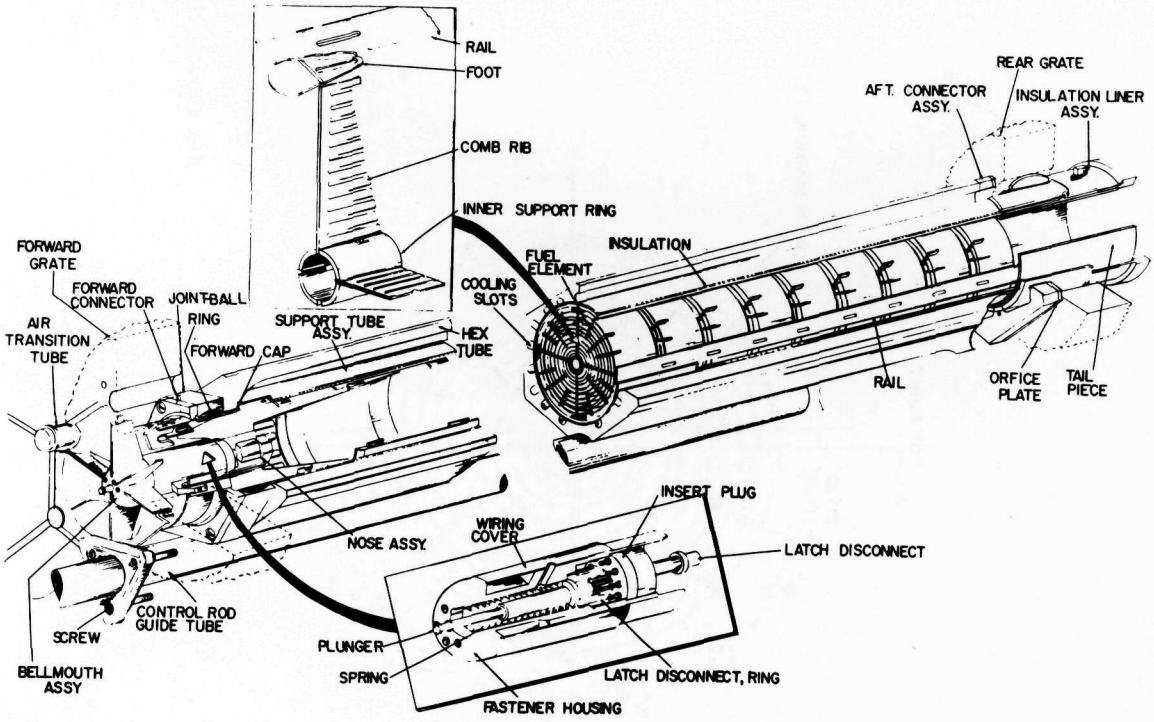

Fig. 4.11 – HTRE No. 3 fuel cell components (G-965)

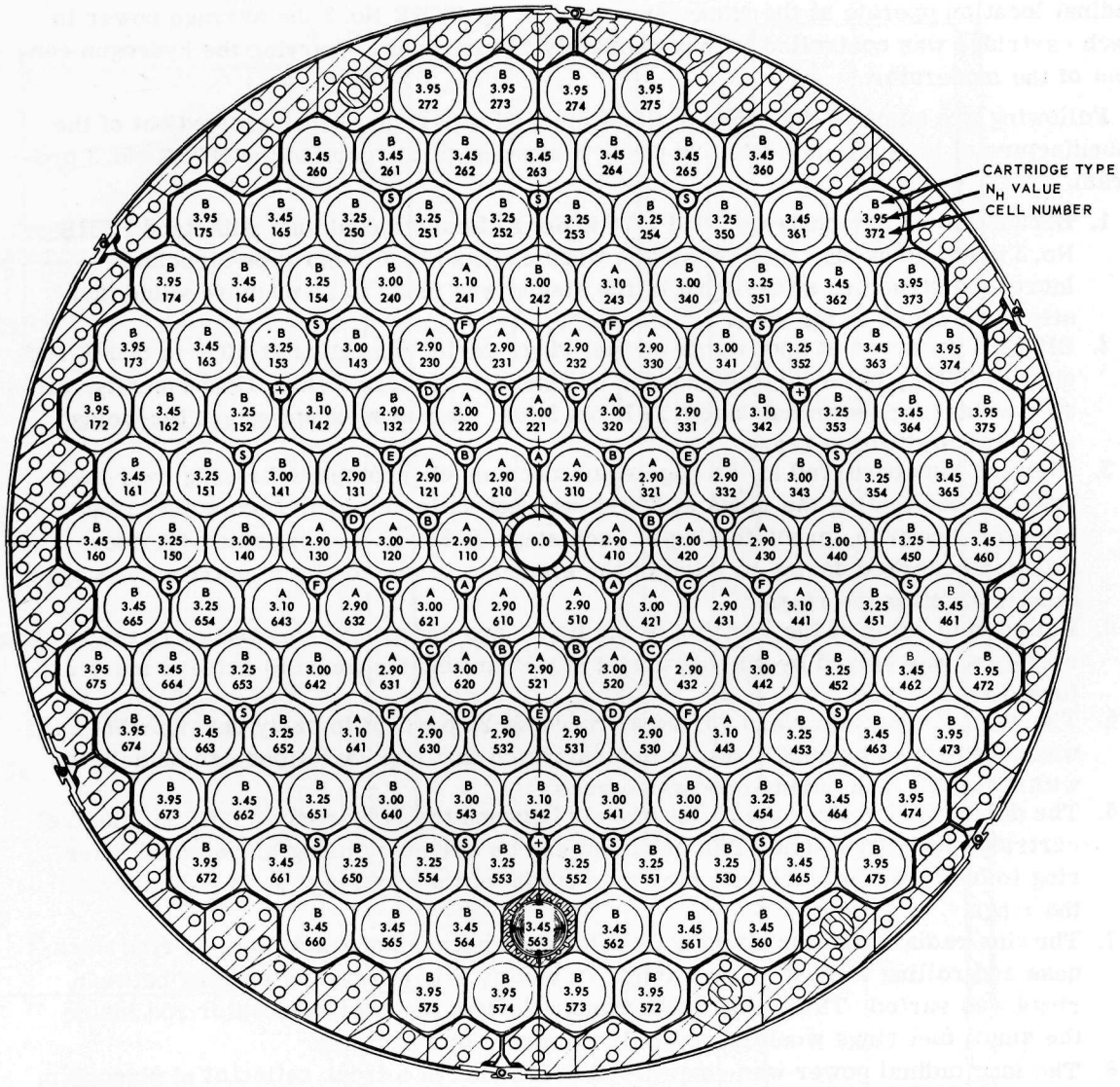

CONTROL RODS

FRAME	TYPE	NUMBER OF RODS
A	SHIM	3
B	SHIM	6
C	SHIM	6
D	SHIM	6
E	SHIM	3
F	SHIM	6
+	DYNAMIC	3
S	SAFETY	15

MODERATOR CELLS

NUMBER OF CELLS	N_H	CARTRIDGE TYPE
24	3.95	B
36	3.45	B
30	3.25	B
9	3.10	A
24	3.00	A
27	2.90	A
1	0	–

Fig. 4.12 – Distribution of control rods, fuel elements, and N_H regions

significantly increased by making the average power of each fuel cartridge identical, by adjusting the longitudinal power so that a fuel cartridge approaches an isothermal temperature, and by equalizing the heat flux from each ring so that all rings at one longitudinal location operate at the same temperature. In HTRE No. 3 the average power in each cartridge was controlled to approximately ±10 percent by varying the hydrogen content of the moderator.

Following are some of the unusual situations and experiences that evolved out of the manufacture of the fuel elements and power flattening of the core in the HTRE No. 3 program.

1. Because tests demonstrated that HTRE No. 1 elements could not withstand HTRE No. 3 dynamic heads, the fuel stages were changed to a comb-type structure. Increased structure at the front of the stages was found to be of more value than structure added at the rear.
2. Blisters occurred at spot welds on fuel rings during operation at 500° to 800°F and above 1700°F, believed to be caused by fissures at these welds. Consequently, all spot welds were eliminated in HTRE No. 3 fuel elements except where the welds were covered with a braze.
3. Blisters also occurred at the edge seals because of incomplete brazing over the edge. Proof-testing the rings at 800°F was not satisfactory in finding fuel ring blisters; however, proof-testing of each stage at 800°F was satisfactory. More blisters occurred during brazing of the elements to the combs in making the stages than in forming the rings.
4. Pulled clad noted at the junction of the fuel rings and combs was traced to the brazing cycle and was solved by placing a heat shield around the piece to achieve more uniform heating.
5. The gap between fuel rings varied as much as 25 percent in early development hardware. Improved brazing fixtures demonstrated that gap variations can be held to within ±0.005 inch during production runs.
6. The desired tolerances could not be held between the larger outer ring and the fuel cartridge insulation tube. This problem can be solved by using an unfueled outer ring to hold the same tolerance on the outside of the cartridge as is held between the rings.
7. The fine radial heat flux could not be flattened because of limitations in ring thickness and rolling radius. In an attempt to modify this effect, the spacing between rings was varied. This is not the optimum design; a center moderator rod inside the small fuel rings would essentially eliminate this problem.
8. The longitudinal power was shaped by the addition of a front reflector of zirconium hydride, thus obtaining a fuel cartridge with a constant hydraulic diameter.
9. Power scallops of more than 20 percent above average were measured. These scallops were reduced to below 10 percent by the addition of borated steel strips to the surface of the insulation liner. This power depression amounted to an estimated 150°F in fuel plate temperature.

4.2.3 MODERATOR

HTRE No. 3 was to have a hollow, hexagonal, hydrided zirconium moderator section with a metal clad on all surfaces, as illustrated in Figures 4.13 and 4.14. Previous design experience with hydrided zirconium and knowledge of its behavior under reactor operating conditions were limited.

Two layers of moderator cladding were to be provided. One layer was to be 0.015 inch of molybdenum for hydrogen retention; the other layer was to be Type 446 stainless steel for external oxidation protection. To provide uniform heat transfer conditions, a continuous metallic bond was needed between the claddings at the zirconium interface.

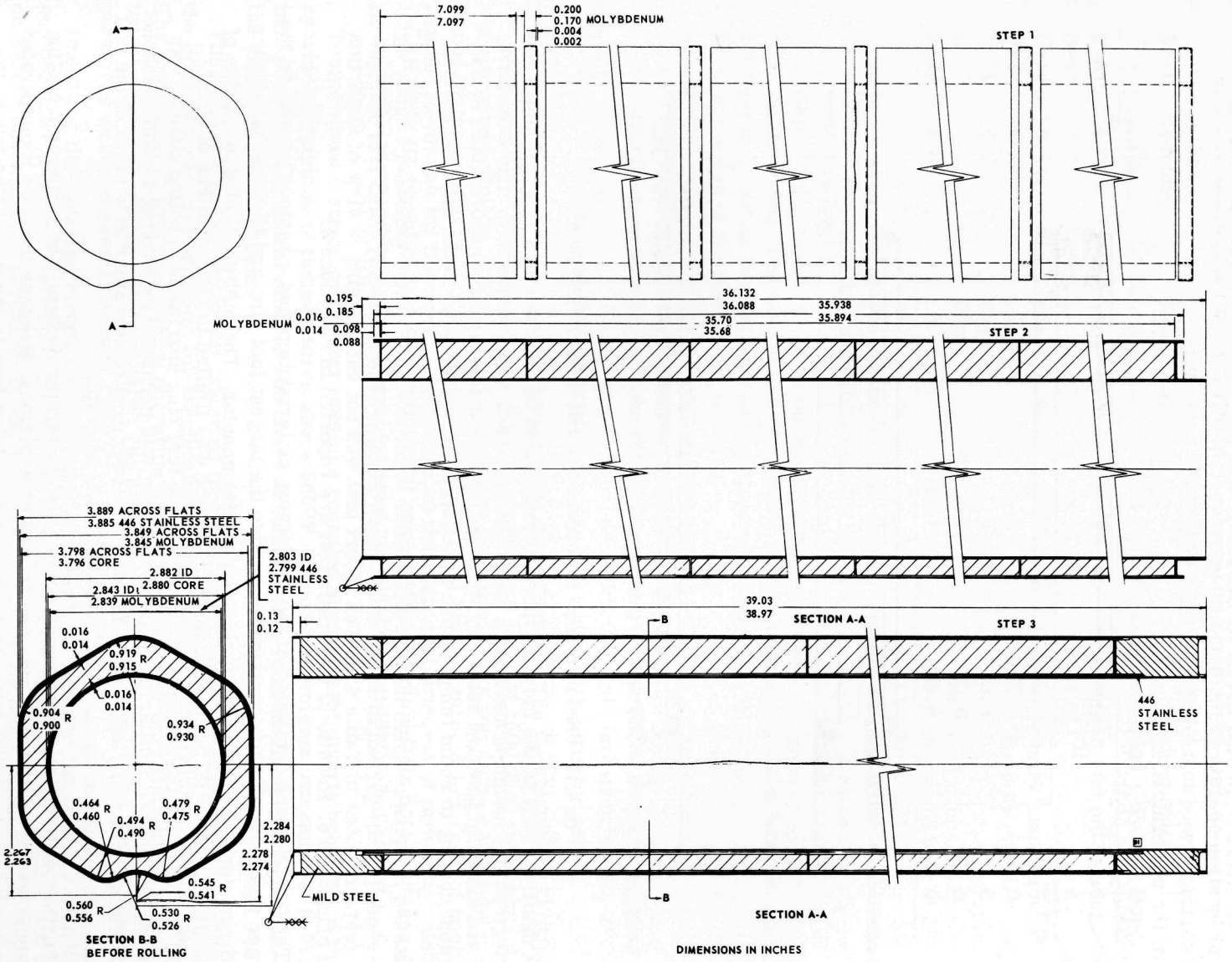

Fig. 4.13 – First three steps in moderator assembly procedure (SK628E660)

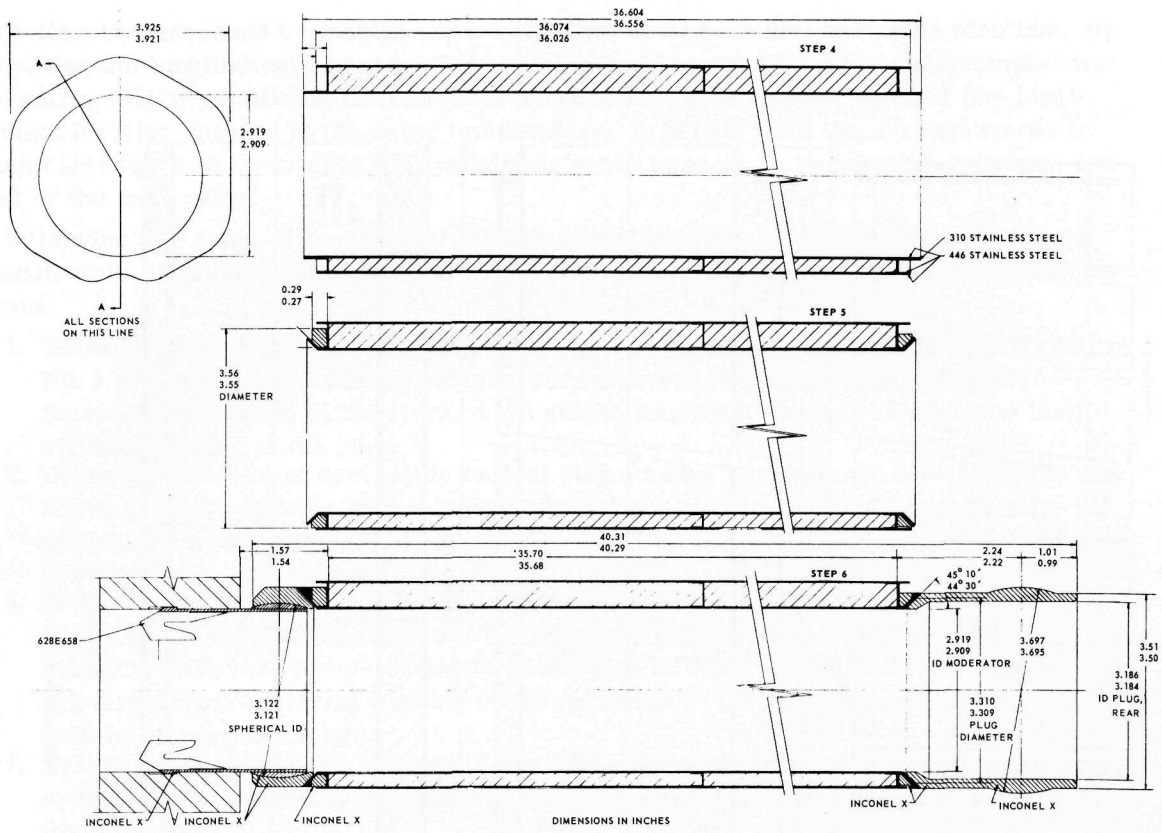

Fig. 4.14 – Final three steps in moderator assembly procedure (SK628E660)

A detailed study of the relative thermal expansions of the claddings and zirconium was performed and a high-temperature fabrication process was investigated. The final forming and sizing of the clad assembly were performed at temperatures above 1000°F. Subsequent cooling to room temperature introduced thermal strains in the clad and core.

A series of clad zirconium assemblies was fabricated for a test in Insert 1B of HTRE No. 2. Limited bonding of the cladding had been achieved for the specimens selected for the test, as noted in Table 4. 3. The insert test was not encouraging in view of distortion and clad failure. Results of the insert test are reported in reference 4.

The temperature limitation of the moderator material imposed a serious penalty on the larger fuel rings of each cartridge, because the largest fuel ring and the internal surface of the moderator cell shared a common cooling annulus. The fuel element was capable of operation at 2000°F, but the moderator surface was limited to temperatures of about 1400°F. Thus the operating temperature of the fuel ring sharing the cooling channel was limited to 1400°F. Similarly, the next fuel ring was penalized by sharing a cooling channel with the largest fuel ring. In this fashion, the operating temperature of several of the fuel rings was penalized by the 1400°F moderator temperature.

Further difficulties were encountered in the moderator design. The moderator cooling channel was not uniform in size and free of obstructions. Because the core was operated in a horizontal position, with the fuel cartridges lying free in the moderator tubes, the manufacturing tolerances and clearances accumulated at the top of the cell and presented a non-uniform channel around the inside diameter of the cell. Also, the cartridge support rails in this channel were obstructions that caused additional cooling problems. In addition, the hexagonal external surfaces of the clad moderator were to be cooled by an annulus

TABLE 4.3

DATA ON HYDROGEN CONTENT AND BONDING OF HTRE NO. 3 MODERATOR SECTIONS SELECTED FOR TESTING IN HTRE NO. 2, INSERT 1B

Part No.	As-Hydrided N_H	Percent Of Area Bonded			
		Hexagonal Exterior		Interior Hole	
		Complete Bond	Partial Bond	Complete Bond	Partial Bond
B-5	4.06	11.4	0	77.4	0
B-11	4.08	1.7	0.7	61.2	0
B-18	4.111	46.4	10.7	90.6	0.8
B-19	4.16	7.3	0	92.7	0
B-21	4.06	26.4	1.0	68.4	0
B-22	4.05	21.5	10.5	90.0	0
B-23	3.99	0.8	22.1	91.6	0

formed by adjacent moderator surfaces. This cooling annulus was far from ideal because of large variations resulting from the following factors.

1. Distance between cell holes in the supporting tube sheets.
2. Clearances required for remote separation of the moderator and the tube sheets.
3. Tolerance across the flats of the moderator sections.
4. Straightness of the moderator sections.
5. Thermal expansion of the supporting tube sheet.
6. Thermal expansion of the moderator section across flats.
7. Bowing of the moderator sections due to temperature differences between opposite flats.
8. Rotation tolerance of the moderator.

The complications of the cooling annuli were compounded by the requirement of cooling the relatively thick moderator wall. With a temperature limit of 1600°F at the midpoint in the zirconium section, the surface temperature was fixed at a lower temperature determined by the conductivity of the material and the local heating rate. A low ratio of cooling surface to volume for the moderator presented the additional problem of providing relatively large coolant passages that operated at lower temperatures than those in parallel passages through the fuel cell. This difference brought about the need for balancing the pressure drop.

Temperature tests on moderator sections revealed a permanent growth behavior of the hydrided zirconium at temperatures above 900°F. Permanent volume increases of 0.010 inch per inch that appeared after 100 hours at temperature introduced additional strains in the cladding and end seals.

The hydrogen in the zirconium migrated from the hotter regions to the colder regions in the body at a rate dependent on the temperature level, temperature gradient, and time. The movement of hydrogen during operation was accompanied by corresponding changes in local power and cooling requirements. The hydrogen tended to accumulate where the temperatures were between 1000° and 1200°F.

Operating the hydrided zirconium at a lower temperature obviated the need for cladding and provided greater precision in the cooling channels. Elimination of the cladding and reduction of operating temperatures brought the design within the scope of immediate capabilities. Hydrogen loss and migration were reduced to acceptable values. Manufacturing problems also came within immediate capabilities; thus the costs and time for production were reduced. The volume previously used for cladding provided room for insulation between the fuel cartridge and the zirconium, and permitted independent cooling channels for each fuel and moderator component.

Figure 4.15, a detail drawing of a typical moderator block, shows the external grooves for the control rod guide tube and the internal cooling slots. Note that the control rod grooves do not extend to the downstream end so that a more uniform cross section for stress considerations exists at the high-temperature end. The cooling slots extend from the exit end to within 0.5 inch of the forward end. This half-inch of material provided a continuous surface for a "push-fit" seal against the support tube of the complete moderator assembly, as shown on Figure 4.16.

Cooling air forward of the fuel rings enters the moderator cooling channels through orifices in the insulation-liner nose section and through slots in the moderator support tube. Cooling air leaving the moderator passes through a channel provided between the moderator tail section and the tube sheet.

During the moderator design and development work, several materials properties were established. Physical properties of the hydrided zirconium were determined and are reported in reference 5. The moderator pieces that contained the most hydrogen ($N_H = 4.0$) were found to be more brittle than pieces hydrided to a lower N_H. The direction of the temperature gradient and its magnitude were of considerable importance to the structural integrity of the hydrided zirconium. Molybdenum was found to be a poorer hydrogen barrier than oxidized stainless steel, and its high neutron-capture cross section and 45-ev resonance level had a pronounced effect on reactivity in this reactor.

A successful procedure for hydriding zirconium was developed. It consisted basically of determining the proper pressure and temperature conditions for particular average hydride levels to be attained. A temperature difference in the furnace of only $5^{\circ}F$ was found to be sufficient to cause the hydrogen content to vary beyond acceptable limits.

4.2.4 REFLECTOR

The relative inability of beryllium, as a reflector material, to absorb thermal shock without cracking was of major concern. However, beryllium samples subjected to various temperature gradients for numerous cycles were found to be more sound than anticipated. Restrained temperature gradients of $40^{\circ}F$ were expected to cause damage, but thermal shock tests introducing temperature gradients of as much as $200^{\circ}F$ caused no damage to the test samples.

Voids in the reflector were not as significant as once thought. Essentially no difference in reactivity was observed in tests in which materials with and without voids were stacked over the reflector.

4.2.5 CONTROL RODS

The original specifications called for boron carbide control rods. Early in the program, however, because of the reactivity of B_4C with available clad material at temperatures above $1200^{\circ}F$, the poison material was changed to europium oxide. Europium oxide in a nickel-chromium matrix was found to grow at high temperatures if exposed to oxygen. In addition to this problem, trapped gas caused bulging of the poison segments. End caps were attached to eliminate the gas expansion as the rod temperature increased.

The control rod slugs are made up of a casing and a matrix of europium oxide and nickel. The density of the matrix must be as high as possible so that the size of the rod is not excessive. Procedures consisting mostly of swaging and compressing techniques were developed wherein 95 percent of theoretical maximum density of this material was achieved. Originally it was thought that the rods had to be centrally grouped in a flight-type design, but the critical experiment revealed that the rod pattern should extend over the entire core.

An extensive investigation of bearing friction at temperature was conducted to insure that parts required to slide during operation did not stick at temperature.[6]

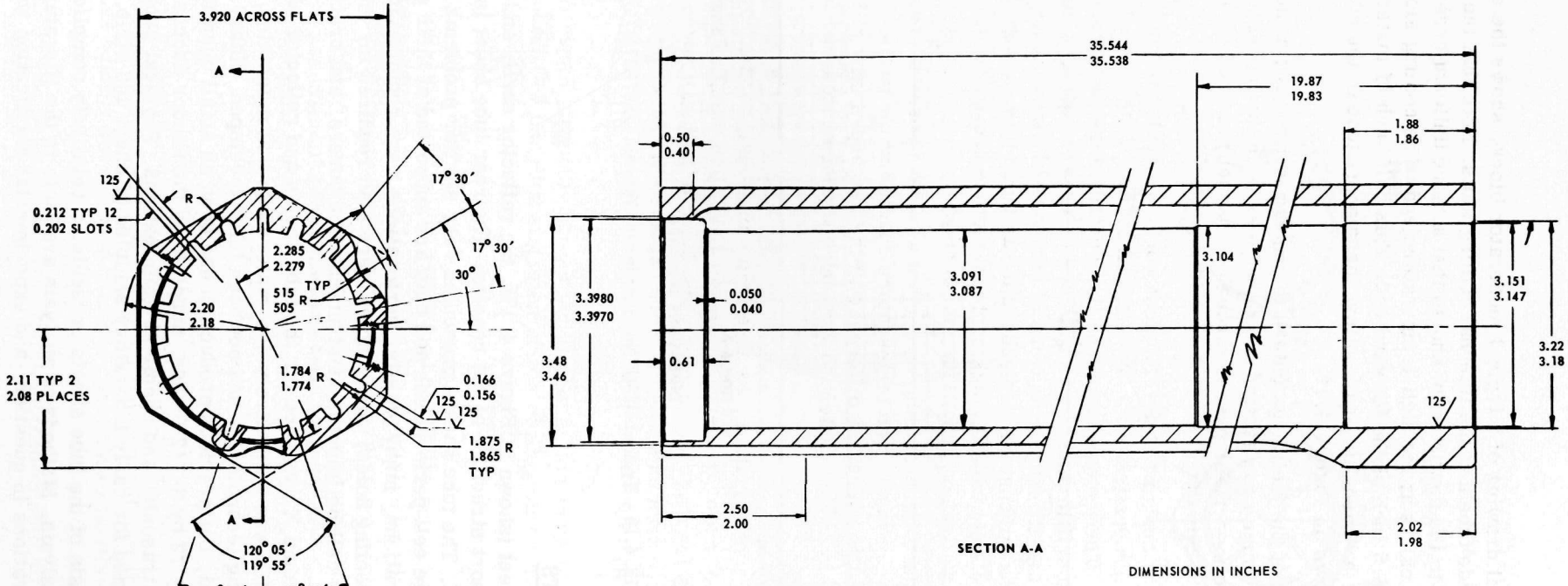

Fig. 4.15 – Typical moderator blocks (665D192)

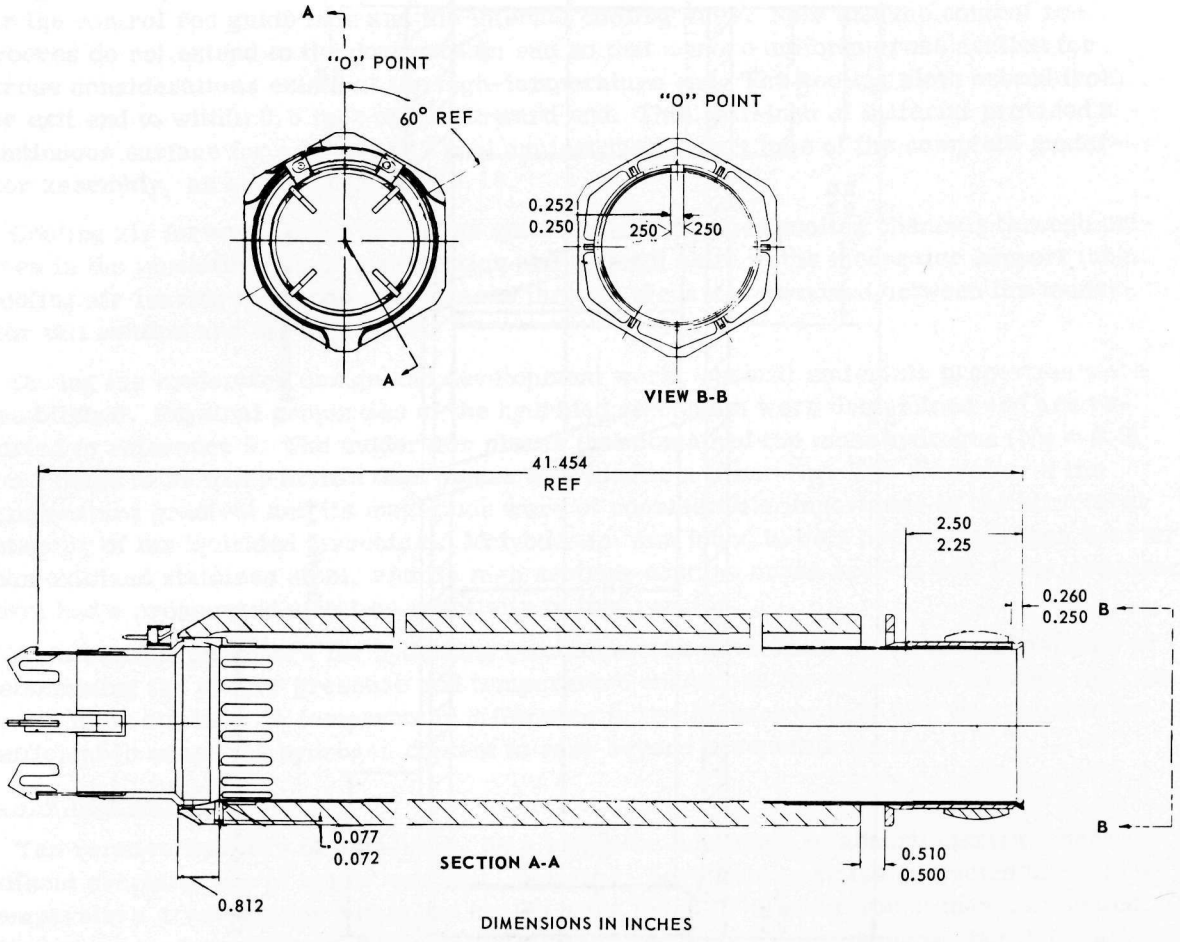

Fig. 4.16 – Typical HTRE No. 3 moderator assembly (567E776)

4.2.6 TUBE SHEETS

The front tube sheet (shown in Figure 4.17), the reflector shell, and the rear tube sheet form the basic support structure of the reactor. The rear tube sheet is about the same as the front tube sheet. The tube sheets presented very similar problems since both are flat plates with 151 large cell perforations and both are supported at their perimeter. In addition to cell perforations, many smaller perforations were required for control rod passages and special cooling holes; tapped holes were also required for mounting special components such as cell bellmouths, instrumentation covers, and brackets.

Age-hardened Inconel X was used for the tube sheets and reflector shell. For these applications Inconel X was a relatively new material in that machining, forming, heat treating, and welding technologies had not been fully developed. Heavy plates without flaws were required, but previous production had been on small quantities of sheet and strip. Plates, 72 by 72 by 3-1/2 inches, supplied by the vendor successfully passed a series of X-ray, ultrasonic, and chemical examinations. Physical properties essentially equaled those obtained for early laboratory samples of sheet and strip.

The stress analysis of the tube sheets presented a relatively complicated problem in perforated plate analysis. Methods of analysis available in the literature were not intended for the large perforations in question, and experimental verification was not available.

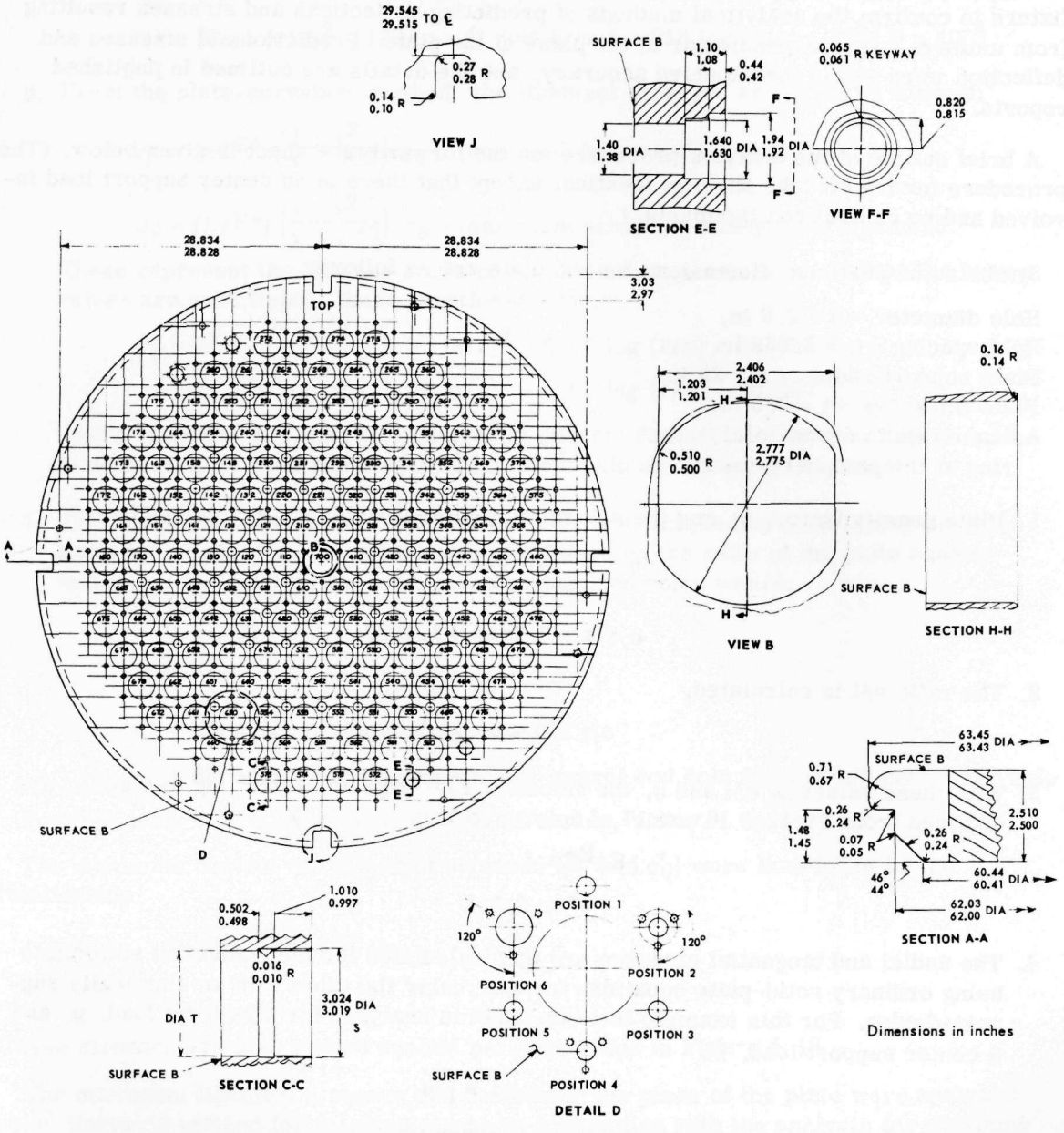

Fig. 4.17 – Front tube sheet detail (Dwg. 628E631)

Also, the analysis was complicated by the requirement for the adjacent holes of unequal size.

A full-size test plate of low carbon steel was prepared and tested in a hydrostatic test fixture to confirm the analytical methods of predicting deflections and stresses resulting from uniform loads perpendicular to the plane of the plate. Predictions of stresses and deflection were within the expected accuracy, and the details are outlined in published reports.[7]

A brief outline of the analysis procedure for the forward tube sheet is given below. (The procedure for the aft tube sheet is identical except that there is no center support load involved and no control rod ligaments.)

Symbols and pertinent dimensions for the plate are as follows:

Hole diameter = d = 2.9 in.
Hole spacing = s = 3.953 in.
Plate support radius = a = 29 in.
Plate thickness = t = 2.5 in.
Assumed width of the solid ring at the periphery = 4 in.

1. Plate density factor, η, and the equivalent ligament width, c, are calculated.

$$\eta = \frac{s - d}{s} = 0.267$$

$$c = s - 0.952d = 1.1953$$

2. The ratio c/t is calculated.

$$c/t = 0.478$$

3. With these values of c/t and η, the values of E/E^* and ν^*, according to Malkin, are obtained from Figures 16 and 17 of reference 7.

$$E/E^* = 5.1$$

$$\nu^* = 0.212$$

4. The radial and tangential stresses are then calculated for the equivalent solid plate using ordinary solid-plate equations for a circular flat plate with an elastically supported edge. For this example the tube sheet is analyzed for a uniform load, p, and a center support load, P.

$$p = 34.6 \text{ psi}$$

$$P = 14,000 \text{ lb}$$

For the uniform load, the radial and tangential stresses are

$$\sigma_{er} = [162.1\,(r/a)^2 - 129]\,p$$

$$\sigma_{e\Theta} = [82.1\,(r/a)^2 - 129]\,p$$

For the center support load, the radial and tangential stresses are

$$\sigma_{er} = [-1.094\,(a/r) + 928 \log (r/a) + 250.2]\,P \times 10^{-4}$$

$$\sigma_{e\theta} = [1.094\,(a/r) + 928 \log (r/a) - 352]\,P \times 10^{-4}$$

5. These stresses are then combined by superposition to obtain the stresses in the equivalent solid plate that result from the combined load.

$$\sigma_{er} = [162.1\ (r/a)^2 - 129]\ p - [-1.094\ (a/r)^2 + 928 \log (r/a) + 250.2]\ P \times 10^{-4}$$

$$\sigma_{e\theta} = [82.1\ (r/a)^2 - 129]\ p - [1.094\ (a/r)^2 + 928 \log (r/a) - 352]\ P \times 10^{-4}$$

6. From the plate-curvature method, the ligament stresses are found as follows:[7]

$$\sigma_r = (E/E^*)\left(\frac{1 - \nu^2}{1 - \nu^{*2}}\right)\sigma_{er} = \text{maximum stress of a radial ligament}$$

$$\sigma_\theta = (E/E^*)\left(\frac{1 - \nu^2}{1 - \nu^{*2}}\right)\ \sigma_\theta = \text{maximum stress of a tangential ligament}$$

These represent the limiting cases of a ligament stress envelope. When the known values are substituted, these equations become:

$$\sigma_r = 29,200\ (r/a)^2 + 7.97\ (a/r)^2 - 6760 \log (r/a) - 25,050$$

$$\sigma_\theta = 14,780\ (r/a)^2 - 7.97\ (a/r)^2 - 6760 \log (r/a) - 20,960$$

These equations are then plotted against percent radius, as shown in Figure 4.18, to obtain the location and magnitude of the maximum ligament stresses.

7. The maximum control rod ligament stresses are obtained by multiplying the main ligament stresses by an empirical factor based on the ratio of the plate density factor, η, for the large holes and the control rod holes where:

$$\eta' = \frac{s' - d + \frac{d'}{2}}{s'}$$

d' = diameter of the control rod hole

s' = distance between centers of a control rod hole and the adjacent large hole

For this case, $s' = 2.28$ inches, $d' = 1.023$ inches, and $\eta' = 0.14$.

The maximum control rod ligament stresses (σ'_r and σ'_θ) were then found by the relationship

$$\sigma'_r = \sigma_r \frac{\eta}{\eta} = 1.906\ \sigma_r$$

$$\sigma'_\theta = \sigma_\theta = 1.906\ \sigma_\theta$$

These stresses are also plotted against percent radius in Figure 4.18.

The maximum ligament stresses due to loads in the plane of the plate were analyzed using Horvay's method for in-plane stress in conjunction with the analysis for obtaining the principal stresses caused in a solid plate by its own weight, when supported in a vertical plane by concentrated shear forces at the ends of the horizontal diameter.

The following is an outline of the procedure followed:

1. The weight load of the moderator plus the weight of the tube sheet itself are treated as uniformly distributed vertical body forces acting on the equivalent solid plate.
2. For this loading the principal stresses are calculated for the equivalent solid plate.
3. The maximum ligament stresses are then calculated by multiplying the numerically larger principal stress of the equivalent solid plate by Horvay's magnification factor.

Figure 4.19 is a plot of the maximum ligament stresses of the rear tube sheet due to in-plane loads for the X211 at 100 percent engine speed.

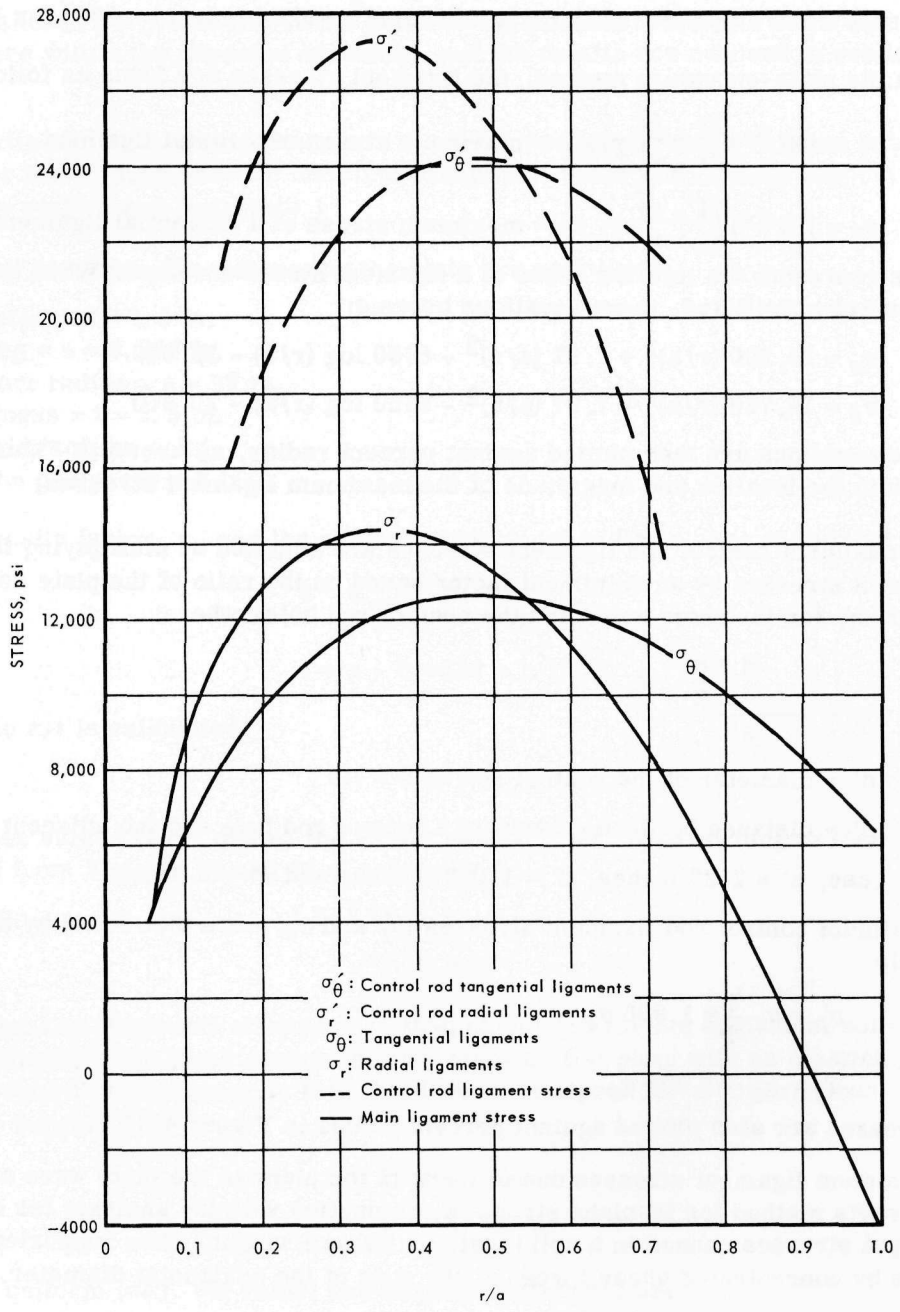

Fig. 4.18 – Maximum ligament stresses in the front tube sheet

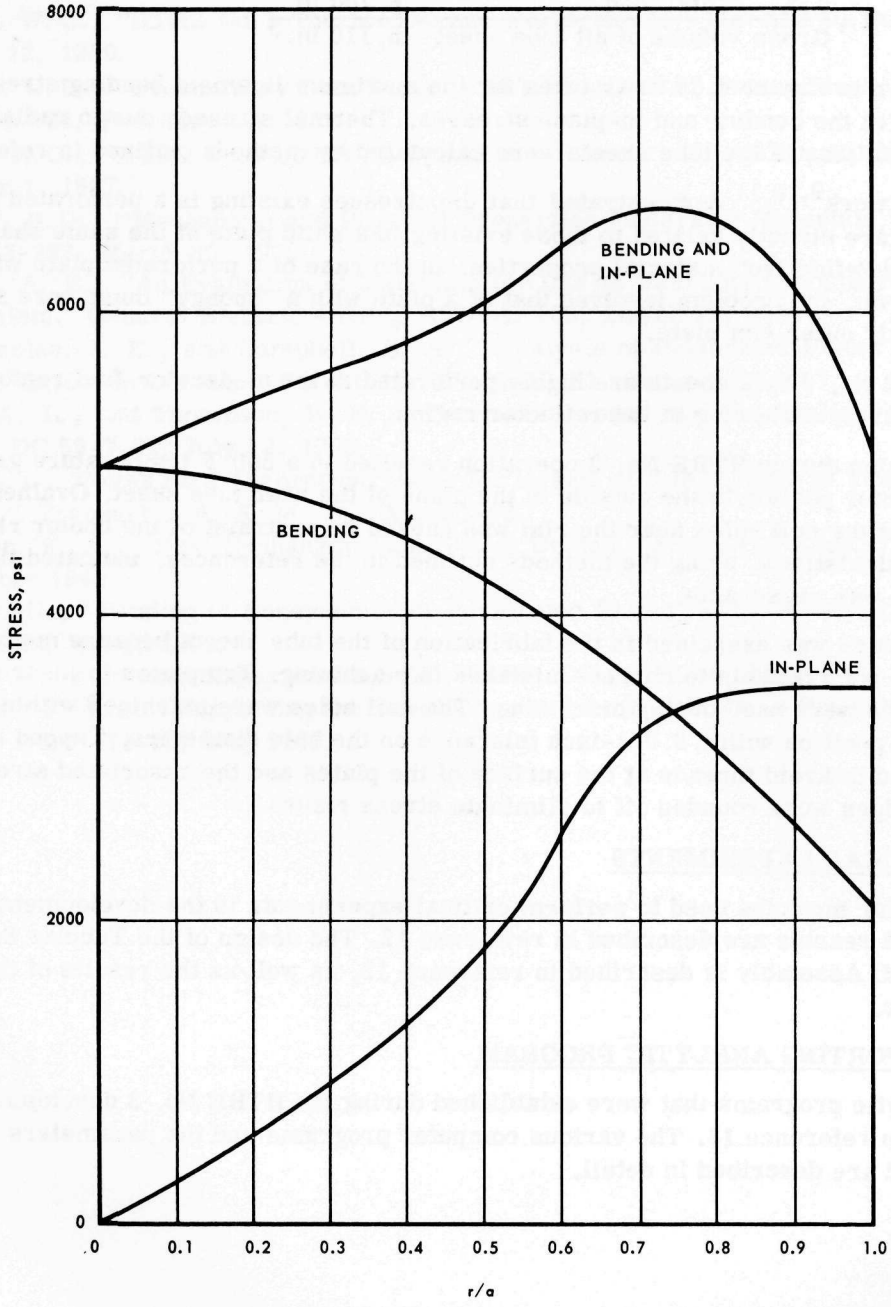

Fig. 4.19 – Maximum ligament stresses in the rear tube sheet

For this case the maximum temperature is 1400°F.

$$\eta = \frac{s - d}{s} = \frac{3.953 - 3.7}{3.953} = 0.064$$

$$p = \frac{\text{Total load}}{\text{Gross volume of aft tube sheet}} = \frac{6,700 \text{ lb}}{5,110 \text{ in.}^3}$$

Also shown in Figure 4.19 are curves for the maximum ligament bending stresses and for the sum of the bending and in-plane stresses. Thermal stresses due to radial temperature gradients in the tube sheets were calculated by methods outlined in reference 8.

Previous work[9,10,11] demonstrated that the stresses existing in a perforated plate (tube sheet) are directly related to those existing in a solid plate of the same shape, but with reduced "effective" material properties. In the case of a perforated plate with an unperforated rim, the problem involves that of a plate with a "spongy" inner core surrounded by a "normal" outer rim plate.

The HTRE No. 3 tube sheets are highly perforated in the moderator-fuel regions, but have a relatively solid ring in the reflector region.

An excursion during HTRE No. 3 operation resulted in a 500°F temperature gradient from the center portion to the outside in the plane of the rear tube sheet. Ovalness of 0.005 inch in the cell holes near the rim was caused by restraint of the cooler rim. Post-operation calculations, using the methods outlined in the references, indicated that the deformation was reasonable.

Extreme care was exercised in the fabrication of the tube sheets because methods of repair were not available to correct mistakes in machining. Templates to insure correct hole positions were used during machining. The cell holes were machined within 0.003 inch of true position with a 0.001-inch tolerance on the hole diameters. Tapped holes were counterbored to avoid threads at the surface of the plates and the associated stress risers. All sharp edges were rounded off to eliminate stress risers.

4.2.7 CRITICAL EXPERIMENTS

The nuclear mockups used to perform critical experiments in the development of the HTRE No. 3 reactor are described in reference 12. The design of the Tubular Solid Moderator (TSM) Assembly is described in reference 12, as well as the results of the critical experiments.

4.2.8 SUPPORTING ANALYTIC PROGRAM

The analytic programs that were established during the HTRE No. 3 development are described in reference 13. The various computer programs and the parameters that were investigated are described in detail.

4.3 REFERENCES

1. Schoenberger, T. W., "102 Project Data Book - 8th Issue," GE-ANPD, DC 59-8-22, July 29, 1959.
2. Powell, W. C., "HTRE No. 3 Thermodynamic Performance," GE-ANPD, DC 60-8-67, August 12, 1960.
3. Cannon, C. B., "Preliminary Data Report - IET 25 - D102A2 Power Plant," GE-ANPD, DC 61-2-724, February 10, 1961.
4. Evans, R. C., "HTRE No. 2 Insert 1B Operations Report," GE-ANPD, XDC 57-10-26, October 1, 1957.
5. Decker, H. D., "Mechanical and Physical Properties Moderator Materials," GE-ANPD, DC 59-3-227, March 30, 1959.
6. Alonzo, A. E., "An Evaluation of Materials for Use as Bearings in a Control Rod Mechanism," General Electric - GEL, R57-GL-105, March 21, 1957.
7. McConnelee, J. E., and Campbell, K. A., "Analysis of Perforated Plates of Triangular Layout in Bending," GE-ANPD, DC 57-10-53, October 8, 1957.
8. Ross, A. L., and Thompson, B. K., "Thermal Stresses in a Composite Disc," GE-ANPD, DC 55-7-67, July 12, 1955.
9. Malkin, I., "Notes on a Theoretical Basis for Design of Tube Sheets of Triangular Layout," Transact of A. S. M. E., April 1952.
10. Gardner, K. A., "Heat Exchanger Tube Sheets Design," Journal of Applied Mechanics, December 1948.
11. Horvay, G., "Bending of Honeycombs of Perforated Plates," Journal of Applied Mechanics, March 1952.
12. "HTRE No. 3 Critical Experiments," GE-NMPO, DC 61-11-14, May 1962.
13. "Analytic Programs Supporting the Development of the HTRE No. 3 Reactor," GE-NMPO, DC 61-11-15, May 1962.

5. SHIELD

5.1 OBJECTIVES AND REQUIREMENTS

The primary function of a reactor shield is to protect the environment around the reactor system to the extent that neutron and gamma radiation levels are within tolerable or prescribed limits, while simultaneously maintaining its own integrity.

Additional objectives and requirements are:

1. Minimum weight.
2. A minimum pressure loss of the primary coolant while passing through the shield.
3. A minimum deviation of the flow distribution to the reactor fuel elements from a specified flow distribution.
4. A minimum quantity of secondary coolant to be utilized for dissipation of heat generated within the shield.

The shield system of the HTRE No. 3 reactor is comparable to a number of tanks containing alternating layers of water and lead with an auxiliary system for dissipating the generated nuclear heat. Since this auxiliary system is independent of the primary reactor circuit, it does not influence the performance of the reactor system. Factors which have major influences on the system performance include:

1. Pressure loss in the scrolls and ducts passing through the shields.
2. Flow distribution to the reactor fuel elements as provided by the ducts and plenums at the forward and aft ends of the reactor.

The design specifications for airflow passages through the shield plugs called for pressure drops not to exceed the following:

Airflow Station	Pressure Loss, psi	
	X39-5	X211
3.2 to 3.4	2.5	3.2
3.4 to 3.5	1.0	3.4
3.6 to 3.7	0.8	3.63

(Airflow stations are defined in Figure 5.1.)

Similarly, the specifications for fuel element flow distribution stated that the flow per tube for a cold reactor should not deviate from the average by more than 3 percent.

The shield system for the HTRE No. 3 reactor is described in detail in reference 1.

In general, the HTRE No. 3 environmental radiation constraints were that radiation levels 18 hours after shutdown should be less than 0.2 r/hr at locations near accessories and engines. The gamma radiation listed below refers to 18 hours after shutdown after

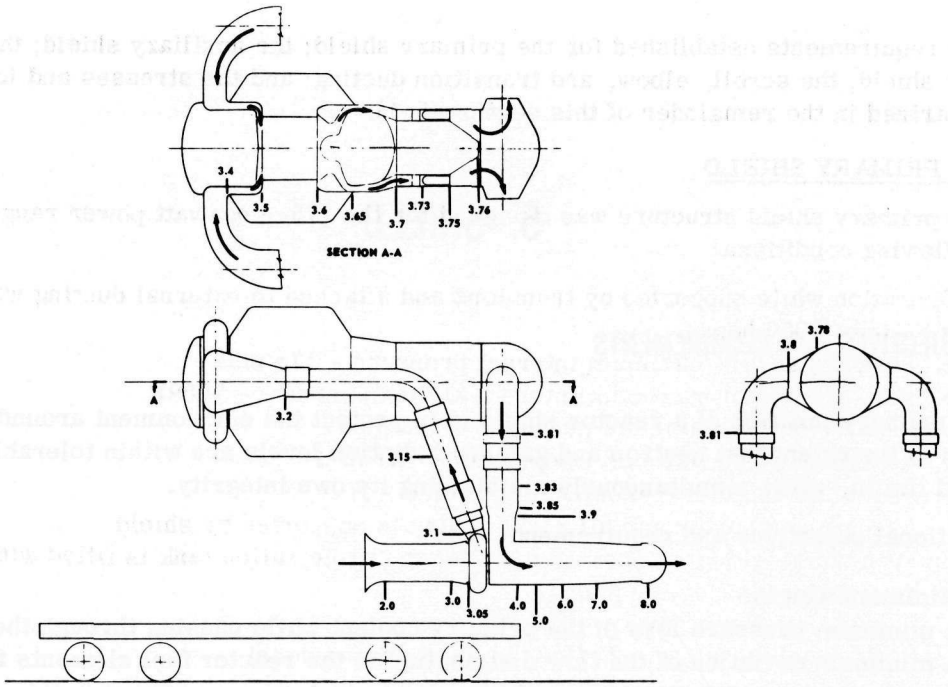

Fig. 5.1 – HTRE No. 3 airflow stations

100 hours of continual operation at a power level of 175 megawatts. During operation at that power level the dose rate at any point on the shield surface should not exceed 1000 r/hr. The specific radiation level requirements for the HTRE No. 3 shield at four locations are given below.

1. At the surface of the lower quadrant of the radial shield

Fast neutrons	10^4 rep/hr
Thermal neutrons	3×10^7 nv
Gammas (after 18 hours)	0.5 r/hr

2. At the surface of the upper quadrant of the radial shield

Fast neutrons	10^5 rep/hr
Thermal neutrons	3×10^8 nv
Gammas (after 18 hours)	2.0 r/hr

3. At the surface of the side quadrants of the radial shield

Fast neutrons	10^4 rep/hr
Thermal neutrons	6×10^7 nv
Gammas (after 18 hours)	2.0 r/hr

4. At the outer surface of the front shield plug (including the effect of duct streaming)

Fast neutrons	10^6 rep/hr
Thermal neutrons	3×10^9 nv
Gammas (after shutdown)	0.6 r/hr

These specifications were determined for a reactor maximum power of 175 megawatts with X211 turbojets. When operating on X39-5 engines, the power level is approximately 35 megawatts.

A more detailed discussion of the nuclear requirements for the HTRE No. 3 shield is contained in reference 2.

The requirements established for the primary shield; the auxiliary shield; the combustor shield; the scroll, elbow, and transition ducting; and the stresses and loads are summarized in the remainder of this section (5.1).

5.1.1 PRIMARY SHIELD

The primary shield structure was designed for the 175-megawatt power range under the following conditions:

1. Operation while supported by trunnions and attached to external ducting with a service life of 1000 hours.
   a. Forward scroll maximum internal pressure - 175 psia
   b. Forward scroll maximum internal air temperature - 700°F
   c. Reactor outlet maximum pressure - 140 psia
   d. Reactor outlet maximum temperature - 1600°F
   e. Maximum structural metal temperature - 1000°F
   f. Assume combustor and all outlet piping is supported by shield
2. Handling of shield after operation and when augmentation tank is filled with mercury.
   a. Internal pressures - 0 psig
   b. Internal air temperature - 150°F
   c. Upward acceleration - 2g (load applied at trunnions)
   d. Fore and aft accelerations - ±1.0g
   e. Lateral accelerations - ±1.0g
3. Shield rotatable 360 degrees while supported by trunnions when augmentation tank does not contain mercury.
4. Shield not rotatable more than ±5 degrees from the normal horizontal attitude while the augmentation tank contains mercury.
5. Loads due to accelerations will be short time only.
6. The reactor-shield assembly (front shield plug and core assembly) designs to permit remote removal and assembly.
7. The pressure shell, forward scrolls, and front and rear shield plug designs to allow replacement of the plugs with flight-type plugs.
8. Drains, fill lines, and internal distribution systems for water and mercury systems in the shield.
9. Accommodate instrumentation of core, shield plugs, and tank.
10. Shield water purity - Maximum allowable impurities and minimum specific resistance shall be as given in column I below (GE-ANPD Specification A50T2001 Grade B). The shield water shall be replaced after contamination reaches the limits set forth in column II below:

Analysis	I	II
Total solids, ppm	8.0	15.0
Al, ppm	0.005	
Ca, Mg, Na, ppm	2.0	4.0
CO_2, ppm	2.0	
SiO_2, ppm	2.0	4.0
Cl, ppm	0.25	0.50
SO_4, ppm	0.50	0.75
Cu, ppm	0.025	0.05
Fe, Ni, Co, ppm	0.20	1.0
B, Cd, ppm	0.10	
pH	5.5 - 7.0	
pH Control	HNO_3	
Specific resistance at 75°F, ohm/cm^3	100,000+	40,000

11. A hydrostatic proof test of the shield internal air passages, before operation, of 190 to 200 psig without yield in any member.
12. The front shield plug supports the center of the core forward tube sheet for axial loads.
13. The front shield plug and core assembly allows the control rods to be in position in the core and in operable condition during the fuel loading operation for the Initial Criticality Experiment.
14. Rear shield area maximum gas temperature is 1600°F.

5.1.2 AUXILIARY SHIELD

The design requirements for the auxiliary shield were also for the 175-megawatt power level under the following conditions:

1. It surrounds the primary reactor-shield assembly using lead, a mixture of borated water and ethylene glycol, and boral (radially outward).
2. It allows contact maintenance and replacement of radiation instrumentation in the side shield and control rod actuators.
3. The lower portion is fixed to and supported by the dolly superstructure. The upper portion is remotely removable. A hoisting load factor of 2.0 is assumed for the design of the upper portion.
4. A 150-gallon auxiliary tank is included in the upper portion of the shield to allow for thermal expansion of the borated water and the ethylene glycol mixture.
5. The lower portion of the shield includes the trunnion supports and the forward support of the primary shield.

5.1.3 COMBUSTOR SHIELD

The combustor shield design included these requirements:

1. Surround the combustor assembly while providing access to fuel nozzles and thermocouples. Shielding materials (radially outward): water, lead, and water.
2. A water system to circulate 13 gallons per minute, serving as coolant as well as shielding.
3. Contact maintenance and replacement for fuel nozzles, thermocouples, etc., in the combustor.
4. The lower portion bolted to and supported by the dolly superstructure. The upper portion is remotely removable. A hoisting load factor of 3.0 is assumed for the upper portion.
5. A nominal clearance of 4 inches between the primary and the auxiliary shield. Additional clearance locally as required for piping, clamps, actuators, etc., located between the shields and on the combustor.

5.1.4 SCROLL, ELBOW, AND TRANSITION DUCTING

The transition ducts, connecting the elbows with the inlet ducts mate to X39-5 engines. The elbow ducts alone would mate to X211 engines.

The foregoing specifications are contained in greater detail in reference 1.

5.1.5 STRESS CRITERIA AND LOADS

The general criteria governing the stress analysis of the HTRE No. 3 shield components are:

1. For steady-state limit loads the allowable stress conditions are:
   a. $F_t = 0.80\ F_{ty}$ for stainless steels.
   b. $F_{tu} = 0.66\ F_t$ for Inconel X.
   c. $F_t = 0.66\ F_R$ for all structural materials, where F_R is the applicable stress-to-rupture value and where $0.66\ F_R$ is less than a or b.

d. $F_s = 0.60\ F_t$ for all structural materials, where F_t is allowable tensile stress, F_{tu} is ultimate tensile stress, F_{ty} is tensile yield stress, and F_s is allowable shear stress.

2. The stress allowable at welds is 90 percent of the applicable stainless steels and Inconel X allowables.
3. Components subject to instability failure are analyzed at a factor of 1.5 times the limit load under operating conditions. The margin of safety is the ultimate stress or load for this condition compared to the limit load or stress.
4. Margins of safety for stresses from mechanical loads are calculated by comparing the maximum principal stress to F_t and/or the maximum shear stress to F_s.
5. When thermal stresses are present, and the combination of thermal and mechanical stresses are not below the allowable stress, a margin of safety (MS) from combined stresses is calculated :

$$MS = \frac{1}{\frac{f_{th}}{2\ F_t} \frac{f_m}{F_t}} - 1$$

where: f_m = maximum stress for mechanical loads
f_{th} = maximum thermal stress calculated elastically
F_t = allowable tensile stress

Greater details on stresses and loads in the HTRE No. 3 reactor shield, and source material from which these data were derived, are contained in references 3 through 8.

5.2 DESIGN DESCRIPTION

5. 2. 1 MECHANICAL DESIGN

5. 2. 1. 1 Over-all Assembly

Shielding for the HTRE No. 3 assembly is composed of the primary (side) shield shown in Figure 2. 3, which consists of three assemblies, and external auxiliary shields, shown in Figures 5. 2 and 5. 3, which radially enclose the primary shield and the combustor.

The primary shield surrounds the core radially, and includes the front and rear shield plugs which allow airflow into and out of the core. The primary shield is designed to demonstrate a flight-type envelope and structure but is not constructed of flight-type shield materials.

The shield inlet scroll, together with the elbows and transition ducting, also shown in Figure 2. 3, are considered part of the shield assembly.

Figure 5. 4 shows the general arrangement of the primary and auxiliary shields.

5. 2. 1. 2 Front Shield

The front shield plug, shown in Figure 5. 5, forms the inside of the inlet air passage, mounts the control rod actuators, and provides sufficient radiation attenuation so that auxiliary shielding is not necessary in this area. It consists of a cylindrical connection between front and rear heads, containing lead slabs and water. The front face is made of 304 stainless steel, the rear head and cylinder of Inconel X, and the lead slabs are canned in 304 stainless steel.

The rear face is connected by 66 structural tubes to the front face. The tubes act as compression members in transferring external air pressure loads from the rear face to the header. Of these tubes, 45 are also designed and situated in such a way as to provide access for and support to the control rods which pass through the front shield plug.

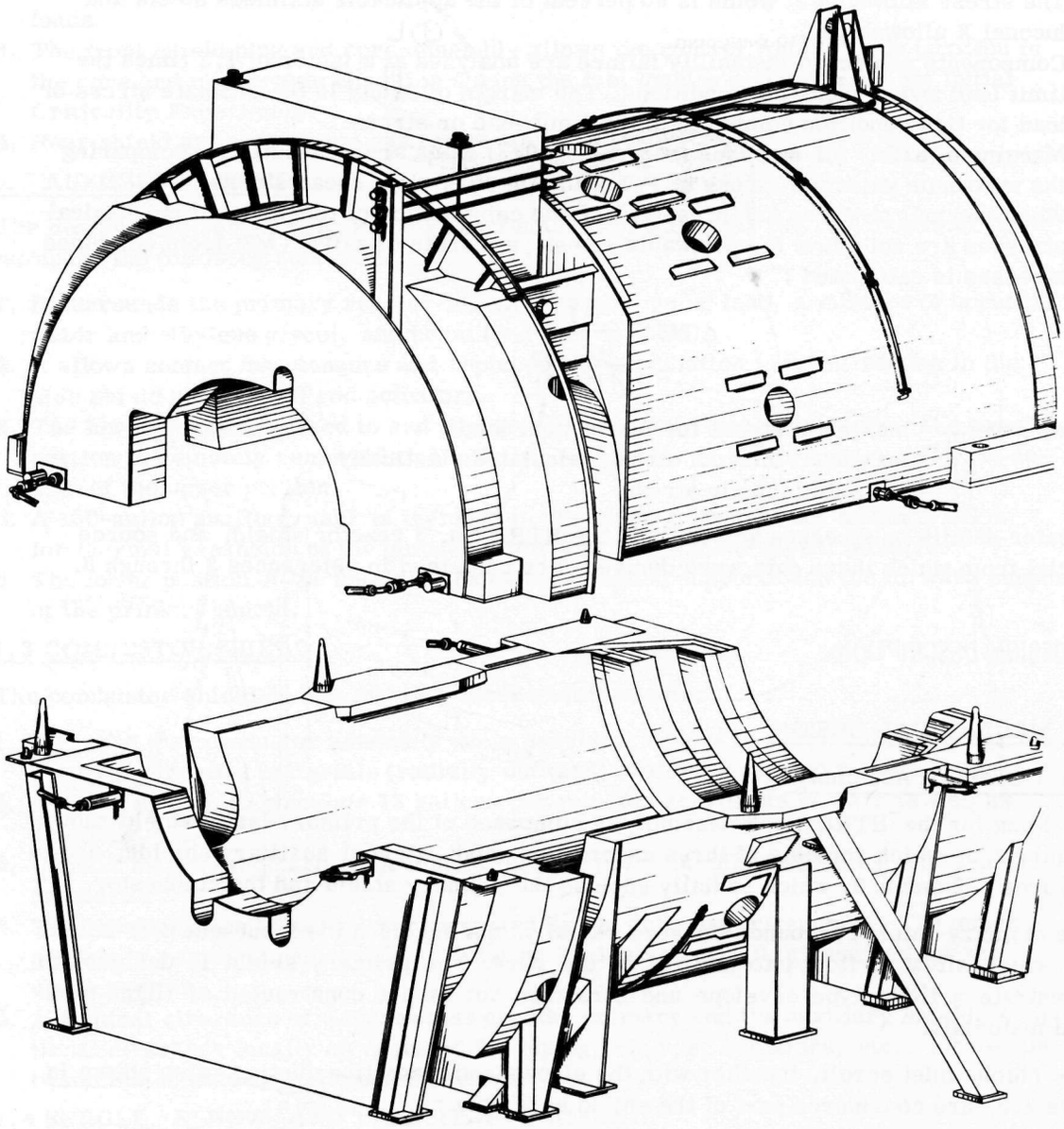

Fig. 5.2 – External auxiliary shield

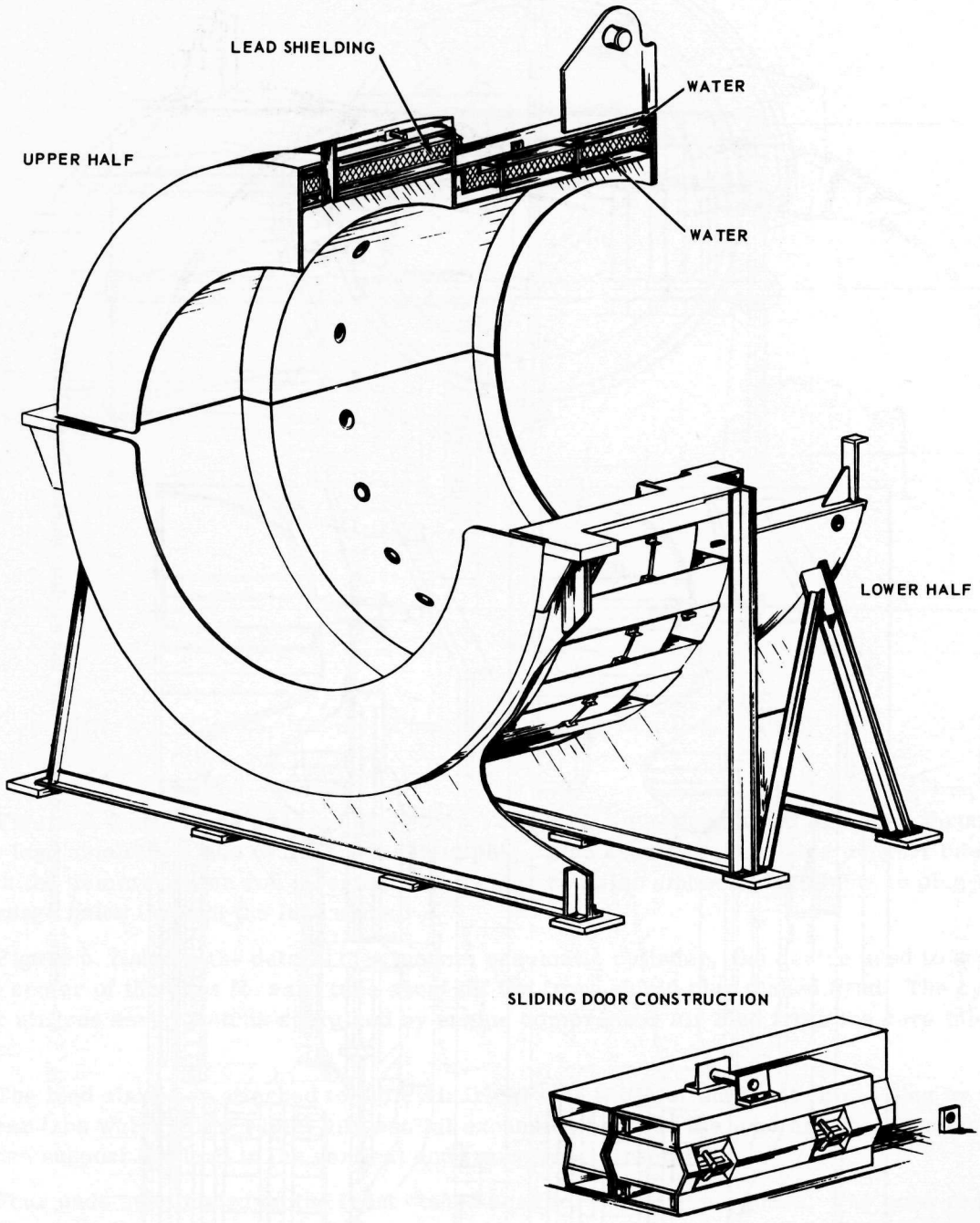

Fig. 5.3 – Combustor shield

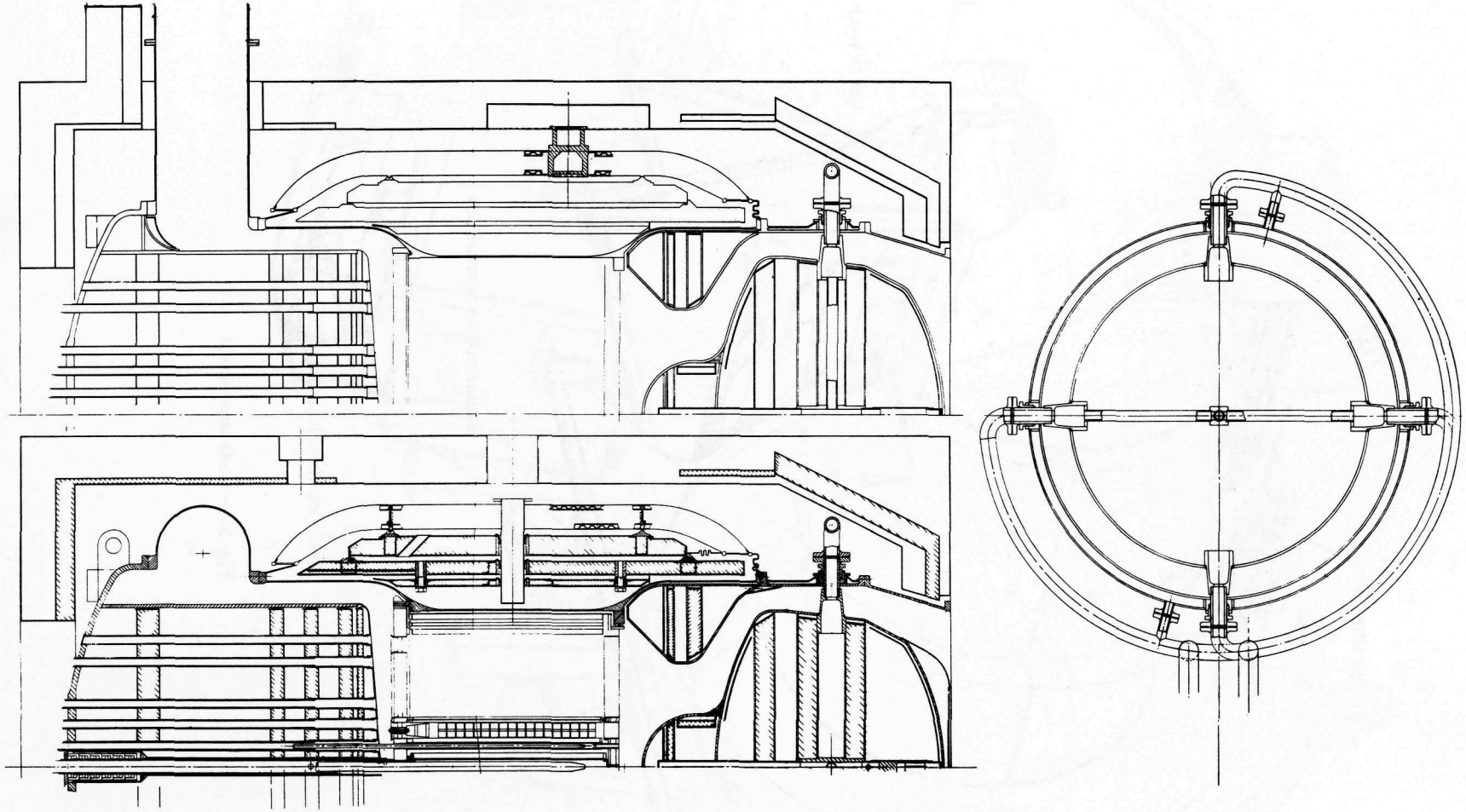

Fig. 5.4 – General arrangement of the primary and auxiliary shields (Dwg. 133R633)

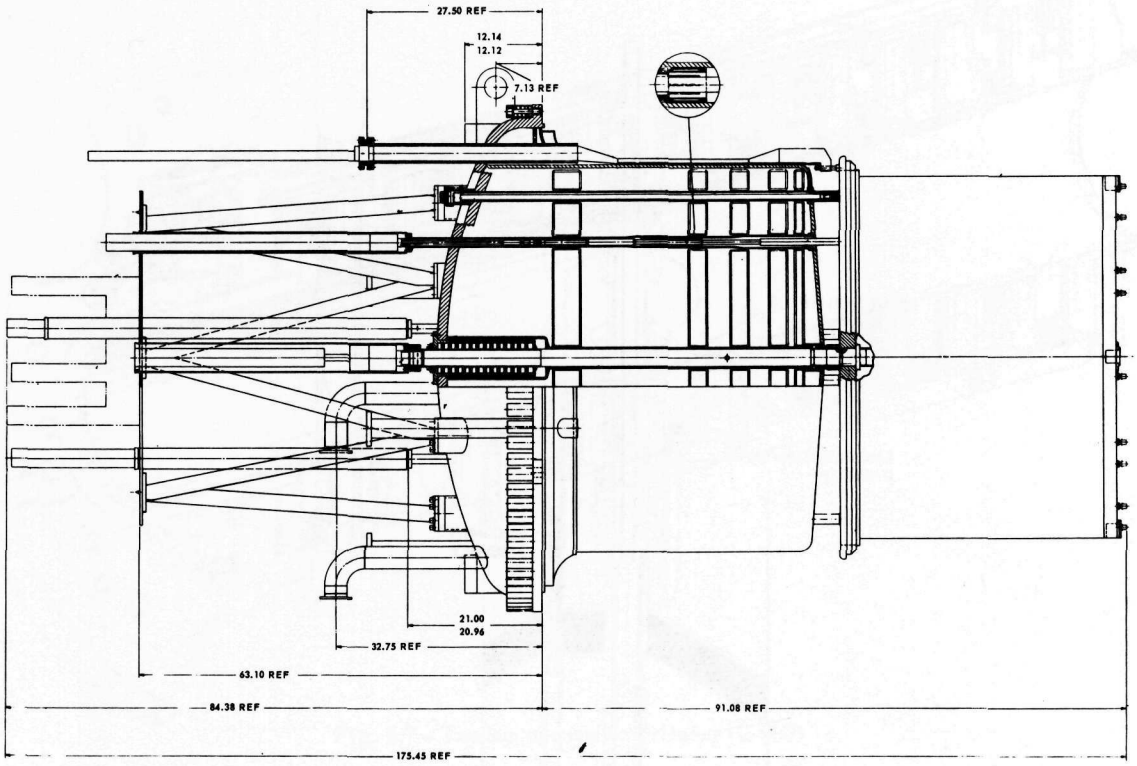

Fig. 5.5 – Side view of front shield plug assembly (Dwg. 134R648)

Figure 5. 6 shows the passage of a control rod with its selfcontained shielding through the lead shielding slabs of the front shield plug. Also shown is the center support tube with the dummy center rod inserted. The center rod also embodies shielding to plug its passage holes through the lead slabs.

Figure 5. 7 shows the details of a tandem pneumatic cylinder, the device used to support the center of the core forward tube sheet off the front shield plug dished head. The cylinder utilizes seven pistons energized by engine compressor air bled from the core inlet duct.

The lead slabs are attached to the cylindrical side walls of the front shield plug by thin shear tabs which allow radial differential expansion between the lead and the cylinder, but which support the lead in the vertical and transverse directions.

Four pads are located on the front dished head for handling purposes. The core removal fixture is bolted to these pads during assembly and disassembly of the front shield plug and core from the upended shield. The pad on the bottom of the vertical centerline of the dished head also provides the third point of support for the primary shield. A special fixture is attached to the two pads on the horizontal centerline for upending the entire primary shield assembly.

Instrumentation leads are brought into the primary shield through four long tubes located near the knuckle radius of the front dished head. The leads follow the outer cylindrical skin of the front shield plug and jump to the core across the four studs located at the outer edge of the forward tube sheet.

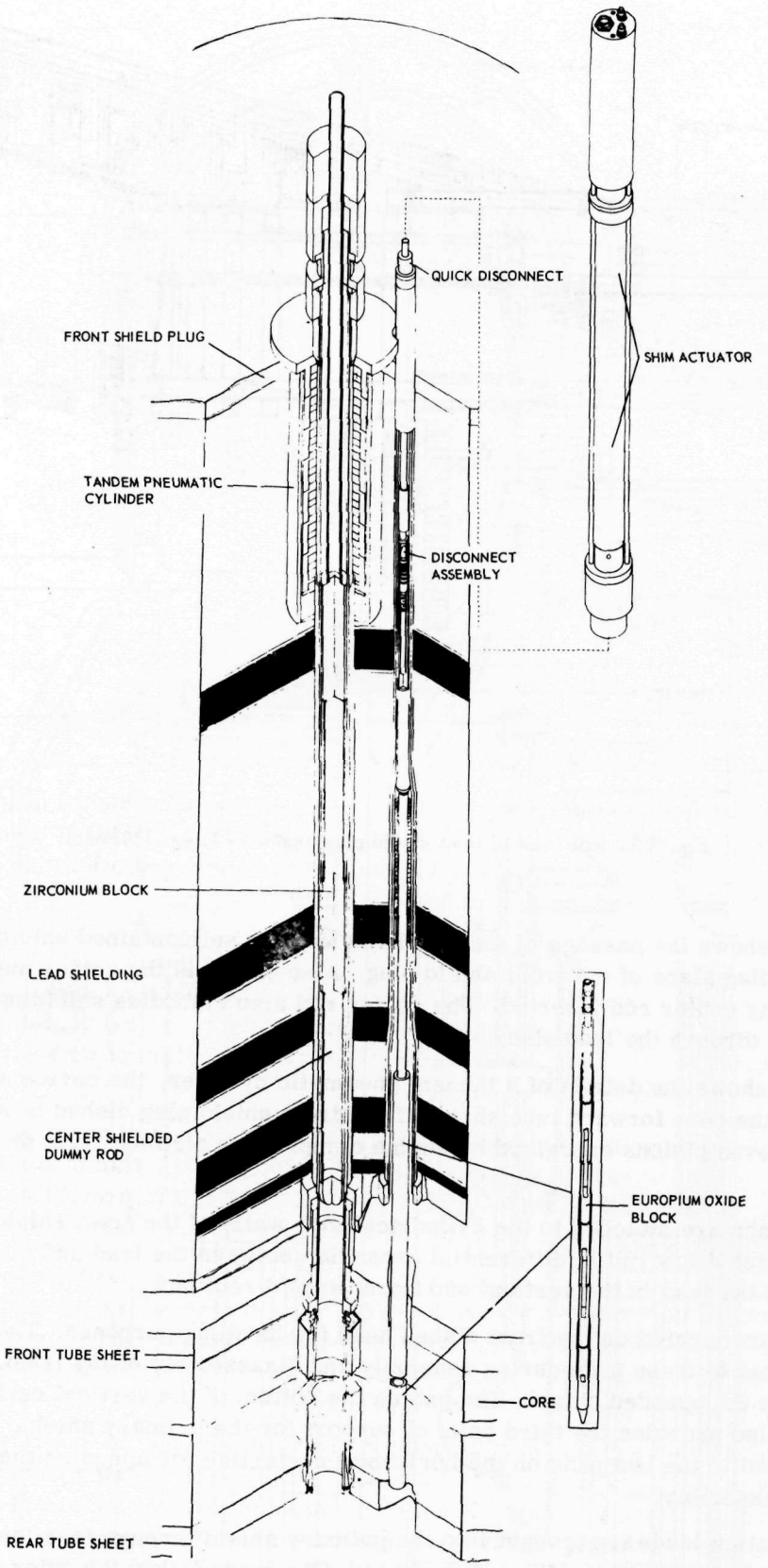

Fig. 5.6 – Control rod passing through front shield plug and core (Dwg. G-995)

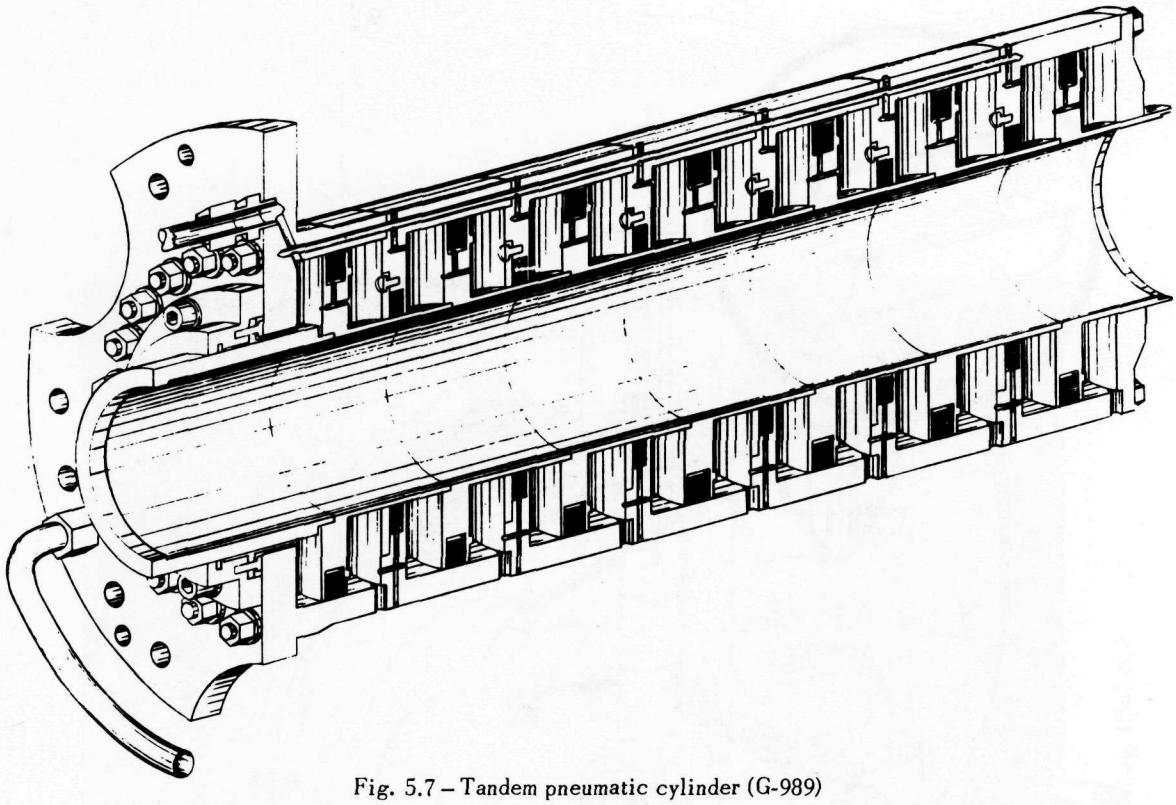

Fig. 5.7 – Tandem pneumatic cylinder (G-989)

Water is introduced into the front shield plug through the front dished head and piped to a point just aft of the rear lead slab near the centerline of the shield. It then flows outward and forward to the front of the shield plug and leaves by an outlet pipe located near the bottom centerline of the forward dished head.

5. 2. 1. 3 Rear Shield

The rear shield plug shown in Figure 5. 8 consists of two parts, the forward annulus (Figure 5. 9), an annular tank housing rings of lead, and the central portion or island plug (Figure 5. 10). Boral sheets are used in the forward section of both parts and also near the rear head of the island.

The structural elements of the annulus, the island, and the lead cans are of type 304 stainless steel. The pressure vessel cylinder is of 304 and 310 stainless steel. Threaded portions of the strut are of type 17-7 stainless steel hardened to prevent galling of the threads on assembly. Inconel is used for the fairing on the rear face of the plug.

The annulus is supported by cantilevering from the cylindrical portion of the pressure vessel. The island is supported within the cylindrical portion of the pressure vessel by four hollow, radially disposed struts. A flange between the cylindrical portion of the pressure vessel and the conical transition section facilitates assembly of the island within the cylinder and allows the plug to be disassembled.

The interior surfaces of the annulus and pressure vessel and the exterior surfaces of the island are protected with a thermal barrier in addition to a water jacket around the cylindrical portion of the pressure vessel to maintain permissible thermal stress levels. The thermal barrier consists of a fibrous insulation covered by discrete pads of thin sheet metal. A schematic drawing of the thermal barrier is shown in Figure 5. 11 and the fasteners used to attach the insulation from one side only, and also provide stiffening, are shown in Figure 5. 12.

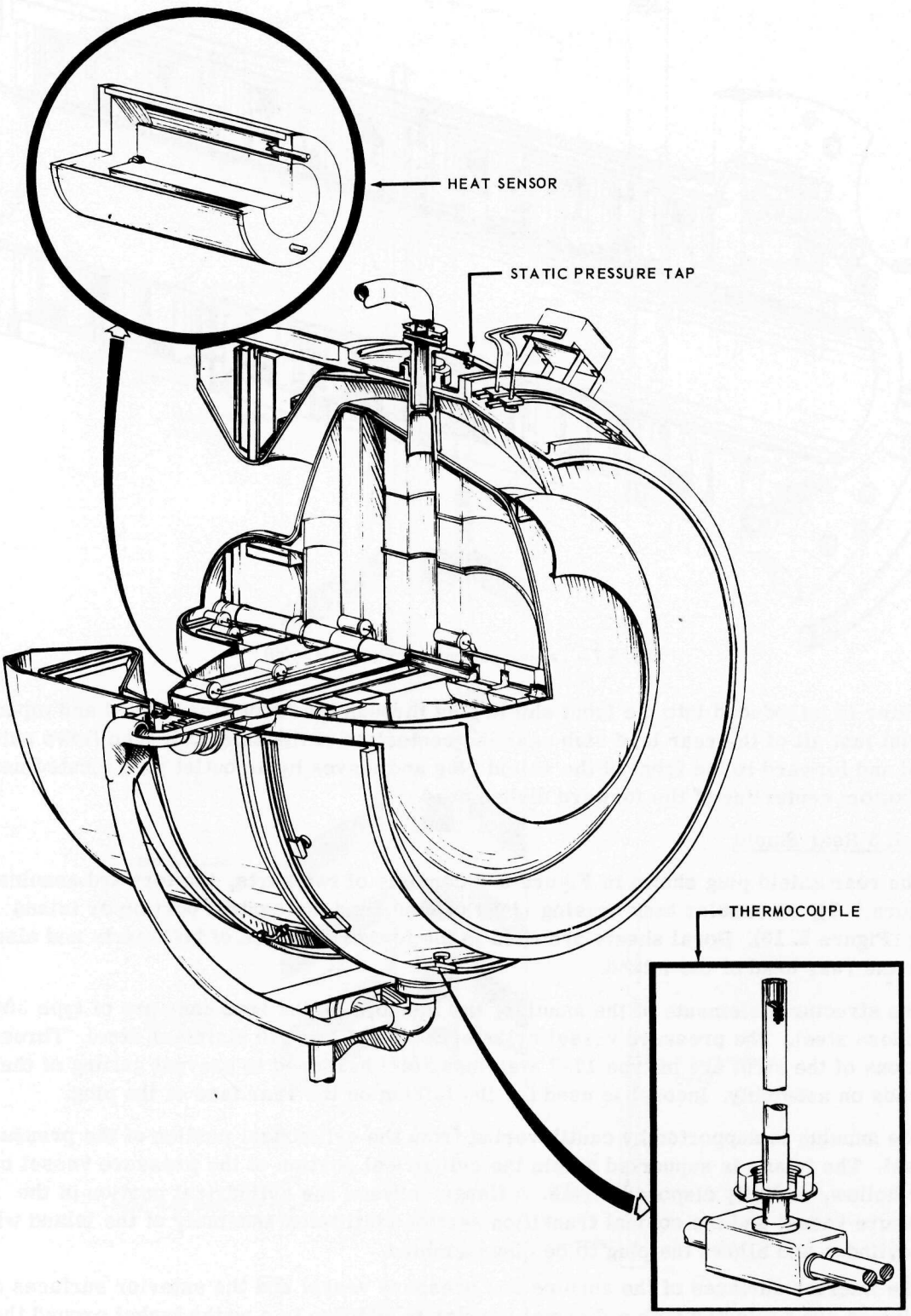

Fig. 5.8 – Rear shield plug assembly (Neg. G-963)

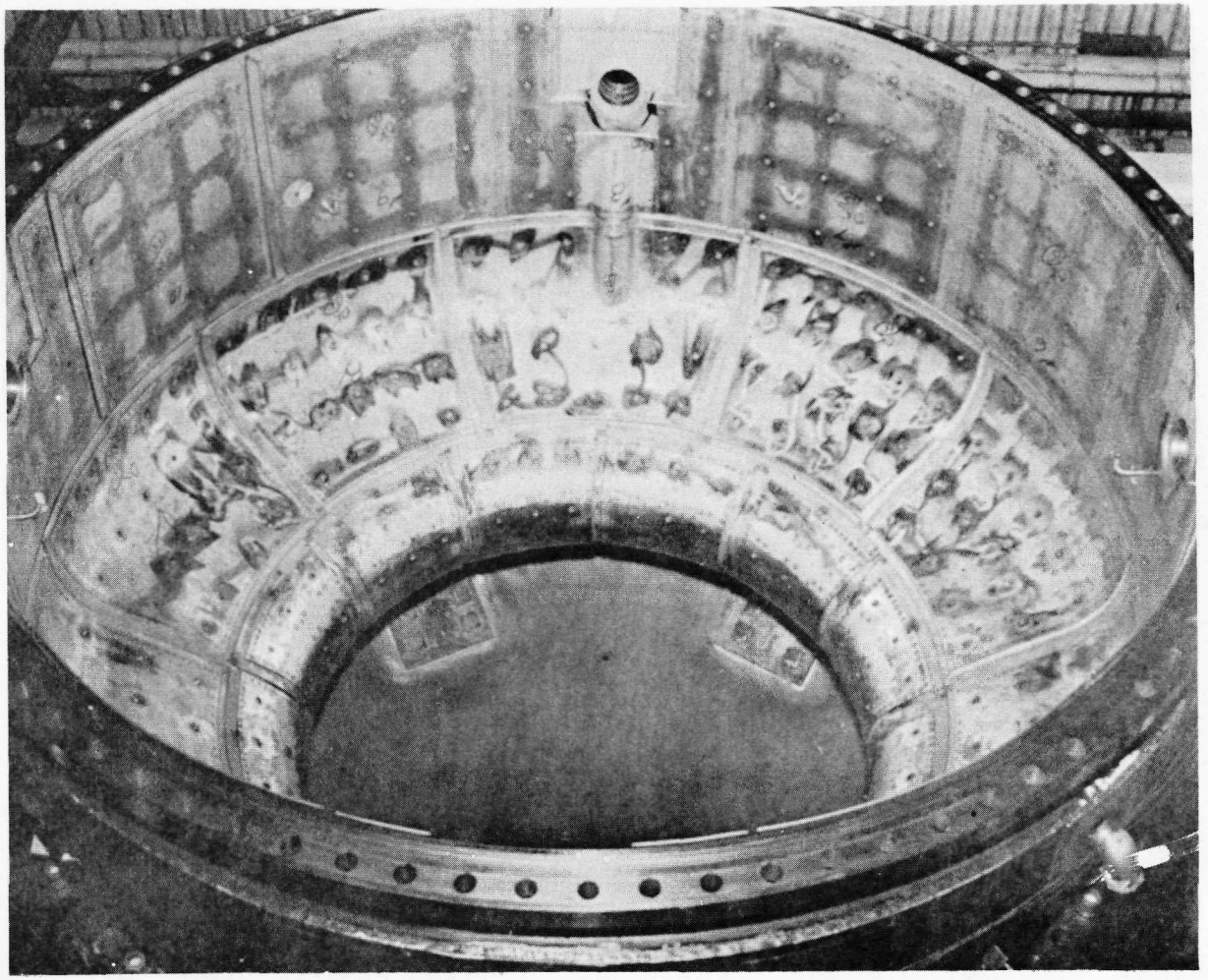

Fig. 5.9 – The forward annulus (Neg. U36136D)

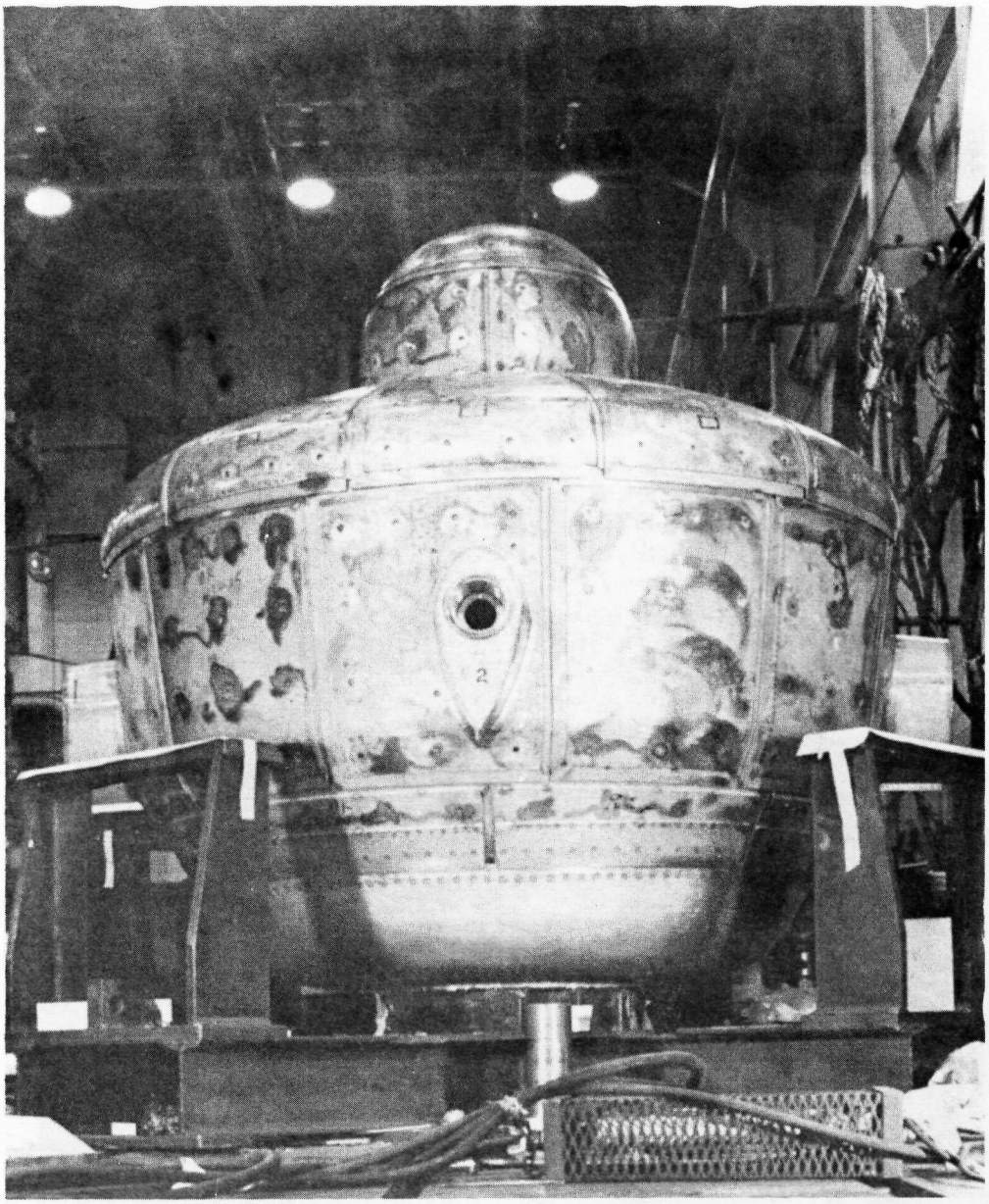

Fig. 5.10 – The island plug (Neg. U36136-B)

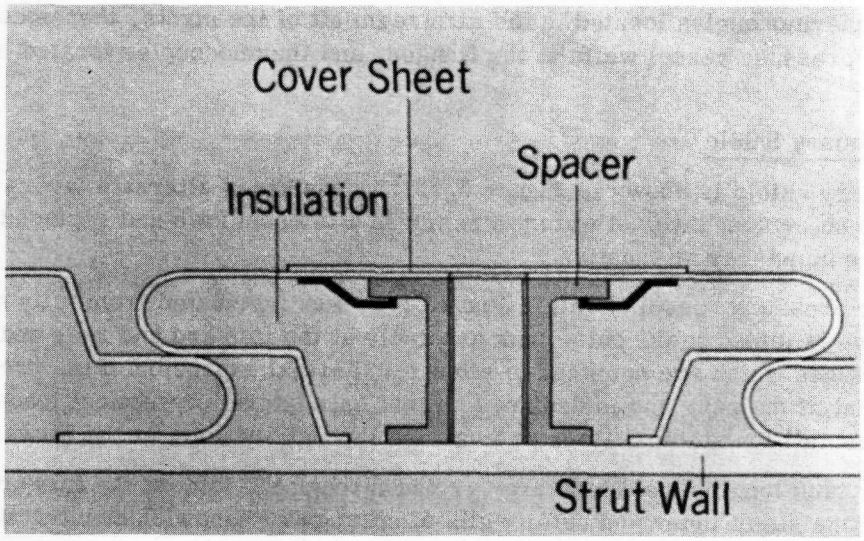

Fig. 5.11 – Thermal barrier (AU-1292)

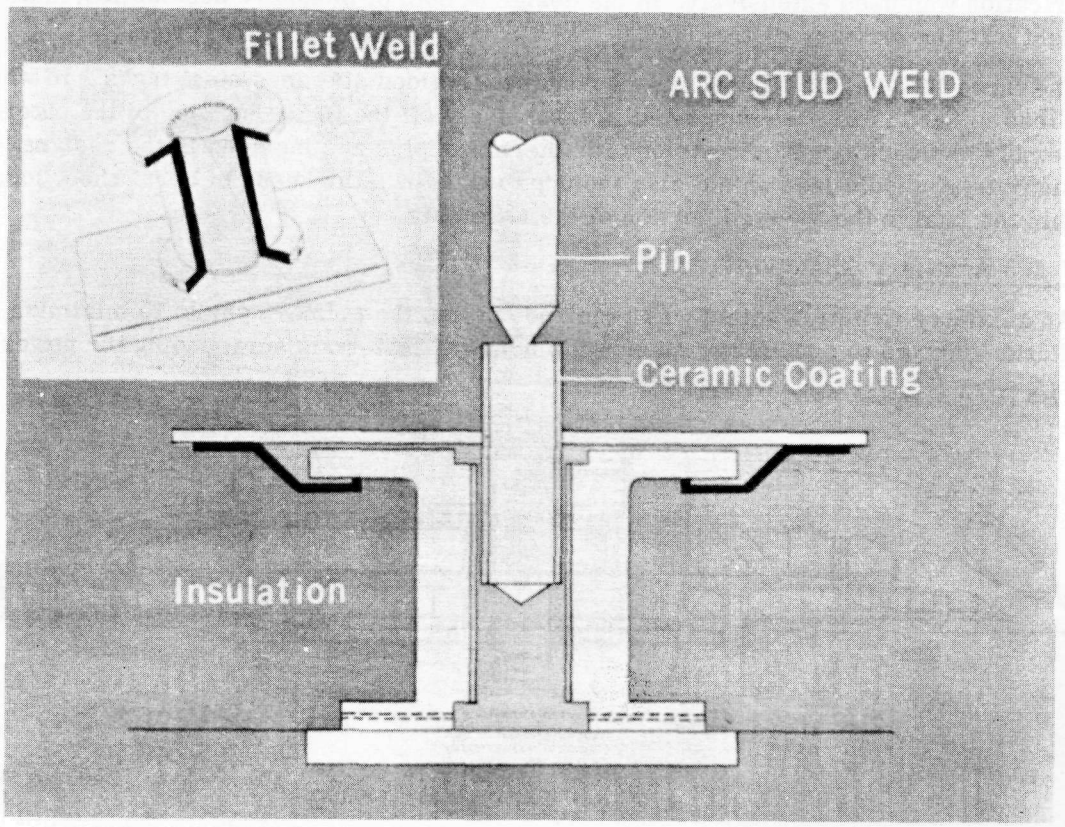

Fig. 5.12 – Thermal barrier fastening device (AU-1289)

The instrumentation consists of pressure probes located in the airstream forward of the struts, thermocouples located in the airstream aft of the struts, thermocouples on the interior pressure vessel walls at the flanges, and thermocouples located in the lead shields.

5. 2. 1. 4 Primary Shield

The primary shield is shown in Figure 5. 13. It consists of alternate layers of lead and water. (The outermost layer of water is removed after shutdown and replaced by mercury for greater gamma-ray attenuation.)

The inner pressure vessel shown in Figure 5. 14 was fabricated from fully age-hardened Inconel X and is joined to the outer tank assembly at the forward and rear ends by small transition pieces which are designed to allow for thermal expansion of the pressure vessel. The joint at the rear end is designed so that only lateral or vertical loads are transmitted. Thus, all longitudinal loads are carried through the joint at the forward end.

The outer tank longitudinal loads are carried through the joint at the forward end. The outer tank consists of inner and outer walls of corrugated sandwich construction. These walls are joined at rings at the ends of the tank, at rings where the conical end wall sections join the cylindrical center wall section, and at the trunnion ring near the center of the tank. The trunnions are attached to the inner and outer walls of the tank through the trunnion rings. All trunnion loads are transmitted to the pressure vessel through the external tank walls. Provisions for instrumentation wells and for hoisting also are built into the external tank. The skins and corrugations are of type 301 stainless steel 1/4 hard and the rings and trunnions are of type 17-7PH stainless steel. Spot weld and arc spot fabrication was used extensively. In the design of both of the above assemblies, minimum weight was the primary criterion.

The three lead shield subassemblies consist of welded stainless steel tanks into which the lead is cast. They are supported progressively off the inside surface of the outer tank assembly and each other. Provisions for thermocouples are included in the designs. The design of the middle lead shield also includes a 1/4-inch thickness of boral sheet located within the lead in the forward portion of the assembly.

5. 2. 1. 5 Auxiliary Shield

An auxiliary radiation shield was required outside the primary shield to minimize both radiation damage to and activation of equipment and materials surrounding the power

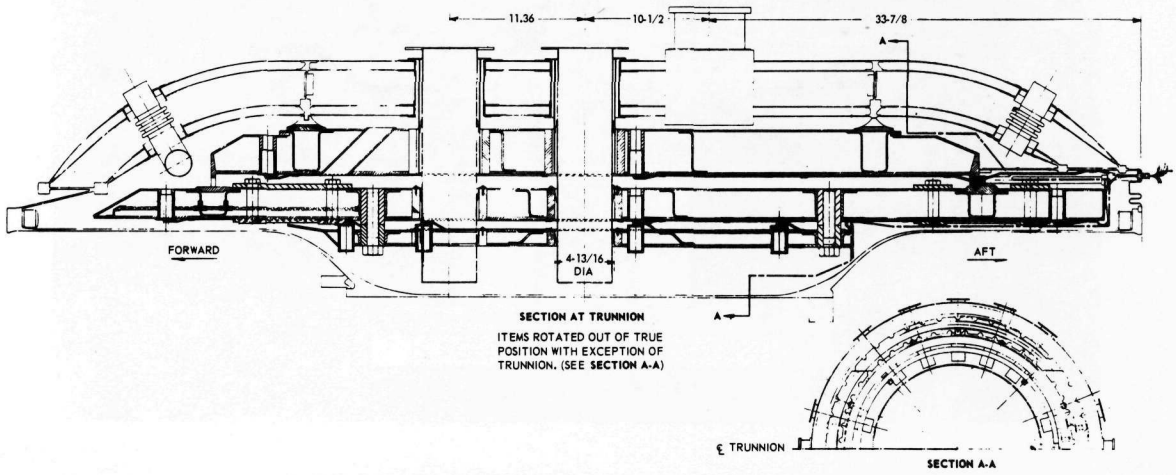

Fig. 5.13 – Primary shield assembly (Dwg. 134R606, Sh. 2)

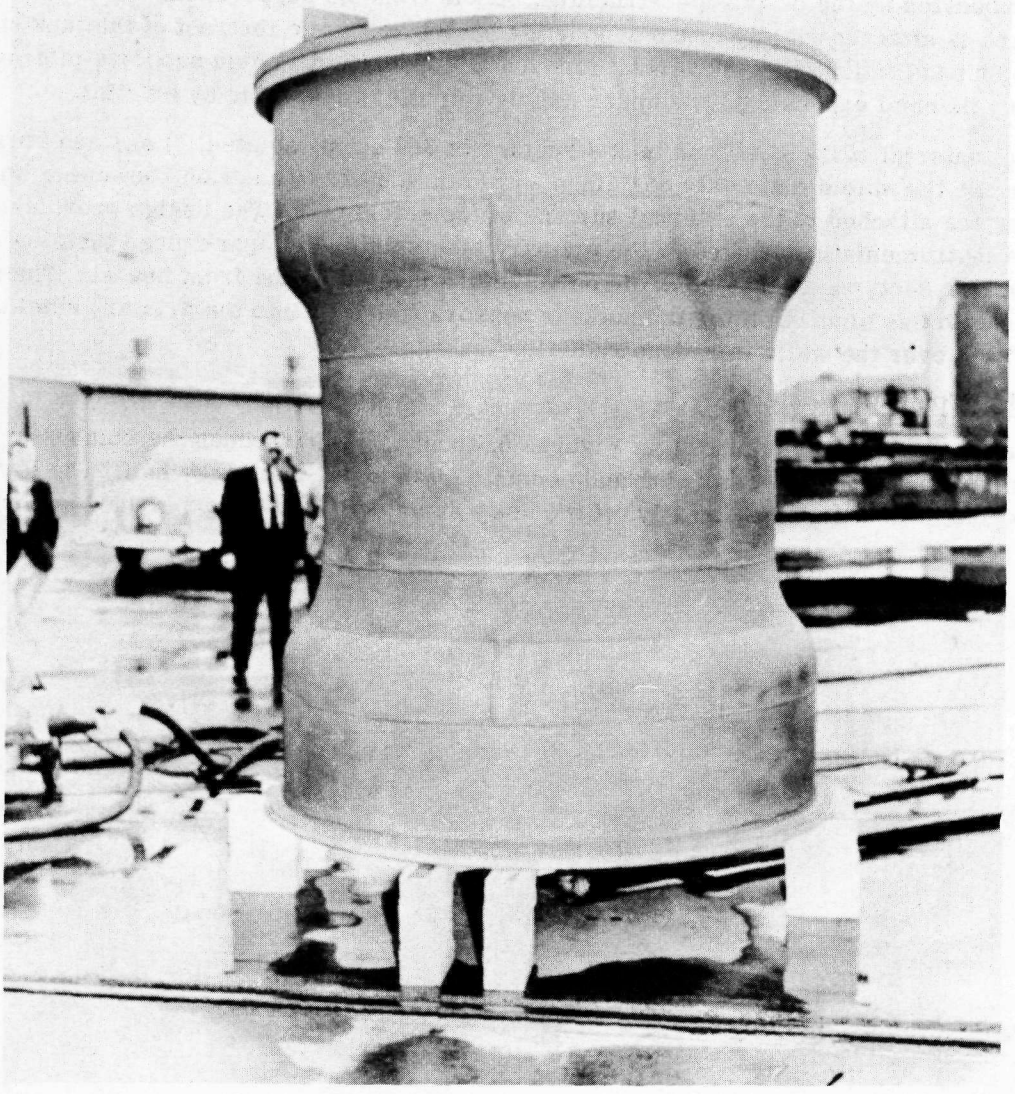

Fig. 5.14 – Inner pressure vessel

plant. This shielding reduces radiation levels to the extent that contact maintenance of equipment adjacent to the power plant can be performed within 18 hours after shutdown following 100 hours of operation at a power level of 175 megawatts. This auxiliary shield, shown in Figures 5. 2 and 5. 15, consists of a large annular tank, made in an upper and lower half, covering the primary shield. The lower half of the auxiliary shield is fixed to and supported by the dolly superstructure. At the trunnion supports for the primary shield the tank is attached rigidly to the supporting structure, while the rest of the tank structure rests on pads which allow movement fore and aft from the trunnion supports to provide for any thermal expansion. The upper half is remotely removable by hoisting.

The material of the shell and tank structure is 304 stainless steel. Lead and borated water are the shield materials contained within the tanks. In addition, however, boral sheets are attached to the external surface of the shield tank. The design provides access to the instrumentation located in the primary side shield, the spark plugs installed in the combustor section, and the control rod actuators located on the front header. The auxiliary shield has nine wells for the nuclear sensors which fit into the primary shield. Doors are fitted over the wells to reduce radiation leakage.

5. 2. 1. 6 Combustor Shield

The combustor shield, shown in Figures 5. 3 and 5. 16, surrounds the combustor which is located just aft of the rear plug and consists of an upper and lower half. The lower half of the shield is supported directly off the dolly structure, and the upper half is supported

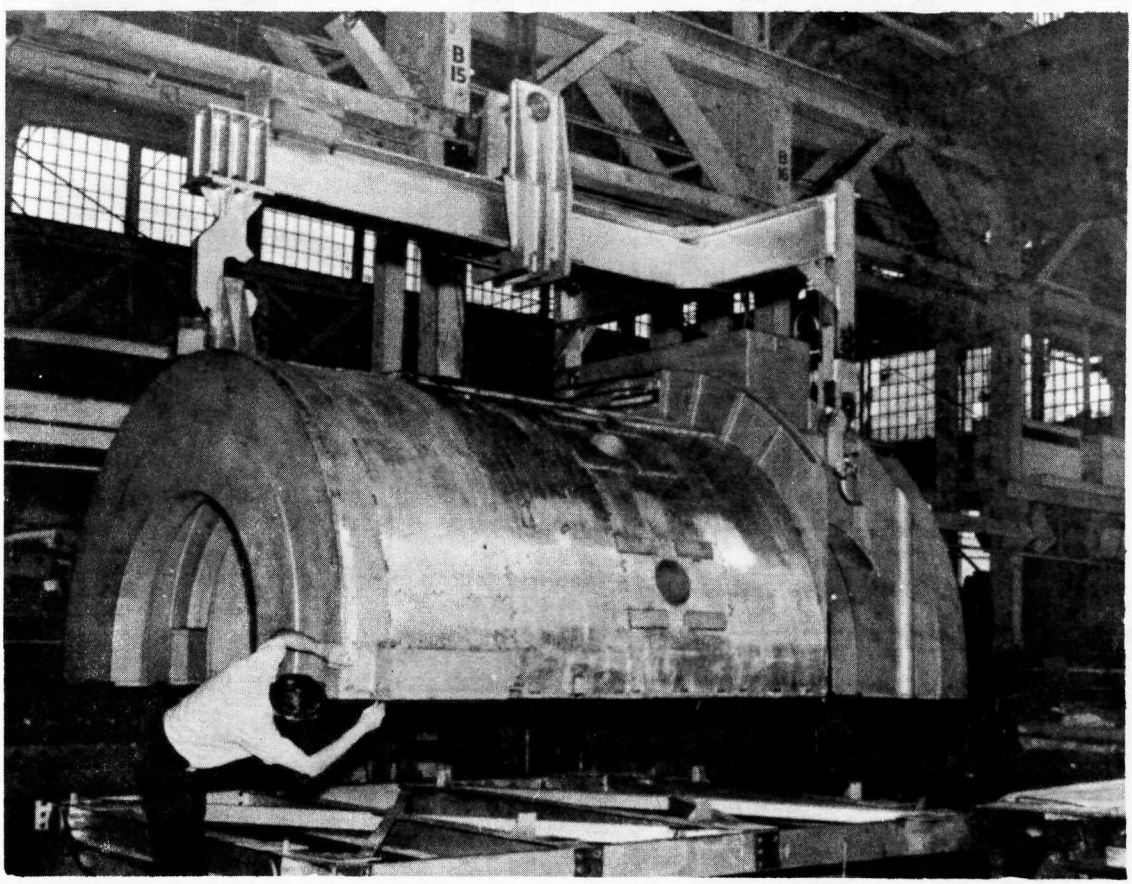

Fig. 5.15 – Upper half of auxiliary shield after installation of boral sheets on outside surface

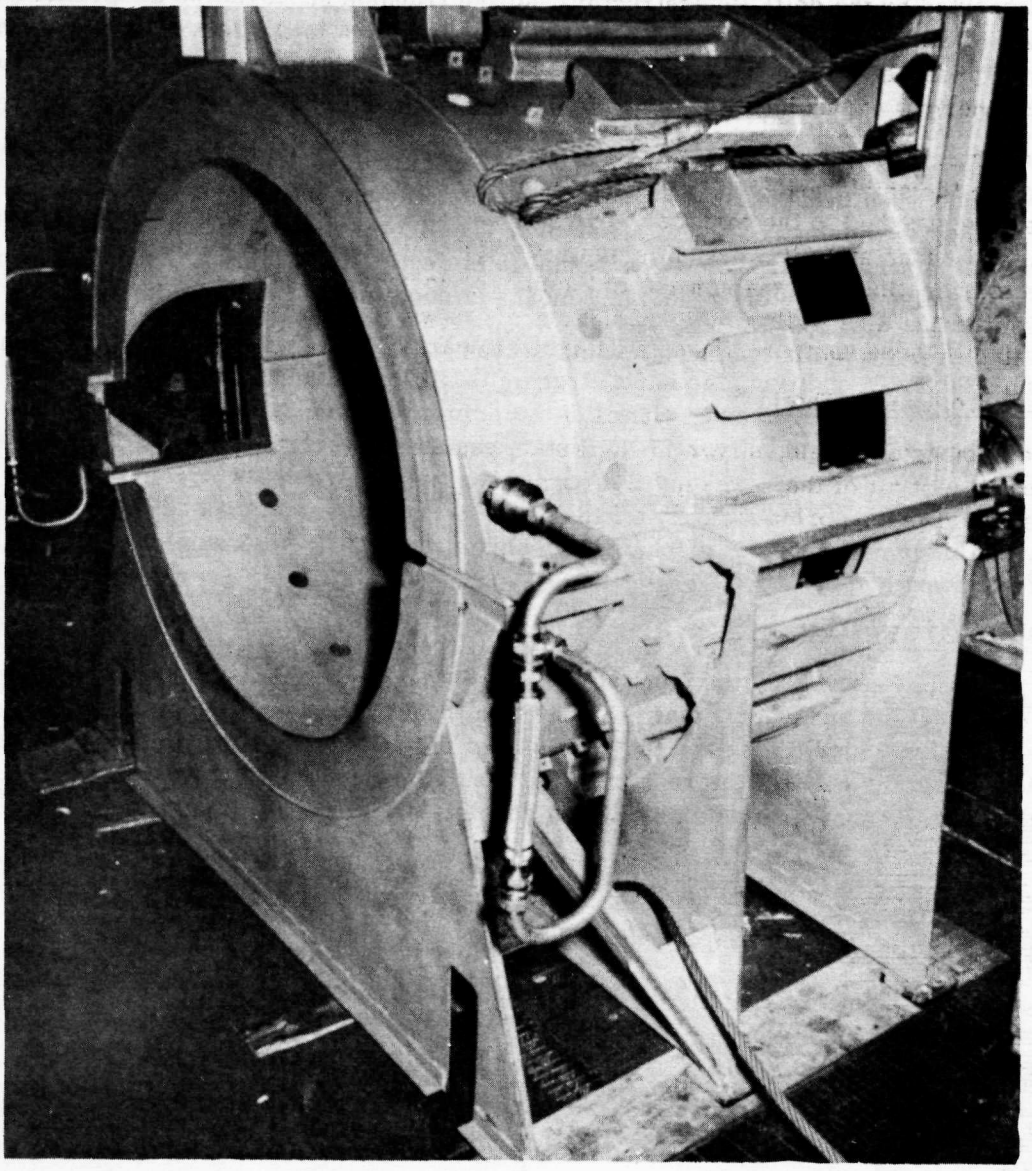

Fig. 5.16 – Combustor shield less sliding doors

by the lower half of the shield. Shielding materials are lead and circulating water. A typical section through the shield consists of 1. 25 inches of water at the inner surface, 2. 5 inches of lead, and 1. 25 inches of water at the outer surface.

There are 18 openings, covered by shielded sliding doors, located radially around the tank in the forward section. These openings provide access to the combustor fuel nozzles and ignitors. The doors are mounted on rollers and may be opened and closed manually or remotely. The doors also contain lead and water; the water is not circulated in the doors, however. A reflective sheet metal plate is provided inside the shield at each door to form a thermal barrier.

5. 2. 1. 7 Scroll, Elbow, and Transition Ducting

The forward scroll is bolted to the pressure vessel and supports the front shield plug. The design is such that the core - shield plug assembly can be removed from the pressure vessel without removing the scroll assembly. The elbows and transition ducts convey compressor discharge air from the external inlet ducting to the forward scroll. After-cooling air is ducted into the reactor by means of ducts which lead into the elbows.

In general these components were designed to carry X211 engine compressor air at 175 psia and 700°F. In addition, the scroll transmits all loads from the front shield plug assembly to the pressure vessel flange of the primary shield. The material used for the scroll, elbow, and ducts is type 17-7PH stainless steel.

These parts are shown in Figures 5. 17, 5. 18, and 5. 19.

Further information on the mechanical design of the HTRE No. 3 shields is contained in references 7 and 9.

5. 2. 2 AEROTHERMAL DESIGN

As shown in Figure 2. 3, the front shield plug is a cylindrical tank, containing alternating layers of lead and water, that is situated in front of the reactor core. The spacing between the front shield plug and the core allows the primary system airflow to distribute itself into the cells of the reactor. The front shield plug and core assembly is contained within the annular side shield which consists of alternating layers of lead and

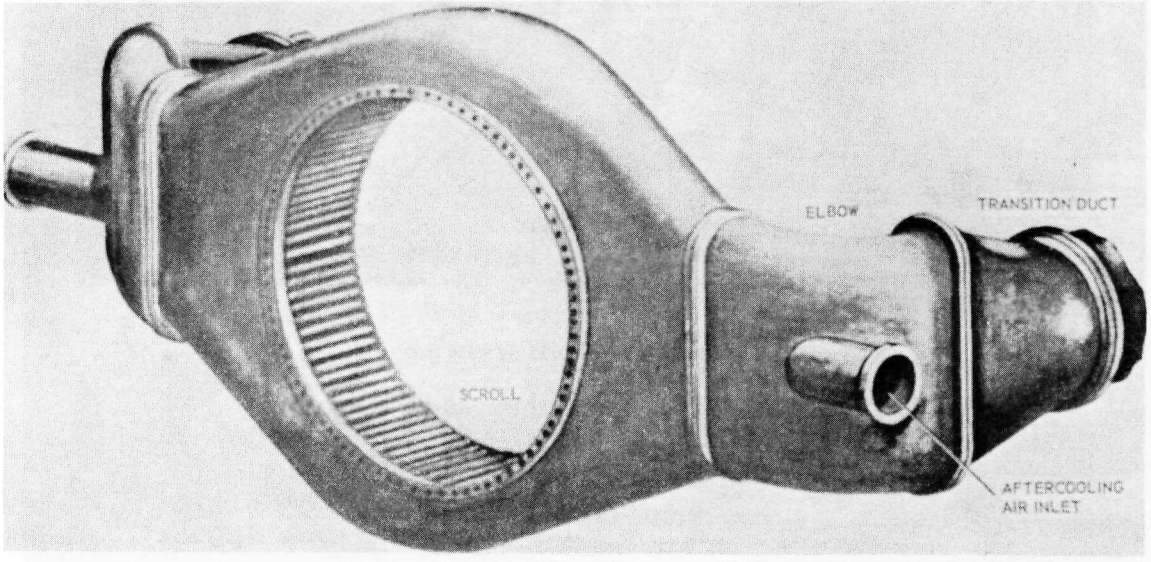

Fig. 5.17 – Scroll, elbows, and transition ducts

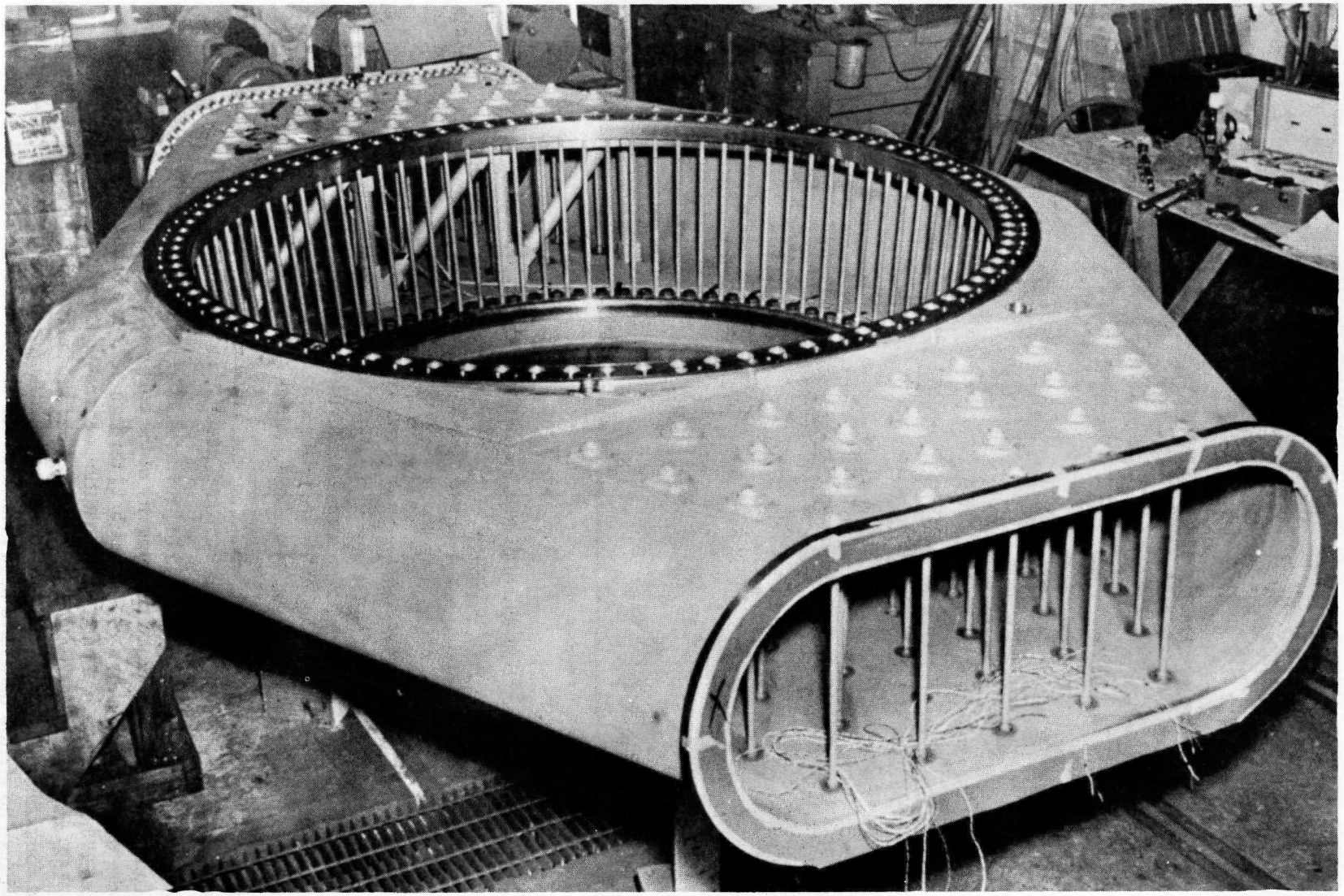

Fig. 5.18 – Scroll

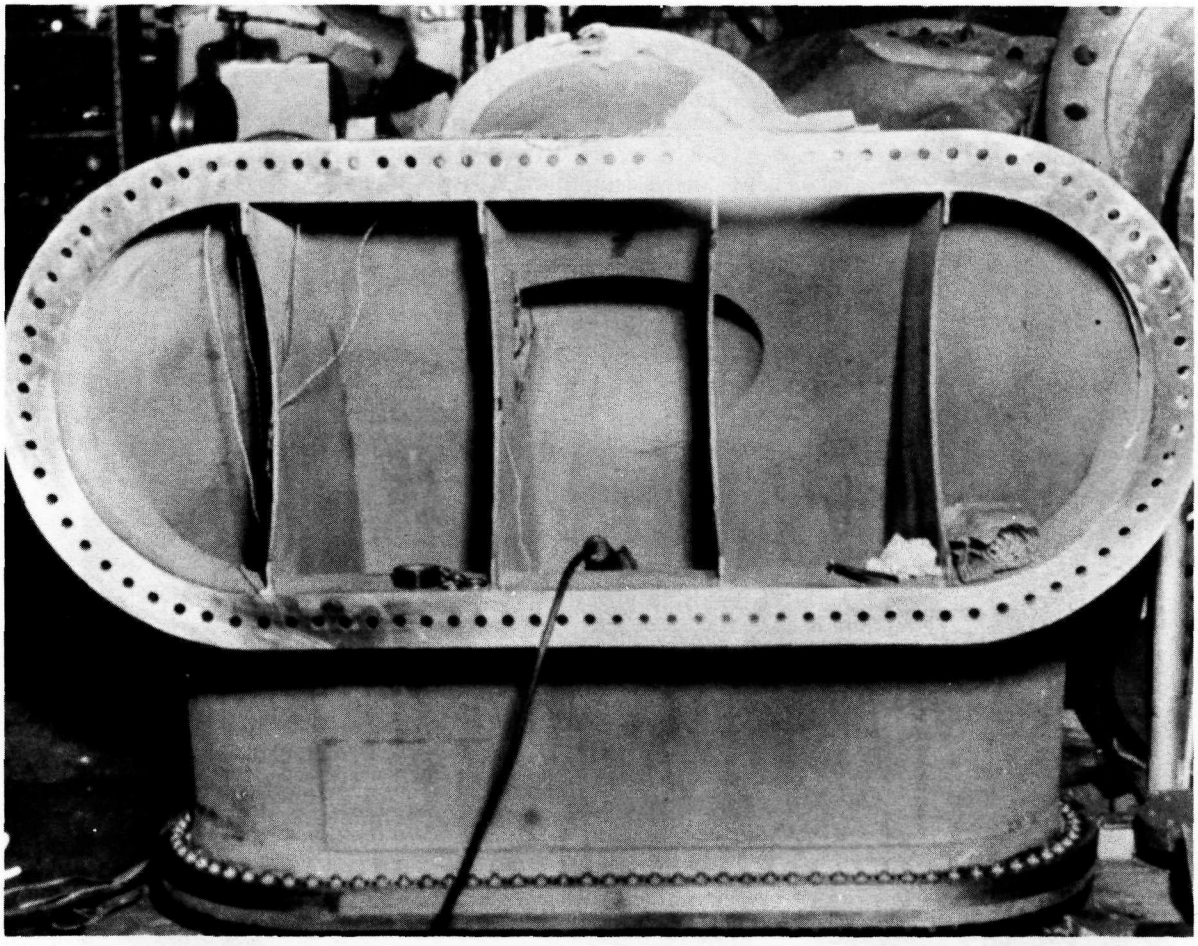

Fig. 5.19 – Elbow

water for shielding. The front shield plug is spaced from the inside wall of the side shield so that an annular air passage is formed to permit airflow to the core. The airflow from the compressor is collected in the scroll and distributed uniformly around the annular air passage.

Aft of the core, and inside the side shield, is the rear shield plug, consisting of an outer annular tank of lead and water and an inner island of lead and water. The rear shield - plug assembly forms a sinuous annular duct which collects the outlet air from the reactor. The rear shield plug is covered with insulation pads on all surfaces to reduce the thermal gradient in the walls and reduce heat loss.

The chemical combustor is aft of the rear shield plug. The system air passes from the combustor to the two turbojet engines through ducts, as shown in Figure 5. 20.

Thermodynamic studies were made to provide the aerodynamic and temperature data required to evaluate the structural integrity of the core and shield components. The temperature distributions shown in Figures 5. 21 through 5. 27 are based on a reactor power level of 175 megawatts and on airflow conditions corresponding to 100 percent rpm on X211 (162-megawatt) operation. This inconsistency arose from the necessity of designing shield components for 175-megawatt operation (maximum power level for X211 operation), but because no airflow data have been generated for an operating point of 175 megawatts, the airflow conditions corresponding to 162-megawatt operation were used.

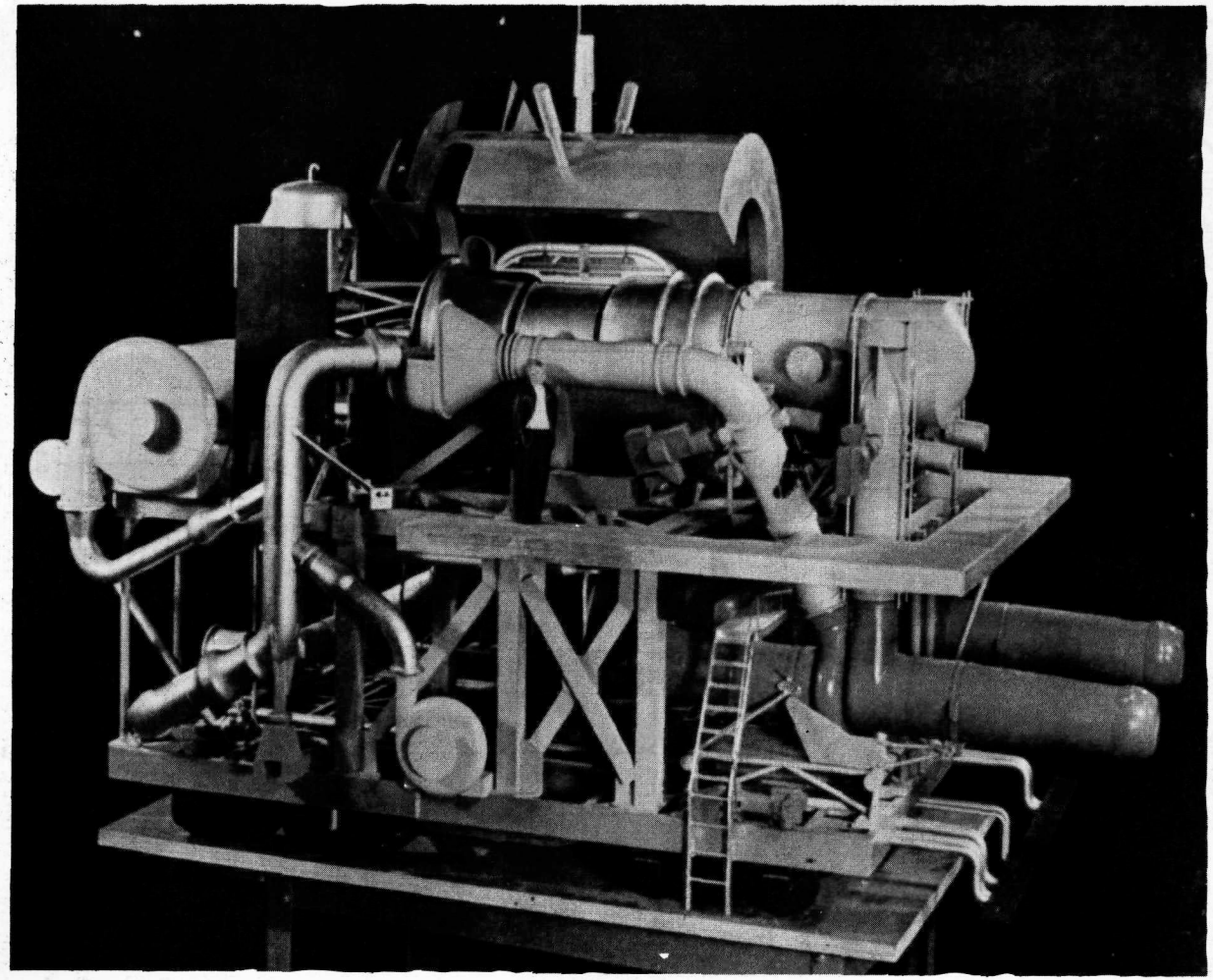

Fig. 5.20 – Mockup of HTRE No. 3 assembly showing external auxiliary shield raised and primary shield cut away (Neg. C-04747)

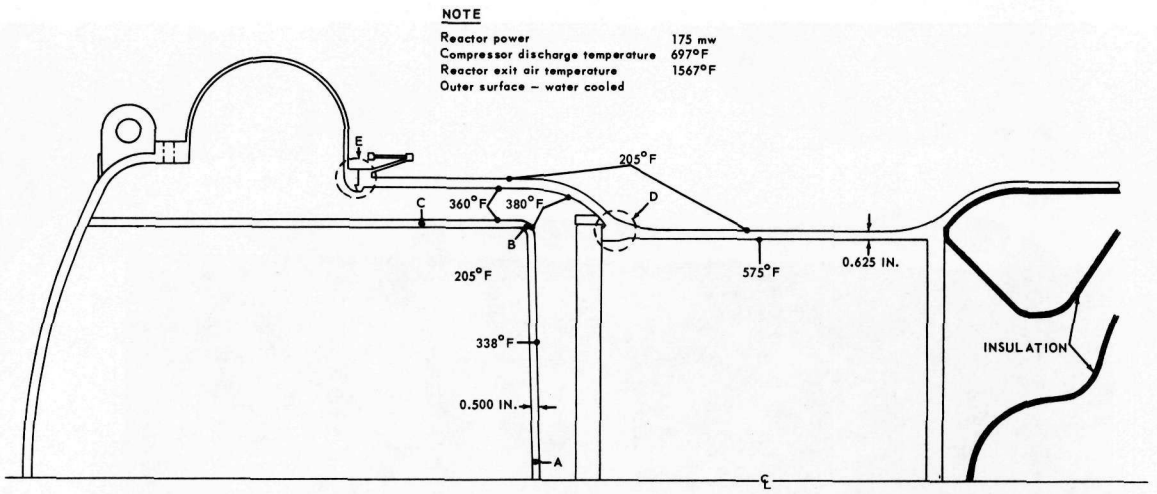

Fig. 5.21 – Primary shield structural temperatures based on X211 engine operation

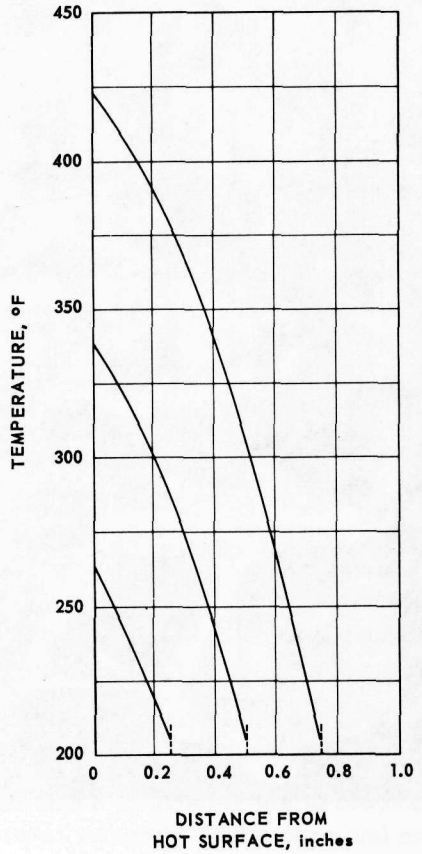

Fig. 5.22 – Temperature profile in front shield plug, point A

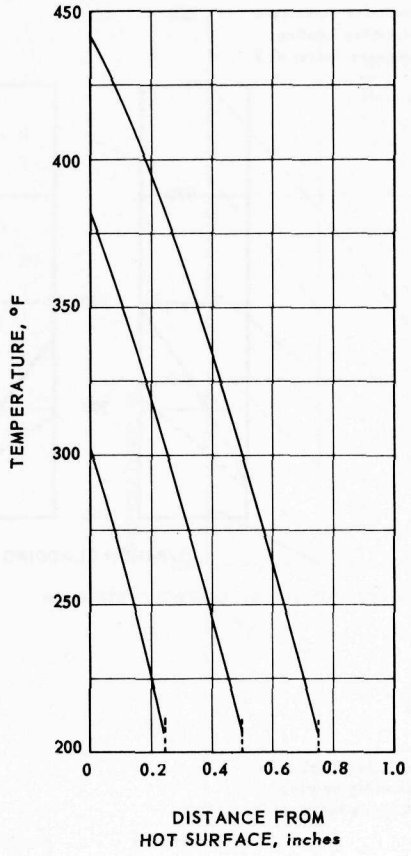

Fig. 5.23 – Temperature profile in front shield plug, point B

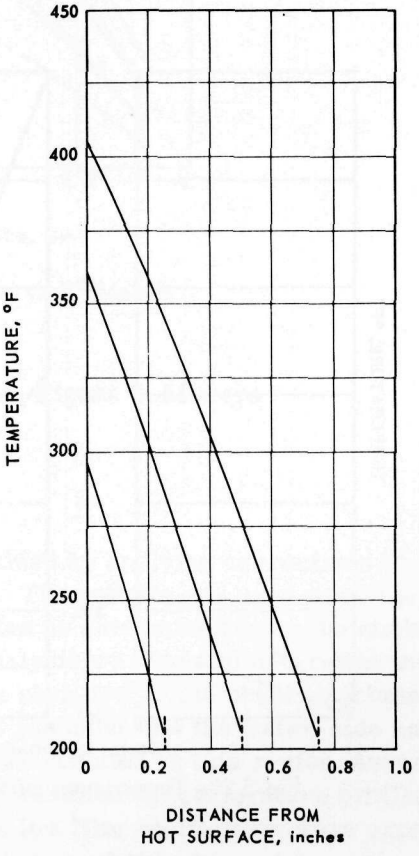

Fig. 5.24 – Temperature profile in front shield plug, point C

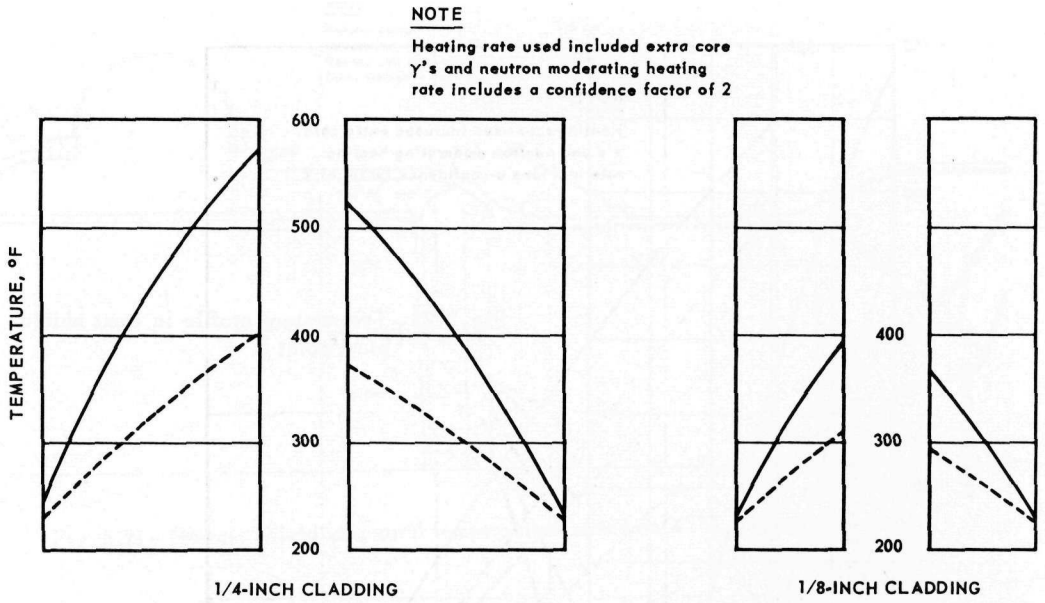

Fig. 5.25 – Temperature profile of side shield considering no contact resistance

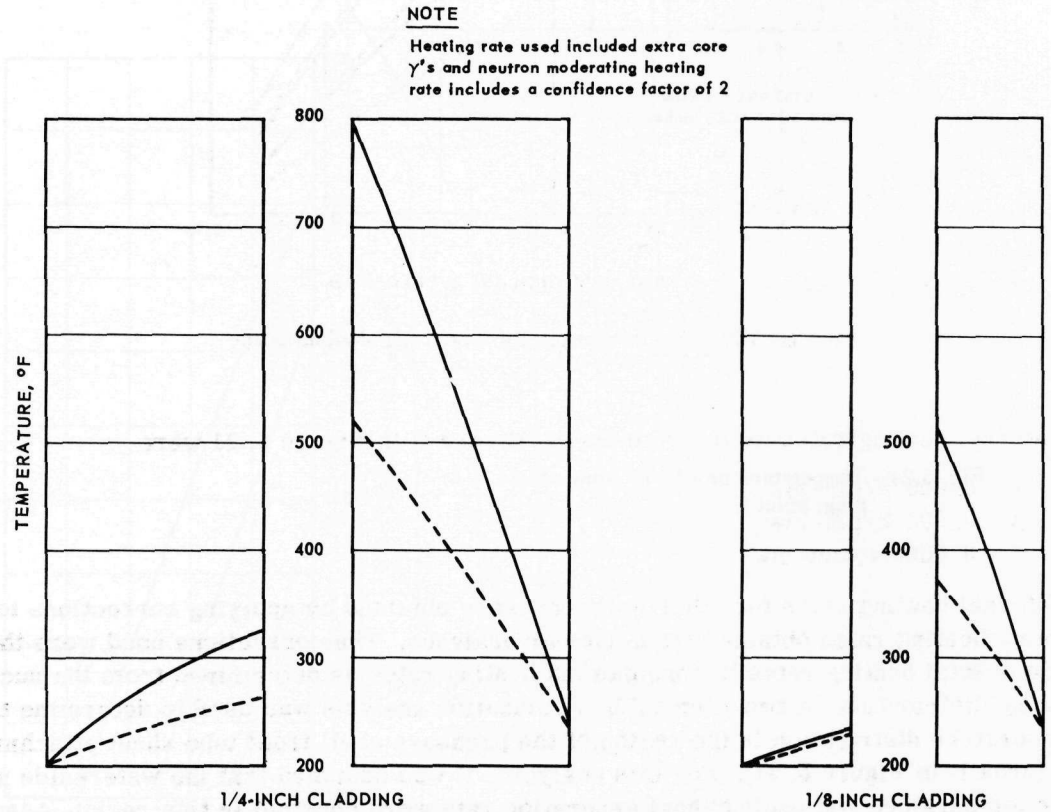

Fig. 5.26 – Temperature profile of side shield considering a 20-mil air gap on one side

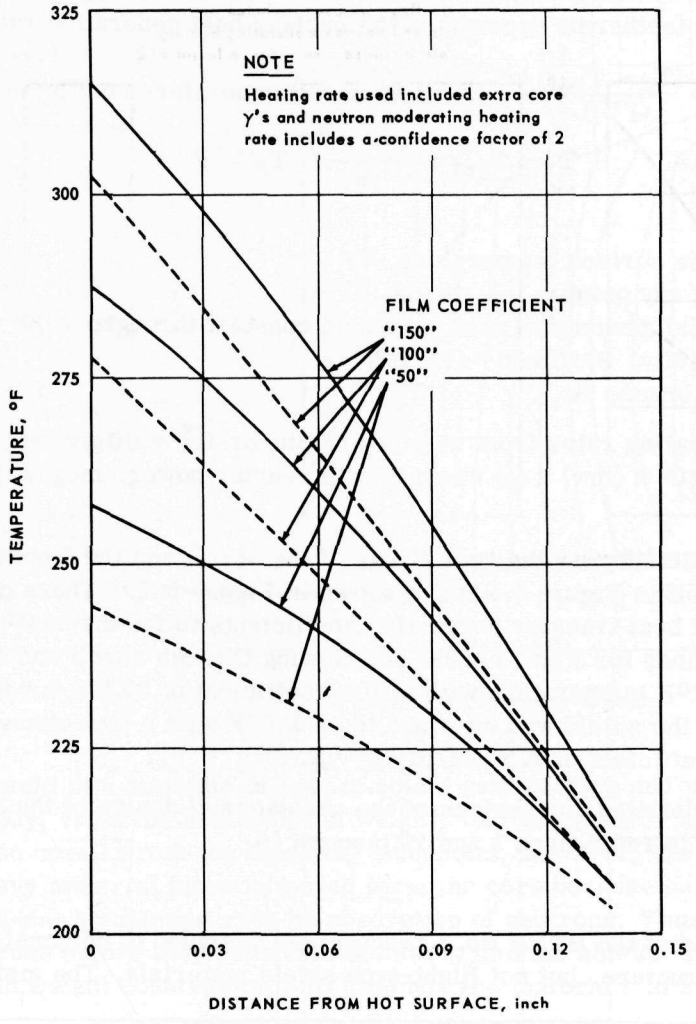

Fig. 5.27 – Temperature profile of pressure shell midplane

Internal heating rates used for points A, B, and C in Figure 5. 21 were

A - 0. 006 w/gm-mw
B - 0. 003 w/gm-mw
C - 0. 0003 w/gm-mw

Internal heating rates for other locations were obtained by applying corrections to the gamma heating rates obtained from nuclear analyses. The corrections used were the ratio of total heating rates to core gamma heating rates as determined from the nuclear heating distribution. A two-dimensional relaxation analysis was used to determine the temperature distribution in the region of the pressure shell front tube sheet attachment lip (area D in Figure 5. 21). For this analysis, it was assumed that the water-side surface temperature and nuclear heat generation rate were constant in this region. Assuming further that the inside surface was perfectly insulated resulted in temperature profiles reaching a maximum temperature on this surface. As low film coefficients were expected in this region and because the inside surface temperature probably was not too different from the air temperature, this assumption was felt to be reasonable.

From the IBM computations, lines of constant temperature coefficient, corresponding to isotherms, are plotted on an enlarged cross section of the lip region (Figure 5. 28). The magnitude of the isotherms depends on the nuclear heat generation rate:

$$T_x'' = \frac{(T_x - T_{ref})\, k}{Q'''\, L^2} \quad \text{Dimensionless temperature coefficient}$$

then

$$T_x = T_{ref} + \frac{(Q'''\, L^2)}{k}\; T_x''\ {}^{o}F$$

Where

T_{ref} is the water-side surface temperature, ^{o}F
T_x is temperature at any point in the region, ^{o}F
Q''' is the nuclear heat generation rate, assumed constant throughout the region, Btu/hr-ft^3
k is thermal conductivity, Btu/hr-ft^2-(^{o}F/ft)
L^2 is characteristic length, ft

NOTE: To convert heating rates from w/g-mw to Btu/hr-ft^3 multiply heating rate in w/g-mw by 9. 664 x 10^4 x (mw) x (ρ) where mw is reactor power, megawatts, ρ is density, gm/cc.

Temperature coefficients for the rear flange of the scroll and the front flange of the pressure shell (area E in Figure 5. 21) are shown in Figure 5. 29. These data are valid only for the ratios of heat transfer convection coefficients to the thermal conductivity used in the computations for Figure 5. 29. Air flowing through scroll and shield was assumed to be at 697^{o}F temperature with a film coefficient of 35 Btu/hr-ft^2-^{o}F. Ambient temperature outside the shield was assumed to be 100^{o}F with a free convection and radiation heat transfer coefficient of 2. 5 Btu/hr-ft^2-^{o}F.

Additional, more detailed discussions of the aerothermal design of the HTRE No. 3 shield are contained in references 1 and 10 through 14.

5. 2. 3 NUCLEAR

The primary shield of the HTRE No. 3 reactor was designed to demonstrate a flight-type envelope and structure, but not flight-type shield materials. The main shielding in

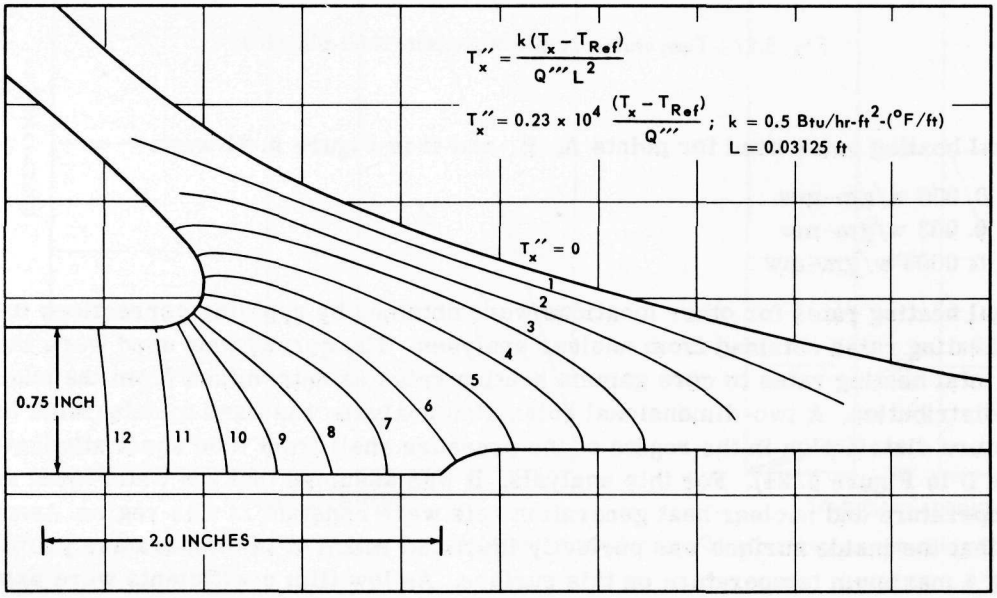

Fig. 5.28 – Temperature distribution in region of point D

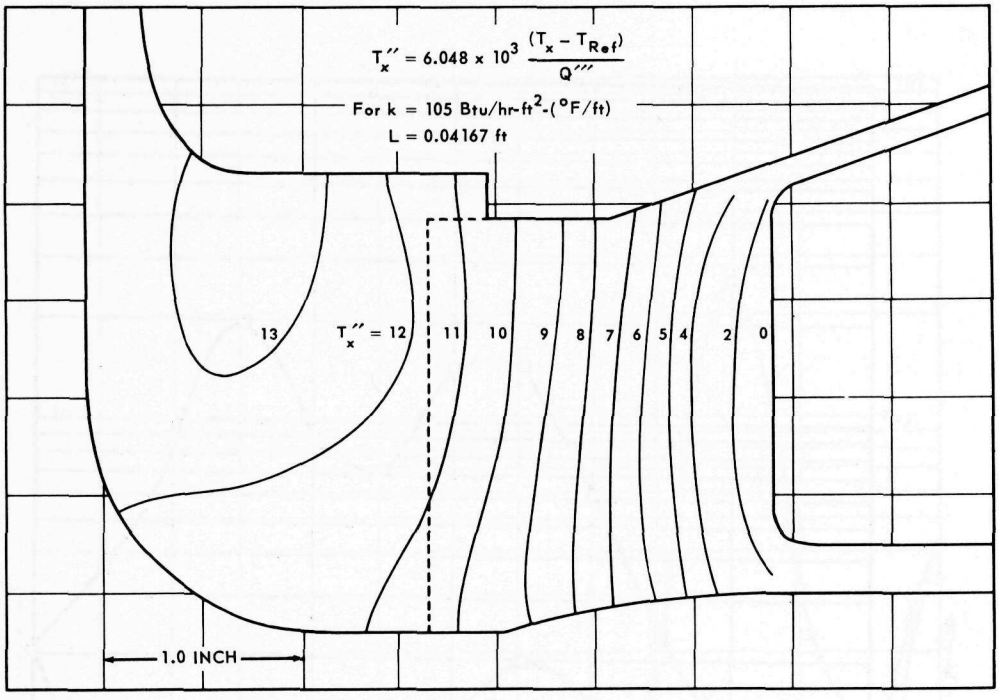

Fig. 5.29 – Temperature distribution in region of point E

the primary shield is a laminate of lead to shield gamma rays and water to attenuate the neutrons. Ideally, from the standpoint of weight, the heavy material would be in close proximity to the core. From the shielding standpoint, however, the ideal configuration is to have the heavy material more removed form the core because heavy materials generate secondary high-energy gamma rays by absorption of neutrons. Thus it is desirable to remove the neutrons before they penetrate the heavy gamma shield. The obvious compromise of shielding and weight constraints is to laminate the materials to arrive at an optimum configuration.

The primary shield is a lead-steel-water configuration consisting of two chambers; the inner chamber contains three layers of lead canned in stainless steel with water circulating throughout, and the outer chamber contains water during operation and can be filled with mercury after shutdown.

Radiation levels expected around the HTRE No. 3 reactor-shield assembly are shown in Figures 5. 30 through 5. 32. The levels were calculated for a distance of 20 feet from the center of the core in a vertical, longitudinal midplane, with and without the auxiliary shield. Dose rates are assumed to be symmetric about the power plant because of the cylindrical symmetry of the configuration. The levels are based on direct radiation originating in the core, radiation scattering through irregularities such as air ducts and control rod channels, and radiation scattered in the air outside the assembly. The gamma-ray dose rates include gamma rays generated by (n, γ) reactions in the shield materials and by the activation of the shield materials. The radiation levels were calculated using point kernel techniques as outlined in reference 15.

Detailed heating rates in the front shield plug and the primary shield are shown in Figures 5. 33 through 5. 36. These data are based on calculations using the point kernel techniques to calculate core gamma heating and the diffusion theory to calculate neutron heating and gamma sources for the secondary gamma heating rates. The importance of

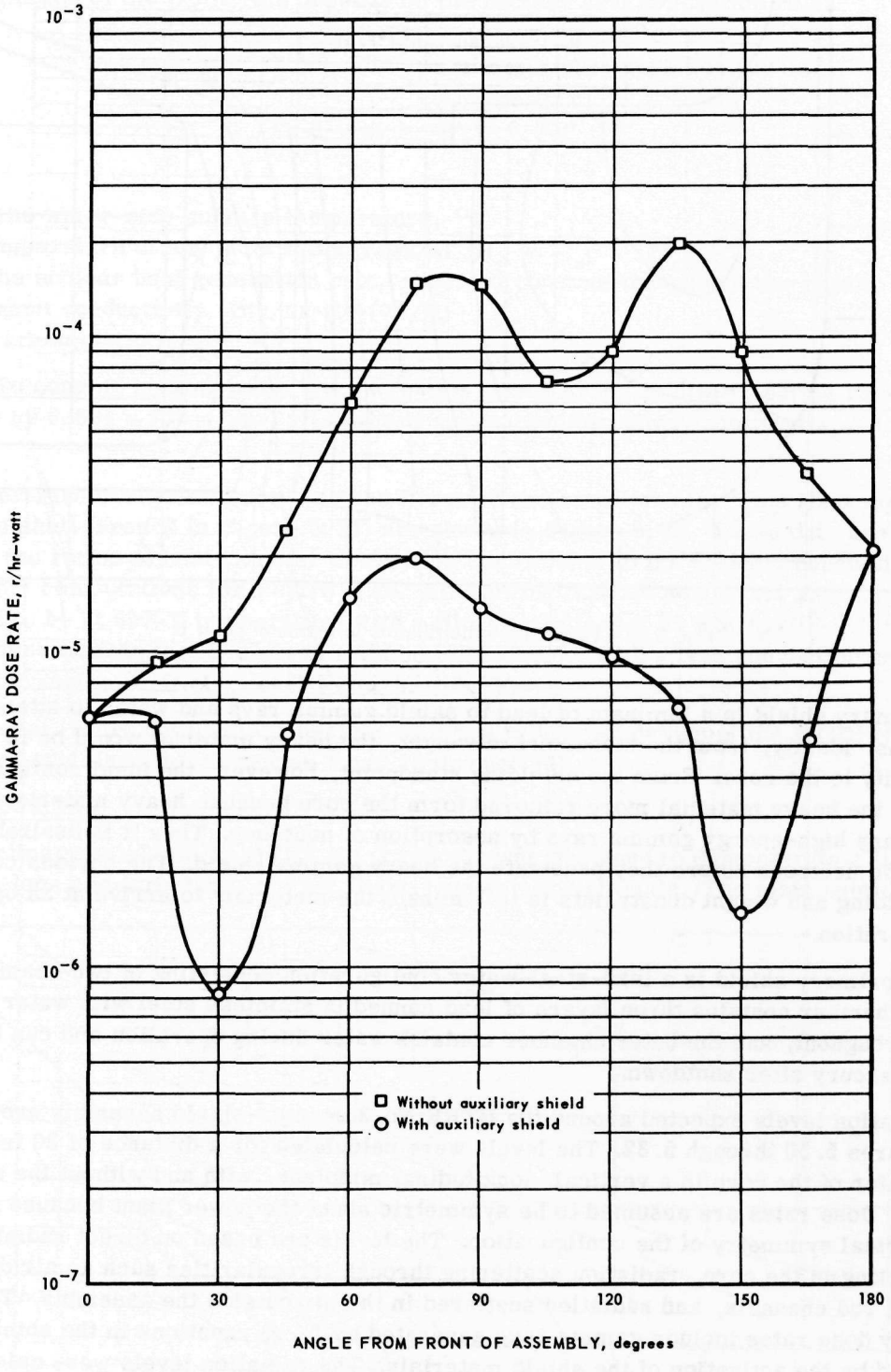

Fig. 5.30 – Calculated HTRE No. 3 gamma-ray dose rate during operation

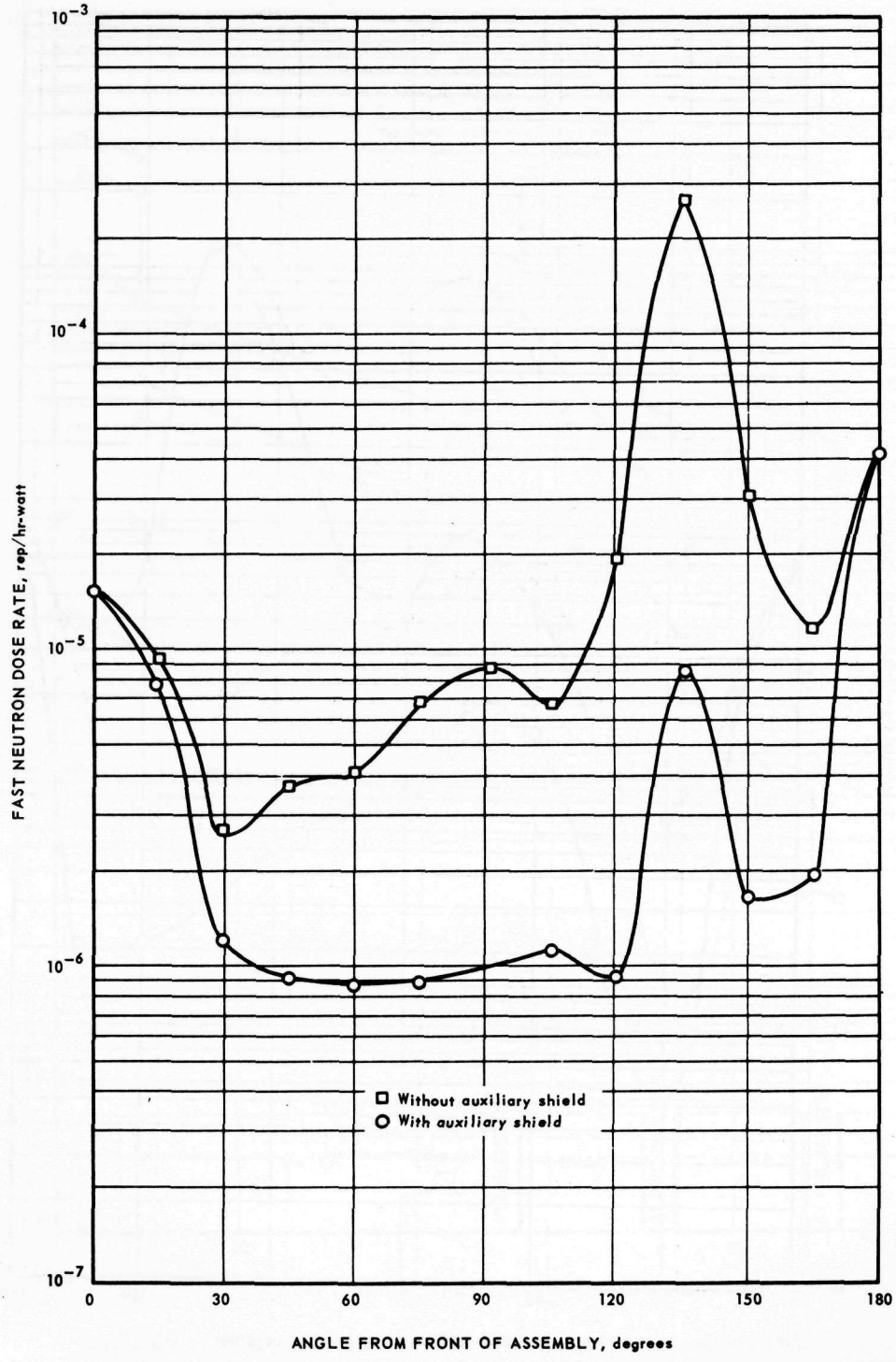

Fig. 5.31 – Calculated HTRE No. 3 fast neutron dose rate during operation

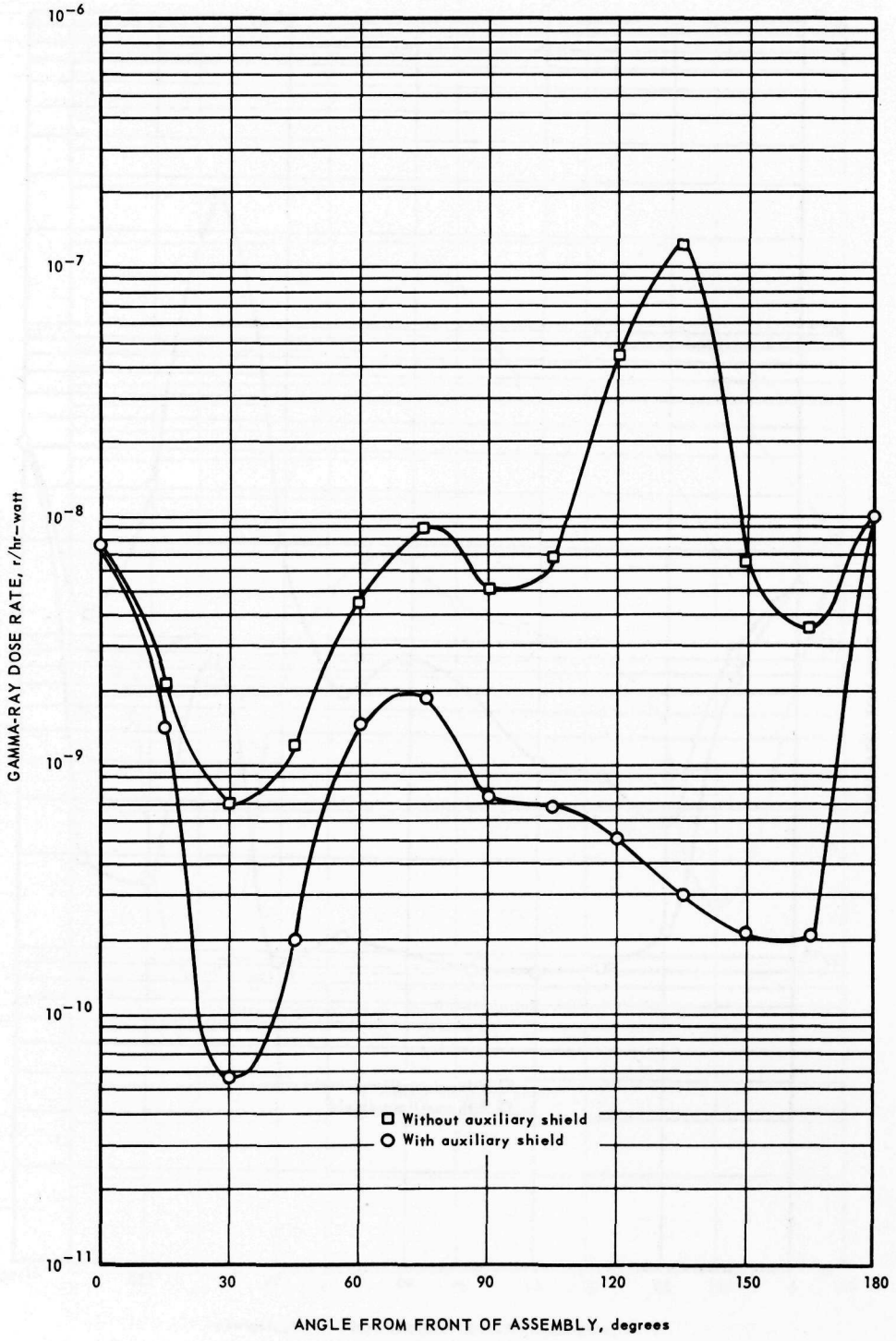

Fig. 5.32 – Calculated HTRE No. 3 gamma-ray dose rate 18 hours following shutdown after 100 continuous hours of operation

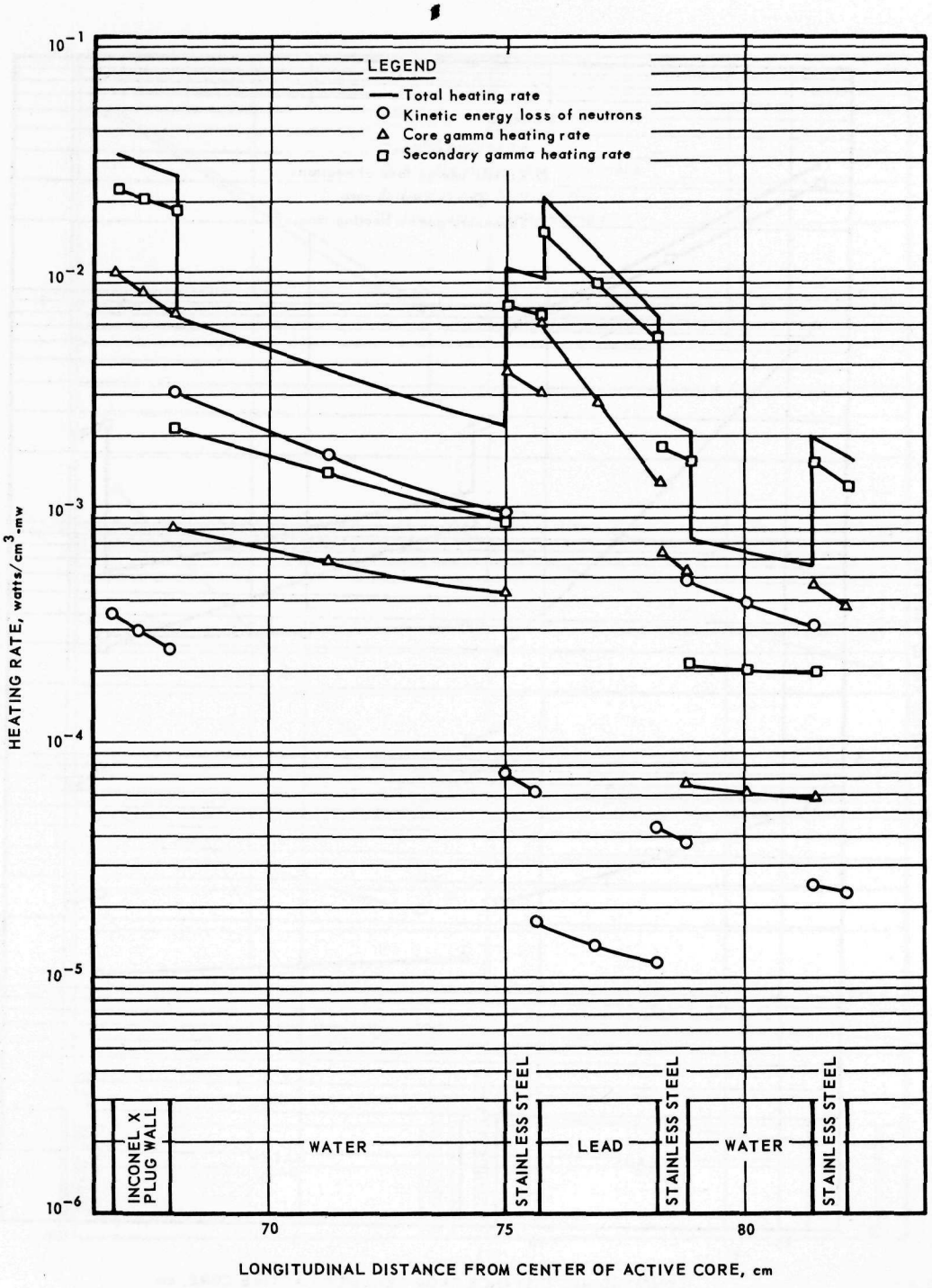

Fig. 5.33a – Calculated heating rates in the longitudinal traverse of the HTRE No. 3 front shield plug

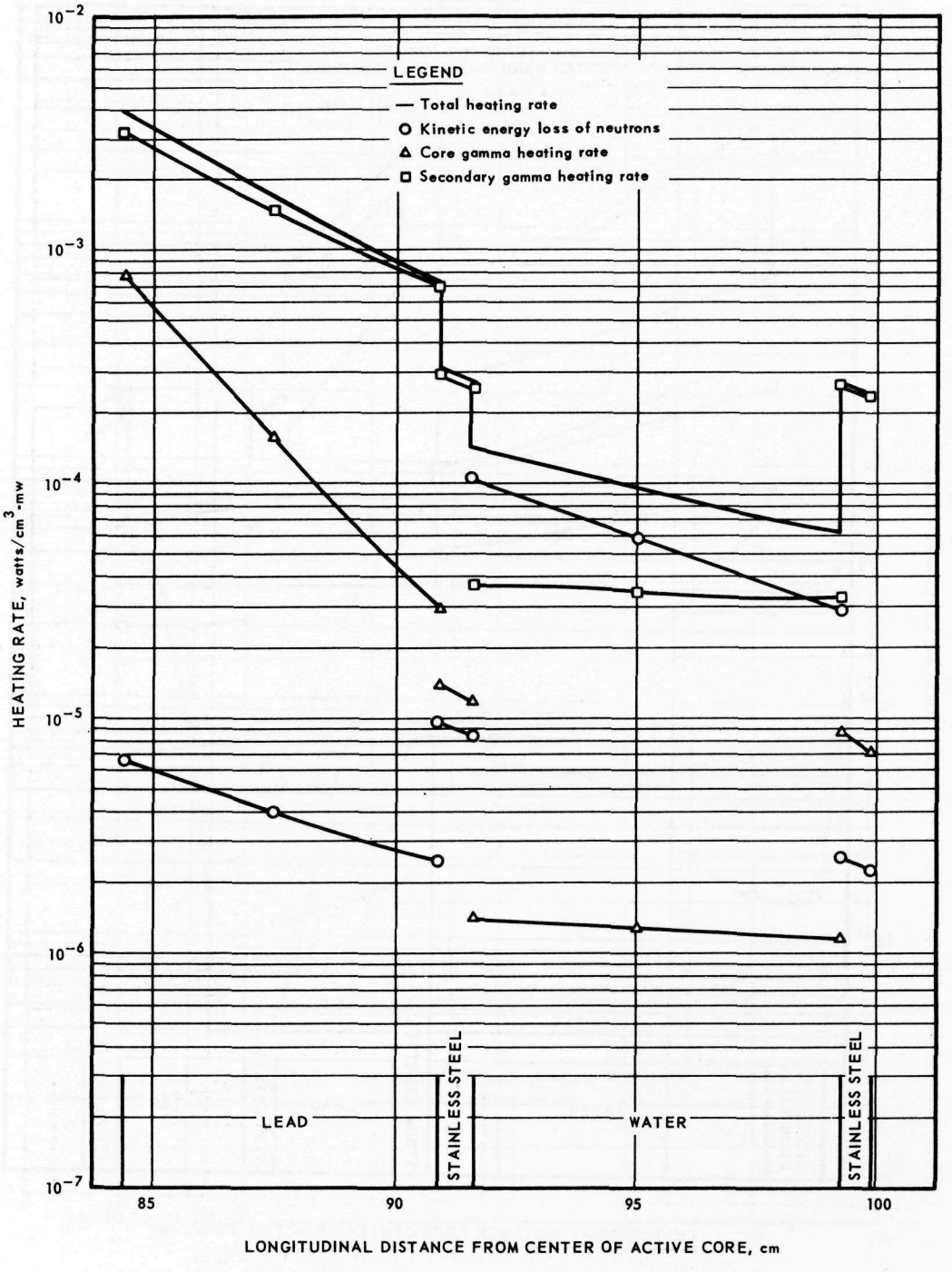

Fig. 5.33b -- Calculated heating rates in the longitudinal traverse of the HTRE No. 3 front shield plug

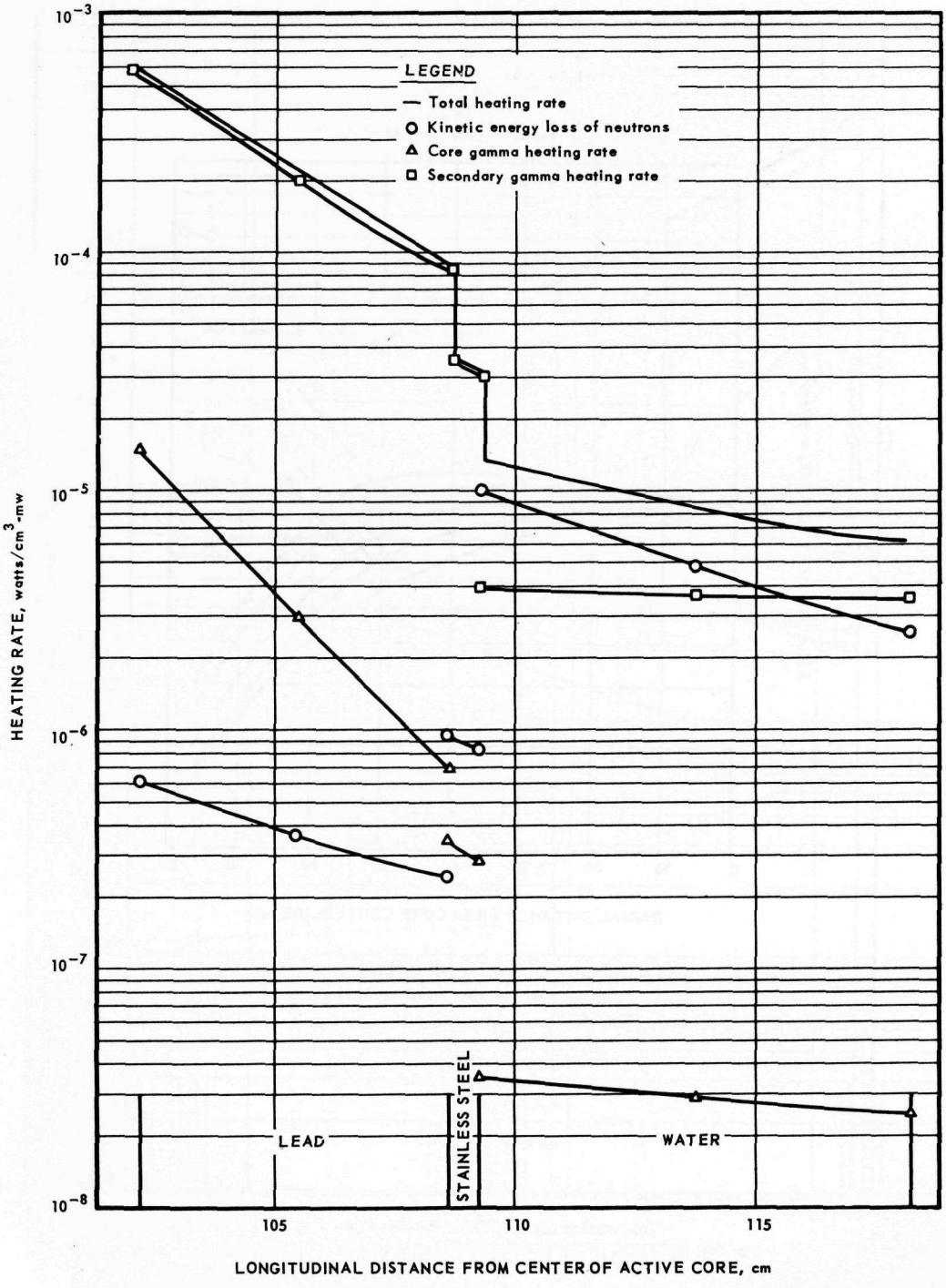

Fig. 5.33c – Calculated heating rates in the longitudinal traverse of the HTRE No. 3 front shield plug

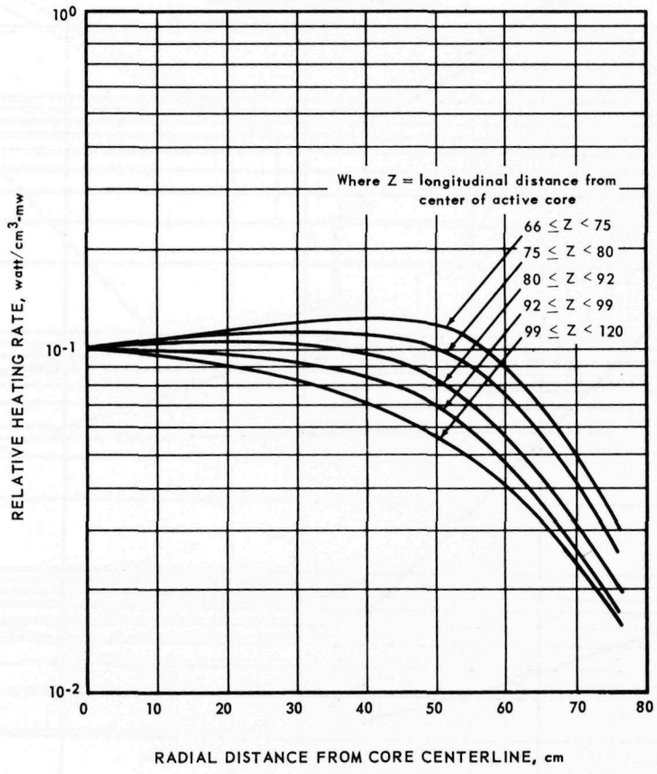

Fig. 5.34 – Calculated radial distribution of the total heating rate in the front shield plug of HTRE No. 3

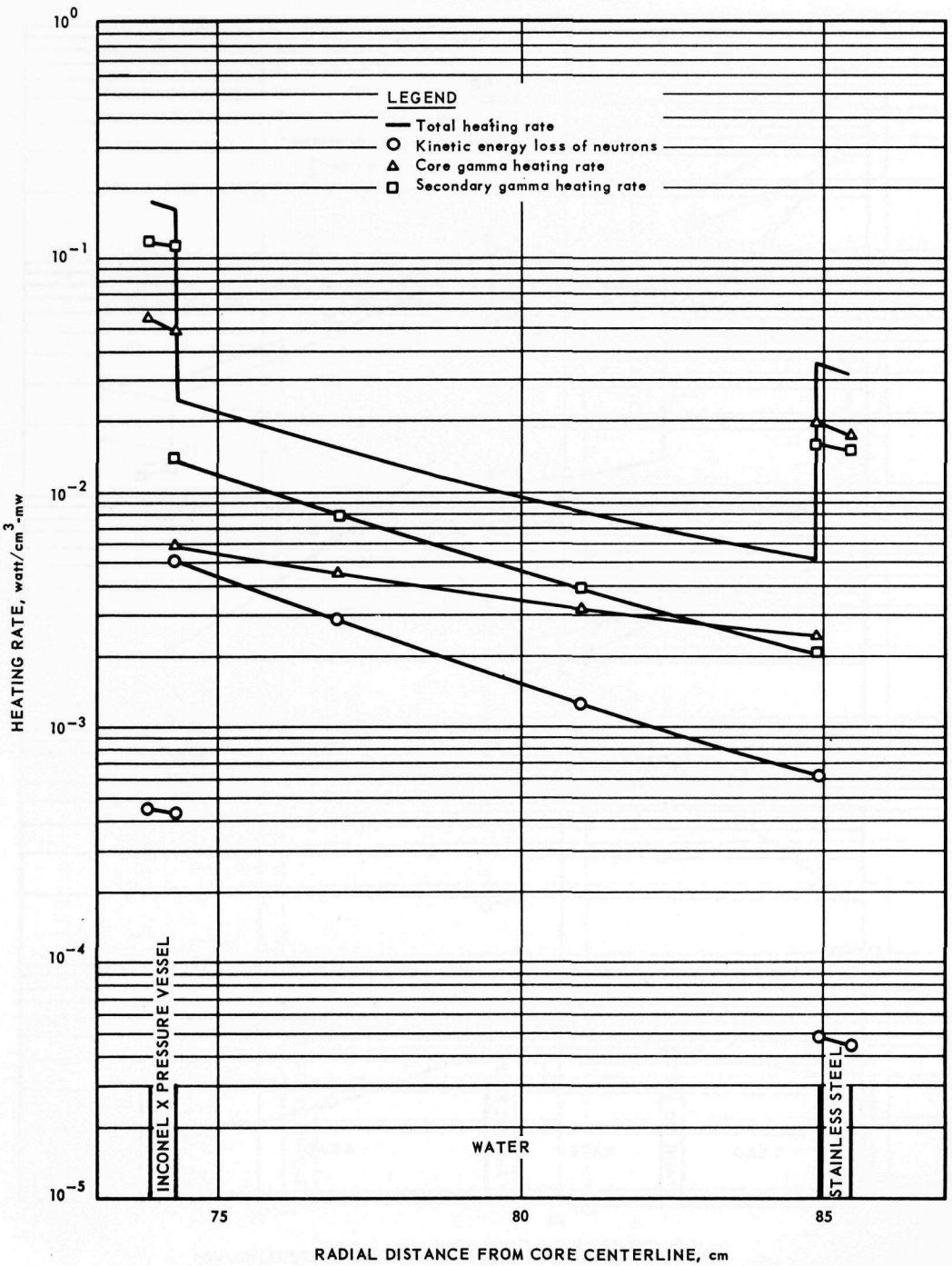

Fig. 5.35a – Calculated heating rates in the radial traverse of the HTRE No. 3 primary shield

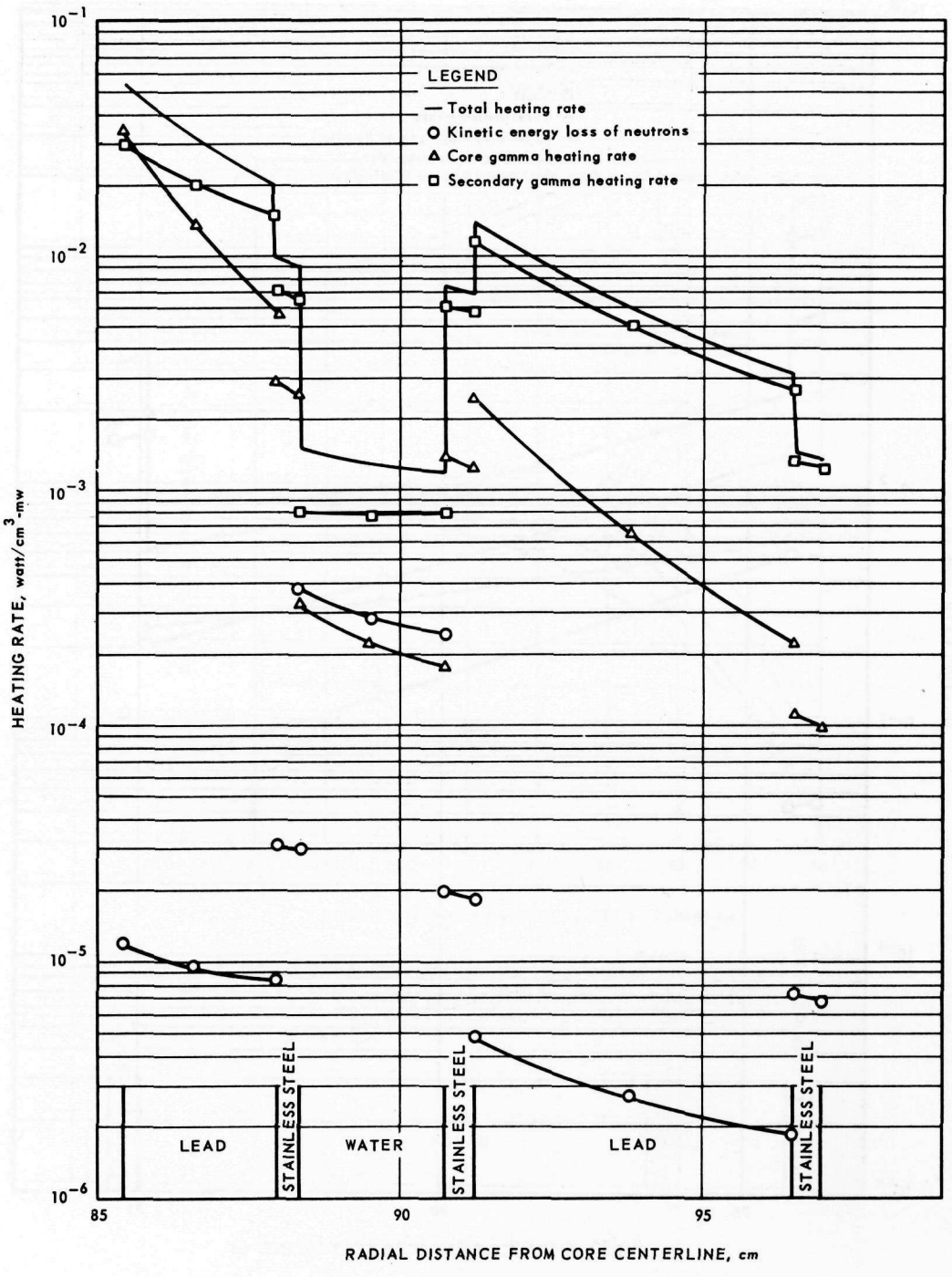

Fig. 5.35b – Calculated heating rates in the radial traverse of the HTRE No. 3 primary shield

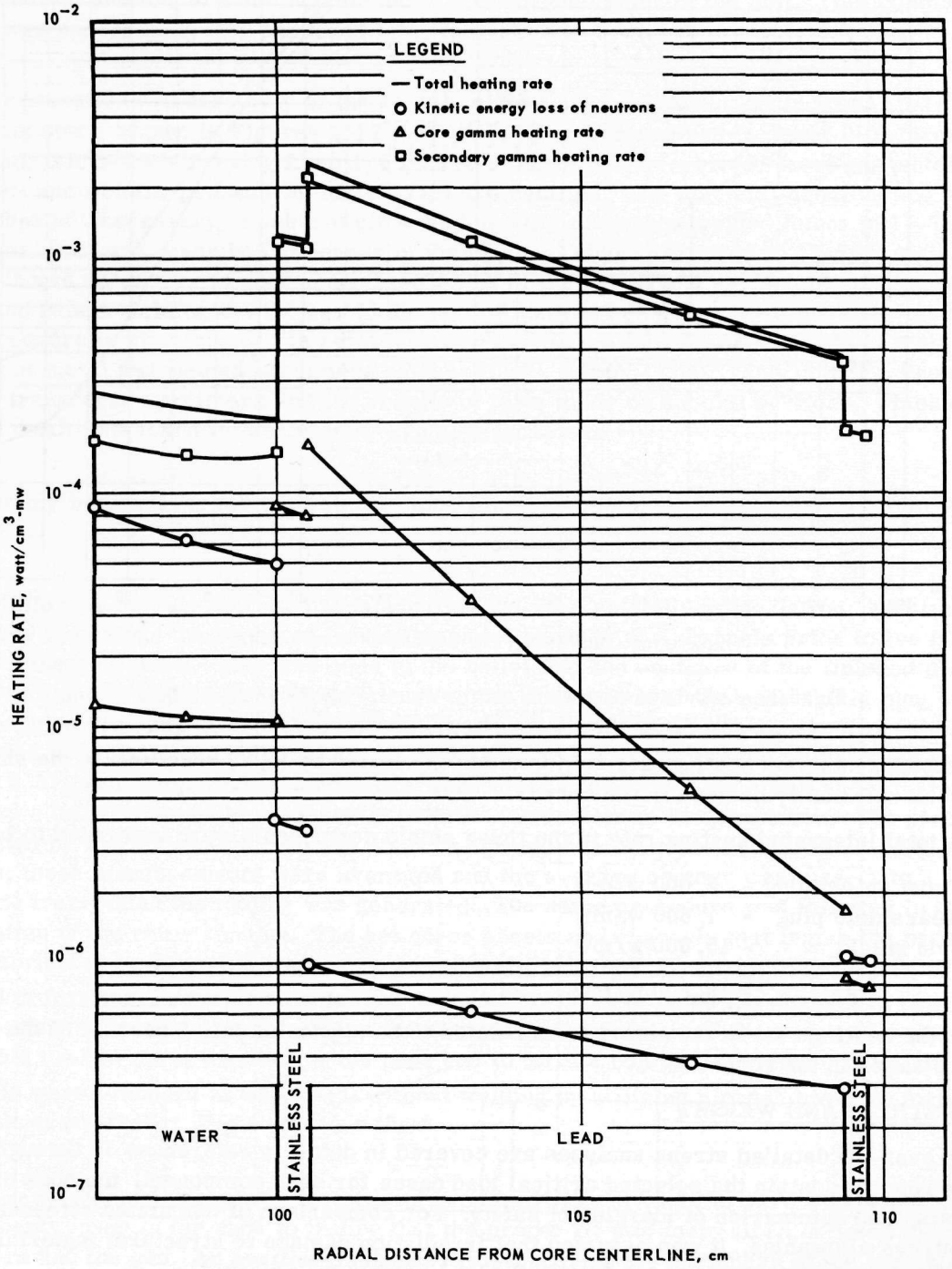

Fig. 5.35c – Calculated heating rates in the radial traverse of the HTRE No. 3 primary shield

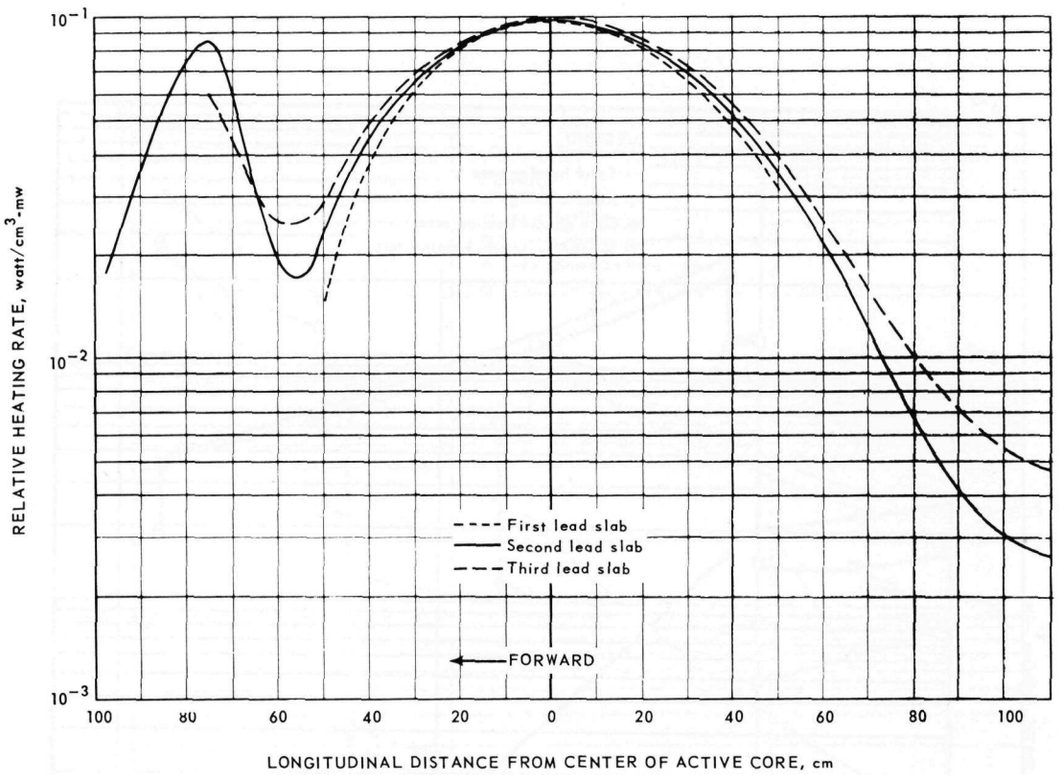

Fig. 5.36 – Calculated longitudinal distribution of the heating rate in the primary shield of HTRE No. 3 for the three lead slabs

the secondary gamma heating rate, i.e., gammas generated by (n, γ) reactions in the shield materials can easily be seen in the curves.

The total integrated heating rate in the three shield components were estimated to be:

Front shield plug	-	2, 000 w/mw
Rear shield plug	-	1, 800 w/mw
Side shield	-	15, 000 w/mw
Total	-	18, 800 w/mw

Thus, the heating rate in the shield is calculated to be approximately 2 percent of the total heat released in the core.

5. 2. 4 STRESS AND WEIGHT

The over-all detailed stress analyses are covered in detail in references 19 through 27. These reports contain the selected critical load cases for each component, methods of analysis, and summaries of margins of safety. For comparison of calculated stresses with stress allowables, it was assumed that irradiation damage to structural material properties was negligible.

5.3 MANUFACTURE AND ASSEMBLY

Many problems were encountered in the fabrication, welding, and heat treatment of Inconel X for the HTRE No. 3 shielding. Reference 28 described in detail the construction of the inner pressure vessel fabricated of Inconel X in thicknesses varying from 0. 146 to

3.5 inches. This vessel, shown in Figure 5.14, is a double-flanged cylinder approximately 95 inches long and 68 inches in diameter at the flanged ends, reducing through a knuckle and transition section to a 58-inch diameter through the center of the unit. This complex vessel was successfully age-hardened after fabrication.

The fabrication and assembly of the scroll, elbows, and transition ducts from 17-7PH stainless steel, shown in Figures 5.17 through 5.19, are described in detail in reference 29. Plate thicknesses varying from 1/4 inch to 3 inches were involved. Inert gas-shielded tungsten-arc welding procedures for 17-7PH are detailed. The material handling and welding techniques necessary to achieve ultra-high quality multipass welded joints in 17-7PH stainless steel are described. Because of the physical characteristics of 17-7PH stainless steel, it was necessary to zone-anneal the edges of the scroll and elbow after heat treatment and before welding the flanges to the unit. A detailed description of the zone-annealing procedure is also included in reference 29, as well as the results of physical tests made on parent metal and welded specimens aged at 1000°, 1050°, 1100°, and 1150°F. Properties of transverse specimens and the results of tests made on special sections, which duplicated conditions found in fabrication, are also included.

Assembly instructions for the shield components are contained in references 30 through 35.

The following method was used in fabricating the rear shield plug insulation. No attempt was made to contour the required insulation cover sheet or the channels prior to the fabrication of the plug itself. This was done in the belief that the contours of the finished plug and outer annulus would not be close enough to the dimensions of the rear shield plug or outer annulus drawings to insure that the contours of the insulation cover sheets could be fabricated to actual plug contours. It was found, however, that after the plug (shown in Figure 5.37) was completed, the contours were close enough that the cover sheet material could have been fabricated concurrently with the fabrication of the plug itself. The plug, fabricated by the Willamette Iron and Steel Company, was contour-measured at eight locations; these measurements were averaged and the average contour was made into a template from which the tooling was generated. The same procedure was followed in the fabrication of the outer annulus. The hot cover sheets and channels that frame the pads were fabricated by Solar Aircraft Corporation and Cyril Bath Company. Solar Aircraft's method of forming the step channels (see Figure 5.11) was to make the channel in two parts, using a die stamping to achieve the stepped arrangement and the required contour, then weld the two parts together at the nose end to form a completed channel. Similar channels were produced at GE-ANPD without welding by utilizing a press brake to form the channel and feeder dies to contour them.

Fitting the completed pads to the structure proved very straightforward with some minor adjustments made in the pads to insure that the proper fit was maintained between the structure and the pad. An auxiliary support system around the periphery of the plug and the outer annulus was required to achieve the forces necessary to insure that the pad was resting against the structure. The last operation was to weld the stud to the structure. A detailed description of arc stud welding is contained in reference 36. Figure 5.38 shows a view of the completely insulated island structure and Figure 5.39 shows a view of the completed outer annulus of the rear plug. Figure 5.40 shows a view of the rear shield plug as a complete unit.

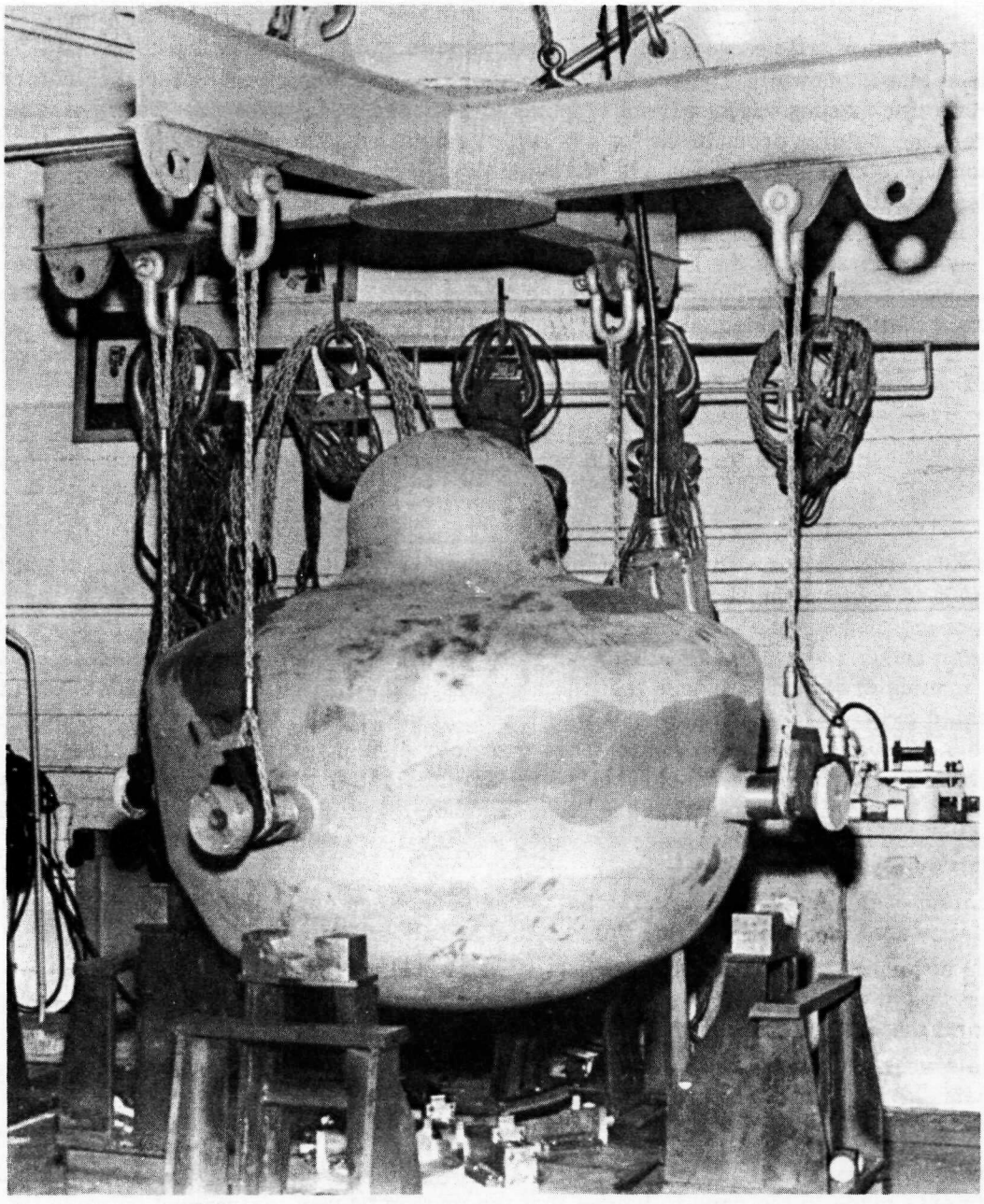

Fig. 5.37 – Insulated rear shield plug (Neg. U35877B)

Fig. 5.38 – Insulated rear shield plug island (Neg. U36136C)

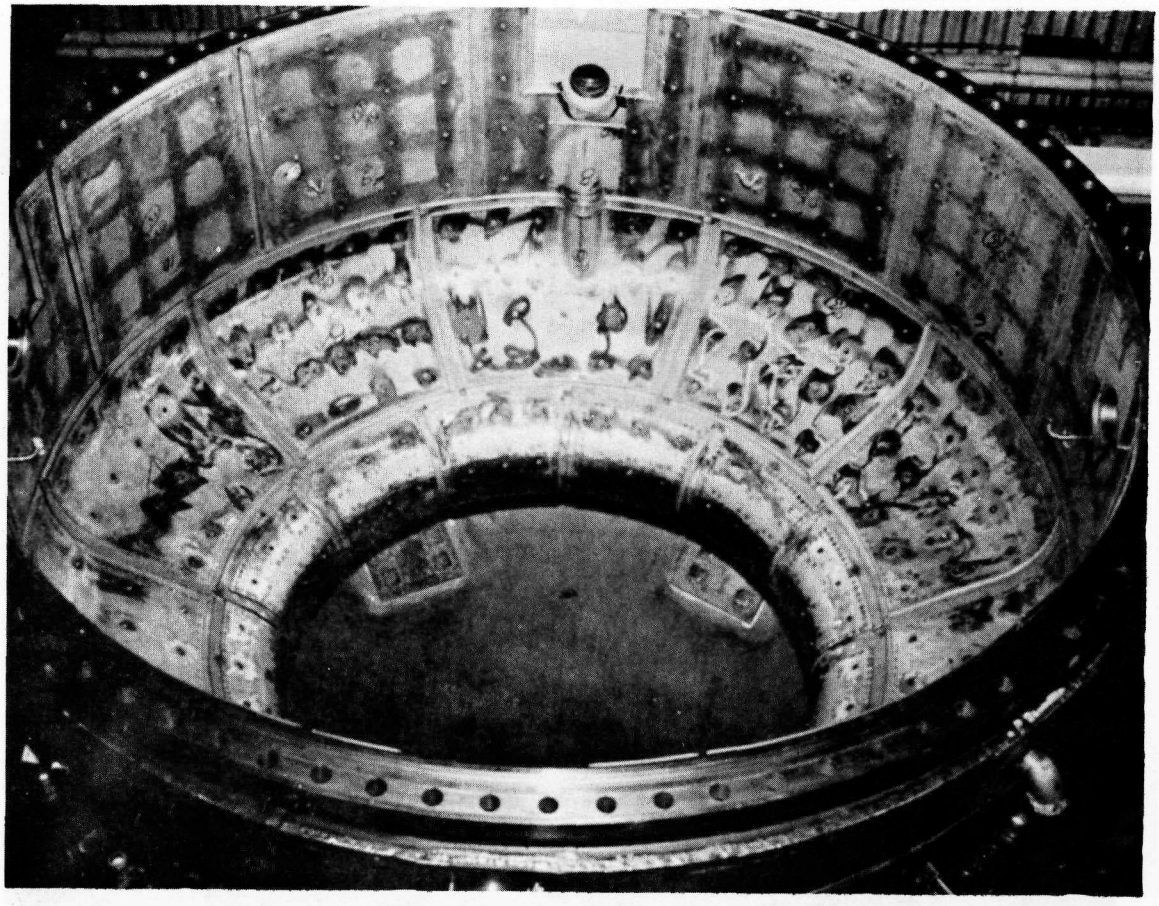

Fig. 5.39 – Rear shield plug annulus (Neg. U36136-D)

5.4 COMPONENT TESTING

5.4.1 MECHANICAL TESTING

5.4.1.1 Front Shield

The following tests were performed on the front shield plug by the manufacturer:

1. The front shield plug was subjected to an external pressure of 220 psi for 1 hour at room temperature.
2. To test for leakage, the front shield plug was filled with water, the outlet closed off, and 25 psig pressure was applied for 1 hour.
3. The time required to drain the shield plug through the outlet in a horizontal position was measured.
4. The pressure drop through the water system of the front shield plug was measured at flow rates of 50, 100, 150, 200, and 250 gpm.

5.4.1.2 Rear Shield

The manufacturer subjected the island plug of the rear shield to an internal hydrostatic pressure of 190 psig at room temperature for 1 hour.

A series of proof tests was performed to determine if the insulation design used in the rear shield would satisfactorily perform for the operating life of the HTRE No. 3 power

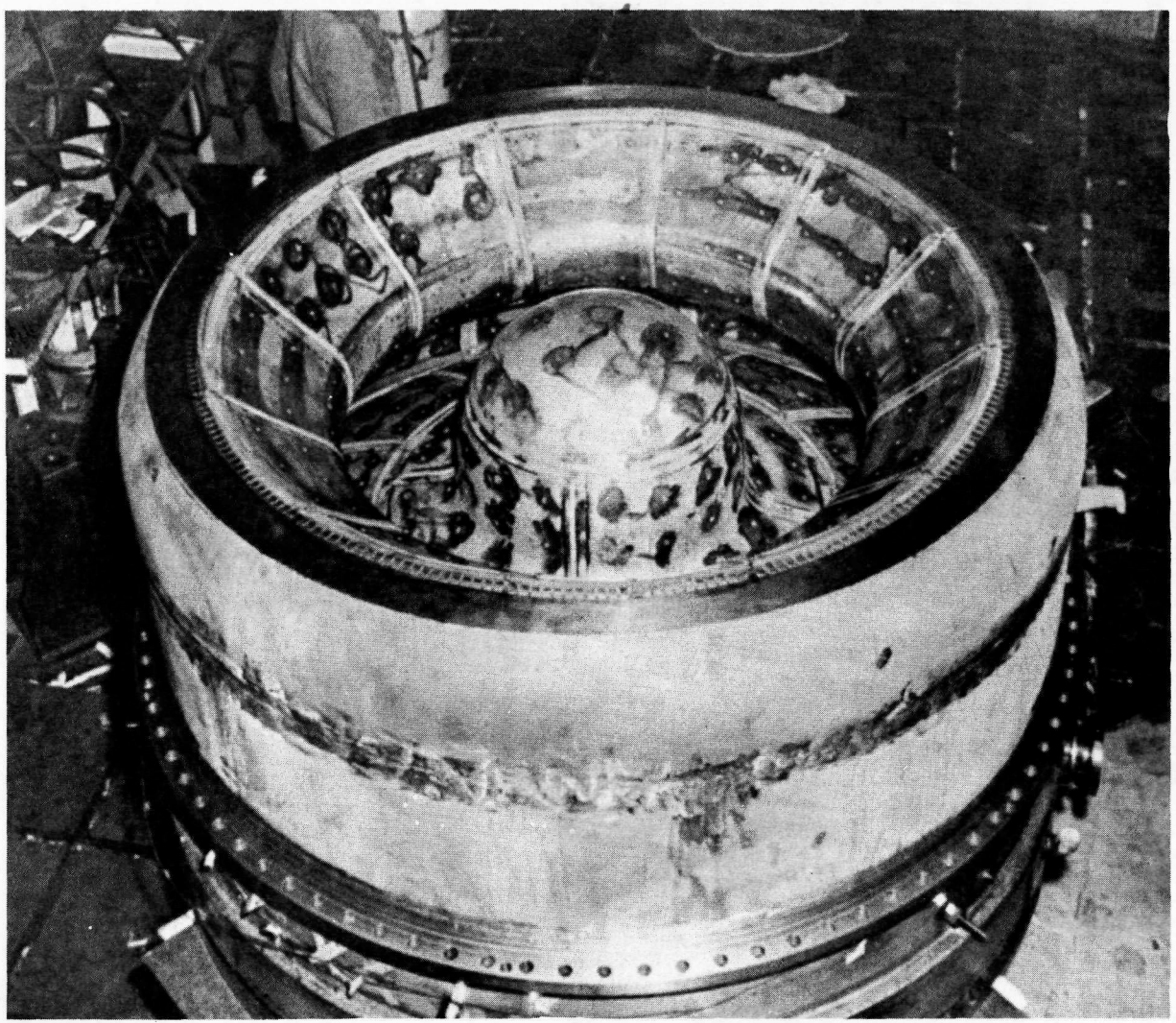

Fig. 5.40 – Rear shield plug assembly (Neg. U36144)

plant. The test tank used for proof testing was a divergent-convergent duct with a plug in the enlarged portion (see Figure 5.41). The smaller diameter was 20 inches and the larger diameter was 30 inches. The plug simulated the island plug of the rear shield. This test tank was insulated as described earlier and as shown in Figure 5.41 with insulation pads similar to those used in the rear plug. Figure 5.42 shows the insulated test tank in the test rig at Wright Air Development Center. The test tank is shown during one of the tests in Figure 5.43.

Various tests were performed on this insulated test vehicle. The test conditions were 150 hours at 1500°F and 100 hours at 1700°F, at Mach 0.23 (pressure = 15 psia). Further tests were performed to determine the effect of JP-4 fuel soaking into the insulation on the possibility of an explosion under the pads during operation. During the ignition tests, high-speed colored photographs were taken of the test tank. These photographs proved that ignition of the fuel did not occur until the vaporized fuel had reached the surface of the insulation pad because of the wicking action of the insulation. Ignition took place at the surface of the pad and fuel was burned. No adverse temperature effects were noted on the structural wall of the insulation. These ignition tests were repeated many times to in-

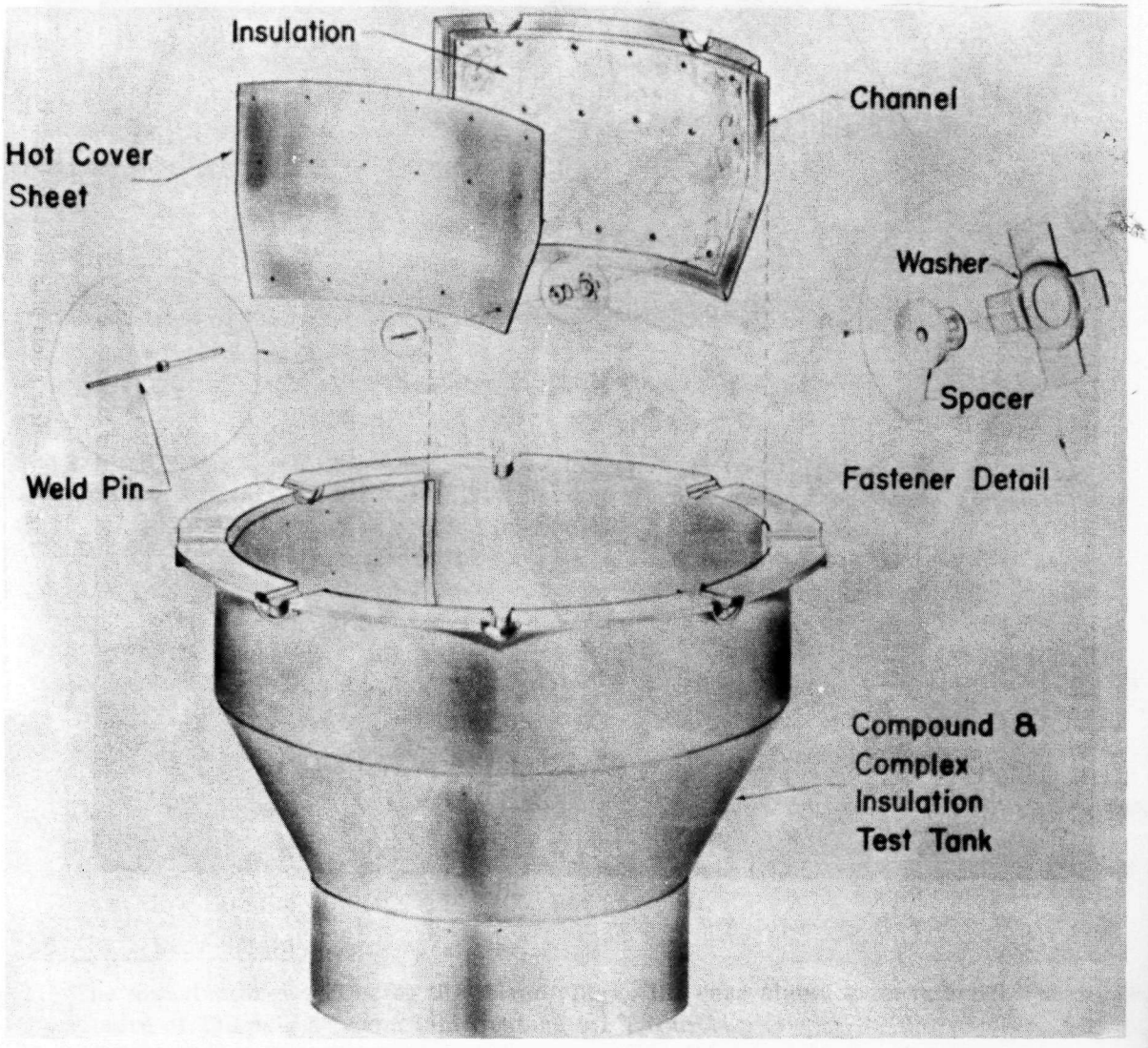

Fig. 5.41 – Portion of the test tank for proof-testing the insulation of the HTRE No. 3 rear shield (G-635)

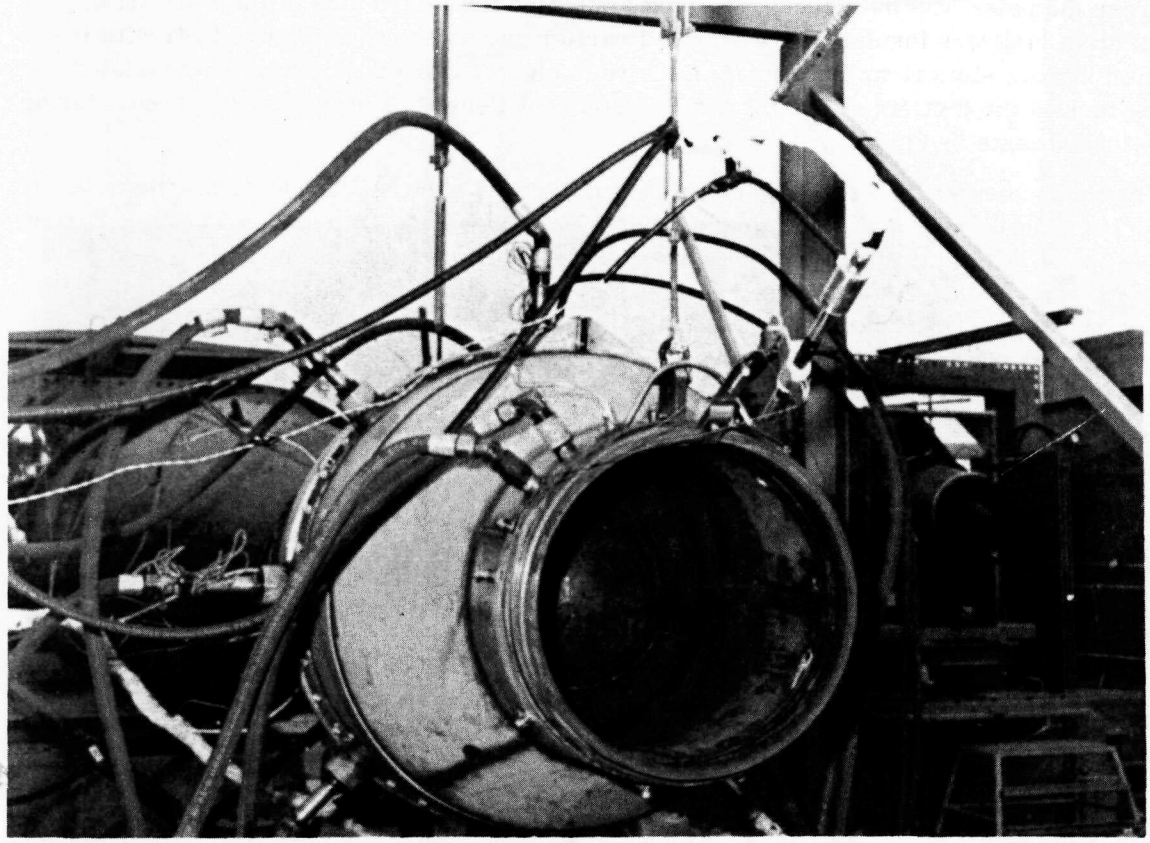

Fig. 5.42 – Insulated rear shield test tank in the test rig

sure that there was no likelihood that ignition would take place. To determine if, under a pressurized system, the ignition characteristics would change sufficiently to cause ignition in the insulation pads, tests were also run under pressures to 60 psi in the Propulsion Unit Test cell at GE-ANPD. These tests also proved that no ignition or explosion occurred under the pad. After all tests were completed, the pads were disassembled to inspect the insulation and fastening components. Figure 5.44 shows a few of the pads. The insulation remained in place and there were no adverse effects from fuel soaking or from the high-temperature gases. Some carbonization from the JP-4 fuel was noted but this had no effect on the insulating value.

A detailed description of insulation designs and testing methods is contained in reference 39.

5.4.1.3 Side Shield

The pressure vessel of the side shield was proof-tested by the manufacturer at a static internal pressure of 240 psig. The test was stopped at 230 psig, however, because the strain gages on the outer surface indicated an approach to local yielding. Because there were no gages on the inside surface of the vessel, the inner surface stresses had to be estimated. Later, the vessel was more fully instrumented as part of the over-all test program and further pressure testing was carried out.[37] The results of these tests showed that the original proof-test could have been continued to 240 psig with safety.

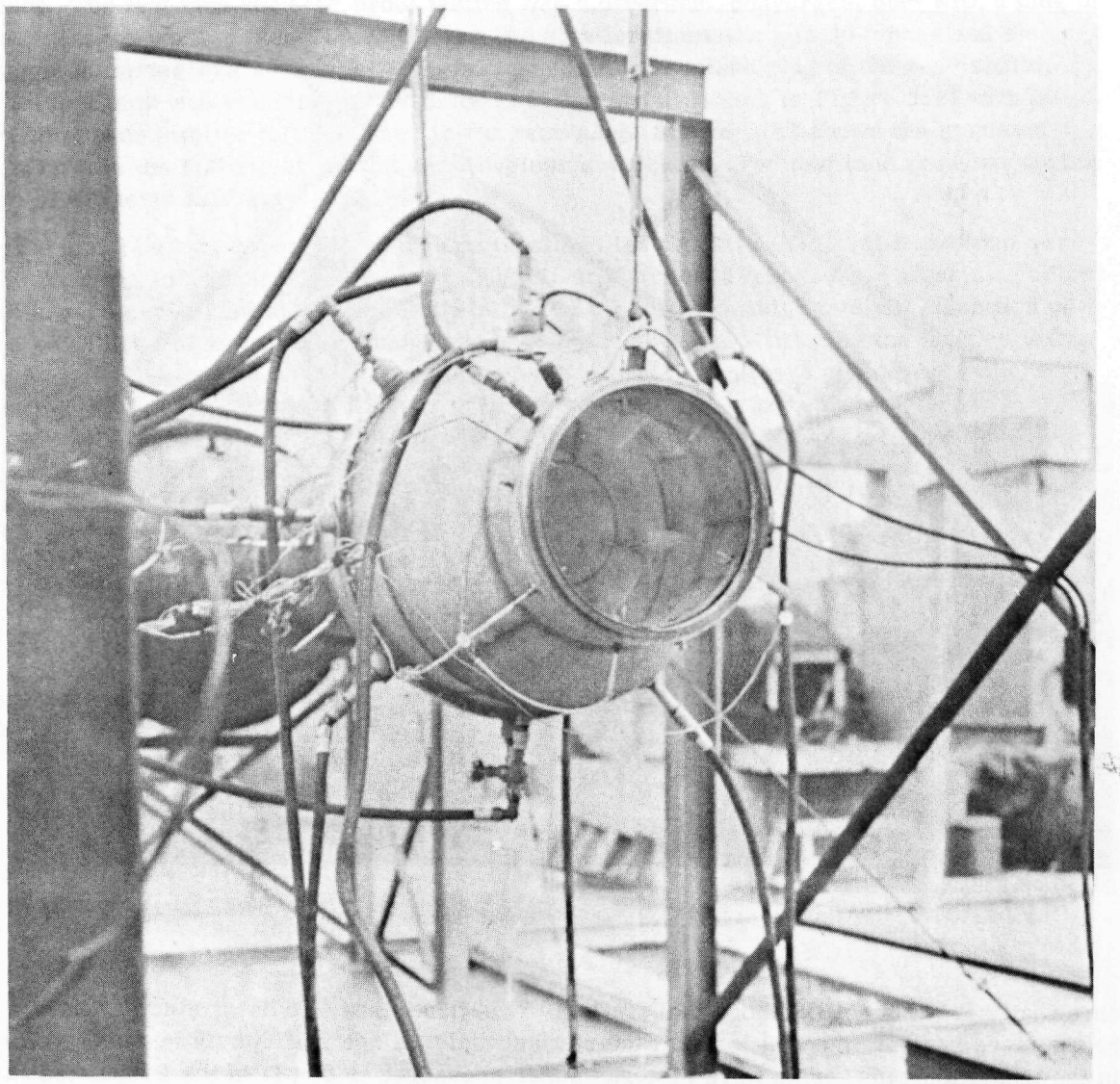

Fig. 5.43 – Insulation test tank during a proof test (Neg. U33731)

After complete assembly of the double-walled cylinder, including the pressure vessel, the following tests were performed:

1. The volumes of the inner and outer tank were measured, as well as the times required to fill them.
2. The pressure drop across the inner tank was measured for a range of water flow rates up to 325 gpm.
3. To check for leaks, the inner tank was filled with water and subjected to an internal pressure of 15 psig.
4. The outer tank assembly was supported at the trunnions and at the forward flange in a horizontal position. The forward support was designed to react only vertical shear loads. Instrumentation in the form of strain gages, dial gages, and photostress was applied to the assembly and the following structural tests were performed.

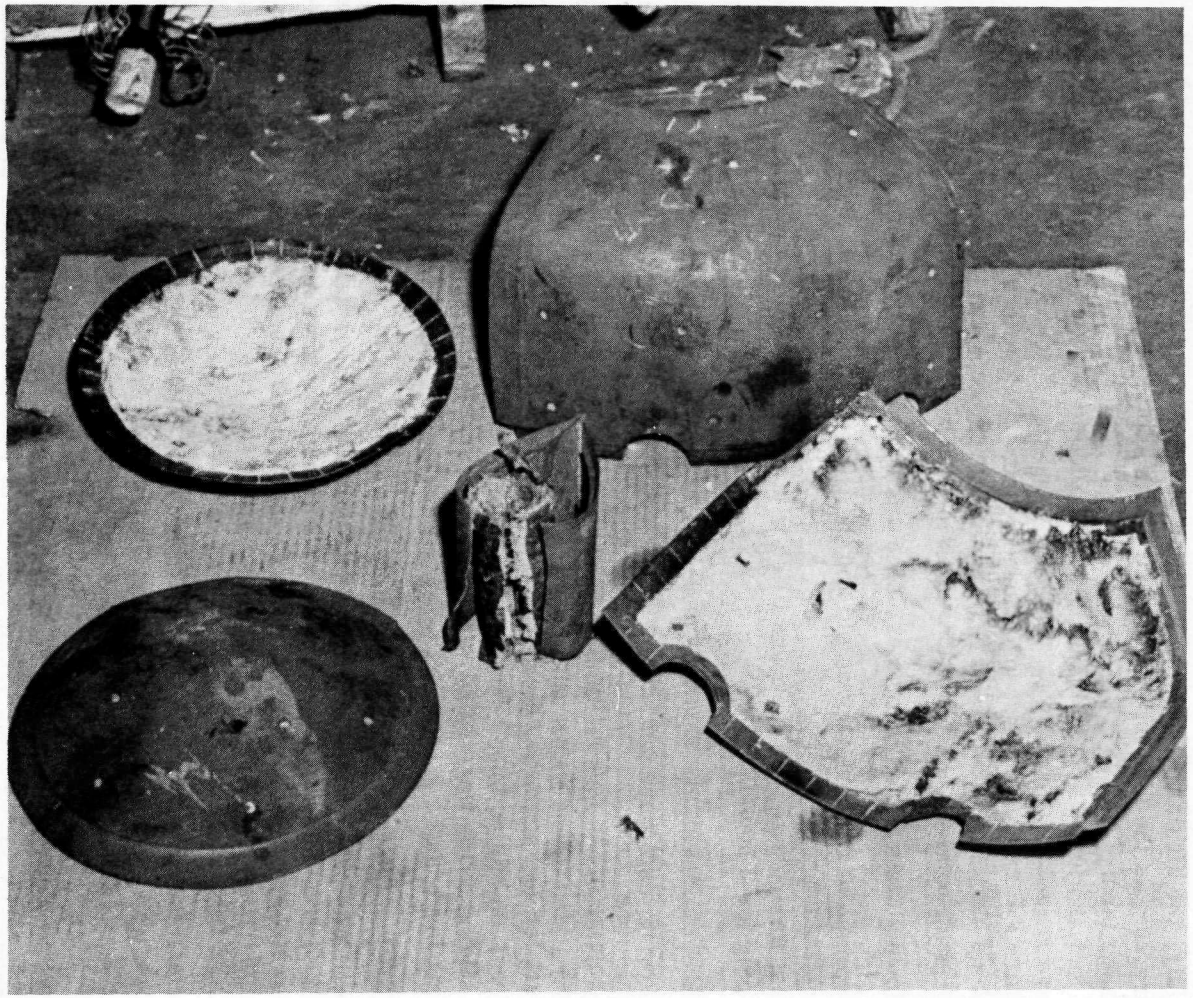

Fig. 5.44 – Insulation pads after proof testing (Neg. U36386D)

a. The outer tank was half filled with mercury.
b. The outer tank was filled with mercury and an additional internal pressure of 48 psig was applied.
c. The forward flange of the pressure vessel was loaded to produce the equivalent of 48, 000-pound down load applied 35 inches forward of the flange face. Simultaneously, the aft flange of the pressure vessel was loaded to the equivalent of a 43, 000-pound down load applied 86. 5 inches aft of the flange face.
d. The forward flange of the pressure vessel was loaded to the equivalent of a 24, 000-pound side load applied 35 inches forward of the flange face. Simultaneously, the aft flange was loaded with a 21, 500-pound side load in the same direction as the load on the forward flange applied 86. 5 inches aft of the aft flange face.
e. A forward load of 86, 000 pounds was applied to the forward flange of the pressure vessel.

The test results are reported in reference 38.

5. 4. 1. 4 Auxiliary Shield

The following tests were performed on the auxiliary shield by the manufacturer.

1. The volume of the auxiliary shield and the time required to fill and drain it were determined.
2. To test for leakage, the tank was filled with water and held to maximum pressure of 5 psig for 2 hours.

5. 4. 1. 5 Combustor Shield

The following tests were performed by the manufacturer of the combustor shield.

1. The volume of the combustor shield and the time to fill and drain it were determined.
2. To test for leakage, the shield was filled with water and an internal pressure of 25 psig was maintained for 1 hour.
3. The sliding doors were filled with water and maintained at an internal pressure of 25 psig for 1 hour.

5. 4. 1. 6 Scroll, Elbow, and Transition Ducting

The scroll was proof-tested by the manufacturer to an internal hydrostatic pressure of 240 psig for 1 hour at room temperature. The transition ducts and elbows were proof-tested to an internal hydrostatic pressure of 250 psig for 1 hour at room temperature.

5. 4. 2 NUCLEAR TESTING

The nuclear tests performed on the HTRE No. 3 are summarized in section 3 of this volume.

5. 4. 3 AEROTHERMAL TESTING

Tests of a One-Fourth Scale Cold-Flow Model

The purpose of tests of a one-fourth scale cold-flow model was primarily to confirm the aerodynamic performance of the preliminary design during the early design stages of HTRE No. 3. The testing program and model design were arranged so that alternative configurations could be tested. However, schedule and time limitations prohibited a systematic testing sequence of each component. Some header development work for air-cooled reactors had been done by the United Aircraft Corporation under contract to NEPA. This work was of a basic nature, however, and did not lend itself directly to current applications since it did not duplicate some of the present design concepts.

These tests utilized air at ambient temperatures and covered a range of projected full-scale Mach numbers at reduced Reynolds numbers and included a number of geometrical variables.

In the design of HTRE No. 3, the airflow is collected forward of the front plugs and ducted through or around the front shield plug, distributing the flow to the reactor fuel tubes. At the reactor discharge, the flow is collected and ducted through or around the rear shield. To obtain maximum aerothermal system performance it is imperative to collect, duct, and distribute this primary coolant flow with a minimum pressure loss, and so that each fuel tube receives its required percentage of the total flow, without compromising the nuclear shielding effectiveness or weight limitations. The nuclear and weight considerations dictate that header or collector sections adjacent to the core be of minimum size, and that ducts piercing the shield plugs follow a tortuous path and also be of a minimum size.

General Arrangement - The cold-flow test mockup is shown in Figures 5.45 and 5.46. Except for instrumentation, the system is symmetrical about the centerlines shown. The complete mockup extended from station 3.2 to station 3.7 and included the following components:

1. Front plug inlet scroll for combining 2-engine flow.
2. Annular front plug with a variable-geometry header.
3. A reactor-simulating tube bundle containing flow-measuring devices.
4. A variable-geometry annular rear plug, and a HTRE No. 3 rear plug.
5. Rear plug discharge plenum.

Inlet Scroll - In addition to the drawing in Figure 5.45, the scroll is shown photographically in Figure 5.47. The scroll receives the airflow from the two turbojet engines through transition sections, turns it 90 degrees through constant-section elbows, and diffuses it through rectangular sections to a hollow "doughnut" plenum at the annular entrance to the front shield plug. Flow obstructions simulating those in the HTRE No. 3 configuration consisted of pins in the transitions, flow splitters in the bends and diffusing sections (not evident in the figure), and pins at the doughnut entrance. The design provides for low-loss airflow Mach numbers which are considerably lower than those in other components, to permit uniform flow conditions in the front shield plug.

Front Shield Plugs - In the mockup, the front plug is a cylindrical, hollow plastic body which, when inserted into a large pipe, provides an annular passage which supplies air to the header plenum. The downstream face of the plug is removable. Figure 5.48 compares the geometries of the various plugs tested, and shows the relationship of tube-bundle geometry. The geometry of front plug No. 5 most closely duplicates that of HTRE No. 3.

Tube Bundle - The simulated core configuration evolved for the tests consists of 216 brass tubes arranged in a hexagonal pattern to form a right cylinder approximately 30 inches long and 13 inches in diameter, as shown in Figure 5.49. This simulated core duplicates the geometry of the fuel tube inlet and exit as well as flow resistance, and is instrumented to determine the flow through each tube and the total header pressure losses.

Rear Plugs - The performance of two types of rear plugs, shown in Figure 5.46, was studied. The proposed HTRE No. 3 type, of which plug Nos. 2 and 3 were examples, was constructed with a removable face so that numerous core-to-face spacings and outlet bend radii were available. The two configurations shown at the top of Figure 5.46 were tested. Because the performance of this type was unsatisfactory, a second plug configuration (bottom of Figure 5.46) was designed. A photograph of this plug is shown in Figure 5.50.

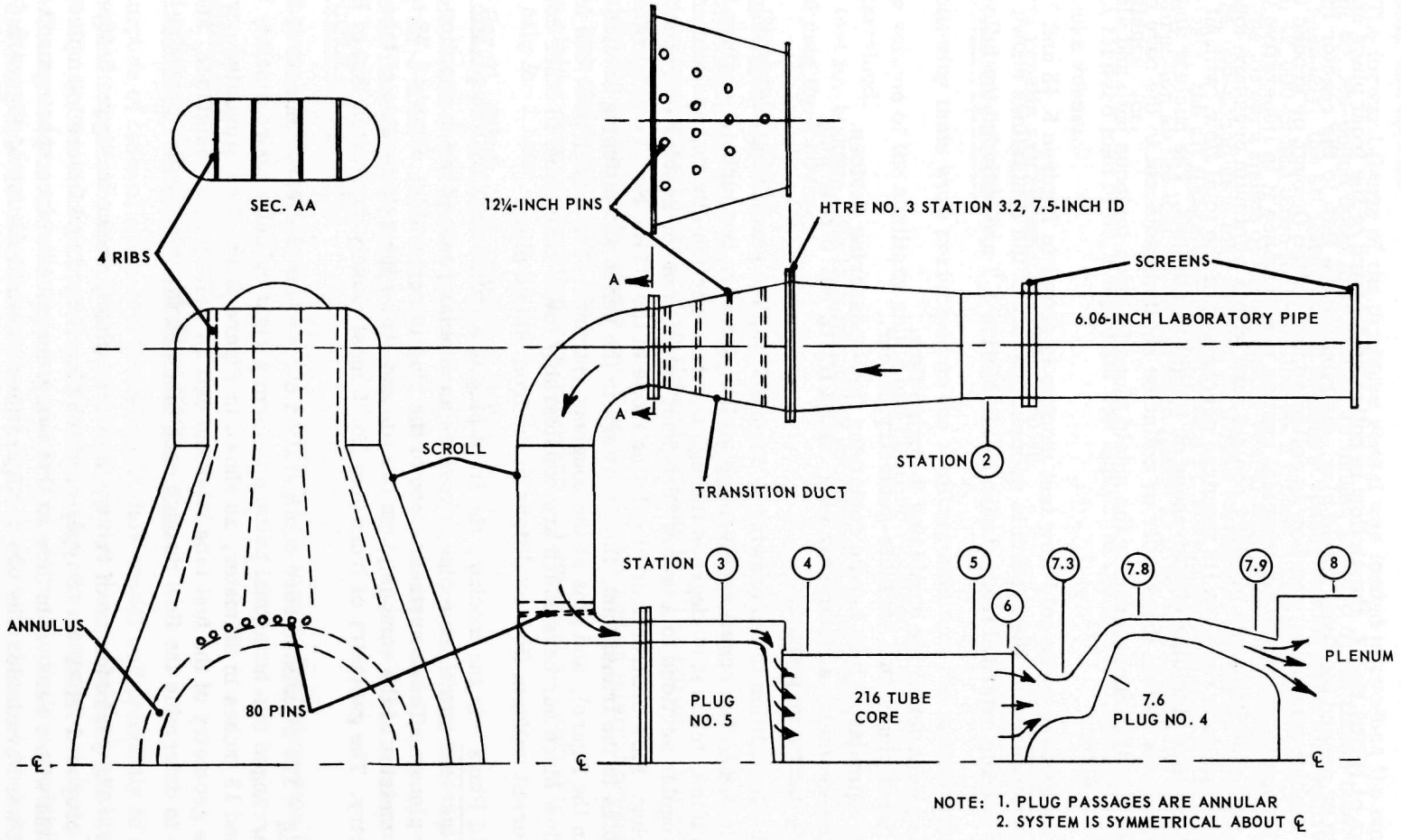

Fig. 5.45 – 1/4-scale scroll-shield-tube bundle mockup for aerodynamic testing

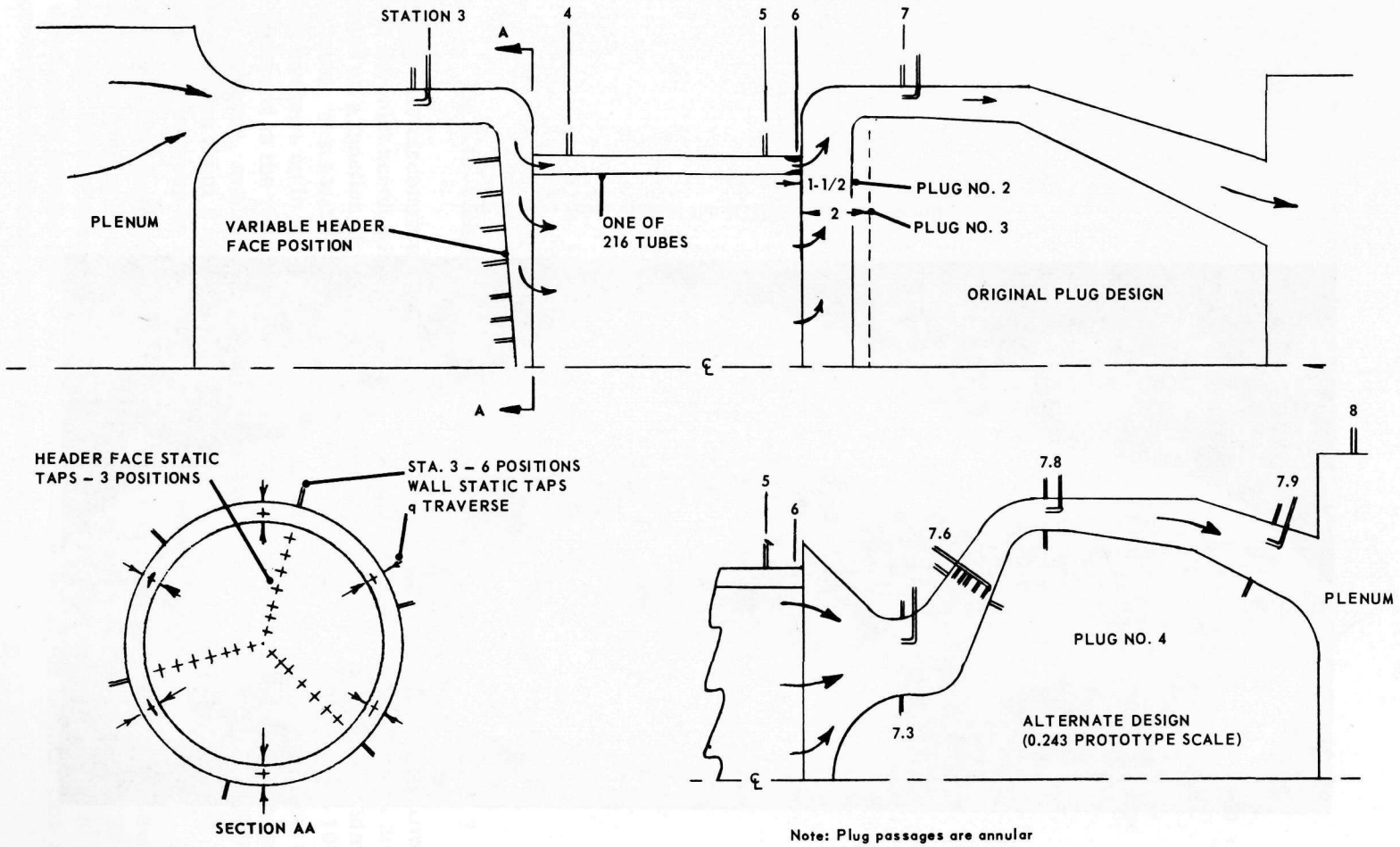

Fig. 5.46 – Alternative configuration of various front and rear header plugs in 1/4-scale aerodynamic test mockup

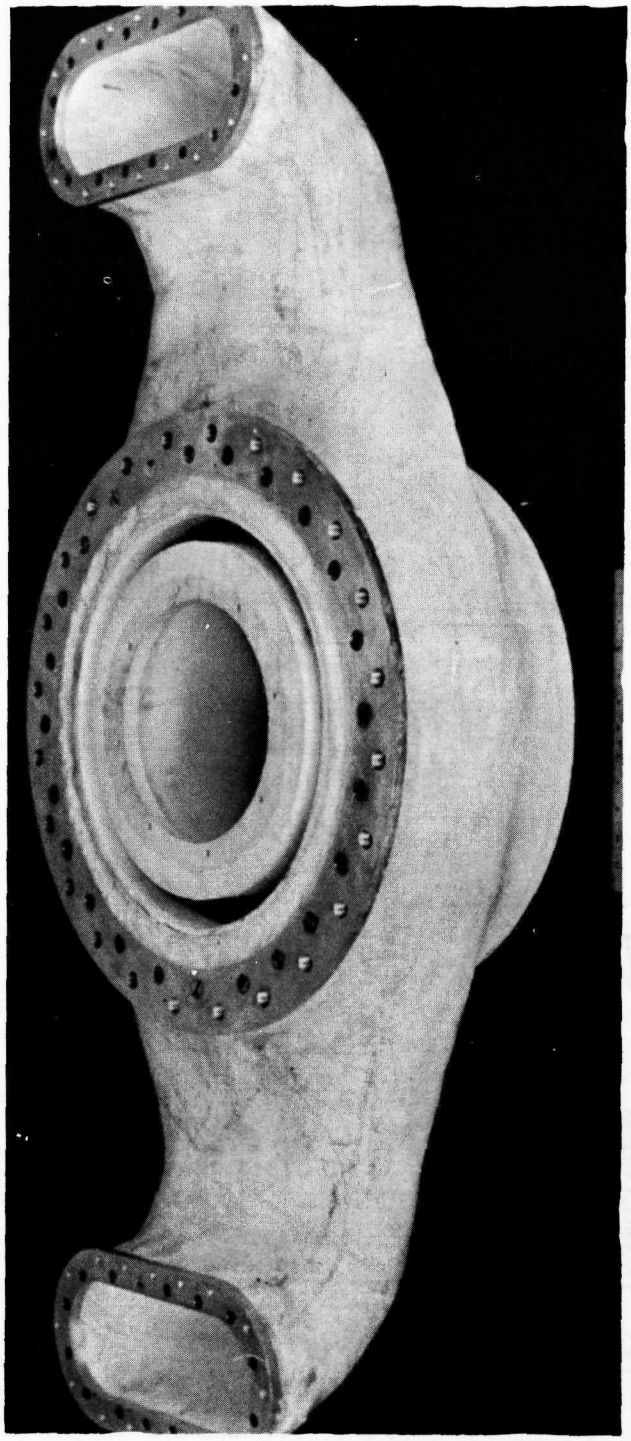

Fig. 5.47 – Front view of the HTRE No. 3 inlet scroll

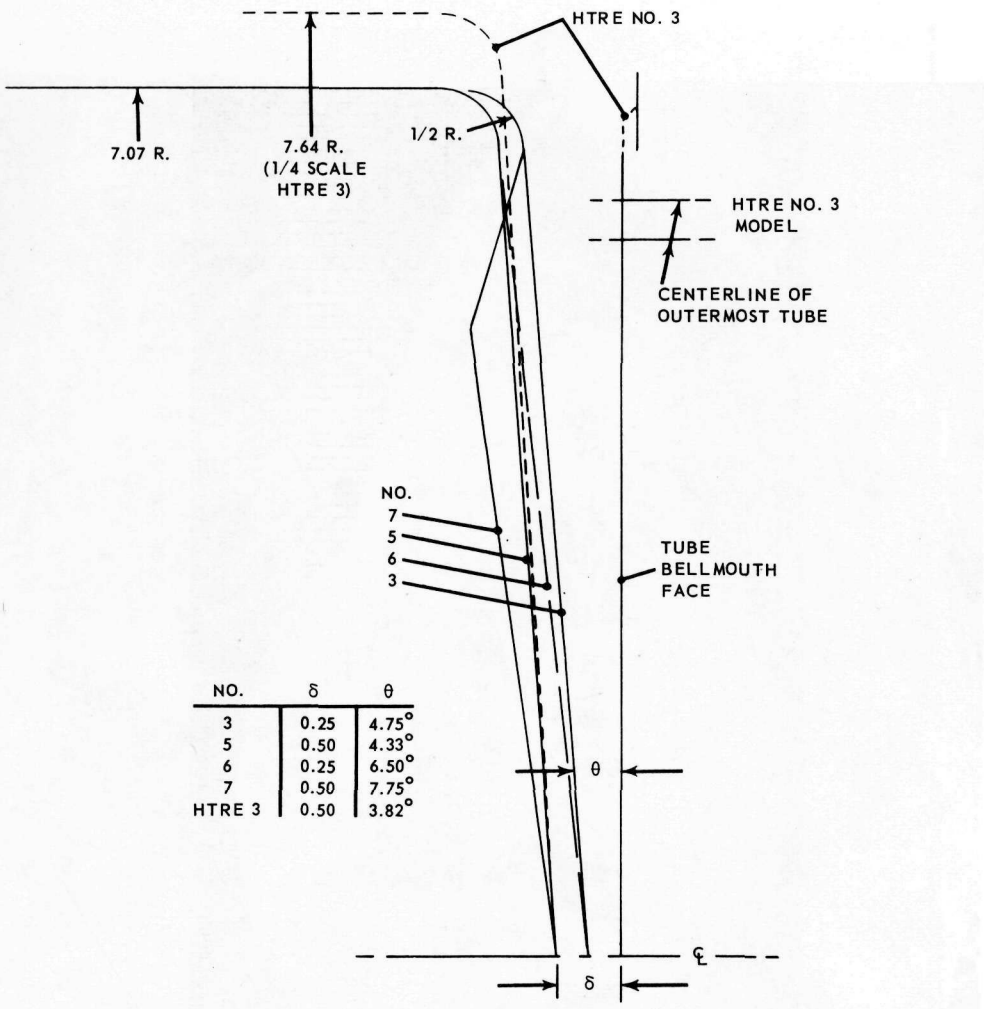

NO.	δ	θ
3	0.25	4.75°
5	0.50	4.33°
6	0.25	6.50°
7	0.50	7.75°
HTRE 3	0.50	3.82°

Fig. 5.48 – Configuration of several front shield plugs tested for the HTRE No. 3

Results - No circumferential variations in reactor flow were noted that could be attributed to the inlet scroll with either 1- or 2-engine operation. No change in distribution was noted as a function of Mach and Reynolds numbers which were varied simultaneously during tests. Tests were run at core Reynolds numbers of about 40, 000 to 100, 000, and at Mach numbers up to those corresponding to X211 operation. No local flow distortions were observed in the vicinity of simulated control rods or tri-rod bolts. Instrument accuracy, however, was such that single-tube flow variations could only be definitely determined within about 1 or 2 percent. The gross flow distribution measured, however, should not be in error by more than about 1/2 percent.

The lowest tube Reynolds number at which it was possible to test the model was about 2, 000, corresponding to a tube pressure drop of about 0. 12 inch of water. At this level, measurement errors were on the order of 5 to 10 percent. Results indicated no local flow deficiencies greater than about 10 percent would occur for laminar flow conditions that prevail during aftercooling blower operation.

Of the four front plug configurations tested, the one most similar to the HTRE No. 3 design had the lowest total pressure loss. Two rear plug configurations were found un-

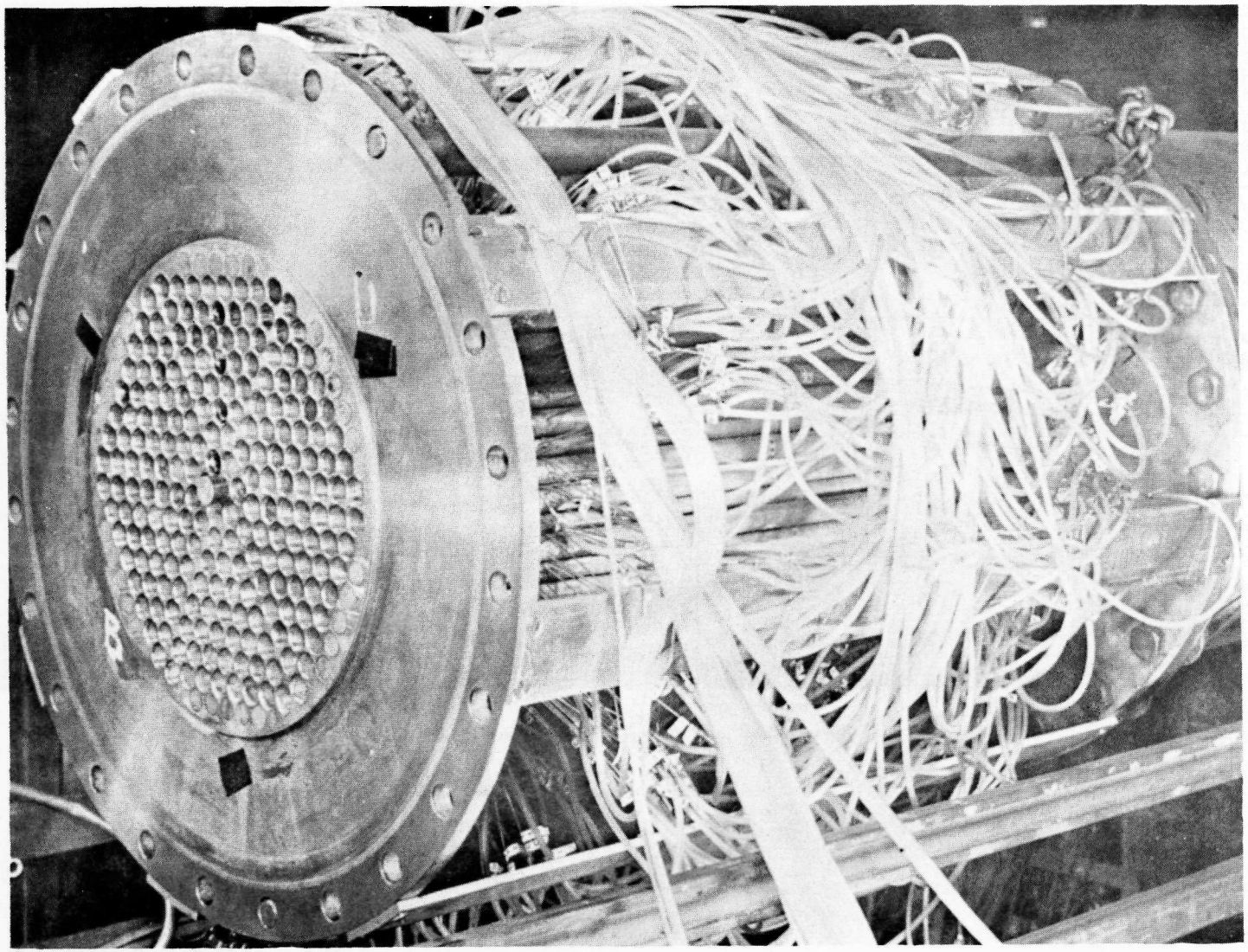

Fig. 5.49 – Reactor simulator showing the tube bundle

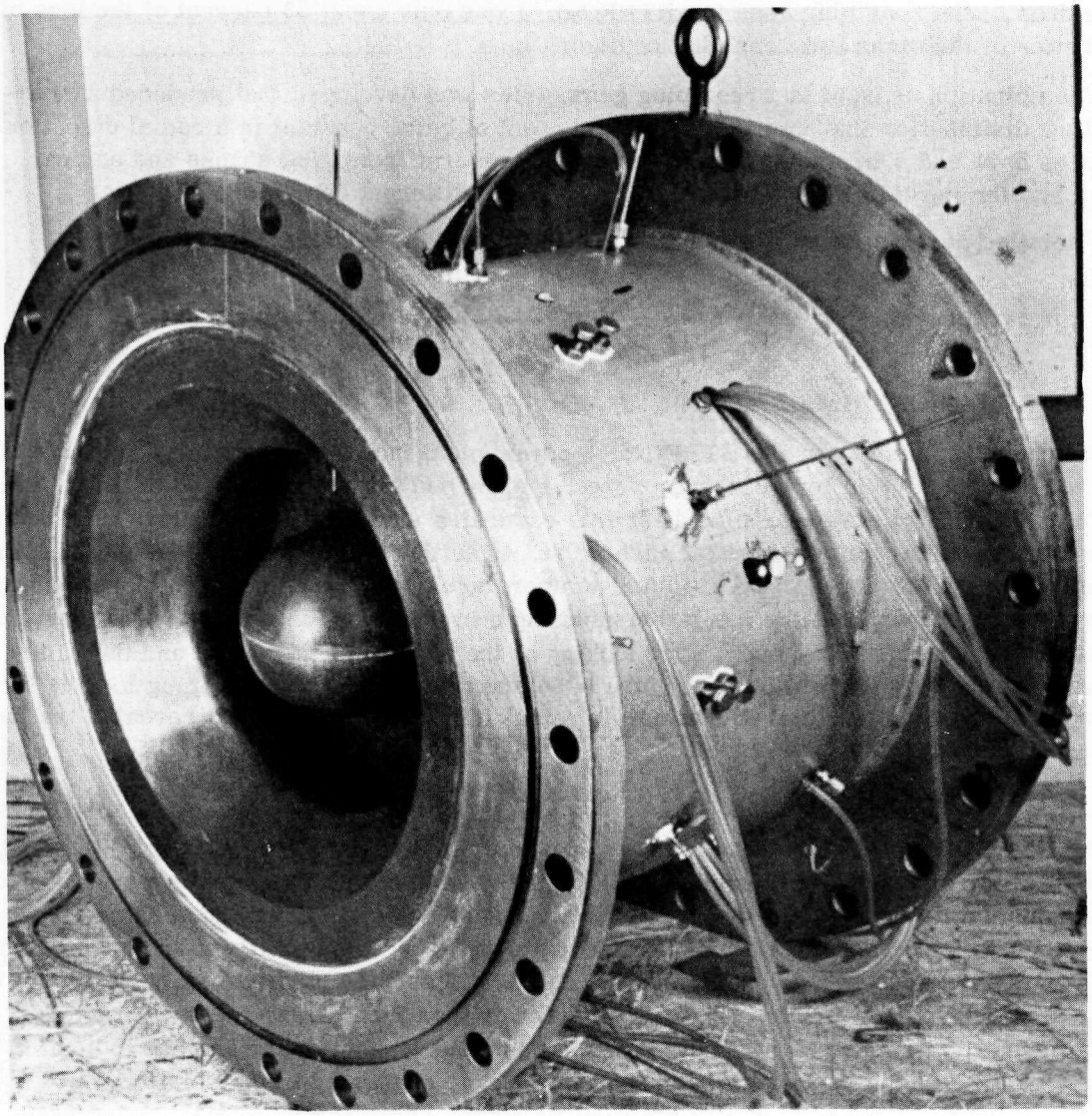

Fig. 5.50 – Rear plug No. 4

acceptable from the standpoint of both reactor flow distribution and pressure loss. A third rear plug configuration, which was chosen for the HTRE No. 3 design, had little effect on the reactor flow distribution produced by the front plug. In addition, the pressure drop in the rear plug used for HTRE No. 3 was only about 53 percent of the loss of the better of the other two rear plug configurations.

A combination of front and rear plug geometries was developed that produced a reactor flow distribution that was within ±2. 5 percent of being constant in a radial direction. Figures 5. 51 and 5. 52 show the test results for several front plug shapes and no rear plug, and for the HTRE No. 3 front plug with three different rear plugs.

A detailed description of the 1/4-scale mockup tests is contained in reference 40.

5.5 OPERATIONS

5. 5. 1 MECHANICAL (INSULATION)

The operating history of the HTRE No. 3 power plant included one reactor runaway in which design maximum temperatures were far exceeded for a short period of time. Inspection of the insulated rear plug after this excursion showed that no damage was experienced by the hot cover sheet or the insulation. After the conclusion of HTRE No. 3 operation (involving 385 hours of operation at temperatures up to about 1400°F), inspection of the rear plug showed that the insulation pads were in place and undamaged. The front end of the rear plug after final operation, looking at the portion of the island and the outer annulus, is shown in Figure 5. 53. Figure 5. 54 shows a view of the rear plug looking through the combustor after the final operation. Physical inspection of this area revealed that no damage had occurred to the insulation.

5. 5. 2 NUCLEAR

The HTRE No. 3 was run in two general phases. Phase I consisted of operation with the top half of the auxiliary shield removed from the assembly. Measurements were taken of environmental fast neutrons, thermal neutron fluxes, and gamma ray dose rates at varying distances from the assembly. Measurements were taken internally in the assembly by locating detectors in sensor wells, control rod passages, and other areas. In general, the calculated dose rates and heating rates were lower than the measured data, especially with respect to gamma-ray measurements. These discrepancies are another indication of the importance of the secondary gamma rays that are generated in the shield itself.

Comparisons of calculated and measured data are presented in Figures 5. 55 through 5. 58 for some of the representative measurements taken during Phase I testing. The total heat generated in the shield components was measured by regulating the flow of cooling water and measuring its change in temperature. The measurements indicated that heat absorbed by the shield was approximately 3. 8 percent of the reactor power. This again is higher than the predicted value of 2 percent.

Phase II testing was primarily an endurance run with the auxiliary shield in place. Some environmental dose rates were measured and the system was monitored after shutdown. The results of Phase II testing can be found in references 41 through 56.

5. 5. 3 AEROTHERMAL

At the start of the Phase II testing at the Idaho Test Station, a great deal of difficulty was experienced with water freezing in the shield system flow valves, lines, etc. In one instance, the expansion of the freezing water was sufficient to rupture the augmentor shield fill and drain line. Considerable operational time was lost in thawing water lines

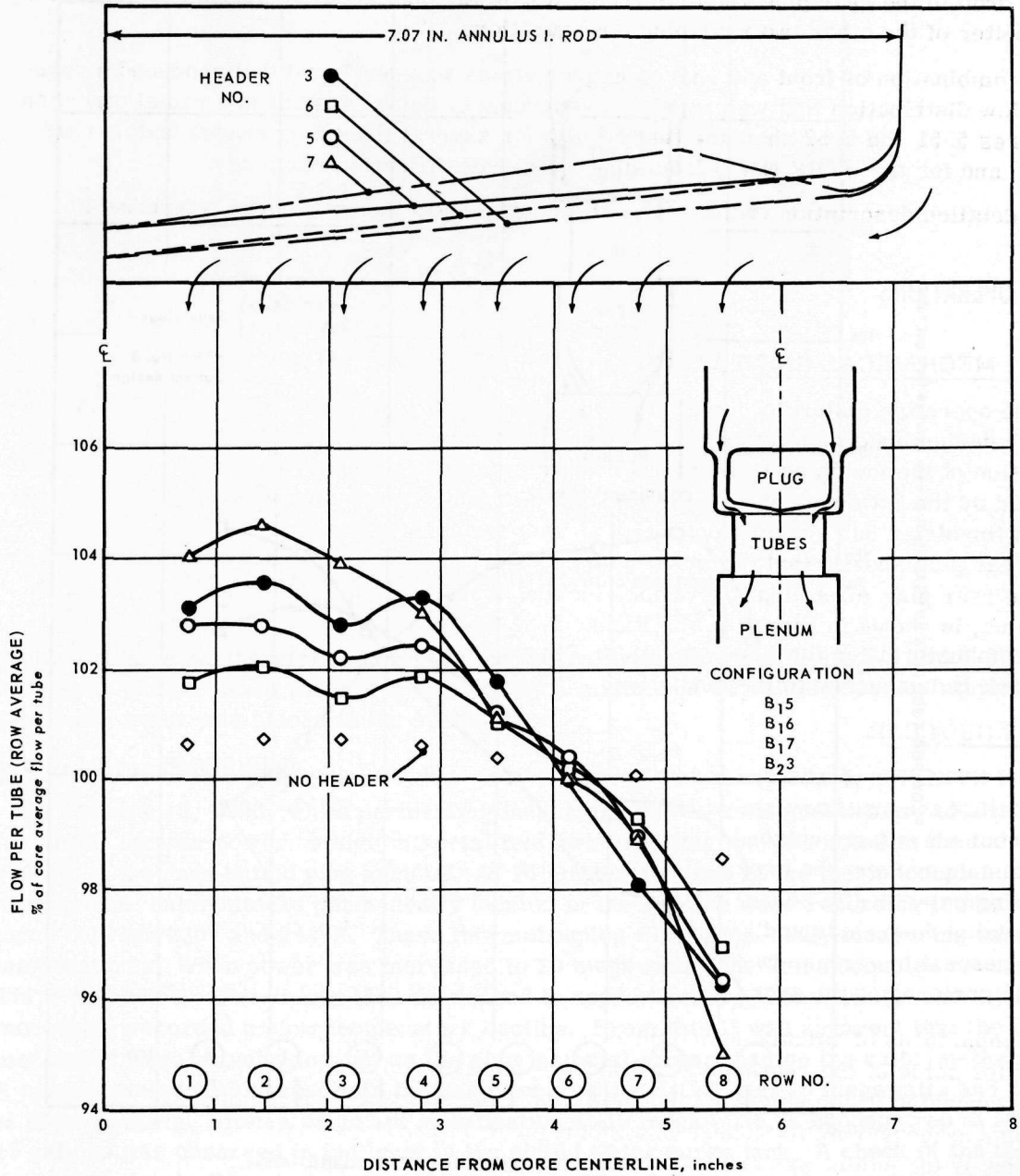

Fig. 5.51 – Weight flow distribution radially in core for various front plug configurations

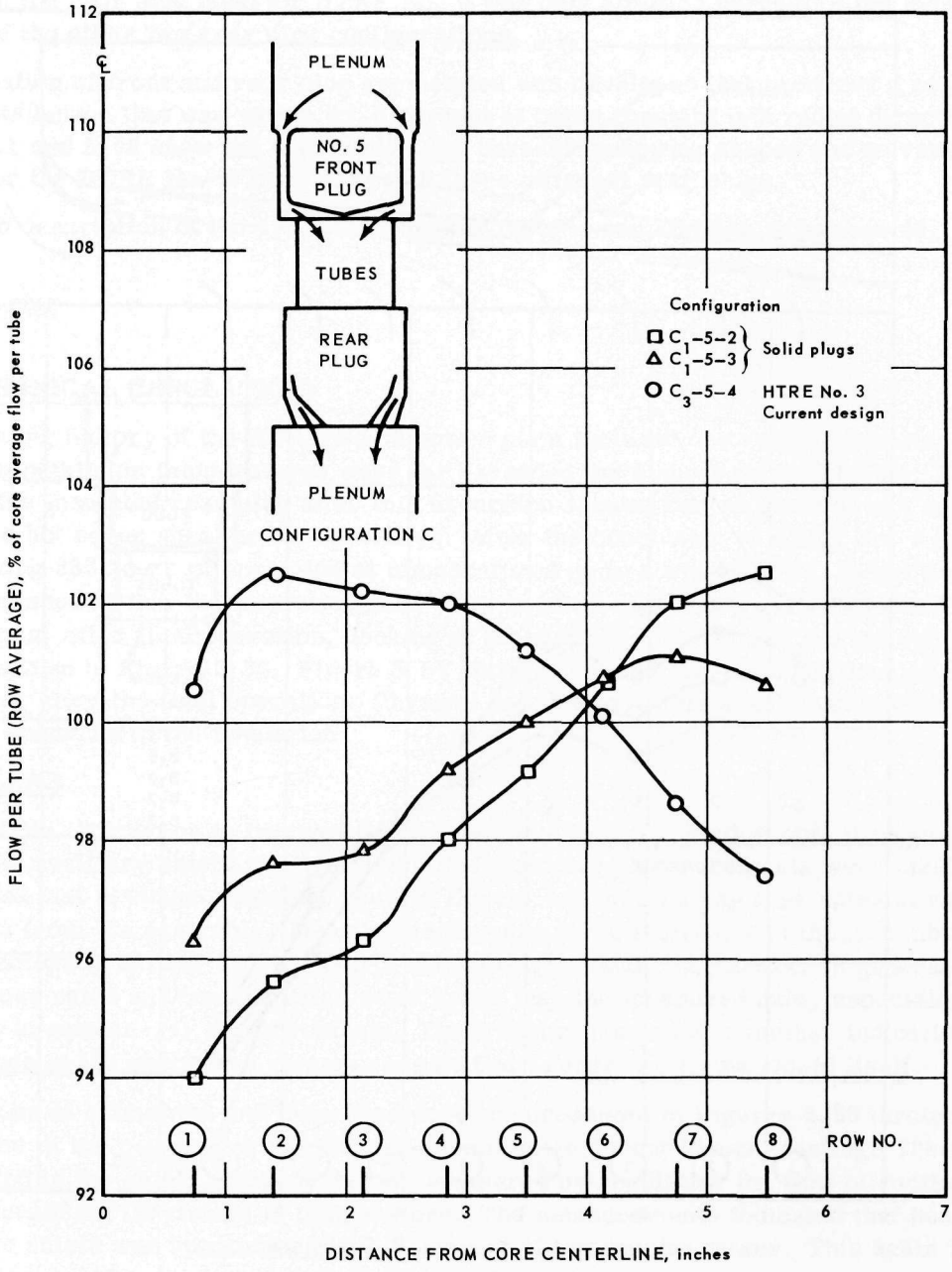

Fig. 5.52 – Weight flow distribution radially in core for various rear plug configurations

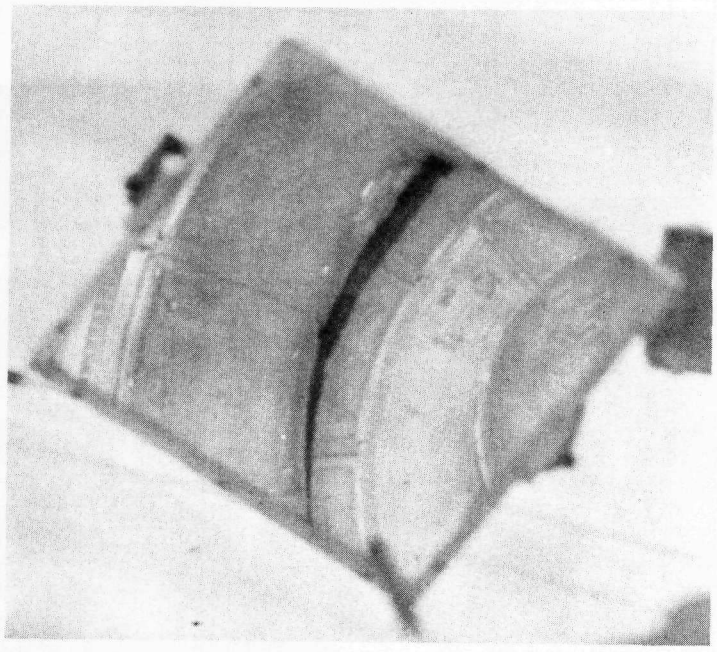

Fig. 5.53 – Front end of insulated HTRE No. 3 rear plug after operation
(Neg. U3323-13)

each morning and, therefore, following the two calorimeter runs (Runs 5-3 and 9-3), the water was drained from the shield system and a mixture of 50 volume percent ethylene glycol and water was placed in the system.

5.5.3.1 Rear Shield Plug

On January 15, 1960, while performing increasing power tests preliminary to a transfer to full nuclear power, a high material temperature situation was noted in the forward portion of the rear shield plug annulus. At 16 megawatts, two of the thermocouples on the heating-rate calorimeters permanently located in the annulus were recording temperatures between 230° and 244°F. These thermocouples were supposedly measuring case temperatures. When power was increased to 20 megawatts, the thermocouples recorded 274°F and 282°F. Power was then decreased to approximately 10 megawatts and the thermocouples recorded a slow temperature decline. From this it was apparent that the thermocouples were actually located on the slug material rather than on the calorimeter case. A case-mounted thermocouple in the same location read 157°F at 10 megawatts and 244°F at 20 megawatts. After a period of stabilization at 10 megawatts, a sudden drop of about 15 gallons was observed in the level in the shield water surge tank. A check of the three thermocouples in the annulus showed a corresponding decrease in temperature. After the temperatures had stabilized, reactor power was again increased to 20 megawatts. For a period during the initial power increase, the case thermocouple and surge tank level remained practically constant. The tank level suddenly rose by 15 gallons, however, and the case temperature climbed rapidly to 250°F at 20 megawatts. The test was repeated with a power decrease to 2 megawatts and the same water level and temperature events were observed. From the data monitored, it was concluded that at sufficiently high power levels the normal water flow into the forward portion of the rear shield annulus was disrupted and localized boiling occurred. It was decided to continue the test with a material limit of 350°F in the rear shield plug annulus as measured by any of the three thermocouples.

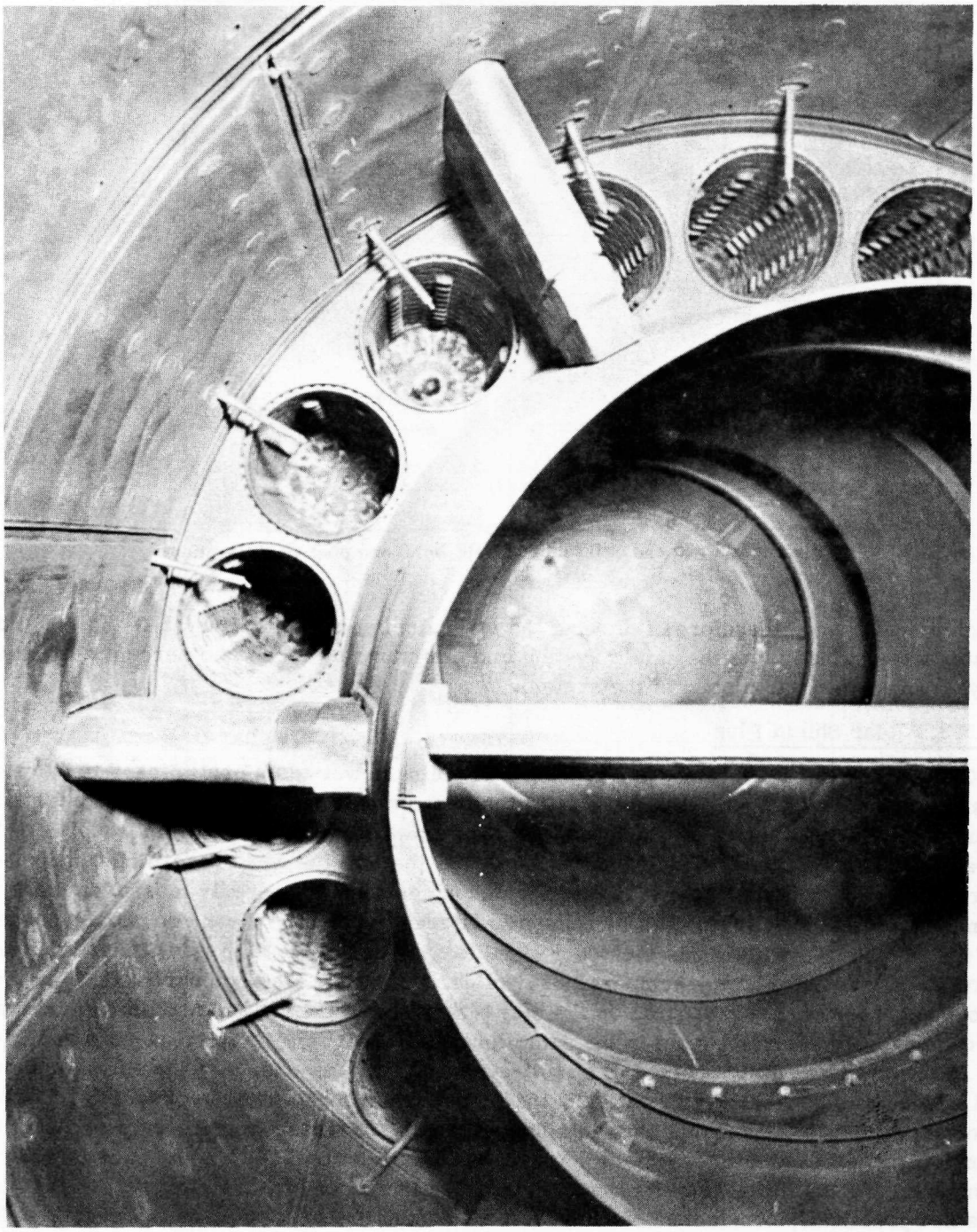

Fig. 5.54 – Aft end of HTRE No. 3 rear plug seen through the combustor (Neg. U3927-2)

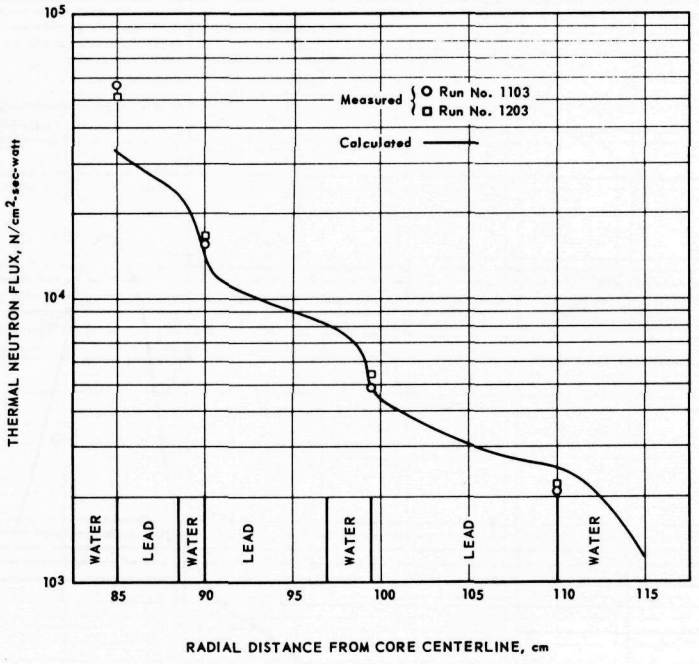

Fig. 5.55 – Comparison of calculated and measured thermal neutron flux distribution in HTRE No. 3 sensor well plug

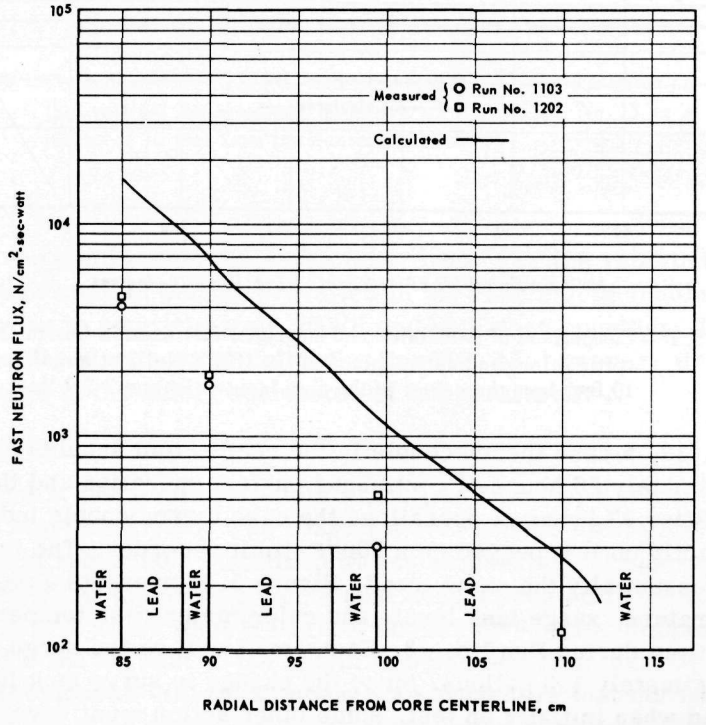

Fig. 5.56 – Comparison of calculated and measured fast neutron flux distribution in HTRE No. 3 sensor well plug (neutron energy > 2.9 Mev)

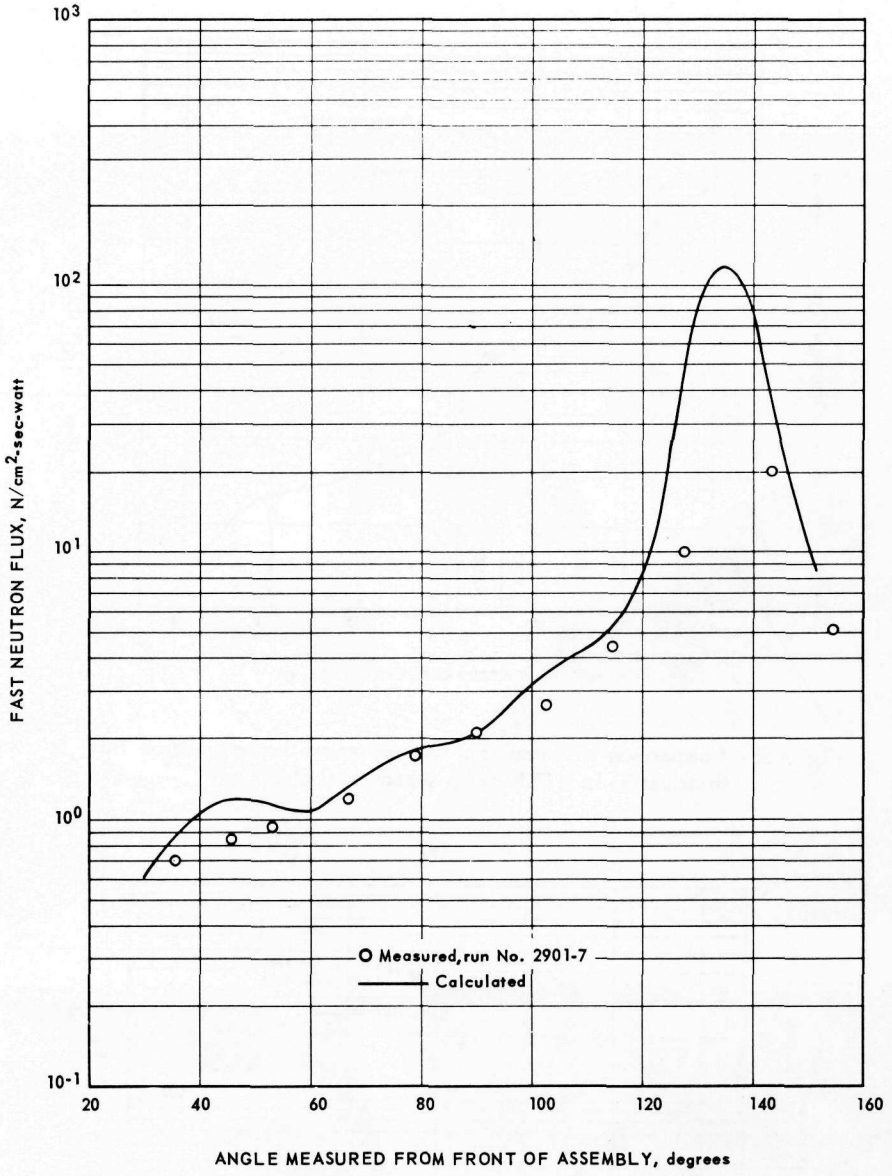

Fig. 5.57 – Comparison of calculated and measured fast neutron flux in the vertical longitudinal midplane of the HTRE No. 3 at a radius of 10 feet from the center of the core (neutron energy > 2.9 Mev)

During Run No. 13, a case thermocouple in the rear shield annulus held constant at 260°F for approximately 26 hours of continuous on-test operation and then suddenly started to increase. After 27 hours of operation, the case thermocouple indicated 320°F and was climbing steadily until it pegged on a 600°F-limit recorder. The two slug thermocouples followed essentially the same trend. Figure 5.59 presents a plot of the core discharge air temperature, surge tank level, and calorimeter case temperature as a function of operating time during Run No. 13. Each small unit on the surge tank level scale represents approximately 1.3 gallons. Since the change in surge tank level did not increase over that observed when initially on test, some other action must have occurred to affect the state that was otherwise in equilibrium. At equilibrium, a small quantity of water probably flows into the annulus; otherwise, the compartment would soon become dry and the structure temperatures would increase rapidly. If this is true, then the further hypothesis can be made that for some unknown reason the flow ceased or at least was reduced to

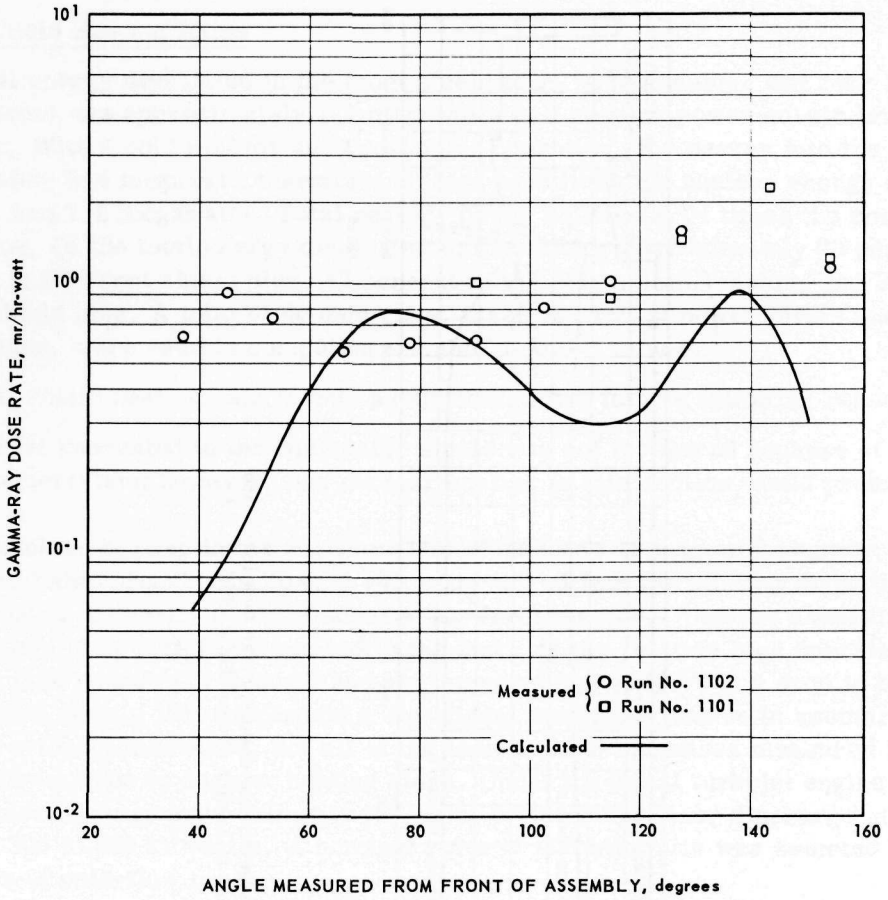

Fig. 5.58 – Comparison of calculated and measured gamma-ray dose rate in the vertical longitudinal midplane of the HTRE No. 3 at a radius of 10 feet from the center of the core

such a low level that the equilibrium state was destroyed. For the remainder of the endurance test, a constant state of boiling prevailed in the rear shield annulus, i.e., the case thermocouples rose to approximately 250°F and remained constant. The ethylene glycol mixture was replaced with water following Run No. 13; however, this did not produce a noticeable change in the shield compartment temperatures.

5.5.3.2 Auxiliary Shield

Boiling was observed in the auxiliary shield which was filled with the 50 volume percent mixture of water and ethylene glycol. The case of a heat sensor located in a lead slab in the aft part of the shield recorded a stabilized water temperature of approximately 225°F during endurance testing. At the same time, a heat sensor located in the forward part of the shield was measuring a water temperature of about 160°F. This temperature difference can be explained if the aft part of the shield is being heated in part by the discharge air from the forward combustor flange. Concern was expressed that the level of the water in the auxiliary shield would be reduced through evaporation to such a level that the lead slabs would not be covered. Therefore, the shield was filled at intervals by means of a rubber hose inserted in a vent on the forward part of the tank. Using a calculated flow rate through the hose, the rate of evaporation was established at between 30 and 40 gallons per hour.

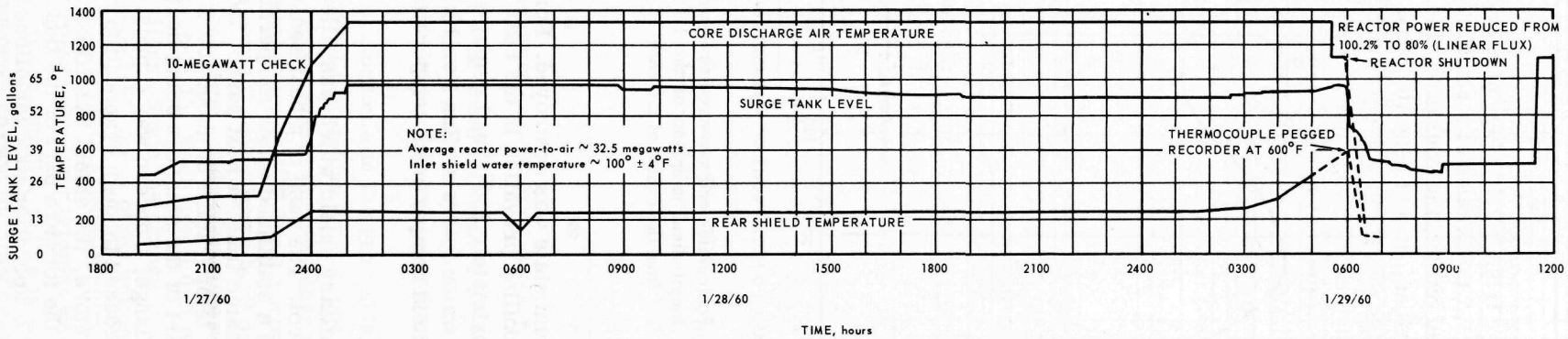

Fig. 5.59 – HTRE No. 3 core discharge air temperature, surge tank level, and rear shield temperature as a function of time during Run No. 13

5.5.3.3 Shield Heating Rates

The total energy dissipated in the front shield plug, side annulus, and rear shield plug compartments was approximately 1.7 megawatts at a reactor power-to-air level of 33.5 megawatts. With a cold reactor and two-engine operation, the energy into the shield was approximately 0.4 megawatt; therefore, at test conditions the nuclear energy released in the shield was 1.2 megawatts. Total reactor power equaled 1.04 times the computed power-to-air value. Of the total energy dissipated in the shield, approximately 20 percent was generated in the front shield plug, 47 percent in the side shield annulus, and 33 percent in the rear shield plug. A total of 40 data runs, taken at various power levels and times during endurance, were used in computing the shield power values.

The total shield heating rate is only an approximation for the following reasons:

1. The heat generated in the combustor shield was not measured because of the lack of instrumentation; however, any nuclear heating in this section would probably be quite low.
2. The nuclear heating in the auxiliary shield tank was an unknown quantity; however, it would also probably be low. It was conjectured that the aft tank structure was being heated primarily by the discharge air from the core, thereby accounting for the high fluid temperatures recorded in the tank. At the relative high operating airflow rates (120 pounds per second) and air temperatures (1330°F), a drop in the air temperature of only 1°F represents a significant heat input source to another system.
3. As previously discussed, not all of the temperature increases measured in the three shields was due to nuclear heating alone. Under chemical turbojet engine operation, measured energy input values to the water from compressor discharge airflow ranged from 300 to 550 kilowatts. A nominal value of 400 kilowatts was selected from a series of cold-flow runs.

5.6 REFERENCES

1. Schoenberger, T. W., "102 Project Data Book - 8th Issue," GE-ANPD, DC 59-8-22, July 29, 1959.
2. Gamertsfelder, C. C., Blumberg, B., and Schoenberger, T. W., "D102A Hazards Report," GE-ANPD, APEX-344, December 12, 1957.
3. Duffy, P. E., "Summary Report of the Stress Analysis of the P-102 Front Plug," GE-ANPD, DC 57-9-39, September 6, 1957.
4. "Tank and Cylinder Assembly Stress Analysis," Allstates Design and Development Company, Report No. 134-R1, April 12, 1957.
5. "Cylinder Assembly - Double Wall," General Electric Engineering Instruction 50922C, June 18, 1956.
6. "Stress Analysis - External Tank Assembly," The Kett Corporation, Report No. K-179,
7. "Design Calculations for Combustor Tank Assembly," Allstates Design and Development Company, Report No. 275-R1, August 6, 1957.
8. "Stress Analysis of Scroll," The Budd Company, Report No. NER-116, December 10, 1956, Revision (A), April 29, 1957.
9. Barron, M. L., "Index of D102A Shields," GE-ANPD, DC 58-8-34, July 28, 1958.
10. Miller, C. L., Nassano, R. N., and Powell, W. C., "Interim Report on HTRE No. 3 Operations," GE-ANPD, DC 60-1-50, January 7, 1960.
11. Powell, W. C., and Ratliff, A. W., "Interim Report on HTRE No. 3 Thermodynamic Data," GE-ANPD, DC 60-4-22, March 31, 1960.
12. "Engineering Progress Report," GE-ANPD, APEX-22, December 1956.
13. "Engineering Progress Report," GE-ANPD, APEX-23, March 31, 1957.
14. "Engineering Progress Report," GE-ANPD, APEX-24, June 30, 1957.
15. Edwards, W. E., "Shielding Computer Program O4-2," GE-ANPD, DC 57-11-101, November 18, 1957.
16. Keppler, J. G., "Heating Rates for D102A Thermodynamic Analysis," GE-ANPD, DC 59-3-85, March 6, 1959.
17. Nassano, R. N., "Radiation Levels After Shutdown HTRE No. 3," GE-ANPD, DCL 58-7-27, June 30, 1958.
18. Schoenberger, T. W., "102 Project Data Book - 8th Issue," GE-ANPD, DC 59-8-22, July 29, 1959.
19. Miklaw, E., "Trunnion Ring Analysis," The Budd Company, Report No. NER-105, June 29, 1956, Revision (A), July 20, 1956.
20. Gorman, F., "Stress Analysis of Pressure Cylinder," The Budd Company, Report No. NER-102, June 27, 1956, Revision (A), July 20, 1956.
21. Gorman, F. T., and Pagon, G., "Stress Analysis of Inner and Outer Tanks," The Budd Company, Report No. NER-106, July 20, 1956.
22. "Stress Analysis of Pressure Cylinder," The Budd Company, Report No. NER-109, October 5, 1956.
23. "Flange Temperatures," The Budd Company, Report No. NER-115, November 1, 1956.
24. "Temperature Distribution Forward Shoulder," The Budd Company, Report No. NER-111, September 28, 1956.
25. "Stress Analysis of Transition Ducts and Duct Elbow," The Budd Company, Report No. NER-118, December 6, 1956.
26. Brown, A. F., and Langenback, C., "Weight and Balance Analysis of the P-102 Primary Shield Assembly," GE-ANPD, DC 57-11-115, November 18, 1957.
27. Wilson, J. F., "Revised Weight Summary of Cylindrical Assembly," The Budd Company, Report No. EP-70-002, July 1956.

28. Smith, G. L., "Fabrication of the Inconel "X" Pressure Vessel," DC 58-5-28, April 14, 1958.
29. Smith, G. L., "Fabrication, Welding and Testing of 17-7PH Stainless Steel," GE-ANPD, XDC 59-1-173, October 10, 1958.
30. Todd, M. J., and Arnold, E. P., "D102A Core - Front Plug Assembly," GE-ANPD, DC 58-5-48, May 29, 1958.
31. McQuin, T. M., "Primary Shield and Upper Half Auxiliary Shield Installation Instructions," GE-ANPD, DC 58-9-72, September 30, 1958.
32. McQuin, T. M., and Sullivan, J. M., "Handbook Assembly Instructions D102A Primary Shield," GE-ANPD, DC 58-5-16, May 29, 1958.
33. McQuin, T. M., "Primary Shield and Upper Half Auxiliary Shield Installation Instructions," GE-ANPD, DC 58-9-72, September 30, 1958.
34. Benke, F. A., "D102A Upper Half Combustor Shield," GE-ANPD, DC 58-7-31, July 25, 1958.
35. Benke, F. A., "Installation and Filling of Combustor Shield Doors," GE-ANPD, DC 58-6-24, June 3, 1958.
36. Reid, R. E., and Breslauer, S. K., "Insulation Attachment by Welding for ANP Power Plants," GE-ANPD, APEX-611, June 30, 1960.
37. Ratterman, E., "Results of Structural Tests Performed on P-102 Inner Pressure Vessel," GE-ANPD, DC 58-5-76, May 8, 1958.
38. "Structural Tests of Double Wall Cylinder," The Budd Company, Report Number NER-164-A2, June 26, 1958.
39. McLay, T. D., "Insulation Designs for Gas Cooled Reactors," GE-ANPD, DC 57-4-76, April 4, 1957.
40. Harper, P. W., et al., "Results of Cold Flow Performance Tests on a One-Fourth Scale HTRE No. 3 Reactor Shield Mockup," GE-ANPD, DC 60-5-112, May 20, 1960.
41. Blumberg, B., "IET Power Tests Requests," GE-ANPD, DC 58-6-161, June 18, 1958.
42. Blumberg, B., "IET Phase I Test Request," GE-ANPD, DC 59-5-221, May 21, 1959.
43. Blumberg, B., "IET Phase II Test Request," GE-ANPD, DC 59-10-154, October 21, 1959.
44. Blumberg, B., "HTRE No. 3 Performance Demonstration," GE-ANPD, DC 60-3-53, March 3, 1960.
45. Cannon, C. B., "D102A-2(A) Power Plant Test Programs and Procedures for IET #18," GE-ANPD, XDCL 59-12-719, December 16, 1959.
46. Cannon, C. B., "Preliminary Data Report, IET Test Series No. 25 D102A2 Power Plant," GE-ANPD, DC 61-2-724, February 10, 1961.
47. Devins, F. G., "Data Report D102A2 Power Plant Testing IET 13," GE-ANPD, DC 59-4-710, April 3, 1959.
48. Feinauer, E., Highberg, J. W., Luke, C. W., Masson, L. S., and Tuck, G., "Summary Report for Testing of the D102A Reactor Assembly During LPT 2," GE-ANPD, DC 58-9-705, August 29, 1958.
49. Hutchins, B. A., "Requests for Shielding Measurements at HTRE No. 3 IET Operation," GE-ANPD, DC 58-2-73, February 6, 1958.
50. Showalter, D. E., "D102A2(A) Power Plant Test Program and Procedures for IET #16," GE-ANPD, XDCL 59-8-719, August 1959.
51. Showalter, D. E., "Preliminary Data Report IET 16 D102A2(A)," GE-ANPD, XDCL 59-11-715, October 28, 1959.
52. McVey, C. I., "HTRE No. 3 Experiment Correlating Calorimetric Heat Rate Detectors and a Bragg Gray Ionization Chamber," GE-ANPD, DC 59-6-255, June 25, 1959.

53. Miller, C. L., Nassano, R. N., and Powell, W. C., "Interim Report on HTRE No. 3 D102A2 Operations," GE-ANPD, DC 60-1-50, January 7, 1960.
54. Nassano, R. N., "Pre-Analysis of Shielding Experiments at HTRE No. 3 IET Operation," GE-ANPD, DC 58-8-125, August 18, 1958.
55. McDonald, W. A., and McLay, T. D., "Trip Report to ITS to Inspect Damaged HTRE No. 3 Duct Insulation," GE-ANPD, DC 61-2-114, February 22, 1961.
56. Highberg, J. W., et al., "Preliminary Data Report IET Test Series, No. 18 Phase II, Testing of the D102A Power Plant," GE-ANPD, DC 60-6-735, June 17, 1960.

6. TURBOMACHINERY

6.1 GENERAL DESCRIPTION

Two X39 turbojet engines are installed on the HTRE No. 3 to provide the cooling airflow for the test reactor. Each engine can operate on energy either from the reactor, from a chemical fuel combustion system, or from both.

The X39-5 engine is a major modification of the J47-GE-11 turbojet engine. The engine was modified by removal of the combustion section and addition of a compressor discharge scroll, which collects compressor discharge air for ducting to the reactor, and a turbine scroll, which takes the hot air from the reactor and/or chemical combustor and distributes it to the turbine inlet annulus. Other major changes include reduction of compressor flow capacity to obtain a suitable match between the compressor and turbine and installation of a new engine control system. Six engines were shipped to the Idaho Test Station for use on the HTRE No. 3. Figure 6.1 shows an X39-5 engine mounted on a dolly.

6.1.1 DESIGN

The design of the HTRE No. 3 turbomachinery reflects consideration of the following guidelines.

1. Modify the standard J47-C11 engine by adding a D17 exhaust nozzle.
2. Utilize the X39-4 engine compressor configuration. Design a new turbine scroll, compressor scroll, and two-engine combustor for low pressure drop, higher turbine inlet temperature, and increased reliability.

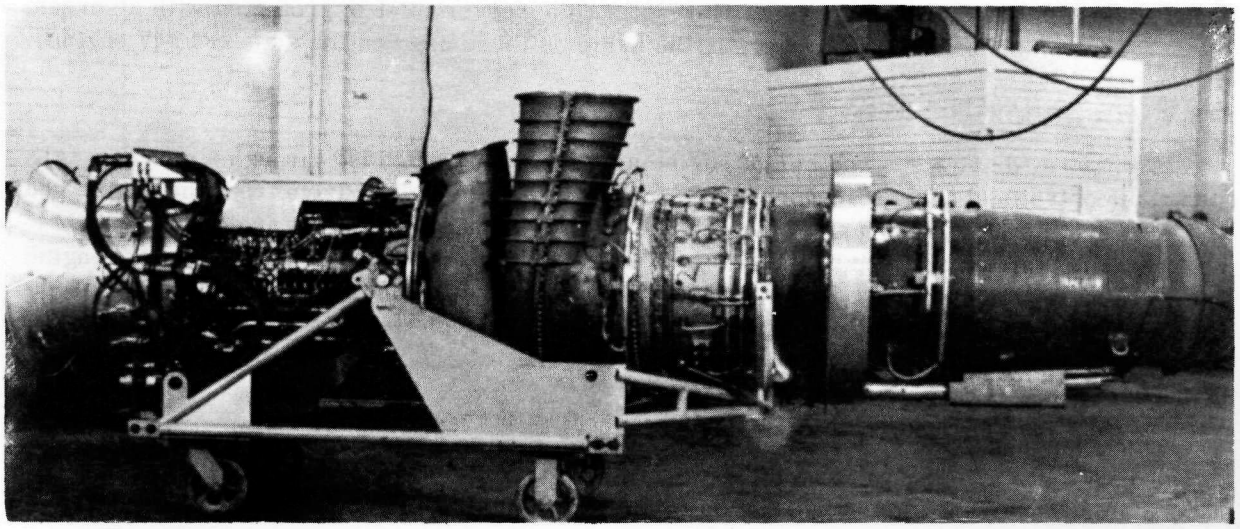

Fig. 6.1 – X39-5 engine (Neg. U35156-C)

3. Modify the J47-C11 engine aft frame to accommodate the new turbine scroll and to allow assembly of scrolls from the rear of the aft frame.
4. Make a design review of all parts of the X39-4 engine to obtain a basis of design for increased reliability.
5. Modify the X39-4 control system for the X39-5 to improve performance, reliability, and manufacturing ease. Modify the temperature control to accommodate the common combustor.

6.1.2 DESIGN REQUIREMENTS

The following performance conditions were established for the HTRE No. 3 turbomachinery:

1. Maximum continuous turbine inlet temperature of 1600°F at 7600 rpm (same as the standard J47 engine). The engine will operate for a minimum of 100 hours at 1600°F T_4 at 7600 rpm or 1500°F T_4 at 8000 rpm. 1000-hour life is achievable by reducing the temperature 100°F for each point.
2. Operation. The engine should be capable of operation in a 100-hour endurance test at 1500°F at 7600 to 7953 rpm. The major change for this endurance test[1] will be an increase in the maximum turbine inlet temperature from 1400° to 1600°F.

Detailed information on the lubrication systems, fuel systems, maintenance, and remote handling of the HTRE No. 3 turbomachinery is contained in references 2 through 5. References 6 through 38 are a chronological series of references covering the development and testing program of the turbomachinery.

6.2 COMPONENTS

A brief description and a statement of the purpose of each of the major mechanical components or sections of the HTRE No. 3 are presented in the following paragraphs.

6.2.1 INLET SECTION

The purpose of the bulletnose, bellmouth, and inlet section is to duct the engine airflow to the compressor inlet with a minimum pressure drop, and to provide a suitable geometry for measuring the compressor inlet flow. The compressor inlet is protected with a screen. All these components are substantially the same as those used on the standard J47 engine.

6.2.2 GEARBOX

Mechanical drive for a number of engine accessories is provided through a gearbox. All engine control and accessory components requiring a mechanical drive from the engine shaft are mounted on the front face of the gear box. This includes the engine fuel pump, lubricating oil pump, overspeed governor, overspeed switch, engine control tachometer, engine indicating tachometer, and engine starter. The gearbox is a modification of that of the basic J47 engine.

6.2.3 COMPRESSOR

The compressor takes in air and raises its pressure to about 5 atomspheres at full speed. The X39-5 compressor is substantially identical to the J47 compressor except that the blade tip diameters were reduced by cutting off the tips of the rotor blades and by manufacturing a compressor casing with a smaller inside diameter and with shorter stator blades. These changes in geometry produce a net compressor airflow about 25 percent lower than that of the basic J47 engine.

6.2.4 MIDFRAME AND AFTFRAME

The midframe provides structural support of the compressor casing, the center bearing, mounting pads, and the aftframe. The aftframe is the nonrotating structural member between the center and rear bearings. The J47 midframe is used in the X39-5 without significant modification. The J47 aftframe is modified for the X39-5 to provide for cooling and for structural support of the turbine scroll. It is removed from the aft end of the engine, thus simplifying remote disassembly.

6.2.5 COMPRESSOR AND TURBINE SCROLLS

The compressor scroll collects the compressor discharge air. The turbine scroll distributes the air to the turbine inlet annulus. Both scrolls are made in the same basic toroidal form. The 8 inlet pipes of the compressor scroll mate with the midframe openings originally provided in the J47 for the combustion cans. Provision is made on the turbine scroll for mounting the turbine nozzle diaphragm and the tailpipe, as shown in Figure 6.2.

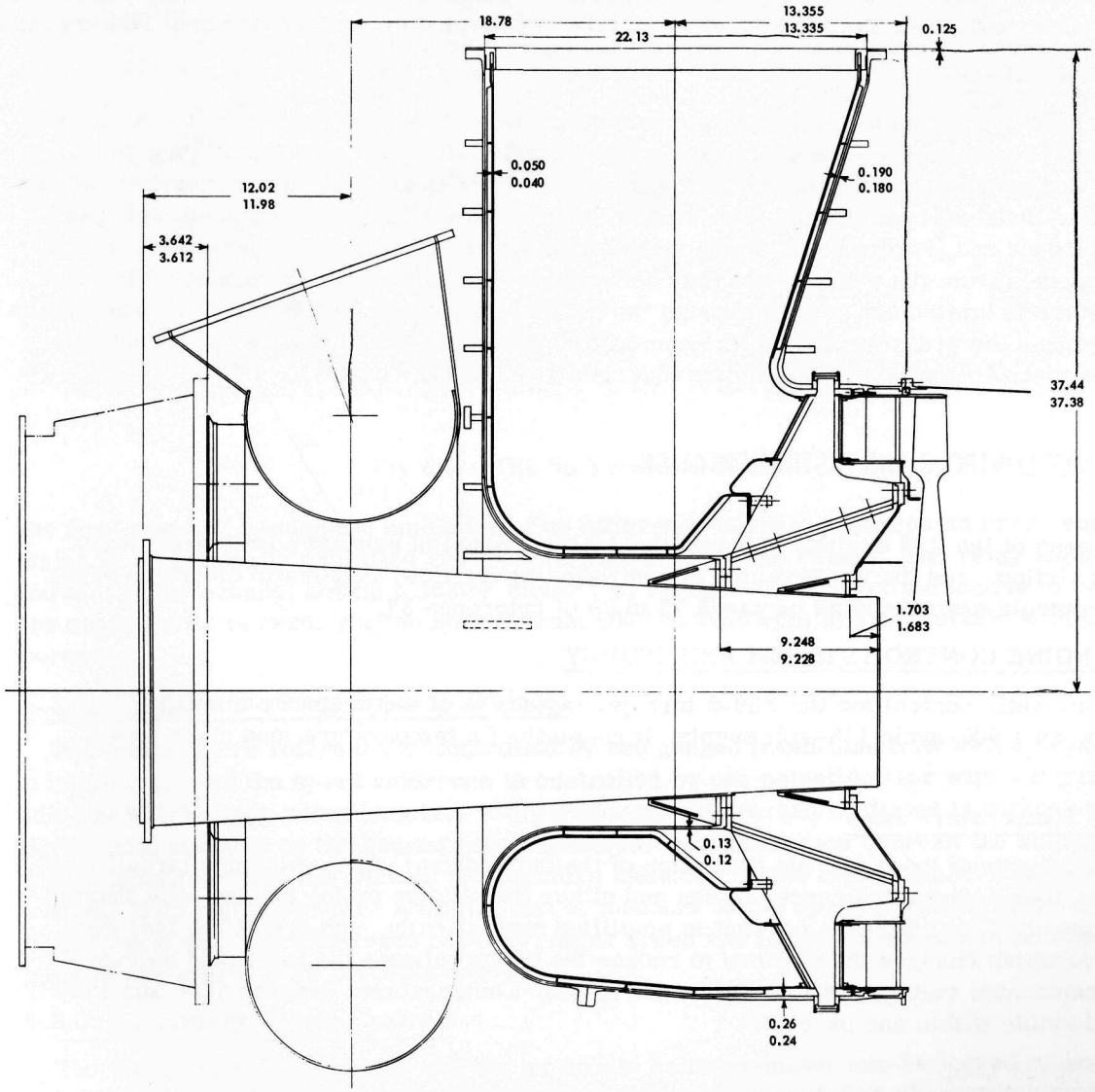

Fig. 6.2– Configuration of HTRE No. 3 engine scrolls (Dwg. 7006R66)

6.2.6 TURBINE

The turbine diaphragm and rotor convert the energy of the hot gases entering the turbine into shaft power. The J47 rotor is used without modification.

6.2.7 EXHAUST NOZZLE

The purpose of the variable area exhaust nozzle is to provide a duct for the exhaust gases and to provide for engine speed control. The X39 exhaust nozzle is the same as that of the J47-GE-17 reheat engine without the reheat fuel nozzles and flameholders. Straightening vanes are provided to minimize tailpipe pressure losses resulting from swirl in the gases leaving the turbine.

6.2.8 AUXILIARY FLOW SYSTEMS

A number of auxiliary flow systems are included in the X39 engine design. Other design features include vents for proper pressure distribution around the oil seals at the various bearings; cooling airflow on the compressor rotor discs and at both the forward and rear faces of the turbine wheel; bleed air from the compressor discharge cooling the aftframe and turbine scroll struts; and cooling for the scroll structure is provided by compressor seal leakage air.

6.2.9 COMBUSTOR

The HTRE No. 3 combustor supplies chemical combustion exhaust gases to the two X39-5 engines as required. The combustor is mounted directly aft of the rear shield plug annulus diffuser and consists of 18 modified J73 combustion liners in an annulus and mounted radially around a cylindrical bypass duct. The bypass duct contains a 32-inch, two-position bypass valve at its aft end (Figure 6.3). When operating on chemical fuel, the bypass valve is shut and air passes from the reactor into the combustion liners where it is mixed with JP-4 fuel. The mixture is ignited and passes through the hot ducting into the turbine scrolls. The bypass valve reduces the pressure drop of the combustor during nuclear operation. It is controlled from the control room at the operator's discretion.

6.3 ENGINE CONTROLS AND INSTRUMENTATION

The speed of the X39 engines is controlled by the amount of exhaust nozzle area available for airflow, and the temperature is controlled by fuelflow. Schematic diagrams of the engine controls are presented on pages 73 to 79 of reference 37.

6.3.1 ENGINE CONTROL SYSTEM PHILOSOPHY

The automatic control for the X39-5 turbojet engines is of the magnetic-amplifier type, operating on a 400-cycle 115-volt supply. It consists of a temperature loop and a speed loop.

6.3.1.1 Temperature Loop

The temperature loop controls the action of the fuel-control valve. A bridge circuit compares the temperature reference voltage and either the tailpipe or the turbine inlet thermocouple output. The difference current is amplified magnetically, and drives the fuel-control valve which changes the fuelflow to reduce the error between the reference voltage and thermocouple voltage until no difference exists. Temperatures between 700° and 1700°F are held stable within one percent.

6.3.1.2 Speed Loop

The speed loop governs the operation of the exhaust nozzle actuator. A speed reference current and a current proportional to engine speed are fed into opposing input windings of

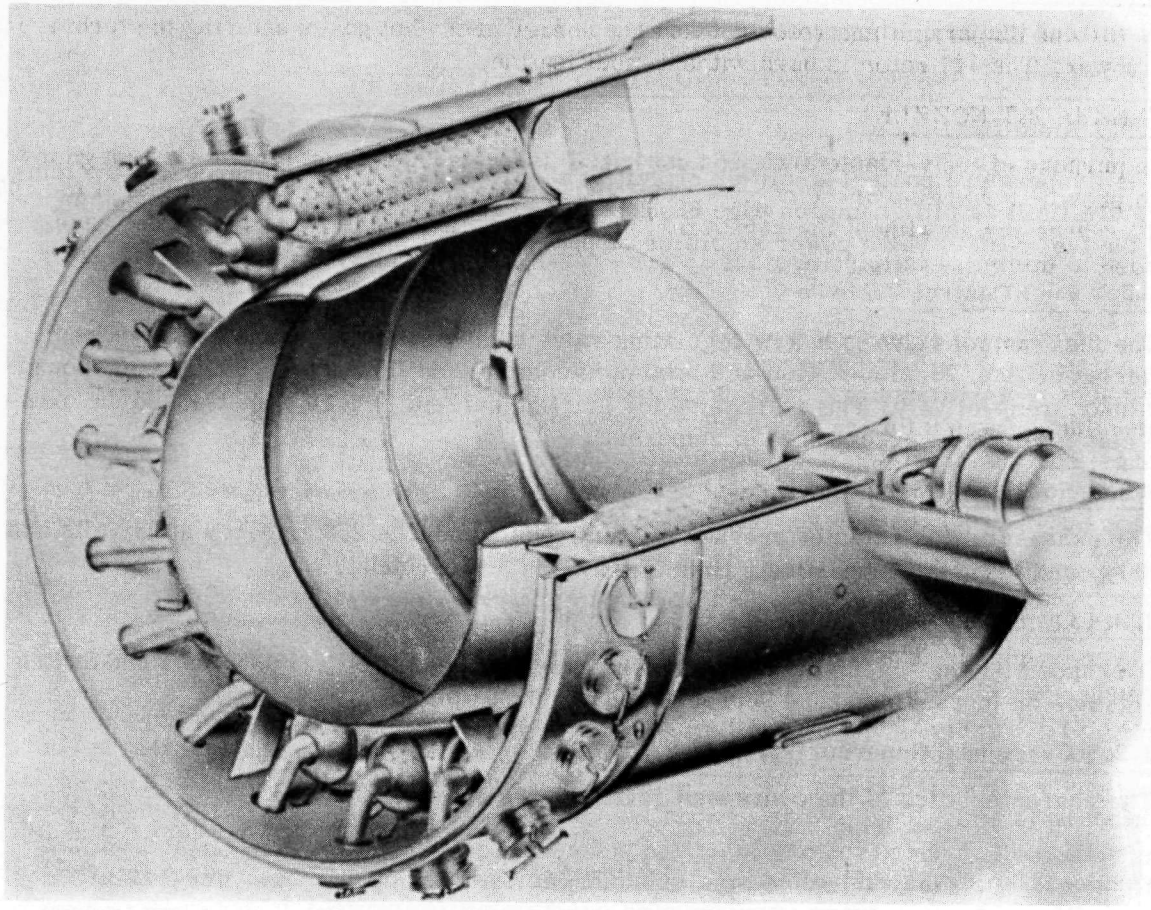

Fig. 6.3 – HTRE No. 3 combustor (G-799)

the first stage of a magnetic amplifier. The difference current produces an error signal which is magnetically amplified and then activates one of two relays. The relay applies a current to the exhaust nozzle actuator motor that changes the area of the nozzle to reduce the speed error to zero. Engine speeds from 4040 to 7950 rpm are held stable within 0.5 percent.

6.3.1.3 Temperature and Speed References

The temperature reference is controlled by two ganged potentiometers with a separate trimming pot and the speed reference is controlled by one potentiometer with a separate idle speed trimming potentiometer. A desired temperature can be dialed in through the digital dial mounted on the ganged potentiometers. Any difference between the stable engine temperature and the demand temperature indicated on the digital dial can be removed with the trim potentiometer. A digital dial is mounted on the speed potentiometer and, when 4040 rpm is set, any difference between engine speed and indicated speed can be removed with the low-speed trim potentiometer.

6.3.1.4 Auxiliary Engine Controls

The fuel control valve motor and the jet nozzle actuator motor can be jogged manually using the 28-volt d-c supply. No serious transients are encountered when switching the transfer switches between manual and automatic operation of either circuit as long as the control pots are positioned for zero output on the amplifier output meters.

A prestart position on the temperature transfer switch allows fuelflow to the fuel nozzles without ignition. This can be used to check fuelflow.

6.3.2 CONTROL SYSTEM DESIGN AND MECHANIZATION

6.3.2.1 Amplifiers

The temperature control amplifier circuit is shown on page 85 of reference 37, the temperature limit amplifier unit on page 88, the speed control amplifier circuit on page 90, and the fuel control valve power amplifier on page 92.

6.3.2.2 Fuel Control Valve

The fuel control valve is a flow regulating valve with constant pressure drop across the metering orifice. Maximum flow and minimum controllable flow are 10,000 and 300 pounds per hour, respectively. The average motor starting current is 1.10 amperes and the average clutch slippage current is 1.75 amperes.

6.3.2.3 Nozzle Actuator

The exhaust nozzle actuator average current requirement is 2.0 amperes at 28 volts and a 500-pound load; the approximate time of travel is 5.5 seconds.

6.3.2.4 Overspeed Switch

Overspeed Switch A actuates on increasing speed between 8000 and 8065 rpm and Switch B actuates on increasing speed between 8168 and 8200 rpm.

6.3.2.5 Overspeed Governor

The characteristics of the overspeed governor are shown in Table 6.1.

TABLE 6.1

CHARACTERISTICS OF THE OVERSPEED GOVERNOR

Engine Speed, rpm	Pressure Drop Across Governor, psig	Bypass Fuelflow, pph
7,950	650 (closed)	0-170
8,100	310	5,200-9,900
8,231	150	10,000-15,000
8,473	30 (full open)	16,000

6.3.3 ENGINE OPERATING INSTRUMENTATION

The engine operating instrumentation is presented in Table 6.2.

6.3.4 ACCESSORY COMPONENTS

6.3.4.1 Starter

The X39-5 turbojet engines are equipped with Hamilton Standard air turbine starters, Model PS-300-4. The starters operate with a regulated inlet pressure of 35 psig, requiring an airflow of 1.33 pounds per second. The starter accelerates the engine rotor to a suitable ignition speed and then assists the engine to its self-sustaining speed; the starters are capable of assisting the engine up to a speed of approximately 3800 rpm. They may be used to motor the engines at approximately 1500 rpm for limited periods to provide approximately 8 pounds of air per second for aftercooling.

TABLE 6.2

ENGINE OPERATING INSTRUMENTATION

Parameter Measured	Operating Limits
Engine speed	7600 rpm at 1600°F T_4 7953 rpm at 1500°F T_4
Fuel supply pressure to engine, nominal psig	15
Engine fuel pump discharge pressure, psig	0 - 400
Small slot pressure, psig	0 - 400
Fuel valve position	10 volts (open) 0 volts (closed)
Jet nozzle position	10 volts (open) 0 volts (closed)
Oil pump discharge pressure, psig	0 - 60
Maximum oil cooler water inlet temperature, °F	158
Position indicator nominal supply voltage	10
D-C line voltage	28 ± 4
400-cycle line voltage	115 ± 3
Supply frequency, cps	385 - 425
Vibration, turbine and compressor bearing, mils	
Average	5
Peak	8
Combustor bypass valve actuator temperature, °F	160
Turbine inlet temperature (T_4), °F	1600 maximum (below 7600 rpm) 1500 continuous
Starter air pressure, psig	34
Exhaust nozzle actuator motor temperature, °F	250
Maximum duct valve actuator temperature, °F	150

6.3.4.2 Ignition System

The 110-volt, 400-cps ignition system includes a capacitor discharge spark generator, surface gap plug, 2-joule approximate spark energy, and a spark rate of 1 to 10 sparks per second at 110 volts.

6.3.4.3 Fuel System

The fuel system is illustrated on page 312 of reference 38. The fuel is pumped by the turbojet engine pump through the lubricating oil cooler and an engine disconnect to the fuel control valves in the combustor control panel. On chemical operation, a metered portion of the fuel is directed to the combustor while the remainder is returned to the Facility tank. During nuclear operation, the control valve returns all the fuel to the Facility tank. This system provides up to 28 gallons per minute of JP-4 fuel at 5 to 20 psig at the turbojet inlet connection.

A drain system drains from 1 to 10 pounds of fuel from the combustor during startup. This fuel represents seepage from the combustor panel controls and from the turbojet engine seepage collection pans under the quick disconnects and fuel and lube pumps and controls. The fuel flows out of the combustor by gravity, through a flame arrestor, to a 3-gallon holdup tank near the floor of the dolly.

6.3.4.4 Lube System

Each turbojet engine has a self-contained lube system. The 32-gallon tank, which is filled to only 28 gallons, supplies oil by gravity through a motor-operated shutoff valve which is controlled from the IET Control Room and then through a disconnect to the engine. Here the engine-driven pump passes the oil to the gear case and all bearings at a flow of about 3 gpm. The scavenger pump returns the oil through the oil cooler and a disconnect and then through a filter and flow switch back to the tank.

6.3.5 DATA INSTRUMENTATION

The X39 engine test instrumentation is shown in Table 6.3.

6.3.6 PARAMETER TABULATION

A complete 5000-foot standard-day engine map for 7000 rpm, taken from test data on the X39 turbomachinery, is shown in Figure 1 of reference 32. Figures 2 through 13 in reference 32 present basic engine parameters plotted against loop pressure drop at constant engine speeds for open-nozzle, 5000-foot, standard-day conditions. Figures 14 through 21 similarly illustrate some of the same basic engine parameters under closed-nozzle, 5000-foot, standard-day conditions. It should be noted in comparison of open and closed nozzle plots that Figures 14 through 21 use half of the total pressure-drop scale used in Figures 2 through 13.

Figures 22 through 25 of reference 32 illustrate low-speed engine characteristics plotted against corrected engine speed for open-nozzle, 5000-foot conditions.

TABLE 6.3

ENGINE TEST INSTRUMENTATION

Parameter Measured	Sensor	Quantity
Bellmouth temperature ($T_{2.0}$)	Copper/Constantan thermocouple	8
Bellmouth to Control Room static pressure ($P_{s2.0}$)	Static probes	4
Compressor discharge total pressure ($P_{t3.0}$)	7 impact probes-manifolded	1 ring
Compressor scroll discharge static pressure ($P_{s3.15}$)	Wall static 3 probes manifolded	3
Combustor inlet temperature ($T_{3.83}$)	4 Cr/Al thermocouples averaged	4 average
Turbine inlet temperature ($T_{4.0}$)	Cr/Al thermocouples averaged in 3 groups	3 average
Exhaust cone static pressure ($P_{s6.0}$)	8 wall static manifolded	1 average
Exhaust cone temperature ($T_{6.0}$)	2 Cr/Al thermocouple rings of 8 thermocouples each	1
Exhaust nozzle static pressure ($P_{s7.0}$)	6 wall static	1
Exhaust nozzle total pressure ($P_{s7.0}$)	4 Kiel probes manifolded	1
Loop total pressure difference between stations ($P_{t3.0}$ - $P_{t3.8}$)	Impact probes	1

6.4 REFERENCES

1. White, H. D., "X39-5 Engine Model Test," GE-ANPD, DC 58-4-162, April 18, 1958.
2. "D102A Turbojet Lube Systems Assembly and Installation," GE-ANPD, DC 57-9-29, September 6, 1957.
3. Evans, W. G., "D102A Turbojet Fuel Systems Assembly and Installation," GE-ANPD, DC 57-9-119, September 16, 1957.
4. Holowach, J., "D102A Combustor - Maintenance Handbook," GE-ANPD, DC 58-7-114, July 17, 1958.
5. Munro, J., "D102A Turbojet Engines Remote Handling," GE-ANPD, DC 57-11-60, March 1, 1958.
6. Halbert, K. P.,. "Engine Performance During S. E. T. #2, The Initial Test of X39 Engine #5002," GE-ANPD, XDC 54-1-30, January 8, 1954.
7. Masson, L. S., "P. U. T. Duct Valve Control," GE-ANPD, XDC 54-5-10, April 28, 1954.
8. King, J. H., et al., "A Preliminary X39 Engine Performance Study," GE-ANPD, DC 54-9-24, September 3, 1954.
9. Fogg, R. G., "X39 Engine Operating Manual," GE-ANPD, XDC 55-2-7, February 1, 1955.
10. Fogg, R. G., "Preliminary Incident Report X39-3 Engine Damage P. U. T. Cell," GE-ANPD, DC 55-4-52, April 11, 1955.
11. Motsinger, R. E., "HTRE No. 1 CTF Operation Instruction Book 20-3. 1 X39-4 Turbojet," GE-ANPD, DC 55-6-127, June 21, 1955.
12. Clavell, G. H., "X39-4 CTF Engine Control System Description," GE-ANPD, DC 55-11-6, November 1, 1955.
13. Jenkins, O. G., "Duct Valve Torques," GE-ANPD, DC 55-12-149, December 1955.
14. Reynold, M. B., and Motsinger, R. E., "Effect of Air Leakage on X39-5 Performance," GE-ANPD, DC 56-5-79, May 16, 1956.
15. Motsinger, R. E., et al., "Final Prediction of Performance of X-39 Engine," GE-ANPD, DC 56-8-201, August 20, 1956.
16. Comassar, S., "Theoretical Analysis of Pressure Losses in P-102 Combustor," GE-ANPD, DC 56-8-46, August 1, 1956.
17. Jordan, L. D., "Component Test Operations Idaho Test Station - Water Injection Tests on the X39-4 Engine at the Idaho Test Pad," GE-ANPD, DC 56-10-74, October 10, 1956.
18. "Test Request No. ITP609 (X39-4)-119," GE-ANPD, November 2, 1956.
19. White, H. D., "X39 Engine 12th Stage Back Pressure Investigation," GE-ANPD, DC 56-11-22, November 2, 1956.
20. "Hot Flow Leakage Test on Development Duct Disconnect," GE-ANPD, November 23, 1956.
21. Motsinger, R. E., and Reynolds, M. B., "Evaluation of the X-39 Engine Starting Characteristics," GE-ANPD, DC 57-1-124, January 25, 1957.
22. "Compressor Rotor - Gear Box Reliability Test for X39-5 Engine," GE-ANPD, February 21, 1957.
23. Comassar, S., and Ogborn, D. M., "Test Effect of Leakage on X-39 Engine Performance," GE-ANPD, DC 57-5-140, May 21, 1957.
24. Anderson, H. E., "Results of Test Request No. ITP 609 (X39-4)-119," GE-ANPD, DC 57-6-703, June 4, 1957.
25. Pincock, G. D., et al., "Assembly Breakdown and Numerical Listing of X39-4 Engine," GE-ANPD, DC 57-7-73, July 1, 1957.
26. Engelbrecht, R. H., "Data Reduction for an X39-5 Engine by the IBM 650 Computer," GE-ANPD, DC 57-9-115, September 13, 1957.
27. Hope, J. I., "Engine Design Unit Presentation on X39-5 Engine Presented to ANPD - 2-27-57," GE-ANPD, DC 57-9-195, September 17, 1957.

28. Reynolds, M. B., and White, H. D., "Report on Testing of Compressor Scrolls in the P. U. T. Cell," GE-ANPD, DC 57-10-90, September 19, 1957.
29. Anderson, H. E., "Checkout and Adjustment Procedure - Modified X39 Engine Automatic Control Amplifiers," GE-ANPD, DC 57-12-726, September 19, 1957.
30. Owen, L. V., "Glossary of X39 Turbojet and Reactor Engineering Terms," GE-ANPD, DC 58-2-120, February 11, 1958.
31. Reynolds, M. B., and Vest, G. E., "Report on Testing of Turbine Scrolls in the P. U. T. Cell," GE-ANPD, DC 58-4-193, April 10, 1958.
32. Warner, C. Y., and Devens, F. G., "Detailed Performance of X39-5 Engine No. 5014-ITP # 125," GE-ANPD, DC 58-4-724, April 18, 1958.
33. Vest, G. E., "Report on the Testing of the P-102 Combustor Disconnect in the P. U. T. Cell," GE-ANPD, DC 58-7-156, May 1, 1958.
34. Anderson, H. E., "Results of 100 Hour Test on X39-5 Automatic Controls," GE-ANPD, DC 58-7-710, June 1958.
35. Brown, A. T., and Hillesheim, C. E., "Report on the Analysis and Tests Conducted on the P-102 Probe Vane Assemblies Instrumentation," GE-ANPD, DC 58-8-96, August 5, 1958.
36. Duffy, P. E., "Summary Report of the Structural Analysis X39-5," GE-ANPD, DC 59-7-66, June 30, 1959.
37. Clavell, G. H., et al., "Handbook, HTRE No. 2, Controls and Instrumentation Systems," GE-ANPD, XDC 60-1-1, December 10, 1959.
38. Schoenberger, T. W., "D102A Data Book - 8th Issue," GE-ANPD, DC 59-8-22, July 29, 1959.

7. CONTROLS

7.1 SYSTEM REQUIREMENTS

In the design of the HTRE No. 3 control system, the requirement was established that the system control either reactor discharge temperature ($T_{3.6}$) or reactor power level (through sensing nuclear flux density) as functions of temperature or power demanded. The initial design could be mechanized for flux control if subsequent conversion to a temperature system was provided for. In this summary, all limits, except those in item 1 below, refer to flux control operation. The specific requirements established for the control systems were:

1. Temperature system - must automatically control $T_{3.6}$ from 1100° to $1400^{\circ}F \pm 10^{\circ}F$.
2. Flux system - must automatically control reactor power from 10^{-6} to 100 percent full power (FP). The 10 to 100 percent FP range must be controlled to ± 1 percent FP.

The HTRE No. 3 control system parameters are shown in Table 7.1.

The system response requirements in the 10^{-1} to 100 percent FP range were:

1. Frequency response - should be flat to 15 radians per second.
2. Transient response - recovery to 90 percent of power setting within 1 second for a step of 0.2 percent Δk.

TABLE 7.1

CONTROL SYSTEM PARAMETERS

Parameter	Sensor Used
Log count rate of flux to 10^{-6}% FP	Fission chambers
Period to 10^{-6}% FP	Fission chambers
Log flux from 10^{-6} to 10^{-1}% FP	Compensated ion chambers
Period from 10^{-6} to 10^{-1}% FP	Compensated ion chambers
Flux level from 10^{-1} to 100% FP	Ion chambers
Outlet air temperature from 10^{-6} to 100% FP	Thermocouples
Servoloop error from 10^{-6} to 100% FP	Difference amplifier
Engine speed from 10^{-6} to 100% FP	Centrifugal switches
Hydraulic oil pressure	Pressure transducer
115-volt 400-cycle power	Relay
28-volt d-c power	Relay
Dynamic rod position	Extensometer
Shim rod position	Potentiometer
Safety rods cocked	Relay

The following safety requirements were established for the HTRE No. 3 control system:

1. Inherent capability. The control system shall be capable of safely controlling the reactor under all operating conditions.
2. Parameter limiting. All parameters should operate through limiter-type circuits which will prevent power level increases or will reduce power, as appropriate, for all abnormal operational conditions.
3. Fail-safe options. As far as possible, all control components shall not be capable of failure in such a manner as to permit any unsafe condition to exist which could jeopardize reliable control of the reactor.
4. Coincident signals. Where more than two channels monitor the same reactor parameter, two of these signals should agree before automatic responses are caused by them. Large numbers of multiple signals may be averaged before causing action.
5. Startup. Shim rod withdrawal shall be impossible unless all conditions are satisfied that protect against equipment failures (open channels, etc.) and operator error or oversight. Low end-scale meter automatic protection shall be incorporated on the log count-rate meter only; other parameter meters may initiate minor or annunciator alarms only.
6. Scram. The scram response shall be incorporated on all critical parameters so that the effectiveness of the preportional safety controls of this system may be evaluated during operation. Perfection of a scram-proof control system is a design goal.

Startup and operation were to be effected by use of the following control subsystems:

1. Source range manual control. The source range manual control was to use as much of the HTRE No. 1 instrumentation and operating philosophy as practical, consistent with the mission of HTRE No. 3.
2. Intermediate range automatic control.
3. Power range automatic control.
4. Manual frame and rod override controls.

The control console will consist of a single-position, desk-type, 40- by 60-inch configuration containing all meters, indicators, and actuators required for one-man operation of the reactor control system.

The following control power requirements were established:

1. Electrical. The control system shall use 115-volt, 400-cycle; 115-volt, 60-cycle; and 28-volt d-c power from external sources.
2. Emergency power. A sufficient number of alternate and emergency power sources, automatically switched, should be made available to insure reasonably well-regulated and reliable control power.
3. Hydraulic oil pressure. Hydraulic oil pressure shall be provided at 1500 psi to actuate the dynamic loop rods.

7.2 CONTROL DESCRIPTION AND OPERATION

There are three general ranges in the HTRE No. 3 control system: the source range control, in which operation is controlled by manual shim control only; the intermediate range control, in which operation is controlled either by automatic servocontrol or by manual shim control; and the power range control, also an automatic servocontrol or manual shim control system.

7. 2. 1 SOURCE RANGE CONTROL

The source range is the range of power from zero to 10^{-6} percent of full power (FP). Control of operation in this range is performed by manual shim control, explained below. A block diagram is shown in Figure 7. 1.

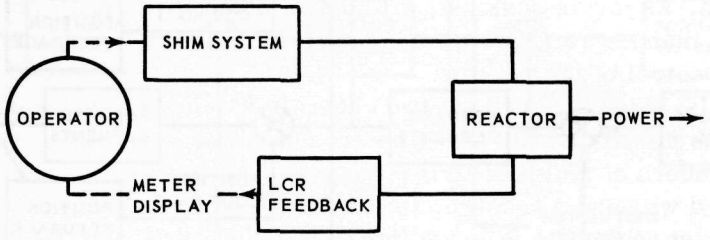

Fig. 7.1 – Source range control

In the source range control system, the power level is sensed by a fission chamber. A signal is sent through a pulse preamplifier, mounted directly on the chamber, to the log count rate (LCR) circuitry. The LCR circuitry computes both the reactor period and the reactor flux level. Both signals are displayed on meters for visual observation by the operator, who achieves the desired power level by positioning the shim rods by means of the shim control system.

In the source range, the reactor period is the only reactor parameter used in the safety circuits. The period is measured by three fissions chambers located in the shield; each transmits a signal to a separate meter on the control panel. One of the periods is recorded on a strip chart. Two period readings shorter than the safety limit are required to initiate safety action.

7. 2. 2 SHIM CONTROL SYSTEM

The shim control system consists of six frames of shim rods, designated Frame A through F. There are three rods in Frames A and B and six in the other four frames. During manual shim operation, the operator can move the shim rods either individually or by frames. If the rods are to be moved by frames, the frame selection is sequential and automatic. Sequential operation is necessary for radial power balancing and is a function of the history of core operation. The sequential system and bypass switching system do not interfere with the operation of the safety system because commands for shim movement from the safety system apply signals directly to the shim rod drive motors.

If individual rods are to be moved, the frame containing the rod to be moved is selected by positioning the frame selector switch and the entire frame is inserted or withdrawn slightly, this clearing the electrical limit switch and allowing power to be applied to individual rods in the frame. Thus, any rod in any frame can be positioned. This procedure permits the selection of one rod in each frame and the operation of all the selected rods simultaneously.

7. 2. 3 INTERMEDIATE RANGE

The intermediate range control system operates in the ring from 10^{-6} to 10^{-1} FP. A block diagram of the system is shown in Figure 7. 2.

The operator's power demand is converted into a voltage signal by the demand servo-unit. The signal is transmitted through the control system and displaces the control rods in the direction necessary to bring reactor power level into correspondence with the de-

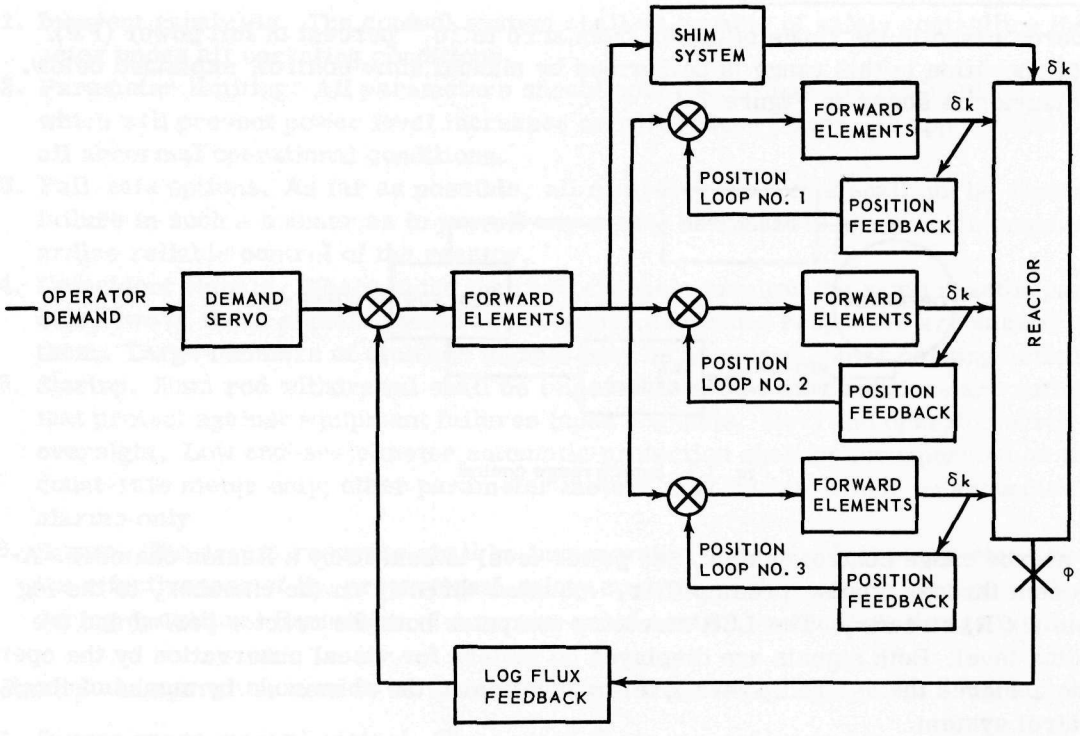

Fig. 7.2 – Intermediate range control

manded power level. If the demand in power level is great enough, both the dynamic and shim rods move during automatic operation.

7.2.4 POWER RANGE

The power range control operates between 10^{-1} and 100 percent FP. A block diagram of the system is shown in Figure 7.3.

The power range demand servo serves two functions. One is to accept the power demand from the operator, convert it into a voltage signal, and schedule it into the system at a predetermined rate. The other function of the power range demand servo is to maintain proper system gain at all power levels.

The automatic control systems of the intermediate and power ranges are multi-channel systems. Any one of three channels can be selected to control the reactor; the selection is left to the operator. The channel selecting circuitry is designed so that not more than two of the three channels can be switched out of the system at any time.

7.2.5 FLUX MONITORING CHANNEL

Two separate linear flux channels serve as monitoring channels to accurately indicate reactor flux level. These channels are also tied into the scram bus for additional protection on flux level settings. They consist of a compensated ion chamber, a high-voltage power supply, a high-voltage filter, and a micromicroammeter which contains an adjustable trip circuit and a remote indicator and range changing switch.

The monitoring circuits cover all ranges of reactor power. The trip setting, being adjustable, can be set to trip at any desired level.

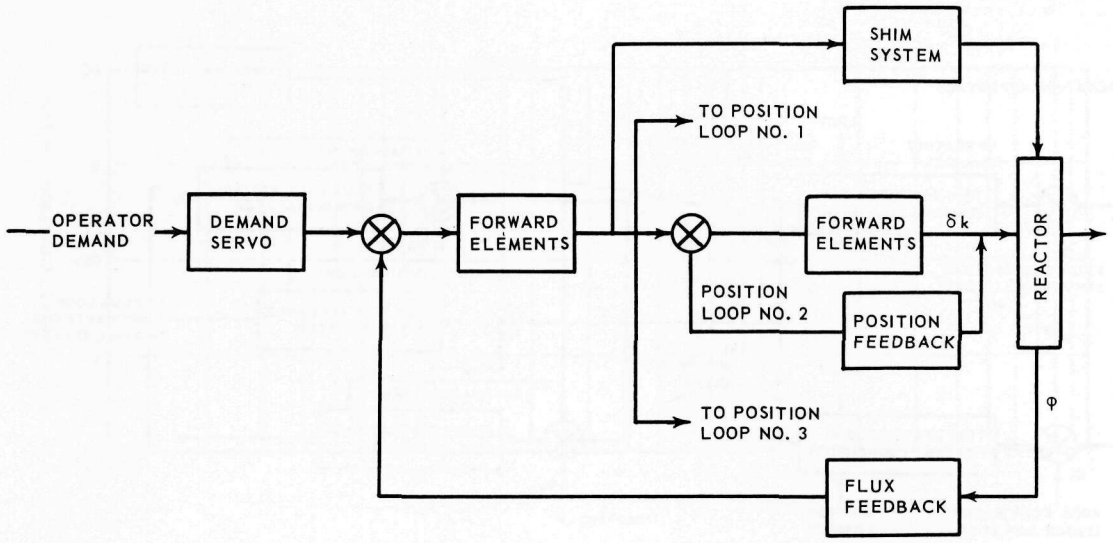

Fig. 7.3 – Power range control

7. 2. 6 TEMPERATURE CONTROL LOOP

7. 2. 6. 1 Description

The HTRE No. 3 temperature control system is a modification of the reactor temperature control of the XMA-1 power plant, in which control was to be accomplished with a single throttle lever. In this system, reference voltage proportional to the demanded temperature is compared to a feedback voltage generated by a reactor exit-air thermocouple. The resulting error is applied to an integrating amplifier and the integrator output is algebraically summed with the flux demand. The output of the integrator is limited to a polarity opposite in sign to the flux demand. It is possible through temperature control to effect a reduction of flux of 40 percent FP.

7. 2. 6. 2 General Requirements

The following requirements were established for the HTRE No. 3 temperature control loop.

1. Control range - 1100° to 1400°F.
2. Mode of operation - servo-controlled temperature regulation.
3. Control parameter - reactor exit-air temperature.
4. Other parameters indicated:
   a. Dynamic rod position
   b. Shim rod position
   c. Fuel element temperature
   d. Flux level
   e. Flux loop error
   f. Temperature loop input.
5. Condition of operation - safety system satisified.
6. Transfer to temperature control - transfer from flux control to temperature control (and back to flux control) must be effected without introducing system transients.

Figure 7. 4 is a block diagram of the temperature control.

The 2-channel temperature loop controls reactor exit-air temperature within ±10°F. The open-loop frequency response is shown in Figure 7. 5, the closed-loop in Figure 7. 6, and the transient response to demand in Figure 7. 7.

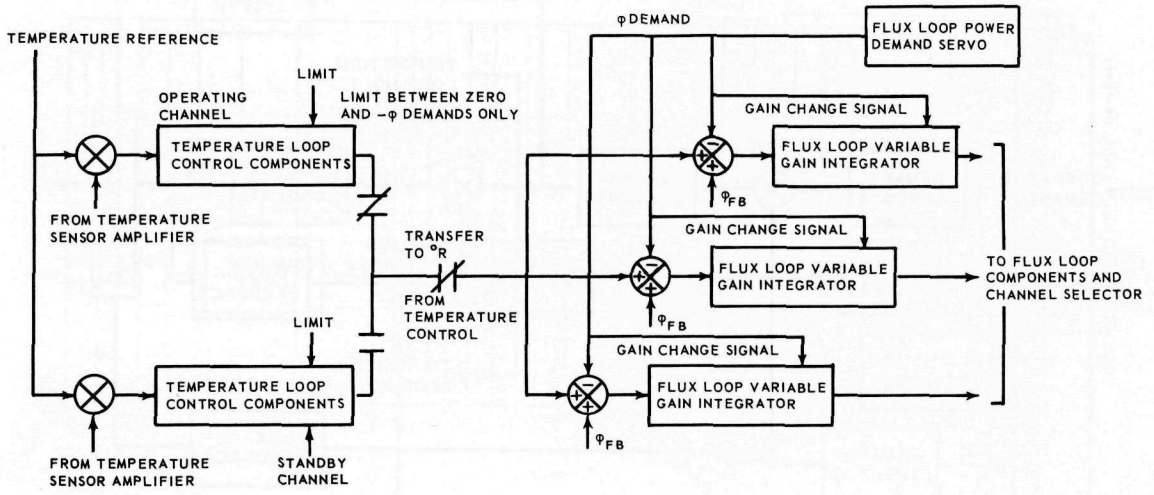

Fig. 7.4 – Temperature loop

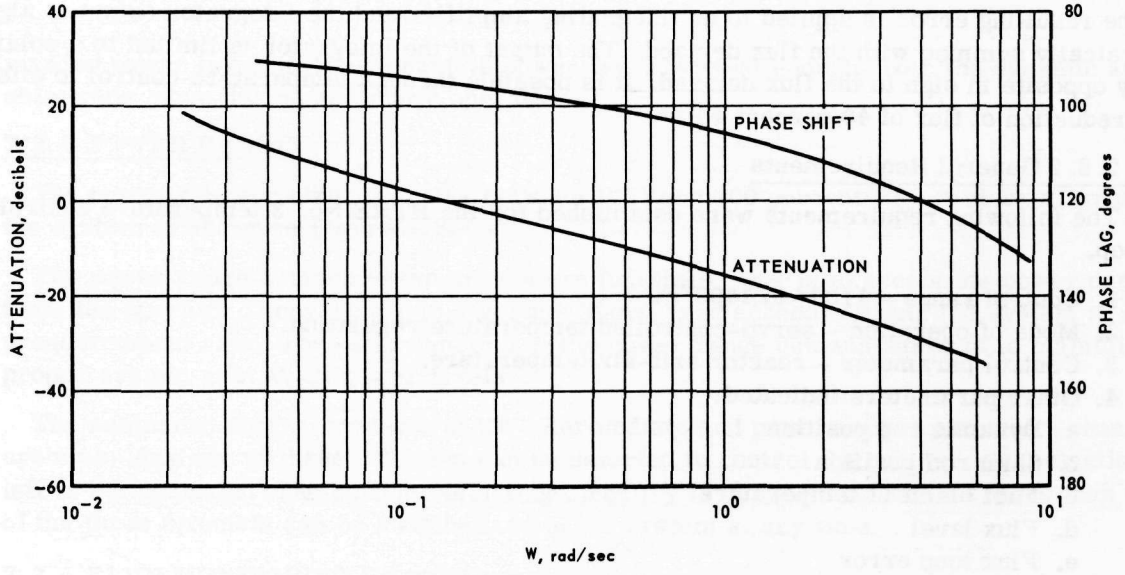

Fig. 7.5 – Measured open loop frequency response of the temperature loop

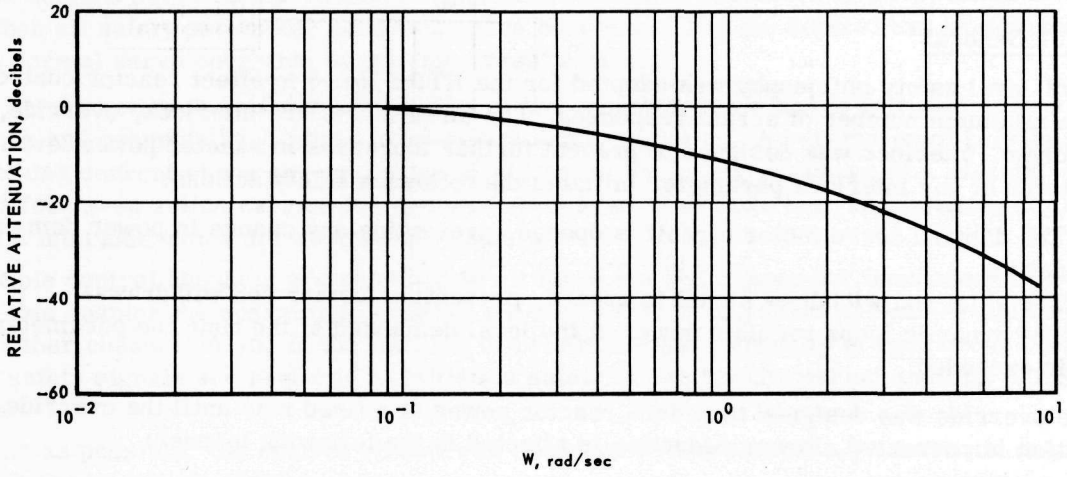

Fig. 7.6 – Measured closed loop attenuation response of the temperature loop

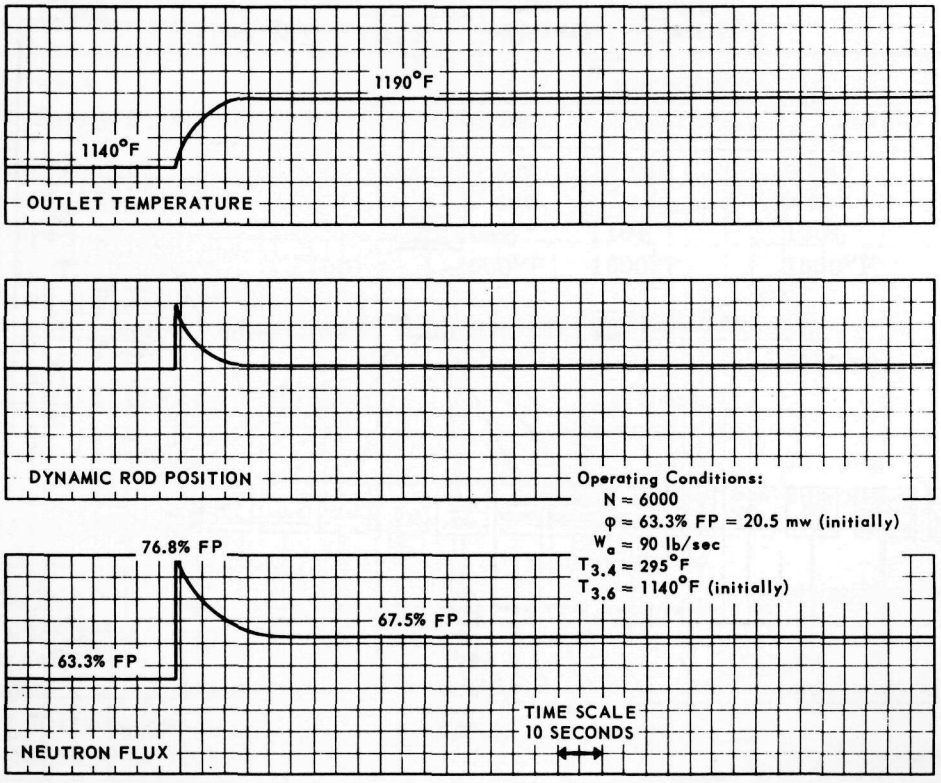

Fig. 7.7 – Temperature loop transient response to demand (50° step input)

7. 2. 7 SAFETY FEATURES

A block diagram of the HTRE No. 3 safety system is shown in Figure 7. 8.

7. 2. 7. 1 General

A tri-level safety philosophy was adopted for the HTRE No. 3 to effect reactor control with a minimum number of scram responses. The three levels are interlock, override, and scram. Interlock was designed to prevent further increases in reactor power level. Violations of any interlock parameter initiates the following safety actions:

1. The demand servo motor circuit is opened, preventing any change in power demand setting.
2. The shim rod withdraw signal is opened, preventing further rod withdrawal.
3. The dynamic loops regulate power at the level demanded at the time the parameter is exceeded.

The override was designed to reduce reactor power at a fixed rate until the override condition is corrected. Power reduction is effected in the following manner:

1. The demand servo output is reduced at a fixed rate causing the dynamic rods to be inserted to reduce power.

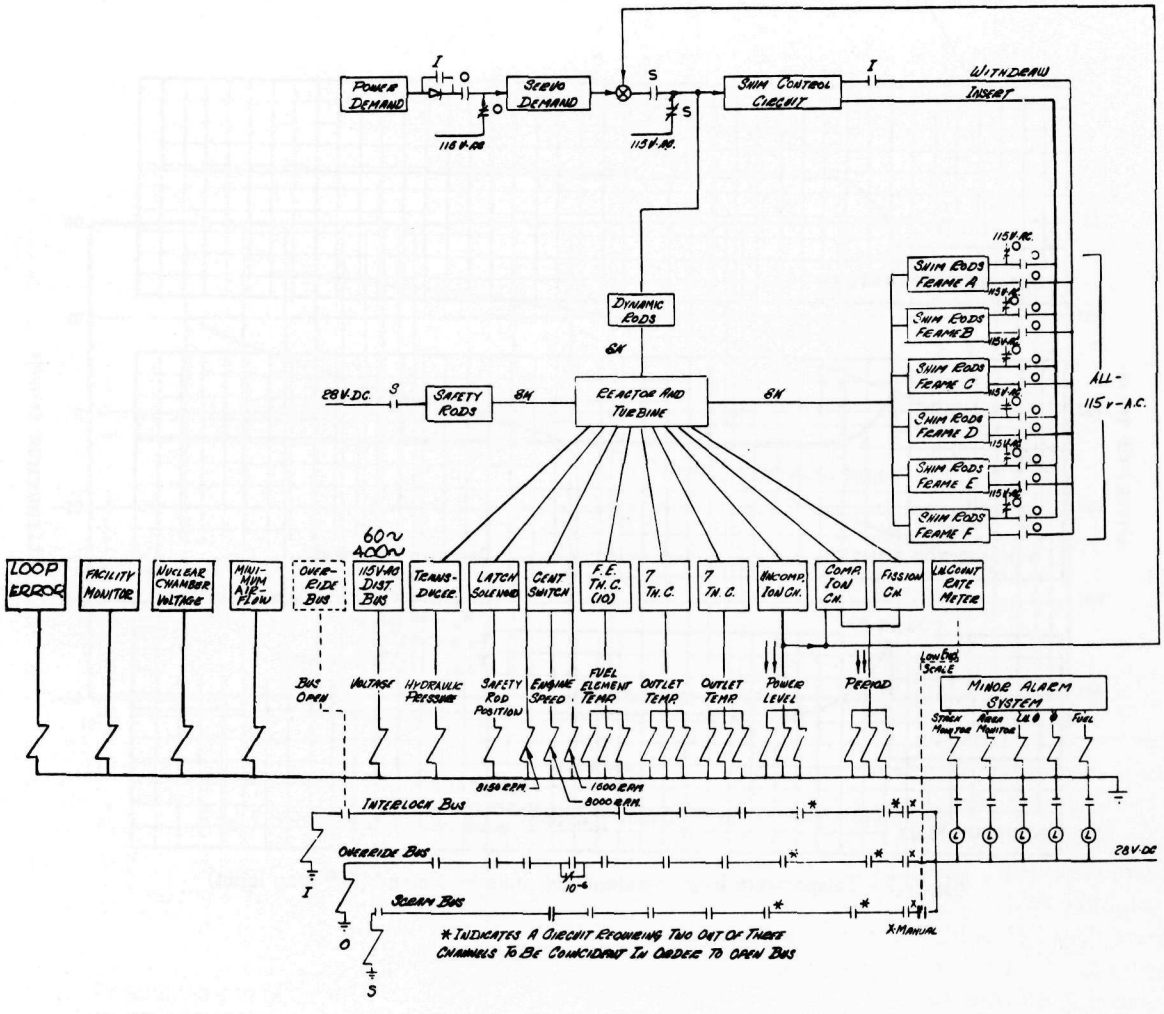

Fig. 7.8 – Safety system

2. All partially or fully withdrawn shim rods are driven into the core at normal speeds (approximately 1% Δk per minute per frame). When the override condition is corrected, the demand servo motor circuit is opened and power is regulated at the reduced level.
3. When all safety parameter conditions have been satisfied, the control can be returned to normal servo operation by operator reset action.

The scram action is entirely independent of the control system and is initiated only after interlock and override have failed to correct a safety violation. A scram signal releases the latching current of the spring-driven safety rods. To insure shutdown at a maximum rate, a follow-up action carries the dynamic rods to be fully inserted, and initiates override and interlock which drives all shim rods in.

Multiple control channels are provided in all three control ranges for increased reliability; this enables the operator to observe the loop error in any control channel and select another channel. Also, in the interest of reliability and continuity of operation, coincident safety signals are required to initiate a safety action for the period and flux parameters.

As far as possible, the control circuit was designed to fail-safe; i.e., circuit or component failures initiate a safety action.

7.2.7.2 Safety Parameters

The safety parameters of the HTRE No. 3 are shown in Table 7.2.

TABLE 7.2

HTRE NO. 3 SAFETY PARAMETERS

Safety Parameter	Response		
	Interlock	Override	Scram
Source range period	15 sec	10 sec	5 sec
10^{-4}% to 10% FP period	10 sec	7 sec	5 sec
Power range flux	105%	110%	120%
Average air temperature	1550°F	1600°F	1650°F
Percent of thermocouples exceeding trip set point (1850°F, adjustable)	10	30	50
Engine speed	-	8050 rpm	8150 rpm
Minimum airflow (above 10^{-4}% FP)	-	ΔP 1 psi across core	-
115-volt, 400-cycle power	-	-	95 volts
28-volt d-c power	-	-	20 volts
Hydraulic oil pressure[a]	-	1000 psi	-
Safety rod latching	-	unlatched	-
Log count rate meter	-	-	off scale low
Dynamics turned off[a]	-	3 off	-
Operator action	yes	yes	yes
Rupture detector (adjustable)	-	-	level exceeded
115-volt, 60-cycle power	-	off	-
Facility power lever monitor (adjustable)	-	-	level exceeded
Power supply undervoltage on ion chambers	-	-	1000 volts
Integral of flux loop error[a] (adjustable)	-	≈10 volts	-
Indicating channels trip setting exceeded (adjustable)	-	-	level exceeded

[a]During automatic servo control.

7. 2. 7. 3 Safety Responses

Figure 7. 9 shows response characteristics of the basic interlock and manual override action. Figure 7. 10 shows the rate of power decrease during a manual scram safety action.

7. 2. 7. 4 Alarm Panel

An alarm panel is provided to receive and display all safety incidents as well as control system safety response status. Acutation of any of the safety response buses provides visual signals for operator notification. Visual signals lock in and require manual resetting to insure operator notification. Figure 7. 11 shows the safety-system monitoring of a demand power rise in the event of a period violation. Figure 7. 12 shows the sequence of events in a scram action.

7. 2. 8 NUCLEAR SENSOR SYSTEM

Being a power reactor control type, the control system for the HTRE No. 3 power plant requires a radiation measuring loop. The measuring devices used are fission and ioniza-

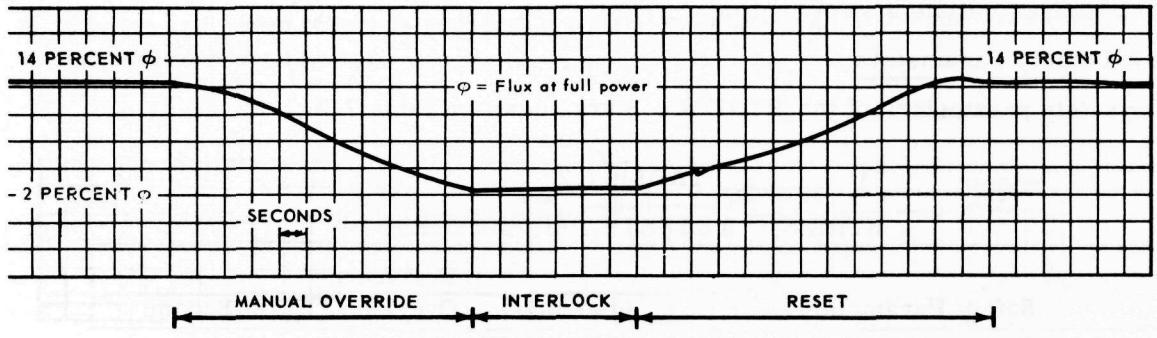

Fig. 7.9 – Response characteristics of the basic interlock and manual override actions

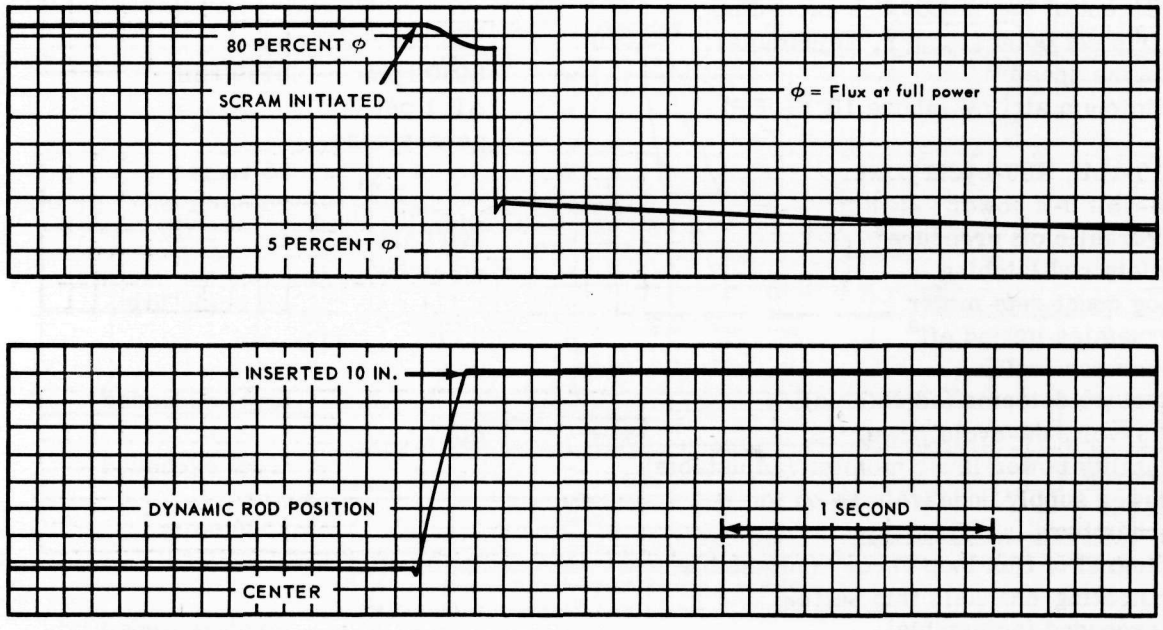

Fig. 7.10 – Rate of power decrease during a manual scram safety action

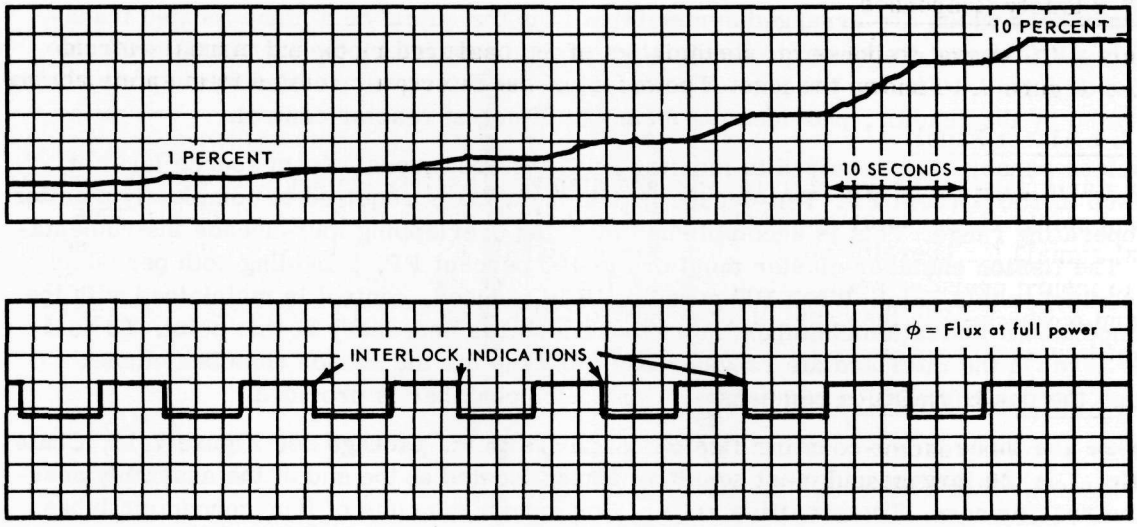

Fig. 7.11 – Safety-system monitoring of a demand power rise in the event of a period violation

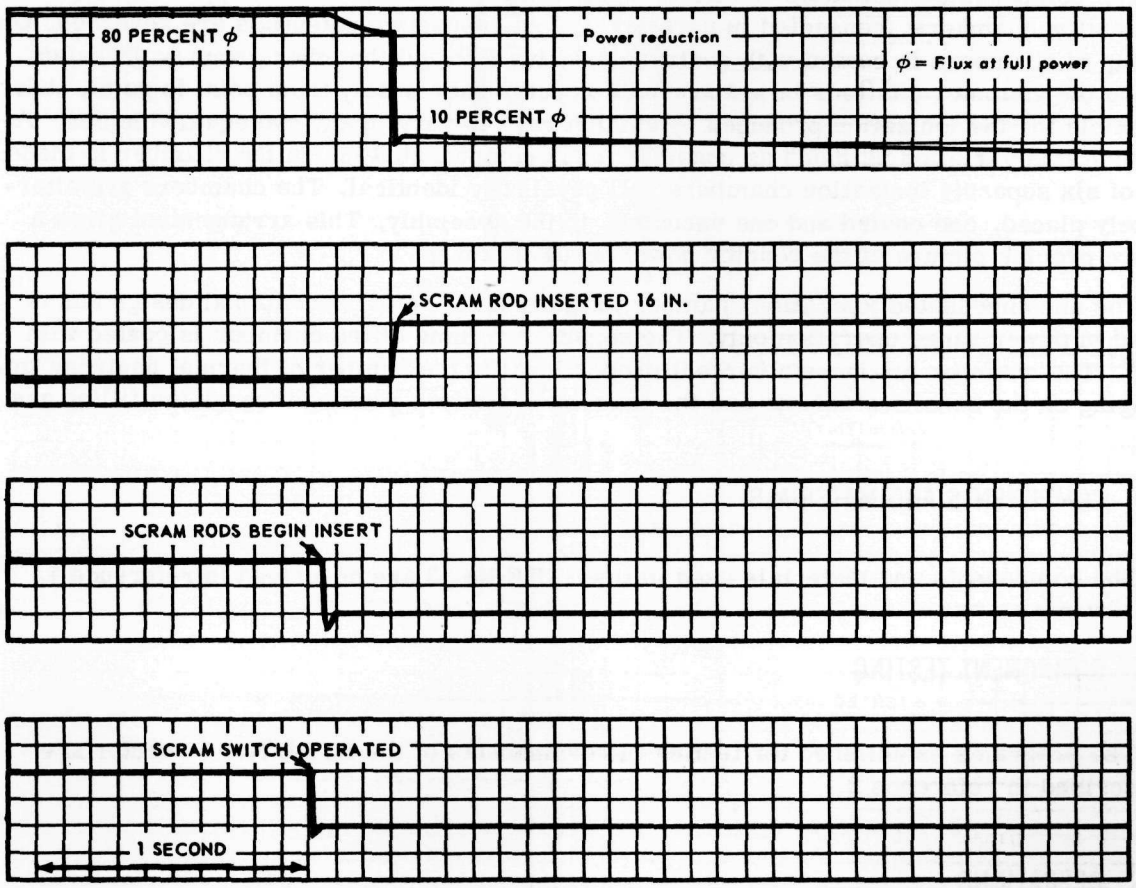

Fig. 7.12 – Sequence of events in a scram action

tion chambers which are arranged symmetrically in the shield on a plane located transversely with respect to the core. Reactor power is measured by the incidental neutrons developed from the fission process. The output of the detectors, related to the power being generated by the reactor, provides the means of effecting reactor control.

Nuclear sensors are required to monitor neutrons continuously from source level at start-up to 150 percent FP. Ten-decade instrumentation is required to completely monitor this operating range. This is accomplished by using overlapping four-decade instrumentation. The fission chamber cluster monitors to 100 percent FP, providing both period and flux control to this point. When 100 percent FP is reached, control is maintained with the uncompensated ionization chamber; no period control is necessary at this point. To hold power level in the intermediate range and as a backup for the fission chamber cluster through the power range, a compensated ionization chamber is provided.

There are three pulse-counting fission chambers in the package see Figure 7.13. Chamber No. 1 is the largest and most sensitive and is located at the end of the assembly nearest the reactor core. The sensitive area of this sensor consists of four concentric tubes which are coated with enriched uranium. The other two chambers of the cluster are of the same design and sensitivity. Their sensitive areas consist of a "cup" coated with enriched uranium. Chamber No. 2 is located just behind No. 1 and No. 3 is located 9 inches behind No. 2.

The compensated ionization chamber, Figure 7.14, consists of two separate groups of ionization chambers, connected in parallel, whose respective potentials are reversed. One group of chambers is coated with neutron sensitive B^{10} and the other group is uncoated. Since the gamma radiations in and around a reactor vary widely from point to point, it is possible for the ionization produced by gamma rays to vary in any two equal volumes. To reduce this variation as much as possible, each compensated ionization chamber is made up of six separate ionization chambers, all physically identical. The chambers are alternately placed, one coated and one uncoated, in the assembly. This arrangement gives a more precise picture of the reactor power level operation.

The uncompensated ionization chamber, Figure 7.15, is of conventional design and is used in power range operation only. The sensitive volume of the chamber is coated with B^{10}. The chamber produces a current proportional to the number of thermal neutrons impinging on the sensitive volume and the ionizing radiations passing through the filling gas.

7.3 COMPONENTS AND MATERIALS

The components and materials used in the HTRE No. 3 are described in reference 1.

7.4 COMPONENT TESTING

The programs established for testing the components of the HTRE No. 3 reactor are described in reference 2.

7.5 OPERATIONS

The HTRE No. 3 control system was the first to be designed and built by GE-ANPD utilizing printed circuits and miniature components in an effort to reduce the weight and volume of the system. This system operated successfully.

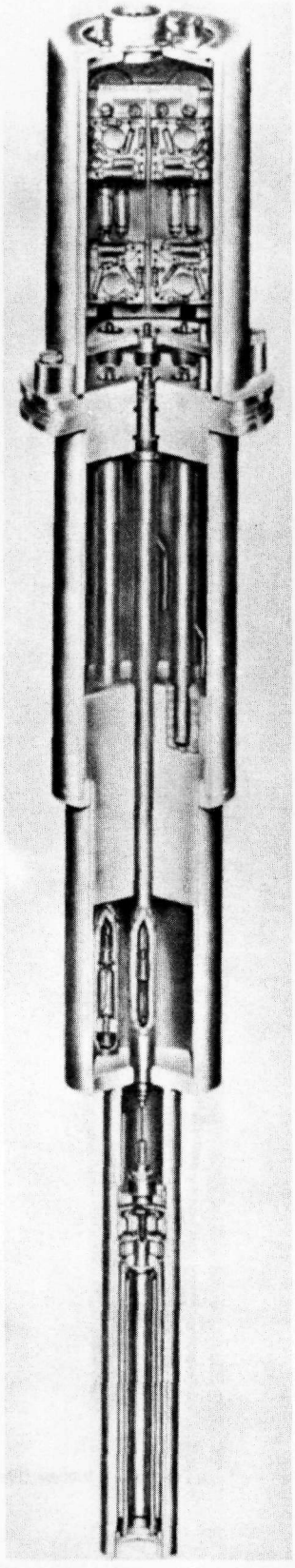

Fig. 7.13 – Fission chamber (Neg. G-994)

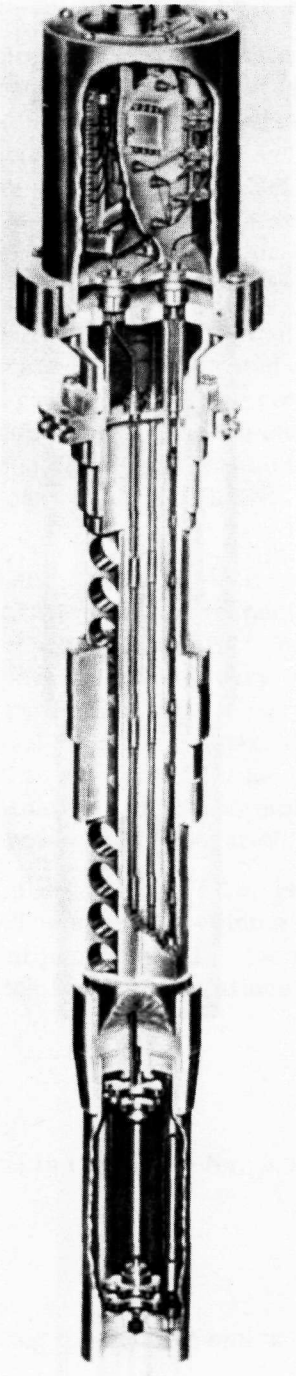

Fig. 7.14 – Compensated ionization chamber (Neg. G-1023)

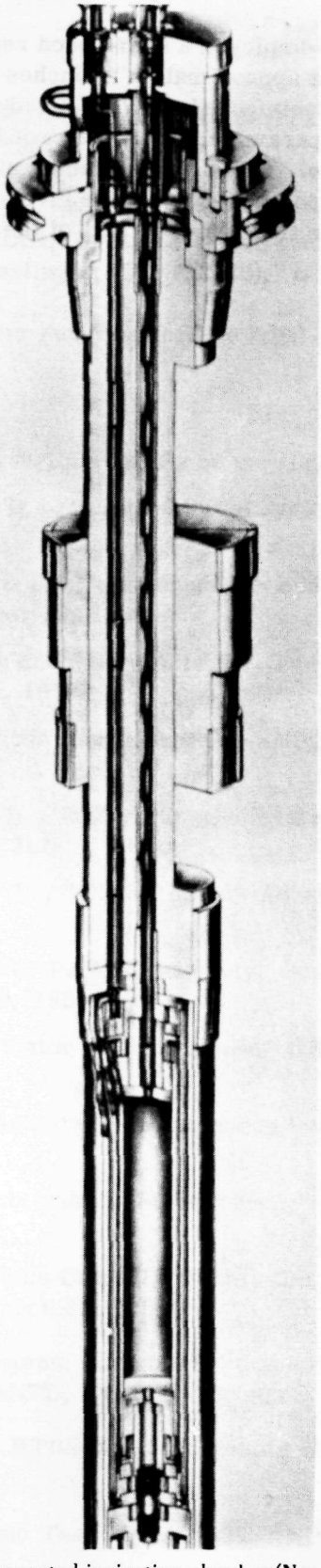

Fig. 7.15 – Uncompensated ionization chamber (Neg. G-972)

The automatic reactor control employed a high-speed regulating control rod capable of following a flux error signal at approximately 45 inches per second. Sinusoidal and step demand variations were superimposed upon the steady-state flux demand and the resulting changes of basic system parameters were recorded. The tests were repeated for a number of operating points; i.e., various flux, temperature, and airflow conditions. The test conditions and the data points recorded are given in reference 3. The test results were analyzed and the basic transfer functions of the reactor and heat transfer are presented in reference 4.

7.6 REFERENCES

1. "Description of the Components and Materials of the HTRE No. 3 Control System," GE-NMPO, DC 61-11-28, May 1961.
2. "Component Testing of the HTRE No. 3 Control System," GE-NMPO, DC 61-11-29, May 1961.
3. Cannon, C. B., "Addenda To XDCL 59-12-719 D102A2 (A) Power Plant Test Programs and Procedures for Phase III Testing at IET (IET 25)," GE-ANPD, XDCL 60-10-725, October 21, 1960.
4. Skow, K. J., "IET #25, Transfer Functions of The D102A2 Core," GE-ANPD, DC 61-6-705, June 19, 1961.

SUPPLEMENTARY REFERENCES

The following references contain further details on the HTRE No. 3 control system.

Miller, W. T., and Ferguson, M. H., "D102A Control System Maintenance," GE-ANPD, DC 59-6-15, June 15, 1959.

Starling, H. C., "System Operation and Maintenance Procedure for D102A Control System," GE-ANPD, DC 57-12-148, December 20, 1957.

Bell, H. E., "Shim Control System and Safety Actuator Control System for D102A," GE-ANPD, DC 58-1-72, January 9, 1958.

Swope, R. R., "D102A Nuclear Sensor Handbook," GE-ANPD, DC 58-8-116, September 1, 1958.

Miller, W. T., and Ferguson, M. H., "D102A Control System Relay, Lamp and Meter Circuit," GE-ANPD, DC 59-6-143, July 1, 1959.

McCarty, L. H., and DeWeese, J. L., "D102A Rotary Actuator - Maintenance," GE-ANPD, DC 58-6-53, June 20, 1958.

Rave, K. B., "D102A Dynamic Power Pack - Assembly, Operation, and Maintenance, GE-ANPD, DC 58-7-204, August 29, 1958.

White, L. C., "D102A Dynamic Actuator - Maintenance," GE-ANPD, DC 58-2-114, February 10, 1958.

Haberman, N., "D102A Shim Rod Actuator - Maintenance," GE-ANPD, DC 58-3-15, March 10, 1958.

Spivak, A. L., "D102A Safety Rod Actuator - Maintenance," GE-ANPD, DC 58-2-115, March 14, 1958.

Humphrey, W. R., "Auxiliary Systems Control - Installation, Operation, and Maintenance," GE-ANPD, DC 58-3-60, March 31, 1958.

Birnbach, S., "D102A Auxiliary Systems Controls System 4500 Blower - Installation, Operation, and Maintenance," GE-ANPD, DC 58-3-39, April 1, 1958.

Emmert, R. I., "The Design of the HTRE No. 3 Automatic Control," GE-ANPD, DC 57-9-107, September 12, 1957.

Hurd, D. E., "P102A Control Mockup Test Report," GE-ANPD, DC 58-1-114, January 15, 1958.

Starling, H. C., and Drummond, J. K., "Final D102A Control System Test Report," GE-ANPD, DC 58-10-209, October 29, 1958.

Miller, W. T., and Ferguson, M. H., "D102A Control System Relay, Lamp, and Meter Circuit," GE-ANPD, DC 58-4-199, April 30, 1958.

Starling, H. C., "Operation Procedure for the D102A Control System," GE-ANPD, DC 59-8-21, August 3, 1959.

Showalter, J. A., "Controls and Instrumentation Schematic Diagrams, Drawings and Photos," GE-ANPD, DC 59-8-127, August 14, 1959.

Coleman, E. M., "200°F Oil Temperature Test on D102A Hydraulic Power Pack," GE-ANPD, DC 60-4-727, April 22, 1960.

Coleman, E. M., "Phase I of -40°F Ambient Temperature Test of D102A Power Pack," GE-ANPD, DC 60-5-707, April 26, 1960.

Coleman, E. M., "Phase II of -40°F Ambient Temperature Test of D102A Power Pack," GE-ANPD, DC 60-5-744, May 13, 1960.

Coleman, E. M., "Room Temperature Endurance Test on D102A Hydraulic Power Pack," GE-ANPD, DC 60-4-726, April 22, 1960.

Gelezunas, V. L., and Betts, R. K., "Revision of D102A Control Rod Mfg. Specs. Part I," GE-ANPD, DC 58-10-183, October 23, 1958.

Gelezunas, V. L., and Betts, R. K., "Revision of D102A Control Rod Mfg. Specs. Part II," GE-ANPD, DC 58-11-89, November 11, 1958.

Gelezunas, V. L., "Control Rods Eu_2O_3 Dispersion," GE-ANPD, DC 59-6-131, June 12, 1959.

Brekken, T., and Tuck, G., "Test Program for D102A Ion Chambers," GE-ANPD, DC 58-12-715, December 10, 1958.

St. Leger-Barter, G., "D102A Ion Chamber Irradiation in the MTR," GE-ANPD, DC 59-2-721, February 23, 1959.

Brekken, T., "Test Program for D102A Ion Chamber Calibration and Endurance Test," GE-ANPD, XDCL 59-2-722, February 20, 1959.

Swope, R. R., "D102A Nuclear Sensors," GE-ANPD, XDCL 59-6-222, June 24, 1959.

Showalter, D. E., "Test Program and Procedures for D102A Fission Chambers in P101 Mockup," GE-ANPD, DC 59-6-713, May 19, 1959.

St. Leger-Barter, G., and Halleck, M. C., "Calibration of D102A Nuclear Sensors," GE-ANPD, DC 59-6-743, June 30, 1959.

Halleck, M. C., "Comparison of D102A Fission Chambers Characteristics with Initial Check-out," GE-ANPD, DC 59-10-721, September 28, 1959.

Swope, R. R., "Recommended Operation of Nuclear Sensors in D102A Phase II Operation," GE-ANPD, DC 59-12-49, December 3, 1959.

8. TEST ASSEMBLIES AND REACTOR ACCESSORIES

This section describes the dolly on which the turbomachinery and reactor are mounted, and the reactor accessory systems (external ducting, shield cooling, and fire control systems).

8.1 DOLLY ASSEMBLY

The HTRE No. 3 dolly is the carriage on which the turbomachinery and the superstructure supporting the reactor, shielding, ducting, and accessory equipment are mounted. The bed, 20 feet wide by 31 feet long, is mounted on four modified 4-wheel railroad trucks. Motive power to the dolly was supplied by a shielded locomotive.

The superstructure consists of three welded rigid platform assemblies. The front platform supports the accessory equipment; the center platform, the reactor-shield assembly; and the rear platform, the turbomachinery, the external ducting, and the combustor shield.

Weather protection for personnel and the power plant is provided by the structure shown in Figure 8.1. Two sections of the side panels are louvered. This structure can withstand steady winds of 40 mph with gusts up to 70 mph.

8.2 REACTOR ACCESSORIES

8.2.1 EXTERNAL DUCTING

The external ducting that conveys compressor discharge air from the two X39-5 turbojet engines to the reactor inlet header and returns the heated air from the common combustor to the engine turbines. Instrumentation and valving are provided in the ducting for data collection and control when operating with either one or both engines. Remote removal of the ducting assemblies from the power plant is accomplished by opening quick-disconnect flanges and lifting the duct assembly out of its support cradle with a suitable hook sling.

Free thermal expansion of the ducts is provided by ten flexible joints to minimize mechanical loading.

The ducting is designed for a maximum loop stress of 6000 to 7000 psi in the thin wall duct members and a maximum temperature of 1000°F at the duct skin.

To protect large surface areas from the effects of high-temperature gas, pad-type insulation was designed that allows the load-carrying members of the duct to operate at relatively low temperatures compared to the gas stream temperature. The 310 stainless steel insulation cover sheet is subject only to the stresses induced by vibration and drag loads from the gases. Thermal expansion of the hot cover sheet is provided in the design by allowing sufficient movement in each of the fasteners and by dividing the insulation

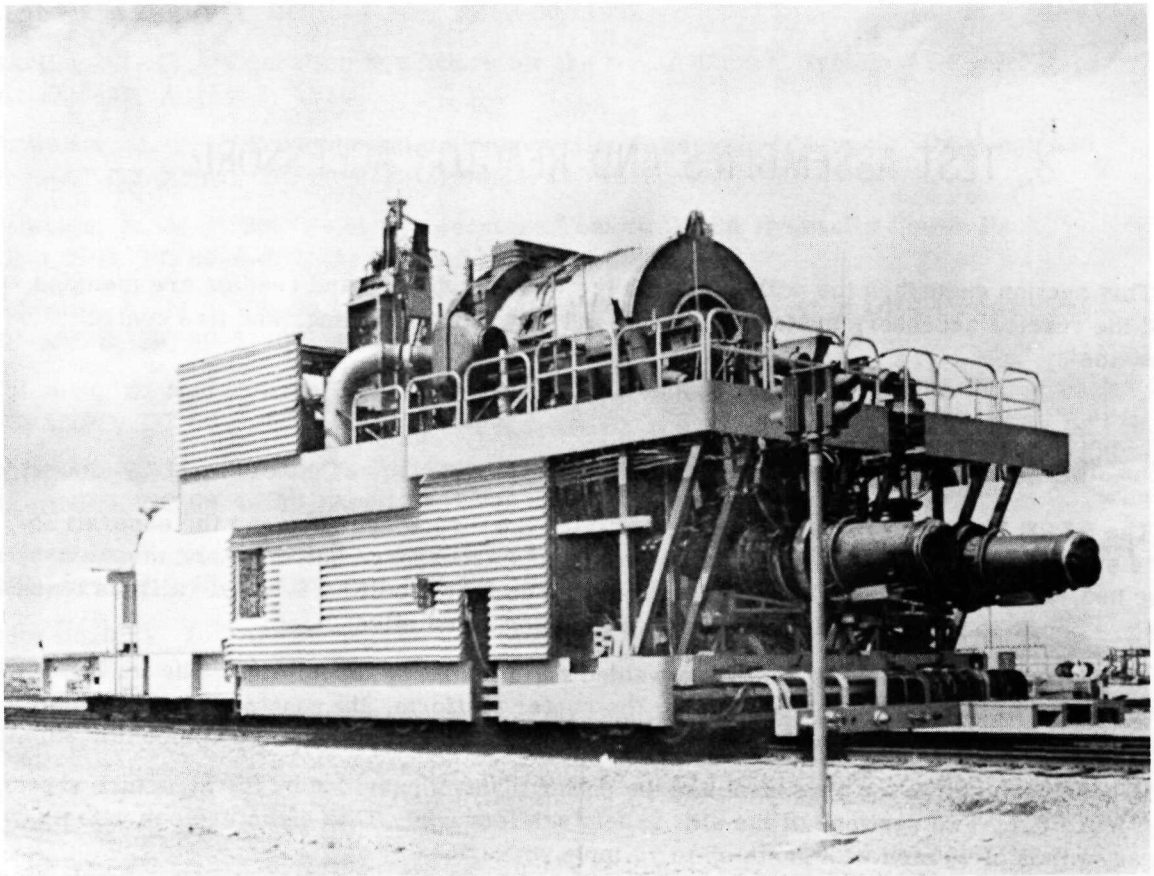

Fig. 8.1 – Louvered weather protection for HTRE No. 3 test assembly (Neg. U2505-3)

cover into a number of relatively small pieces. This design can be applied to any complex curved surface. This large duct area insulation has been experimentally tested at temperatures of 1500°F and 1700°F and Mach 0.23 for a total of 325 hours.

8.2.2 DUCT VALVES AND ACTUATORS

The actuator assembly embodies three principal elements, the main actuator, dynamic brake, and static brake, which are mounted in series on an axial extension of the valve shaft.

The entire actuator is connected to the valve by an interlocking housing arrangement which is secured with pip pins.

The main actuator is a rotary type unit, with displacement of approximately 188 cubic inches which is operated by 200 psig of lubricated air. It is capable of 100-degree rotation with output torques up to 20,000 inch pounds. Lubrication of the operating air is provided on the actuator assembly.

The dynamic brake is a hydraulic damper unit which is similar in construction to the main actuator except that it is built for higher pressure operation (proof pressure 2500 psig) 300°F ambient temperatures and operates on hydraulic fluid. It functions to reduce the valve operating speed, providing for slow jog operation and preventing high velocity impact of the blade against the stops.

The static brake is a standard dry disc type with twin, rubber faced discs splined directly to the actuator shaft. The brake is normally on and is released only by application of 200 psig air to the air cylinder. This brake is provided to allow positive locking of the valve in any position and also as a means of arresting the valve motion in the event of interlock violation or failure of the air and/or power supplies.

The HTRE No. 3 assembly uses four duct valves. Two 20-inch valves are used in the cold ducting. Two 24-inch valves are used in the hot ducting. These valves are of the same basic design. They differ in that the hot ducting valves are larger and insulated. More detailed information on the duct valves and actuators is presented in references 1 and 2.

8.2.3 SERVICE-AIR SYSTEM

The service-air system is made up of three separate air systems: a 200-psi system, a 100-psi system, and a 90-psi system. The 200-psi system, supplied from the permanent IET air compressor, is used primarily for operating actuators. The air is brought onto the dolly through a 2-inch facility plug quick-disconnect. From the 2-inch line, smaller lines are run to the duct-valve actuators, combustor bypass-valve actuator, the scram-rod actuators, and the shield-plug pressure cylinder.

The 100-psi system, supplied from portable air compressors at the IET, is used primarily for starting. The air is brought onto the dolly through a 3-inch quick-disconnect on the facility plug. This line tees into a 2-inch manifold which runs across the dolly under the combustor panel. A line is run from each end of this manifold to the nose of each turbojet engine where it is used for operating the starters. Other lines run from the manifold to the duct-valve actuators to cool the actuators. Air is run to the combustor panel where it is distributed for nozzle purging, nozzle cooling, and combustor bypass-valve cooling. A 1-1/2-inch line is run to the front of the dolly to an automatic quick-disconnect. This air is used for starting the aftercooler blower engines on the service dolly.

A 90-psi system is used only in the hot shop and operates from the hot shop air supply. This air is used only for operating the air cylinders which pull the pins from the turbojet dolly mounts so the turbojet dollies may be removed remotely.

The service air system is more fully described in references 3 and 4.

8.2.4 PRIMARY SHIELD LIQUID SYSTEM

The shield liquid system is designed to remove the heat generated in the shield during operation of the HTRE No. 3 assembly and the heat remaining after shutdown while at the coupling station. The system provides for filling and draining of the shield components and maintaining the proper water level.

There are two flow systems: (1) the process water or shield water system, and (2) the coolant water system.

8.2.4.1 Process Water System

The process water is circulated through the primary radial shield, front shield plug, rear shield plug, and combustor shield at a constant flow rate of 600 gpm. Three pumps are provided to circulate the water. Two are required for the design flow while one is a stand-by.

The flow distribution between the cooled components is adjusted by motor-driven valves. The flow to each component is measured by flow meters in each component's supply line, and an exit-water temperature is recorded for each component. The inlet temperature to the components is recorded at the heat-exchanger outlets. With this information, the shield's total heating can be evaluated and the flow can be properly distributed.

After the process water leaves the shield, it is piped to the pumps and taken to the tube-side of the heat exchanger, then back to the shield. A surge tank of 150-gallon capacity is provided. This tank is normally half-filled. This system drains through the pumps or by gravity. Quick-disconnects are provided in inlet and outlet lines to the shield for remote-handling of the reactor-shield assembly.

8.2.4.2 Coolant Water System

The coolant water is obtained from wells located at the ITS. The water is pumped to the shell side of the heat exchanger. The heat exchanger is rated at 15 million Btu per hour with maximum design flow rates. After the coolant water leaves the heat exchanger, it is piped to a location directly above the drainage trench where it is dumped.

A provision has been incorporated into the process water system to permit the independent filling or draining of the front shield plug, side shield, rear shield plug, and combustor shield. Each of these units may be isolated from the process water system during the cooling operation in a low-power test run. For example, the entire system can be filled, the side shield remain filled or drained completely when isolated from the balance of the system, and a low-power test run with the process water flowing through the front shield plug, rear shield plug, and combustor shield. It is also possible to isolate combinations of the shield units. This provision has been made for test purposes only.

References 5, 6, 7, and 8 present more detailed information on the shield liquid system's control, safety, and vent accessory systems.

8.2.5 SHIELD AUGMENTATION SYSTEM

The purpose of the shield augmentation is to provide additional shielding for the reactor after shutdown by replacing the water in the primary shield outer tank with gamma shielding mercury. The mercury provides the necessary mass around the reactor to permit contact maintenance.

The system operates in the following manner: the shield outer-tank water drain valve is manually opened. After this water is evacuated, the water valves are closed and the augmentation drain-and-fill valve is opened. The augmentation fluid is pumped from the storage tank through stainless steel piping, through the opened valve and into the primary-shield outer tank. The shield fills from the bottom. Filling forces the air in the shield tank out through a vent line at the top of the shield. A pressure switch, located in the vent line and operated by the overflow of mercury, signals the operator that the tank is filled.

The vent line is routed back into the storage tank, thus forming a closed system. In the vent line, there is a water and foreign material separator. This separator is so constructed that it returns any mercury and its toxic vapors to the storage tank and shunts water overboard.

A system of valve interlocks prevents the mercury from draining into the water drain-and-fill lines.

Draining of the augmentation fluid takes place through the same valve and line used to fill the tank with mercury.

The shield augmentation system is more fully described in references 5 and 6.

8.3 REFERENCES

1. McDonald, W. A., "D102-A Duct Valves Actuator System - Operation and Maintenance," GE-ANPD, DC 58-6-131, June 2, 1958.
2. McDonald, W. A., "D102-A Duct Valves - Assembly and Installation," GE-ANPD, DC 58-6-130, June 2, 1958.
3. Evans, W. G., "D102-A Service Air Systems - Assembly and Installation," GE-ANPD, DC 57-10-135, November 1, 1957.
4. Evans, W. G., and Ferguson, M. H., "D102-A Service Air System - Operation and Maintenance," GE-ANPD, DC 57-12-76, December 30, 1957.
5. Goodhart, F. W., Jr., and Ferguson, M. H., "D102-A Shield Liquid System and Shield Augmentation System - Assembly Instructions," GE-ANPD, DC 57-11-10, November 10, 1957.
6. Evans, W. G., and Ferguson, M. H., "D102-A Shield Liquid System and Shield Augmentation System - Operation and Maintenance," GE-ANPD, DC 57-12-14, December 13, 1957.
7. Evans, W. G., and Sullivan, J. M., "D102-A Shield Vent System - Assembly and Installation," GE-ANPD, DC 57-12-62, December 20, 1957.
8. Evans, W. G., and Arnold, E. P., "D102-A Shield Vent Systems - Operation and Maintenance," GE-ANPD, DC 57-12-63, December 20, 1957.

9. REMOTE HANDLING EQUIPMENT

9.1 OBJECTIVES AND REQUIREMENTS

The objectives of the HTRE No. 3 remote handling planning were to provide the necessary equipment to allow maintenance of the power plant assembly after it had been operated under nuclear power. The radiation after reactor shutdown would continue for long periods of time and to such intensity that all work on the core itself would require remote maintenance.

Induced activity and contamination required that components located in close proximity to the core be handled remotely. Other components, separable from the core could be handled manually, limiting the remote handling work to operations necessary to remove the component from the core area.

All of the HTRE No. 3 remote handling equipment is described in detail in reference 1.

9.2 REFERENCES

1. Ridgeway, C. L., "Remote-Handling Equipment Catalog," GE-ANPD, XDC 61-1-133, February 1961.

10. HAZARDS

Hazards reports for the HTRE No. 3 power plant are contained in references 1 and 2. APEX-921, "Nuclear Safety," of this Report summarizes the over-all approach to the safety aspects of the direct-air-cycle nuclear propulsion program.

10.1 REFERENCES

1. Gamertsfelder, C. C., Blumberg, B., and Schoenberger, T. W., "D102A Hazards Report," GE-ANPD, APEX-344, December 12, 1957.
2. Gamertsfelder, C. C., Blumberg, B., and Schoenberger, T. W., "Addendum to D102A Hazards Report," GE-ANPD, APEX-482, June 16, 1961.